Processes at the Interfaces of Electro- and Organic Chemistries

by

Anuska Shrestha

A dissertation submitted in partial fulfillment
of the requirements for the degree of
Doctor of Philosophy
(Chemistry)
in the University of Michigan
2020

Doctoral Committee:

Professor Melanie S. Sanford, Chair
Professor Adam J. Matzger
Assistant Professor Charles C. L. McCrory
Professor Johannes Schwank

Anuska Shrestha

ashresth@umich.edu

ORCID iD: 0000-0002-3880-3736

For my family

Acknowledgements

It is strange to be defending my thesis in a time when the world is suffering from a pandemic. But this situation stands as an example of my fortune to have a graduate mentor like Melanie. You have always watched out for your students' health and well-being. Thank you for giving me an opportunity to work in your lab, under your mentorship. You let me work on projects that I had no background on and gave me the time and resources to learn and grow as a chemist. This is the most valuable lesson that I take away from graduate school. I will miss your enthusiasm and energy, that is so infectious, and helped lift me up when I struggled in lab.

I want to thank Professor Adam Matzger for all your valuable teachings and mentorships. I got to explore a completely new area of chemistry in your lab during my rotation. You were patient with me through failed MOF syntheses and several MOF characterizations lessons. Your feedbacks and advices were crucial for a successful Karle Symposium (2018).

I also want to thank Professor Charles McCrory for your valuable feedback on my work during my candidacy and data meeting. Those conversations helped shape some of the projects that we were working on and we are grateful for the valuable discussions. Professor Matzger, McCrory and Schwank, thank you for serving in my committee and for your valuable feedback during my time in graduate school.

A big shout out to my undergraduate mentor, Professor Emily McLaughlin. You have always been there when I needed someone to talk and make (what I thought were) life-changing decisions. I am so proud to be one of your students. You have worked effortlessly to improve college experience of a student like me, and I will always be grateful for your support throughout my career.

I also had an opportunity to be a part of JCESR and specifically the redoxmers sub-thrust. The biweekly meetings gave us a platform to share our research and gain

valuable insights from researchers with different backgrounds and perspective. This was also a great opportunity for a graduate student like me to learn and grow as a scientist. I want to specifically thank our collaborators Professor Matthew S. Sigman and Professor Shelley D. Minteer at the University of Utah for all your help during my graduate school. Thank you for taking your time to address my questions. Zayn Rhodes at the University of Utah, it was great to share our knowledge of flow batteries with you and in turn learn a lot from you as well. I also want to thank the batteries/echem subgroup for the interesting discussions and suggestions when the data did not make sense, or when the experiments did not work as intended.

Graduate school would have been a lot harder without mentorship of amazing mentors and colleagues throughout. Firstly, thank you Pablo, my first mentor in graduate school. I learnt a lot about synthesis and organic chemistry from you. You were a great mentor and friend, despite your poor choice in sports team. I want to give a huge shout out to Koen. My PhD would not have been the same without your guidance and mentorship. I learnt so much about redox flow batteries and electrochemistry from you and continue to do so. Whenever I have any questions, I know I can always turn to you. Thank you for answering all my frantic WhatsApp messages. Christo, thank you for the helpful discussions and teaching me about electrochemistry as well.

I want to thank all the graduate students and post-docs that I interacted with during my time in the Sanford group. I have learnt so much from each and every one of you. I also made great and life-long friends in the Sanford group. I got really fortunate that I got Katarina as my cubby-mate in my first few years. You helped me boost my confidence when I was a young and a timid graduate student, helped me with all the small things that stressed me out, listened to me complain and found a way to make me feel better. Kuam, I don’t even know where to begin thanking you. You have seen me cry and you have seen me rant. But you have put up with it all and I will be forever grateful to your friendship. Yiyang and Scott, thank you for putting up with me and making sure I was never short of wine in my life. I have highly appreciated your feedback on my work and chemistry and owe much of my success to you guys. Pronay, I have always enjoyed our conversations about (Indian) politics, some stupid cultures back home and other random and ridiculous topics. You have also given me some thoughtful advices, that I’ll always be grateful for.

Courtney, you been such an inspiration. I have always valued your dedication to uplift women in science. Christian, thank you for all the late-night pep-talks. Melissa, I really enjoyed collaborating with for the C–H functionalization project. Thank you for your continued support even after you graduated. Mark, I could not have asked for anyone better to share the unique experience that my final year graduate school has been. I also want to thank Devin, Liz, Liam, Ellen, and Conor for all the helpful discussions about chemistry and otherwise. Also, thank you Liam and Katarina for letting me play with Obe, Salem and Jasper.

During my time in the Sanford group, I also got an opportunity to mentor some amazing graduate students: Ryan and Brianna. I cannot wait to see all the wonderful things that you guys are going to do in your respective careers. Yichao, you always make everyone around you laugh with your crazy impressions and ideas. That made lab a fun place to be.

I want to thank my family for their continued support. Mamu and Papa, you have sacrificed so much to get me to where I am today. I am blessed to have you as my parents. I owe all my success to you. Thank you for believing in me, encouraging me to pursue my dreams and letting me fly. Mamu, you are the most amazing person and the best of friend; I aspire to have your level of patience and dedication to family. To all my extended family, thank you for loving me endlessly and motivating me to work harder every day.

I have been very fortunate to have emotional support systems outside of lab. Ramesh and India, I have always look forward to our adventures together, and taking the much-needed breaks from lab. Ayousha, Sudeshana, and Shilva, I had never realized I had been missing out on so much fun without girlfriends like you in my life. Thank you for being the emotional support system I didn’t realize I needed.

Finally, big shout out to the unsung hero of my graduate school, Bijay. No words are enough to express how grateful I am to you. You have made sure I stayed sane throughout graduate school, oftentimes at the expense of your own sanity. Every time I doubted myself or was low in confidence (which was fairly often), you were there to lift me up. You showed me the world of adventure. I could not have made it through this time without your endless love, support and encouragement. Thank you for always being there for me.

Table of Contents

List of Figures

List of Schemes

List of Tables

List of Abbreviations

Ac_2O	acetic anhydride
AcOH	acetic acid
AEM	anion exchange membrane
BE	bulk electrolysis
Boc	*tert*-butyloxycarbonyl
BQ	benzoquinone
CAES	compressed air energy storage
Cbz	carboxybenzyl
CP	cyclopropenium salts
CV	cyclic voltammetry
DCM	dichloromethane
DMA	*N,N*-dimethylacetamide
DMAP	4-dimethylaminopyridine
DMF	*N,N*-dimethylformamide
DMP	Dess-Martin periodinane
DMSO	dimethyl sulfoxide
EDC	1-ethyl-3-(3-dimethylaminopropyl)carbodiimide
EES	electrical energy storage
Fc	ferrocene
Fc^+	ferrocenium
HRMS	high resolution mass spectrometry
KPF_6	potassium hexafluorophosphate
MeCN	acetonitrile
MeOH	methanol

MSA	Molecular Surface Area
Ns	nosyl
OMs	mesylate
$PhI(OAc)_2$	(diacetoxyiodo)benzene
PhOH	phenol
PHP	pumped hydropower
PIM	polymers of intrinsic microporosity
Py	pyridinium salts
RAO	redox active oligomers
RAP	redox active polymers
RFB	redox flow batteries
ROM	redox-active organic molecules
RVC	reticulated vitreous carbon
TEMPO	2,2,6,6-retramethylpiperidine-*N*-oxyl
THF	tetrahydrofuran
THP	tetrahydropyran
TMABF4	tetramethylammonium tetrafluoroborate
TMAOAc	tetramethylammonium acetate
TMAPF6	tetramethylammonium hexafluorophosphate
TMB	trimethoxybenzene
Ts	tosyl
TsOH	*p*-toluenesulfonic acid

Abstract

Electrochemistry is a powerful tool that has recently been revisited and reimagined for application in the 21st century. Operating at the interface of electricity (i.e. flow of electrons) and chemistry, electrochemistry provides a unique platform to approach certain challenges in both fields from alternative angles. My thesis addresses two distinct challenges using electrochemistry, namely the design of new reaction modes using electricity and energy storage using organic molecules.

Chapter 1 introduces the emerging field of synthetic organic electrochemistry and discusses examples of electrochemical reactions that demonstrate impact of several electrochemical parameters. Previous work in the field of electrochemical C–H functionalization as well as design of organic electrolyte for redox flow batteries are discussed.

Chapter 2 elaborates our efforts to improve the atom economy of known C–H functionalization reactions by replacing the expensive and unsustainable chemical oxidants for electric current. High-valent palladium catalytic intermediates were accessed through an anodic oxidation. Scope of the reaction was evaluated to include a variety of functional groups and directing groups.

Chapter 3 focuses on design and development of organic electrolytes for asymmetric non-aqueous redox flow batteries. Multiple pathways leading to loss of storage capacity were identified in a system using pyridinium and cyclopropenium salts as electrolytes. New generation of electrolytes were designed and synthesized to tackle these mechanisms of decay.

Chapter 4 continues to explore one of the major challenges in the field of redox flow batteries: crossover. Extensive investigation of factors that affect crossover identified an impact of the charge and the size of the electrolyte when using an anion exchange

membrane. Future directions, including a solvent study, calculation of kinetic molecular diameter, and different anion exchange membranes is detailed.

Chapter 5 describes our efforts to understand impact of three-dimensional arrangement on physical and electrochemical properties through synthesis of several trimeric cyclopropenium species. Cyclic trimer with different spacing in between the redox active units were synthesized and their electrochemical behavior evaluated using cyclic voltammetry. Efforts toward synthesis of other oligoamine scaffolds is also detailed in this chapter.

This dissertation describes processes operating at the interface of electrochemistry and organic chemistry. Ultimately, we can use the understanding we gained in these studies of how organic compounds react to electrochemical stimuli to develop new approaches to both fine chemical synthesis and energy storage.

Chapter 1
Introduction

Since the industrial revolution, fossil fuels have been a key driver of transportation and chemical energy production due to their abundance, availability and affordability.[1] More recently, the factors of cost and sustainability have shifted focus to include the ecological footprints of current technologies.[1–3] Deriving energy from sustainable and renewable sources is becoming increasingly important to tackle pollution, carbon dioxide emission, and waste generation. Electrochemical processes can play a pivotal role in this global phenomenon. These processes involve interconversion of electrical and chemical energies through movement of electrons. This interconversion can enable design of new technologies for fine chemical manufacturing or deployment of greener technologies to decarbonize the electric grid.[4] This thesis will explore both the utilization of electrochemistry to design greener organic transformations for fine chemical synthesis (Chapter 2) as well as the design and development of energy storage technology (Chapters 3-5) to incorporate renewable energy sources into the grid.

1.1. Synthetic Organic Electrochemistry

With a mass movement to develop greener chemical processes, the field of synthetic organic electrochemistry is experiencing a renaissance.[5–12] In electrochemical reactions, the conventional oxidizing or reducing agents can be replaced by electric current, which is increasingly derived from renewable sources of energy. These systems utilize an electrical circuit that is broken, with an electrode on the either side of the break.[7] The electrodes mediate an electron transfer reaction with a substrate in the solution (Figure 1.1) with the two electrodes facilitating two separate processes. At the anode, electrons are transferred from the reaction mixture to the electrode, oxidizing the

molecules in solution. Simultaneously, at the cathode, the electrons flow from the electrode to the reaction mixture, reducing the molecules in solution (Figure 1.1).[5,7,12,13] The net result of this process a is flow of electrons from the cathode to the anode. A key feature of electrochemical reactions is that, unlike reagent-based oxidation/reduction, these are heterogeneous processes.[10,14] The electron transfer event occurs at the electrode-electrolyte interface. Therefore, the identity of both the electrode and electrolyte (supporting electrolyte salt and solvent) is crucial for efficient reactions.[8,14]

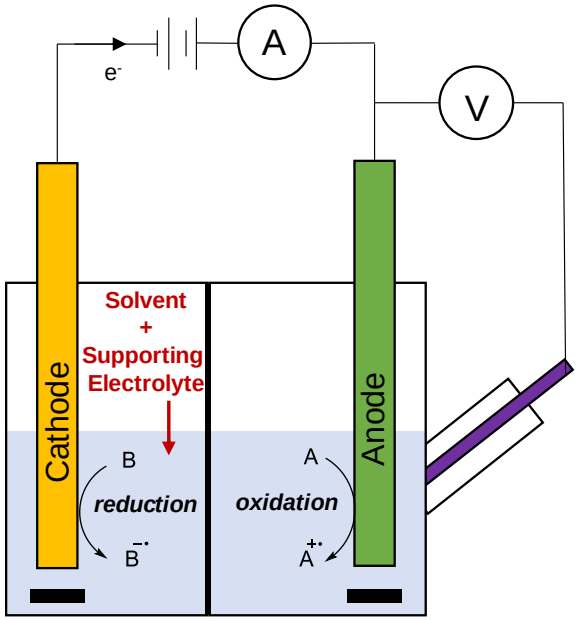

Figure 1.1. A schematic representation of an electrochemical cell with an oxidation event occurring at anode and reduction event occurring at cathode

In a 1991 study, Hudson and coworkers demonstrated the impact of the electrode material on the outcome of an oxidative cyclization reaction (Scheme 1.1).[15] In this study, substrate **1** underwent an initial anodic oxidation to generate a radical cation of the electron rich alkene, that was then attacked by the nucleophilic allylsilane forming a five-membered ring. Through a subsequent oxidation and coupling with MeOH in solution, the desired product **2** was formed in lower than desired yield (46%). During the reaction using a Pt-wire anode, a vinylsilane side product **4** was observed. Under the hypothesized mode of reactivity, this side product would not be formed, indicating that a competing was in play to form **4**. Such vinylsilanes could be formed after a loss of hydrogen atom from a *β*-silyl radical. Therefore, this byproduct indicated incomplete oxidation using the Pt-

anode. When using an RVC anode, significantly higher yields of the desired product **2** (83%) were observed. More importantly, no vinylsilane byproduct was generated under these conditions. These observations are hypothesized to be a result of Pt-anodes typically struggling to promote two electron organic transformations due to fouling of the surface upon the first oxidation.[8,10] This example shows the impact that the electrode material can have on the overall reactivity.

Scheme 1.1. Representative example of effect of electrode on outcome of the reaction

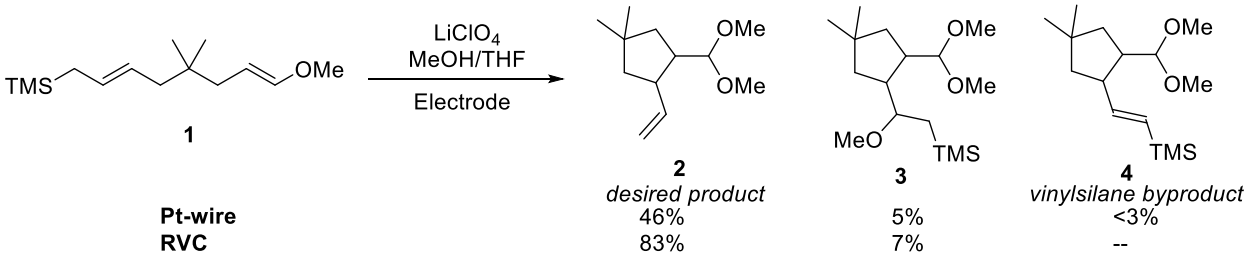

Similar effects have also been observed on the outcome of the reactions based on the identity of the supporting electrolyte (Scheme 1.2). Supporting electrolytes contribute to the double layer that forms during electrolysis at an electrode surface, thereby controlling the environment at the electrode-electrolyte interface (where the redox reaction happens). Supporting electrolytes with higher ionic strength, such as $LiClO_4$, form a more hydrophilic double layer, while electrolytes such as Et_4NOTs form a more hydrophobic double layer. Such a difference in the environment at the electrode can affect the overall reaction. For instance, in the electrochemical cyclization of substrate **5**, lower yields of cyclized product **6** (20%) were observed with $LiClO_4$, along with a large amount of overoxidized (**7**) or uncyclized (**8**) products (Scheme 1.2a).[16] The side products were believed to result from faster trapping of the dithioketal radical with MeOH than the desired cyclization to form product **6**. To prevent this reactivity with MeOH, the authors use Et_4NOTs as supporting electrolyte, which excluded MeOH from the double layer, thereby suppressing the deleterious side reactions and increasing the yield of desired product to 60%. In contrast to this example, in the cyclization shown in Scheme 1.2b, lower yields were observed with Et_4NOTs. The polar substrate **9** was being expelled from the double layer, as Et_4NOTs forms a greasier interface.[17] This issue was circumvented by using a more polar supporting electrolyte $LiClO_4$ to increase the effective concentration of the

substrate in the electrode-electrolyte interface, thereby increasing the yield of the reaction from 40% to 85%.[17]

Scheme 1.2. Representative example of effect of supporting electrolyte on the outcome of the reaction

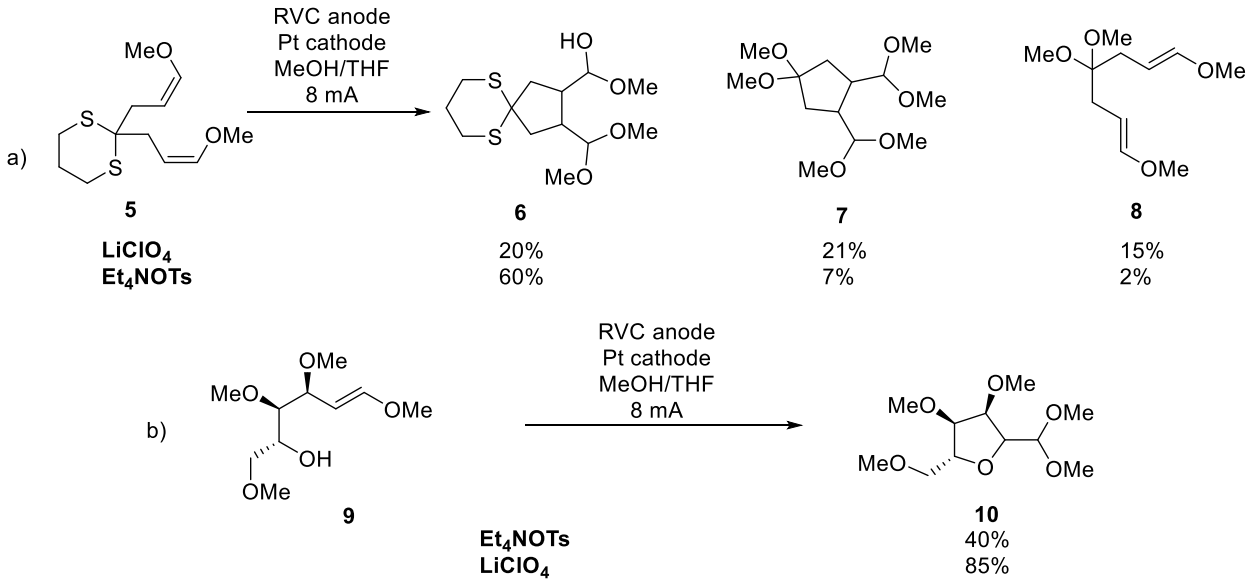

One of the big advantages of electrochemical reactions is the control over several reaction parameters, such as precise control over strength of oxidation (redox potential) or over concentration of electrons (current density). A reaction can either be subjected to *potentiostatic* (controlled potential) or *galvanostatic* (constant current) conditions. Under *potentiostatic* conditions, a reference electrode is used to control the potential of the working electrode, which is held constant at a certain potential. This potential corresponds to the redox potential needed for desired oxidation or reduction reaction (as determined by cyclic voltammetry).[5,8] This setting gives a high level of control over the species undergoing the redox event and prevents any over-oxidation or -reduction. However, as the starting material is consumed, the current flowing through the reaction decreases, which shuts down the reaction before completion. As a consequence, most electrochemical reactions are run *galvanostatically*,[5] where the current passing through the reaction is kept at a constant value, and the potential of the reaction is allowed to adjust freely to match the potential of the substrate with lowest oxidation potential.[8] The working electrode then remains at this potential until most of the substrate is consumed. These reactions do not require a reference electrode and can be simpler to implement

than *potentiostatic* reactions. However, as the substrate is consumed, the reaction can lose selectivity.[5]

The power of galvanostatic electrolysis is demonstrated by a pair of oxidative cyclization reactions to yield either a tetrahydrofuran product (**12**)[18] or a pyrrolidine derivative (**14**)[19] (Scheme 1.3).[8] Both the reactions are triggered by oxidation of the dithioketene acetal functional group. The oxidation of the first substrate **11** occurs at +1.06 V vs Ag/AgCl while the second substrate **13** undergoes oxidation at a much lower potential of +0.6 V vs Ag/AgCl. At higher potentials, the pyrrolidine ring can undergo over-oxidation. Therefore, no single chemical oxidizing reagent can be successfully employed for both of these reactions. However, by using galvanostatic electrolysis, both the reactions can be performed *under similar reaction conditions* (i.e. without changing the oxidant), where the potential of the reaction automatically adjusts to accommodate the potential of each reaction.[8]

Scheme 1.3. Two representative examples of galvanostatic oxidation with different oxidation potentials of the starting materials

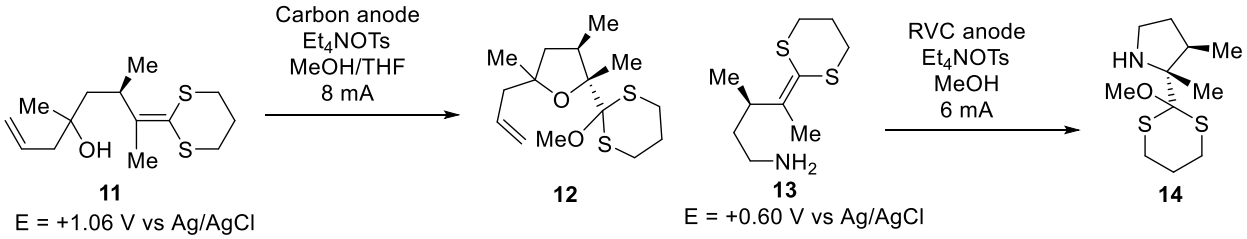

1.2. Electrocatalysis in C–H Functionalization

Transition metal catalyzed C–H functionalization reactions have emerged as a powerful tool in synthetic chemistry. These reactions allow for conversion of ubiquitous C–H bonds to a diverse variety of functional groups without the need for prefunctionalization of the substrate. These reactions typically involve oxidation of a transition metal intermediate as a key step in the catalytic cycle. This typically requires the use of stoichiometric amounts of expensive or toxic chemical oxidants such as copper(II) or silver(I) salts, hypervalent iodine, peroxides, persulfates, etc. Use of large quantities of these external oxidizing agents lower the overall atom economy of the

reaction and typically generate a stoichiometric byproduct that can cause difficulty in separation. The oxidation step in these catalytic systems presents an exciting opportunity for the merger of transition-metal catalyzed C–H functionalization with electrocatalysis to design a transformation that is more environmentally benign. Electric current would then serve as a greener alternative to the expensive chemical oxidants. Notably, metal-free oxidations of C–H bonds, that exploit innate electronic reactivity of the substrate, have been explored electrocatalytically by Baran, Waldvogel, Yoshida, and others.[5,12,13] In contrast, the use of electrochemistry in transition metal catalyzed C–H functionalization remains underexplored.

An early example of this merger of electrochemistry and metal-catalyzed C–H functionalization was presented by Jutand and coworkers in 2007, where they utilized benzoquinone as a redox mediator in a palladium-catalyzed alkenylation reaction (Scheme 1.4).[20] The reaction was initiated through a base-assisted C–H activation of the benzamide substrate (**15**), followed by a migratory insertion into the alkene (**16**). A *β*-hydride elimination generates product **17**, and reductive elimination generates AcOH and Pd(0). Co-catalytic amounts of benzoquinone in the reaction solution reoxidize Pd(0) to Pd(II). This benzoquinone is then regenerated through oxidation at the anode. In this process, instead of direct oxidation of the metal center at the anode, benzoquinone acts as a redox shuttle.

Scheme 1.4. Electrocatalytic C–H alkenylation reaction catalyzed by palladium

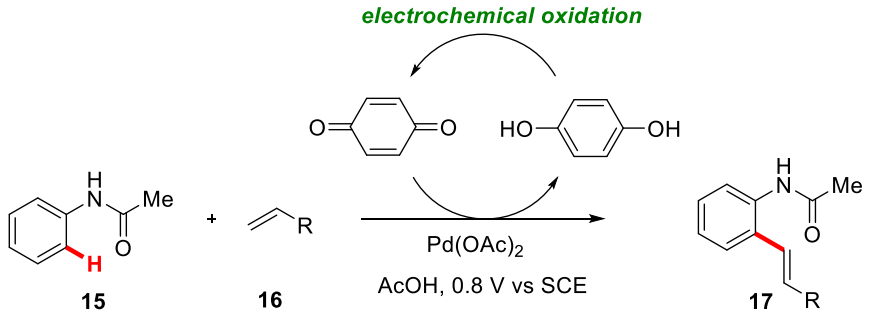

This report was followed by a Pd-catalyzed chlorination reaction by Kakiuchi *et al.* in 2009 (Scheme 1.5). In this system, the authors replaced halogenating reagents such as *N*-halosuccinimides and instead generate the electrophilic chloronium ion (Cl^+)

electrochemically from HCl. This chloronium ion then oxidizes the Pd(II) to a putative Pd(IV) intermediate, which facilitates a C–Cl bond-forming reductive elimination.

Scheme 1.5. Palladium-catalyzed electrochemical C–H chlorination

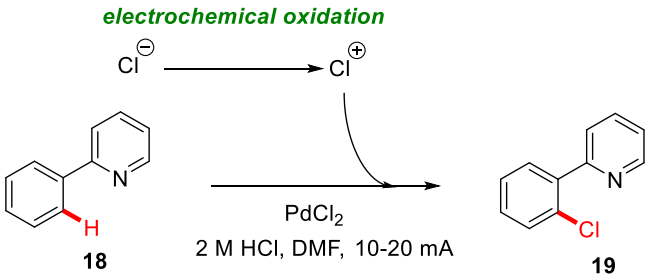

In the examples presented above, while the transformations were promoted by an electrochemical oxidation, the metal centers themselves did not undergo a direct oxidation at the anode. Direct oxidation of metal centers at the anode are quite rare, with only a few groups such as that of Budnikova exploring such a possibility at the start of our work in this field.[21–23] This thesis describes the systematic realization of the anodic oxidation of a Pd(II) center to Pd(IV) stoichiometrically, and ultimately translating this reactivity into a catalytic transformation (Chapter 2).

1.3. Redox Flow Batteries

A switch from unsustainable fossil fuels to sustainable and renewable sources of energy is imminent. However, there is discrepancy between the availability of renewable sources of energy, such as solar or wind power, and times of peak demand, which limit their applicability on the grid scale. Introduction of an intermediary energy storage technology can address this limitation. There is a growing interest in various electrical energy storage (EES) systems.[24–28] EES can represent a range of technologies including pumped hydropower (PHP), compressed air energy storage (CAES), or a range of electrochemical energy storage systems such as solid state batteries (Li-ion or Pb-acid) or redox flow batteries (RFBs).[25,27]

Solid state battery systems have been well studied and recognized for decades, including a recent Nobel Prize for Li-ion batteries.[29] While these systems are well suited for portable electronics and electric vehicles, large scale energy storage requires a more scalable and cost-effective system.[25,27,28] Redox flow batteries (RFBs), on the other hand, are well suited for applications in larger scales because the energy is stored in solutions

of redox active species in external reservoirs, rather than in the electrodes themselves.[30–35] In these systems, the energy output is dictated by the amount and identity of the redox active material, while the power output is dictated by the size of the electrodes. Critically, the energy and power outputs are independent of each other, allowing for economical and scalable large-scale storage, which is in contrast to conventional solid-state battery technology.[25,27,28]

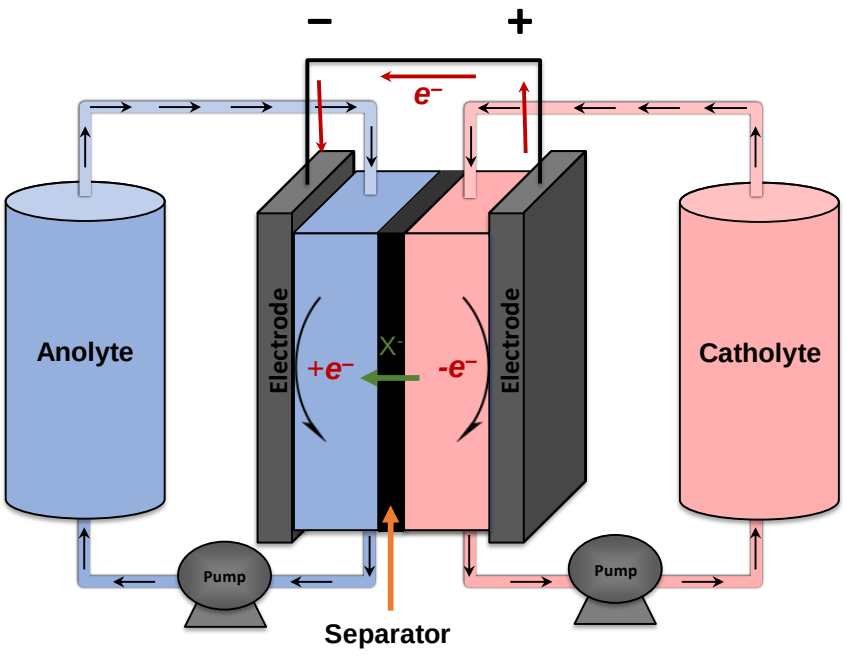

Figure 1.2. A schematic representation of a redox flow battery

A schematic of redox flow batteries is shown in Figure 1.2. RFBs store electrical potential in form of chemical energy. From external reservoirs, solutions of redox active molecules are pumped through an electrochemical cell that is composed of two half-cells separated by a selectively permeable membrane. These batteries undergo cycles of charge and discharge, where anolytes are molecules that undergo reduction and catholytes are molecules that undergo oxidation during the charging process.

The electrodes in RFBs are inert. They facilitate an electron transfer process to oxidize/reduce the redox active species (a chemical change), instead of undergoing any physical changes themselves during the charge/discharge process. This contrasts with conventional batteries, where the electrodes materials undergo expansion and contraction during the charge/discharge cycles, limiting the lifetime of those

batteries.[25,27,28] Therefore, RFBs are also designed to have significantly longer lifetimes than solid state batteries, which is desirable for a technology used to supply energy to the electric grid.[25,27,28]

Metal complexes that occupy distinct oxidation states were the initial targets as redox active species in RFBs.[26,36] Among these complexes, vanadium oxide systems have been extensively studied (with >20 demonstrations) and commercialized in flow battery technologies. These metal-based systems, particularly the vanadium oxide, suffer from a relatively high market price for the cost of vanadium, moderate solubility of vanadium oxide at certain oxidation states, as well as lack of tunability of the physical and electrochemical properties. In contrast, organic molecules are gaining attention for the feasibility of their structural optimization in order to tune various physical and electrochemical properties.[24,37–42] Some classes of organic molecules can be easily attained through preexisting distribution sources and therefore can be a cheaper alternative to metal-based electrolytes.

1.4. Organic Molecules in Redox Flow Batteries

As discussed above, organic molecules are attractive electrolytes for redox flow batteries because their molecular structure can be easily altered to optimize for desired physical and electrochemical properties (Figure 1.3).[43–47] Several examples are available where properties such as redox potential, solubility, stability, and crossover behavior of organic electrolytes were improved by addition or variation of the functional groups in the core of the molecules.[43–47] It is known that electronically biased functional groups can have a profound impact on the redox potential of the electrolytes. Different functional groups have also been identified to facilitate solubility of these electrolytes in various solvents such as water or acetonitrile. A few examples of molecular engineering to enhance some of these properties are discussed below.

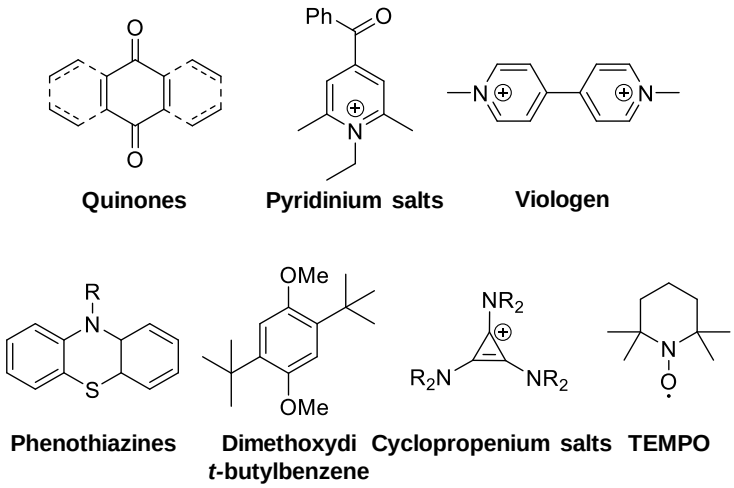

Figure 1.3. Examples of organic electrolytes

The reversible quinone/hydroquinone redox couple had been previously used as solid active electrode material in fuel cells and rechargeable lithium batteries, as well as overcharge protection mediators.[26,36] Their rapid proton coupled electron-transfer was first exploited in an aqueous RFB by the Aziz group in 2014 (Scheme 1.6).[48] By pairing benzoquinone with bromine/bromide couple as catholyte in sulfuric acid, the group achieved high current densities (150 $mAcm^{-2}$) and power densities (35 $mWcm^{-2}$). However, other properties of this molecule, such as solubility and crossover across the membrane, remained far from desirable. These limitations were addressed by investigating a different member of the quinone family: anthraquinones. First, 9,10-anthraquinone-2,7-disulfonic acid (**AQDS**) was tested in a RFB (Figure 1.4).[31] **AQDS** is significantly larger than benzoquinone, helping lower the rate of crossover in the system. In addition, the polar sulfonic acid groups enhances in solubility in aqueous solutions, achieving >1 M concentrations in pH 0.

Scheme 1.6. Redox reaction of quinones under acidic and basic conditions

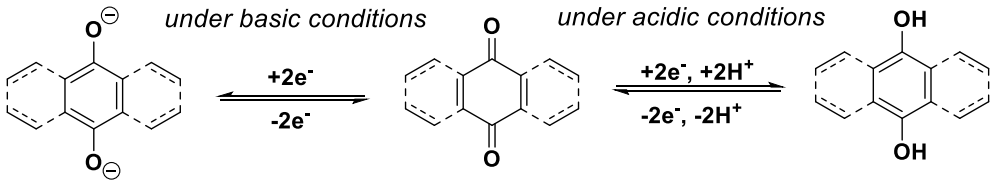

Although better solubility was achieved with AQDS, the electron-withdrawing sulfonic acid substituent had a detrimental impact on the redox potential (+213 mV vs

SHE, Figure 1.4). As a demonstration of tunability of organic electrolytes, later reports studied replacement of the electron-withdrawing sulfonic acid substituent with electron-donating hydroxyl groups. In alkaline media, the hydroxyl groups in 2,6-dihydroanthraquinone (**DHAQ**) are deprotonated, leading to an even larger impact on the redox potential. **DHAQ** thus has a potential of −0.687 V vs SHE, which is a 47% improvement from the previously studied electrolytes in acidic media (Scheme 1.7).[49]

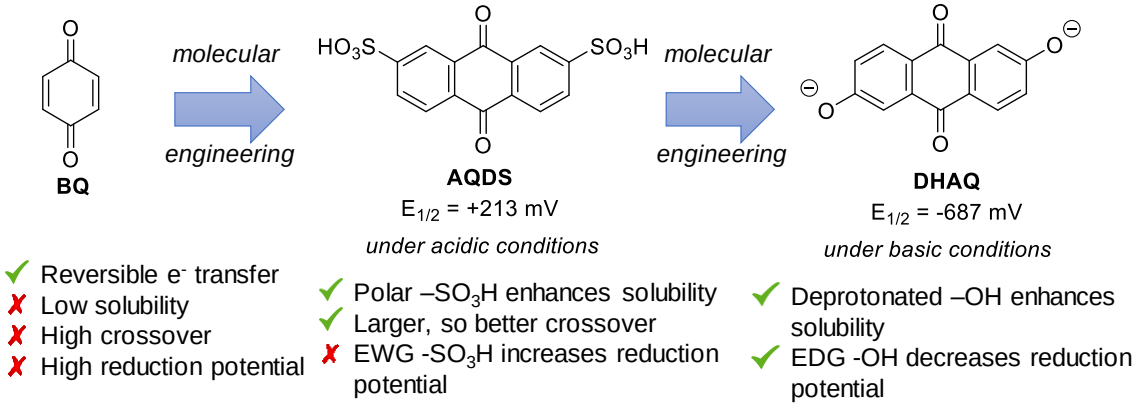

Figure 1.4. A systematic improvement of properties such as solubility, redox potential, and crossover in the quinone/hydroquinone system for application in RFB

The significance of molecular engineering of these organic electrolytes was further established when the stability of **DHAQ** to the electrochemical charge/discharge cycling is significantly improved upon a simple functional group replacement. **DHAQ** underwent decomposition during the electrochemical cycling through a conproportionation with an equivalent amount of charged **DHAQ** followed by irreversible oxidative dimerization.[50] The instability of **DHAQ** was hypothesized to arise due to the high concentration of anionic charge in the molecule and was successfully suppressed by substituting the hydroxyl groups with ether alkyl carboxylic acids ((anthraquinone-diyl)dioxydibutyrate; 2,6-DBEAQ) or phosphonic acids (dioxo-dihydroanthracene-diyl; 2,6-DPPEAQ).[51,52] Although this protection of hydroxyl group led to an increase in reduction potential to -0.51 V vs SHE for 2,6-DBEAQ and -0.49 V vs SHE for 2,6-DPPEAQ at pH 12, it was overshadowed by the significant increase in stability of these compounds as observed in electrochemical cycling experiments (<0.014% capacity fade per day). These compounds demonstrated one of the longest calendar lives of organic molecules in RFBs with half-lives on the order of 5 years, showing tremendous potential for commercialization in the future.

Scheme 1.7. Proposed decomposition pathway for **DHAQ** and engineering of the molecule to suppress such decomposition

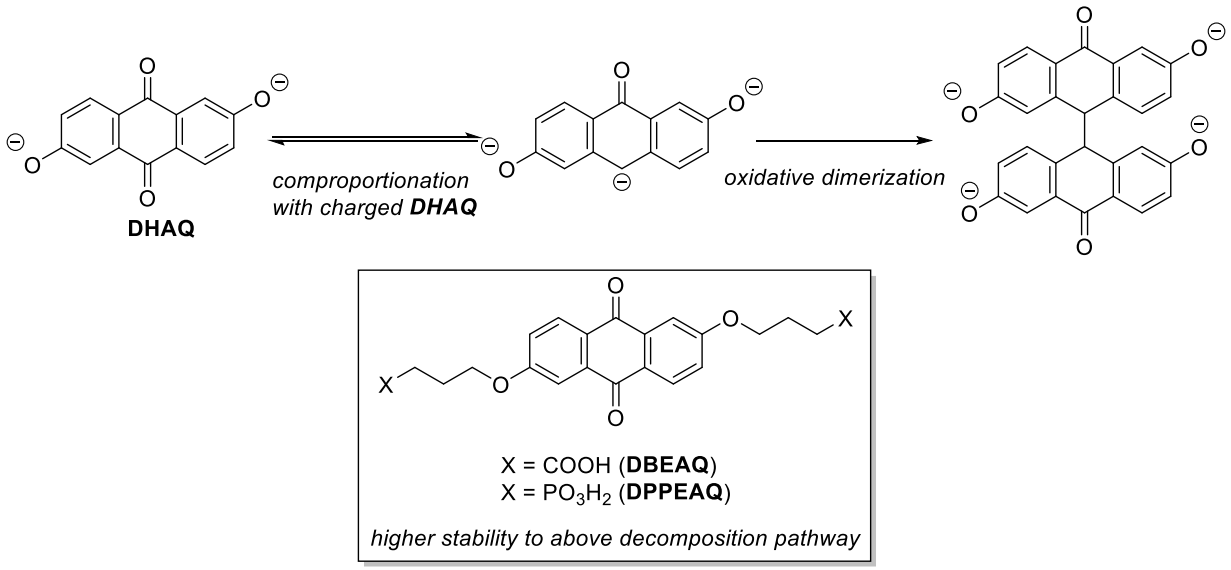

Another study of molecular engineering of an electrolyte core to enhance physical and electrochemical properties was achieved through a collaborative effort between the Sanford group and the Sigman and Minteer groups. Cyclopropenium salts (CP) demonstrated desirable properties to be utilized as catholytes for non-aqueous RFBs. Tris-(bis-alkyl-amino)-cyclopropenium salts exhibit higher oxidation potentials (>+0.8 V vs Fc/Fc^+) than other commonly used catholytes (e.g., 2,2,4,4-tetramethylpiperidine (TEMPO), ferrocene, and quinones, which have oxidation potentials in the range of 0 – +0.4 V vs Fc/Fc^+).[43] These CP molecules are particularly interesting for application in RFBs due to their synthetic modularity, where a wide variety of electronically or sterically differentiated CPs can be easily accessed in a single synthetic step.

Initial studies on this scaffold investigated the effect of changing electronics and sterics on the amine. Favorable increase in oxidation potential (of up to ~150 mV) were observed when the electron donating alkyl *N*-substituent was substituted for an electron withdrawing phenyl group.[43] This increase in oxidation potential, however, was overshadowed by a dramatic decrease in electrochemical cycling stability of these molecules. Stabilization was observed when adding steric bulk around the nitrogen, using diisopropylamine instead of a dimethylamine.[43] Later, to demonstrate the utility of organic principles in RFBs, the Sanford and Sigman groups modified the

trisaminocyclopropeniums, to further increase the oxidation potential.[53] Trisaminocyclopropeniums are stabilized through three strongly π-donating amine functionalities. The replacement of one of these strongly donating groups with a weaker π-donor thioether group yielded alkylthiobis(dialkylamino)cyclopropenium salts (alkylthio CP), which have oxidation potentials of >+1.3 V vs Fc/Fc^+.[53]

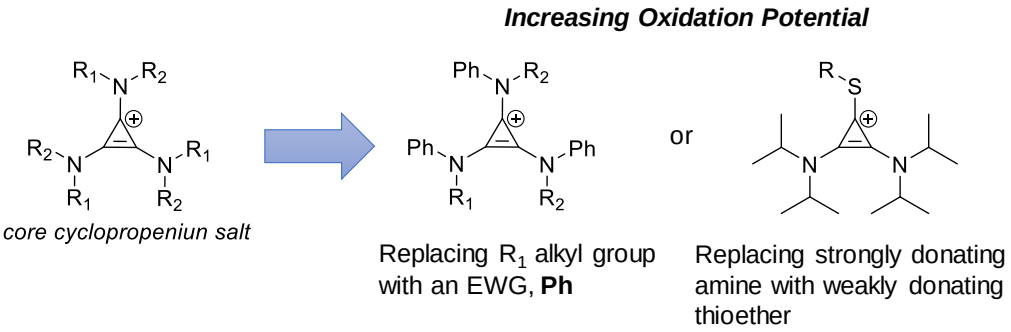

Figure 1.5. Strategies to increase oxidation potential for cyclopropenium catholyte

While tris(diisopropylamine)cyclopropenium salt exhibit high redox potentials and high cycling stabilities, the reported solubility of the oxidized dication radical was 20-fold less (0.081 M) than the parent compound (1.5 M), which limited the energy density of the battery. A collaboration between the Sanford and the Sigman groups computed a predictive solubility model to improve on the solubility of oxidized cyclopropenium salts.[54] The best statistical model was comprised of two parameters: average of maximum Sterimol B5 values (for the width of the molecules) and the molecular surface area (MSA) for the conformer of CP with lowest energy. An unsymmetrical CP, containing an ethyl and a butyl chain on the amine (Figure 1.6) was identified to have the highest solubility of 1.66 M at its oxidized state through this study, which is a >20 fold increase in solubility from original diisopropyl CP. This derivative also retained the high oxidation potential achieved by the CP core. A RFB with no supporting electrolyte was demonstrated at 1 M concentration of CP.[54]

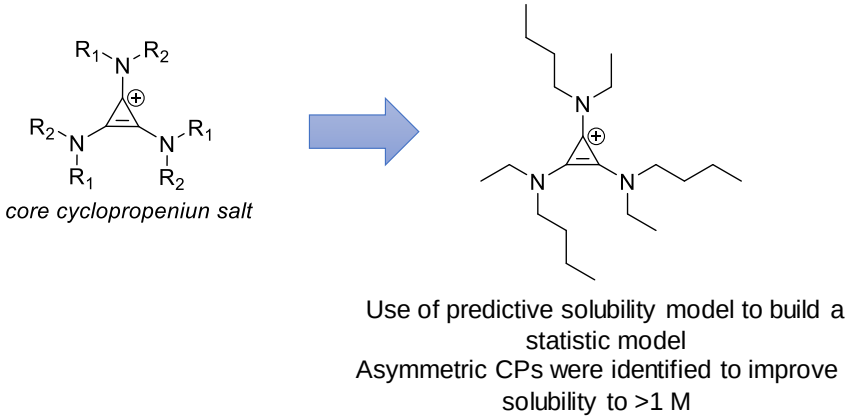

Figure 1.6. A strategy to improve solubility identified through a statistical model

Crossover is another major challenge in the field of organic RFBs, especially at such high concentrations. Most of the membranes that are currently employed in RFBs are designed for aqueous systems, and often undergo mechanical failures in nonaqueous RFBs. To that end, a collaborative effort between the Helms and Sanford groups identified a size exclusion system that utilizes polymers of intrinsic microporosity (PIM) and oligomeric versions of CP as a promising solution (Figure 1.7).[45] Given enough spacing between the redox active moieties (≥4 carbon linker), the trimer and tetramer of CP exhibit similar electrochemical behavior to the monomeric species both by CV ($E_{1/2}$ = +0.86 V vs Ag/Ag^{+}) and bulk electrolysis (<5% fade in discharge capacity over 100 cycles). With <4 carbon linker, electronic coupling between the redox active CPs was observed which led to less reversibility in electron transfer (as determined by CV), as well as lower stability of the molecule (as determined by bulk electrolysis cycling).[45] A proof-of-concept RFB with the tetramer and a PIM-1 membrane demonstrated no detectable crossover after 6 days of flowing the catholyte solution through the RFB.

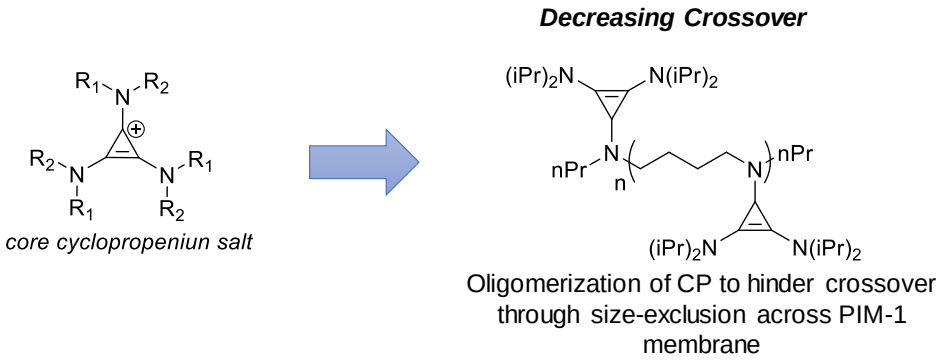

Figure 1.7. A strategy to mitigate crossover through oligomerization and utilization of PIM-1, a size exclusion membrane

These examples demonstrate the systematic and property specific derivatization that occurs when identifying new redox active organic materials. Many in the field are conducting systematic studies to answer fundamental questions that can lead the design of next generation of organic electrolytes. This thesis explores molecular engineering of organic electrolytes (pyridinium and cyclopropenium salts) to achieve improved performance in an asymmetric non-aqueous redox flow battery (Chapter 3). We also attempt to understand the effects of several parameters on crossover, which is a largely unaddressed challenge in the field (Chapter 4), and finally we synthesize and study oligomeric cyclopropenium catholytes as a potential solution to this problem (Chapter 5).

1.5. References

(1) Farhani, S.; Rejeb, J. B. Energy Consumption, Economic Growth and CO2 Emissions: Evidence from Panel Data for MENA Region. *Int. J. Energy Econ. Policy* **2012**, *2* (2), 71–81.

(2) PBL. Trends in global CO2 emissions: 2016 Report https://www.pbl.nl/en/publications/trends-in-global-co2-emissions-2016-report (accessed Mar 24, 2020).

(3) International Energy Outlook 2016. **2016**, 290.

(4) Orella, M. J.; Román-Leshkov, Y.; Brushett, F. R. Emerging Opportunities for Electrochemical Processing to Enable Sustainable Chemical Manufacturing. *Curr. Opin. Chem. Eng.* **2018**, *20*, 159–167. https://doi.org/10.1016/j.coche.2018.05.002.

(5) Yan, M.; Kawamata, Y.; Baran, P. S. Synthetic Organic Electrochemical Methods Since 2000: On the Verge of a Renaissance. *Chem. Rev.* **2017**, *117* (21), 13230–13319. https://doi.org/10.1021/acs.chemrev.7b00397.

(6) Horn, E. J.; Rosen, B. R.; Baran, P. S. Synthetic Organic Electrochemistry: An Enabling and Innately Sustainable Method. *ACS Cent. Sci.* **2016**, *2* (5), 302–308. https://doi.org/10.1021/acscentsci.6b00091.

(7) Moeller, K. D. Synthetic Applications of Anodic Electrochemistry. *Tetrahedron* **2000**, *56* (49), 9527–9554. https://doi.org/10.1016/S0040-4020(00)00840-1.

(8) Moeller, K. D. Using Physical Organic Chemistry To Shape the Course of Electrochemical Reactions. *Chem. Rev.* **2018**, *118* (9), 4817–4833. https://doi.org/10.1021/acs.chemrev.7b00656.

(9) Jing, Q.; Moeller, K. D. From Molecules to Molecular Surfaces. Exploiting the Interplay Between Organic Synthesis and Electrochemistry. *Acc. Chem. Res.* **2020**, *53* (1), 135–143. https://doi.org/10.1021/acs.accounts.9b00578.

(10) Hammerich, O.; Speiser, B.; Speiser, B. *Organic Electrochemistry : Revised and Expanded*; CRC Press, 2015. https://doi.org/10.1201/b19122.

(11) Lund, H. A Century of Organic Electrochemistry. *J. Electrochem. Soc.* **2002**, *149* (4), S21. https://doi.org/10.1149/1.1462037.

(12) Wiebe, A.; Gieshoff, T.; Möhle, S.; Rodrigo, E.; Zirbes, M.; Waldvogel, S. R. Electrifying Organic Synthesis. *Angew. Chem. Int. Ed.* **2018**, *57* (20), 5594–5619. https://doi.org/10.1002/anie.201711060.

(13) Yoshida, J.; Kataoka, K.; Horcajada, R.; Nagaki, A. Modern Strategies in Electroorganic Synthesis. *Chem. Rev.* **2008**, *108* (7), 2265–2299. https://doi.org/10.1021/cr0680843.

(14) Sperry, J. B.; Wright, D. L. The Application of Cathodic Reductions and Anodic Oxidations in the Synthesis of Complex Molecules. *Chem. Soc. Rev.* **2006**, *35* (7), 605–621. https://doi.org/10.1039/B512308A.

(15) Hudson, C. M.; Marzabadi, M. R.; Moeller, K. D.; New, D. G. Intramolecular Anodic Olefin Coupling Reactions: A Useful Method for Carbon-Carbon Bond Formation. *J. Am. Chem. Soc.* **1991**, *113* (19), 7372–7385. https://doi.org/10.1021/ja00019a038.

(16) Redden, A.; Moeller, K. D. Anodic Coupling Reactions: Exploring the Generality of Curtin−Hammett Controlled Reactions. *Org. Lett.* **2011**, *13* (7), 1678–1681. https://doi.org/10.1021/ol200182f.

(17) Xu, G.; Moeller, K. D. Anodic Coupling Reactions and the Synthesis of C-Glycosides. *Org. Lett.* **2010**, *12* (11), 2590–2593. https://doi.org/10.1021/ol100800u.

(18) Liu, B.; Duan, S.; Sutterer, A. C.; Moeller, K. D. Oxidative Cyclization Based on Reversing the Polarity of Enol Ethers and Ketene Dithioacetals. Construction of a Tetrahydrofuran Ring and Application to the Synthesis of (+)-Nemorensic Acid. *J. Am. Chem. Soc.* **2002**, *124* (34), 10101–10111. https://doi.org/10.1021/ja026739l.

(19) Xu, H.-C.; Moeller, K. D. Intramolecular Anodic Olefin Coupling Reactions: Use of the Reaction Rate To Control Substrate/Product Selectivity. *Angew. Chem. Int. Ed.* **2010**, *49* (43), 8004–8007. https://doi.org/10.1002/anie.201003924.

(20) Amatore, C.; Cammoun, C.; Jutand, A. Electrochemical Recycling of Benzoquinone in the Pd/Benzoquinone-Catalyzed Heck-Type Reactions from Arenes. *Adv. Synth. Catal.* **2007**, *349* (3), 292–296. https://doi.org/10.1002/adsc.200600389.

(21) Dudkina, Yu. B.; Gryaznova, T. V.; Sinyashin, O. G.; Budnikova, Yu. H. Ligand-Directed Electrochemical Functionalization of C(Sp2)—H Bonds in the Presence of the Palladium and Nickel Compounds. *Russ. Chem. Bull.* **2015**, *64* (8), 1713–1725. https://doi.org/10.1007/s11172-015-1067-3.

(22) Dudkina, Y. B.; Mikhaylov, D. Y.; Gryaznova, T. V.; Sinyashin, O. G.; Vicic, D. A.; Budnikova, Y. H. MII/MIII-Catalyzed Ortho-Fluoroalkylation of 2-Phenylpyridine. *Eur. J. Org. Chem.* **2012**, *2012* (11), 2114–2117. https://doi.org/10.1002/ejoc.201200050.

(23) Dudkina, Y. B.; Mikhaylov, D. Y.; Gryaznova, T. V.; Tufatullin, A. I.; Kataeva, O. N.; Vicic, D. A.; Budnikova, Y. H. Electrochemical Ortho Functionalization of 2-Phenylpyridine with Perfluorocarboxylic Acids Catalyzed by Palladium in Higher Oxidation States. *Organometallics* **2013**, *32* (17), 4785–4792. https://doi.org/10.1021/om400492g.

(24) Wang, W.; Luo, Q.; Li, B.; Wei, X.; Li, L.; Yang, Z. Recent Progress in Redox Flow Battery Research and Development. *Adv. Funct. Mater.* **2013**, *23* (8), 970–986. https://doi.org/10.1002/adfm.201200694.

(25) Chalamala, B. R.; Soundappan, T.; Fisher, G. R.; Anstey, M. R.; Viswanathan, V. V.; Perry, M. L. Redox Flow Batteries: An Engineering Perspective. *Proc. IEEE* **2014**, *102* (6), 976–999. https://doi.org/10.1109/JPROC.2014.2320317.

(26) Soloveichik, G. L. Flow Batteries: Current Status and Trends. *Chem. Rev.* **2015**, *115* (20), 11533–11558. https://doi.org/10.1021/cr500720t.

(27) Perry, M. L.; Weber, A. Z. Advanced Redox-Flow Batteries: A Perspective. *J. Electrochem. Soc.* **2015**, *163* (1), A5064. https://doi.org/10.1149/2.0101601jes.

(28) Weber, A. Z.; Mench, M. M.; Meyers, J. P.; Ross, P. N.; Gostick, J. T.; Liu, Q. Redox Flow Batteries: A Review. *J. Appl. Electrochem.* **2011**, *41* (10), 1137. https://doi.org/10.1007/s10800-011-0348-2.

(29) The Nobel Prize in Chemistry 2019 https://www.nobelprize.org/prizes/chemistry/2019/press-release/ (accessed Mar 25, 2020).

(30) Ding, Y.; Zhao, Y.; Li, Y.; Goodenough, J. B.; Yu, G. A High-Performance All-Metallocene-Based, Non-Aqueous Redox Flow Battery. *Energy Environ. Sci.* **2017**, *10* (2), 491–497. https://doi.org/10.1039/C6EE02057G.

(31) Huskinson, B.; Marshak, M. P.; Suh, C.; Er, S.; Gerhardt, M. R.; Galvin, C. J.; Chen, X.; Aspuru-Guzik, A.; Gordon, R. G.; Aziz, M. J. A Metal-Free Organic–Inorganic Aqueous Flow Battery. *Nature* **2014**, *505* (7482), 195–198. https://doi.org/10.1038/nature12909.

(32) Lin, K.; Gómez-Bombarelli, R.; Beh, E. S.; Tong, L.; Chen, Q.; Valle, A.; Aspuru-Guzik, A.; Aziz, M. J.; Gordon, R. G. A Redox-Flow Battery with an Alloxazine-Based Organic Electrolyte. *Nat. Energy* **2016**, *1* (9), 1–8. https://doi.org/10.1038/nenergy.2016.102.

(33) Janoschka, T.; Martin, N.; Hager, M. D.; Schubert, U. S. An Aqueous Redox-Flow Battery with High Capacity and Power: The TEMPTMA/MV System. *Angew. Chem. Int. Ed Engl.* **2016**, *55* (46), 14427–14430. https://doi.org/10.1002/anie.201606472.

(34) Hu, B.; DeBruler, C.; Rhodes, Z.; Liu, T. L. Long-Cycling Aqueous Organic Redox Flow Battery (AORFB) toward Sustainable and Safe Energy Storage. *J. Am. Chem. Soc.* **2017**, *139* (3), 1207–1214. https://doi.org/10.1021/jacs.6b10984.

(35) Schon, T. B.; McAllister, B. T.; Li, P.-F.; Seferos, D. S. The Rise of Organic Electrode Materials for Energy Storage. *Chem. Soc. Rev.* **2016**, *45* (22), 6345–6404. https://doi.org/10.1039/C6CS00173D.

(36) Li, B.; Liu, J. Progress and Directions in Low-Cost Redox-Flow Batteries for Large-Scale Energy Storage. *Natl. Sci. Rev.* **2017**, *4* (1), 91–105. https://doi.org/10.1093/nsr/nww098.

(37) Zhang, J.; Yang, Z.; Shkrob, I. A.; Assary, R. S.; Tung, S. on; Silcox, B.; Duan, W.; Zhang, J.; Su, C. C.; Hu, B.; Pan, B.; Liao, C.; Zhang, Z.; Wang, W.; Curtiss, L. A.; Thompson, L. T.; Wei, X.; Zhang, L. Annulated Dialkoxybenzenes as Catholyte Materials for Non-Aqueous Redox Flow Batteries: Achieving High Chemical Stability through Bicyclic Substitution. *Adv. Energy Mater.* **2017**, *7* (21), 1701272. https://doi.org/10.1002/aenm.201701272.

(38) Su, L.; Ferrandon, M.; Kowalski, J. A.; Vaughey, J. T.; Brushett, F. R. Electrolyte Development for Non-Aqueous Redox Flow Batteries Using a High-Throughput Screening Platform. *J. Electrochem. Soc.* **2014**, *161* (12), A1905. https://doi.org/10.1149/2.0811412jes.

(39) Wang, W.; Sprenkle, V. Redox Flow Batteries Go Organic. *Nat. Chem.* **2016**, *8* (3), 204–206. https://doi.org/10.1038/nchem.2466.

(40) Winsberg, J.; Hagemann, T.; Muench, S.; Friebe, C.; Häupler, B.; Janoschka, T.; Morgenstern, S.; Hager, M. D.; Schubert, U. S. Poly(Boron-Dipyrromethene)—A Redox-Active Polymer Class for Polymer Redox-Flow Batteries. *Chem. Mater.* **2016**, *28* (10), 3401–3405. https://doi.org/10.1021/acs.chemmater.6b00640.

(41) Montoto, E. C.; Nagarjuna, G.; Moore, J. S.; Rodríguez-López, J. Redox Active Polymers for Non-Aqueous Redox Flow Batteries: Validation of the Size-Exclusion Approach. *J. Electrochem. Soc.* **2017**, *164* (7), A1688. https://doi.org/10.1149/2.1511707jes.

(42) Burgess, M.; Moore, J. S.; Rodríguez-López, J. Redox Active Polymers as Soluble Nanomaterials for Energy Storage. *Acc. Chem. Res.* **2016**, *49* (11), 2649–2657. https://doi.org/10.1021/acs.accounts.6b00341.

(43) Sevov, C. S.; Samaroo, S. K.; Sanford, M. S. Cyclopropenium Salts as Cyclable, High-Potential Catholytes in Nonaqueous Media. *Adv. Energy Mater.* **2017**, *7* (5), 1602027. https://doi.org/10.1002/aenm.201602027.

(44) Sevov, C. S.; Hickey, D. P.; Cook, M. E.; Robinson, S. G.; Barnett, S.; Minteer, S. D.; Sigman, M. S.; Sanford, M. S. Physical Organic Approach to Persistent, Cyclable, Low-Potential Electrolytes for Flow Battery Applications. *J. Am. Chem. Soc.* **2017**, *139* (8), 2924–2927. https://doi.org/10.1021/jacs.7b00147.

(45) Hendriks, K. H.; Robinson, S. G.; Braten, M. N.; Sevov, C. S.; Helms, B. A.; Sigman, M. S.; Minteer, S. D.; Sanford, M. S. High-Performance Oligomeric Catholytes for Effective Macromolecular Separation in Nonaqueous Redox Flow Batteries. *ACS Cent. Sci.* **2018**, *4* (2), 189–196. https://doi.org/10.1021/acscentsci.7b00544.

(46) Wei, X.; Xu, W.; Vijayakumar, M.; Cosimbescu, L.; Liu, T.; Sprenkle, V.; Wang, W. TEMPO-Based Catholyte for High-Energy Density Nonaqueous Redox Flow Batteries. *Adv. Mater.* **2014**, *26* (45), 7649–7653. https://doi.org/10.1002/adma.201403746.

(47) Hu, B.; Liu, T. L. Two Electron Utilization of Methyl Viologen Anolyte in Nonaqueous Organic Redox Flow Battery. *J. Energy Chem.* **2018**, *27* (5), 1326–1332. https://doi.org/10.1016/j.jechem.2018.02.014.

(48) Nawar, S.; Huskinson, B.; Aziz, M. Benzoquinone-Hydroquinone Couple for Flow Battery. *MRS Online Proc. Libr. Arch.* **2013**, *1491*. https://doi.org/10.1557/opl.2012.1737.

(49) Lin, K.; Chen, Q.; Gerhardt, M. R.; Tong, L.; Kim, S. B.; Eisenach, L.; Valle, A. W.; Hardee, D.; Gordon, R. G.; Aziz, M. J.; Marshak, M. P. Alkaline Quinone Flow Battery. *Science* **2015**, *349* (6255), 1529–1532. https://doi.org/10.1126/science.aab3033.

(50) Goulet, M.-A.; Tong, L.; Pollack, D. A.; Tabor, D. P.; Odom, S. A.; Aspuru-Guzik, A.; Kwan, E. E.; Gordon, R. G.; Aziz, M. J. Extending the Lifetime of Organic Flow Batteries via Redox State Management. *J. Am. Chem. Soc.* **2019**, *141* (20), 8014–8019. https://doi.org/10.1021/jacs.8b13295.

(51) Kwabi, D. G.; Lin, K.; Ji, Y.; Kerr, E. F.; Goulet, M.-A.; Porcellinis, D. D.; Tabor, D. P.; Pollack, D. A.; Aspuru-Guzik, A.; Gordon, R. G.; Aziz, M. J. Alkaline Quinone Flow Battery with Long Lifetime at PH 12. *Joule* **2018**, *2* (9), 1894–1906. https://doi.org/10.1016/j.joule.2018.07.005.

(52) Ji, Y.; Goulet, M.-A.; Pollack, D. A.; Kwabi, D. G.; Jin, S.; Porcellinis, D. D.; Kerr, E. F.; Gordon, R. G.; Aziz, M. J. A Phosphonate-Functionalized Quinone Redox Flow Battery at Near-Neutral PH with Record Capacity Retention Rate. *Adv. Energy Mater.* **2019**, *9* (12), 1900039. https://doi.org/10.1002/aenm.201900039.

(53) Yan, Y.; Robinson, S. G.; Sigman, M. S.; Sanford, M. S. Mechanism-Based Design of a High-Potential Catholyte Enables a 3.2 V All-Organic Nonaqueous Redox Flow Battery. *J. Am. Chem. Soc.* **2019**, *141* (38), 15301–15306. https://doi.org/10.1021/jacs.9b07345.

(54) Robinson, S. G.; Yan, Y.; Hendriks, K. H.; Sanford, M. S.; Sigman, M. S. Developing a Predictive Solubility Model for Monomeric and Oligomeric Cyclopropenium-Based Flow Battery Catholytes. *J. Am. Chem. Soc.* **2019**, *141* (26), 10171–10176. https://doi.org/10.1021/jacs.9b04270.

Chapter 2

Pd-Catalyzed C–H Bond Acetoxylation via Electrochemical Oxidation

(A part of this work has been published in Shrestha, A.; Lee, M.; Dunn, A. L.; Sanford, M. S.* "Palladium-Catalyzed C–H Bond Acetoxylation via Electrochemical Oxidation" *Organic Letters* **2018**, *20*, 204-207.)

2.1. Introduction

Transition metal catalyzed C–H functionalization reactions have emerged as a powerful tool that allows access to a diverse pool of functional groups in fewer synthetic steps starting from ubiquitous C–H bonds.[1–8] Our group has been successful in developing palladium-catalyzed C–H bond functionalization reactions for both $C(sp^2)$–H and $C(sp^3)$–H bonds.[9–15] Installation of various functional groups have been explored, including halogenation,[9,10] oxygenation,[11,12] arylation,[13,14] amination,[15] and many other transformations. As shown in Figure 2.1a, these transformations are believed to proceed via an initial C–H bond activation at Pd^{II} to form an intermediate of general structure **A**. A two-electron oxidation of **A**, typically with a chemical oxidant such as hypervalent iodine reagent, phenyliododiacetate ($PhI(OAc)_2$), then forms a transient high-valent Pd^{IV} intermediate such as **B**. C–O bond-forming reductive elimination from **B** then affords the product (**C**) while regenerating the Pd^{II} catayst.[16] These transformations proceed efficiently with a diverse range $C(sp^2)$–H and $C(sp^3)$–H substrates, and have been widely applied to the synthesis and diversification of natural products and pharmaceutical candidates.[17–20] Nonetheless, these transformations are limited by the use of a chemical oxidant to facilitate the oxidation to high-valent metal centers. These transformations require stoichiometric amounts of chemical oxidants such as hypervalent

iodine reagents, peroxides, persulfates, metal oxidants, etc.[1-8] Use of these oxidants typically results in generation of an equivalent amount of byproduct, thus lowering the overall atom economy of the reaction.[21,22] Additionally, application of these reactions on large scale is limited by the need to separate the byproduct(s) from the desired product of the reaction.

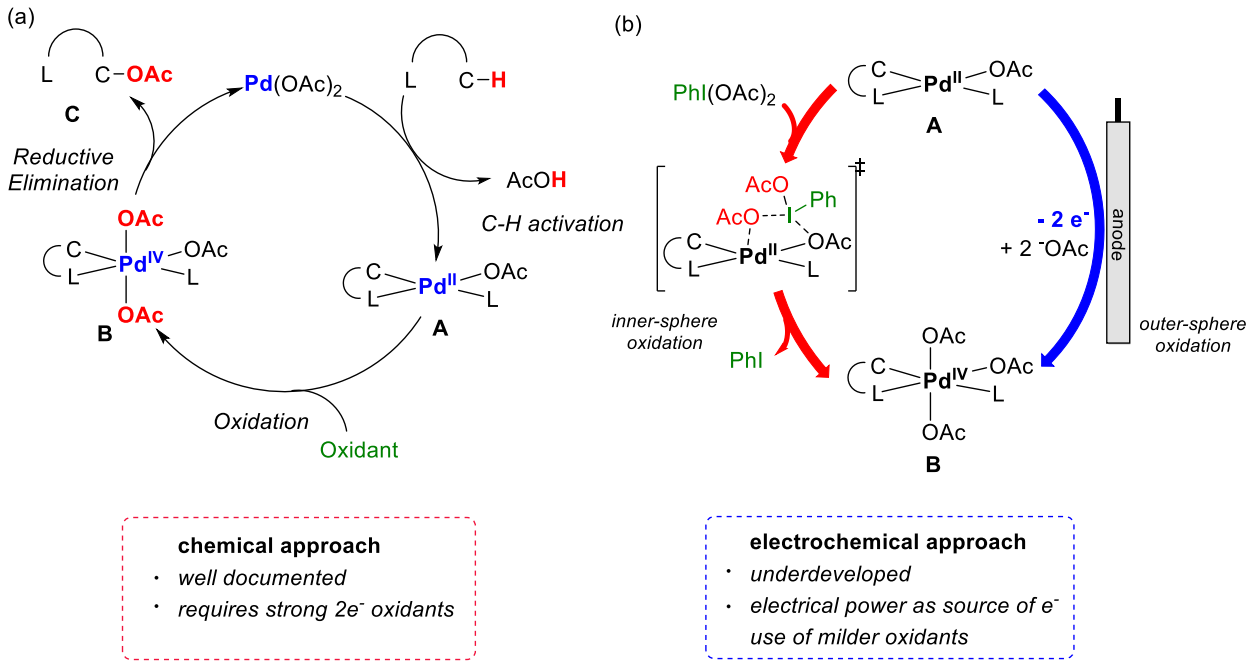

Figure 2.1. (a) Proposed mechanism for palladium catalyzed C–H oxidation; (b) Comparison of chemical oxidation of Pd^{II} – Pd^{IV} to electrochemical oxidation at anode

This Chapter reports an attractive alternative to achieving this overall transformation using an anodic oxidation event in place of an external chemical oxidant.[23–35] As shown in Figure 2.1b, this requires a change in mechanism from an inner sphere chemical oxidation of the Pd^{II} intermediate **A** to an outer sphere oxidation of **A** at an electrode surface. The supporting electrolyte would then serve as a ligand/nucleophile for the functionalization of the resulting high valent intermediate **B**. A seminal report by Kakiuchi et al. showed the viability of this approach by demonstrating the Pd-catalyzed electrochemical C(sp^2)–H chlorination of 2-phenylpyridine derivatives with HCl as both the supporting electrolyte and the nucleophile (Scheme 2.1a).[36] More recently, Budnikova demonstrated the Pd-catalyzed electrochemical C(sp^2)–H oxygenation of 2-

phenylpyridine, and conducted a detailed investigation of the speciation and stoichiometric electrolysis of key cyclopalladated intermediates (Scheme 2.1b).[37–39]

Scheme 2.1. Preliminary proof-of-concept report from (a) Kakiuchi and (b) Budnikova groups on Pd-catalyzed electrochemical C–H oxidation reactions

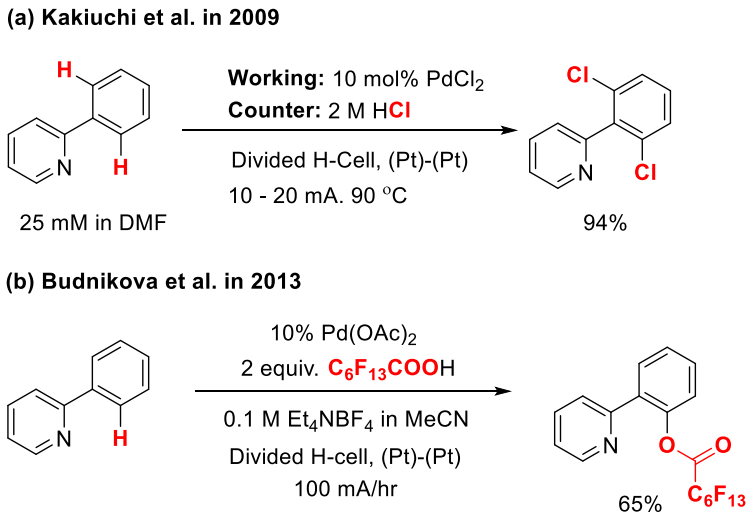

Despite these advances, general methods for Pd-catalyzed electrochemical C–H oxidation remain limited. At the time that we initiated this study, the substrate scope of such transformations was limited to the oxidative functionalization of C(sp^2)–H bonds in molecules containing pyridine-type directing groups. In addition, there was minimal systematic data regarding the impact of different electrochemical conditions (particularly the chemistry occurring at the counter electrode) on the outcome of these transformations. Finally, the complementary scope and side reactions of chemical versus electrochemical oxidation conditions had yet to be explored in detail. The work described in this chapter focuses on development of a Pd-catalyzed electrochemical acetoxylation of a variety of C(sp^3)–H and C(sp^2)–H substrates. The optimal electrochemical conditions as well as several key side reactions are explored, and complementary reactivities between electrochemical and chemical oxidation using $PhI(OAc)_2$ are described in detail. Notably, while our studies were underway, the Mei group reported several elegant examples of related Pd-catalyzed electrochemical C–H oxygenation reactions.[40,41]

2.2. Results and Discussion

2.2.1. Initial Stoichiometric Studies

Initial studies focused on establishing the feasibility of the electrochemical oxidation of Pd^{II} to Pd^{IV}. For this, 8-methylquinoline was selected as a model substrate to assess the feasibility of electrochemical C(sp^3)–H acetoxylation. This substrate is designed to undergo facile C(sp^3)–H activation with a Pd-catalyst to generate a stable, 5-membered palladacycle; indeed, C(sp^3)–H functionalization of this substrate had been studied in depth by various groups.[3,4] In the Pd-catalyzed C–H functionalization reactions, the C(sp^3)–H activation is typically rate limiting. In order to study the oxidation step, decoupling of C(sp^3)–H activation step from the electrochemical oxidation is necessary. Thus, the putative intermediate of the catalytic cycle formed from the C(sp^3)–H activation of 8-methylquinoline, palladacycle **2**, was synthesized and isolated. The anodic oxidation of this intermediate was examined stoichiometrically. Cyclic voltammograms of **2** were obtained in MeCN using tetramethylammonium tetrafluoroborate ($TMABF_4$, a weak nucleophile) and tetramethylammonium acetate (TMAOAc, a much stronger nucleophile) as the supporting electrolyte. When the experiment was performed with $TMABF_4$, two quasi-reversible peaks were observed with onset potential for oxidative peak at ~0.21 V and ~0.66 V versus $Ag/AgBF_4$ (red trace, Figure 2.2). In contrast, with TMAOAc as the supporting electrolyte, the CV showed two irreversible oxidation peaks with onset potentials of ~0.04 V and ~0.33 V, respectively (black trace, Figure 2.2).[i] This result is consistent with electrochemical oxidation being followed by an irreversible chemical reaction with the TMAOAc electrolyte to potentially form acetoxylated product **3.**

(i) These CV studies were conducted in collaboration with Dr. Anna L. Dunn.

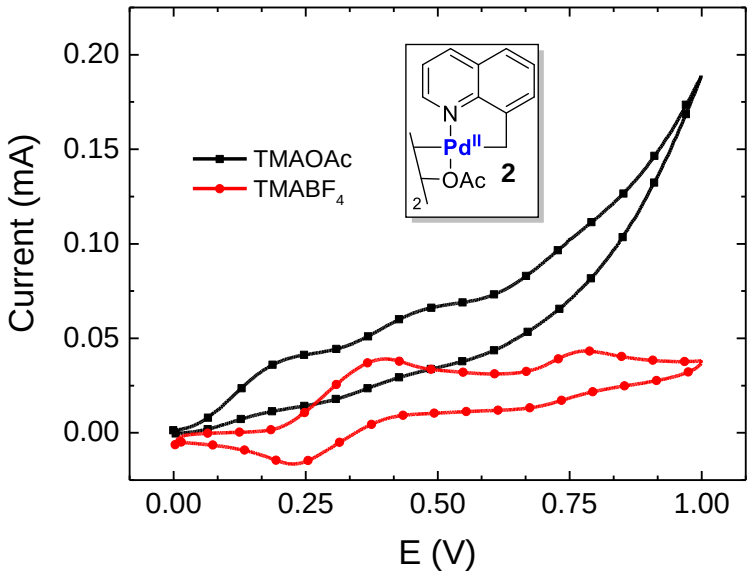

Figure 2.2. Cyclic voltammogram of palladacycle **2** with NMe_4BF_4 (black) and NMe_4OAc (red) as supporting electrolyte in MeCN. The experiment was conducted using glassy carbon working electrode, platinum wire counter electrode and $Ag/AgBF_4$ as reference electrode.

However, CV is an analytical technique; as such, the redox event only occurs on the surface of the electrode (not in the bulk solution). Thus, isolation of the product of the observed irreversible oxidation with TMAOAc was not feasible from the CV experiment. In order to confirm the identity of then product, bulk electrolysis (BE) of **2** in MeCN/TMAOAc was conducted.[ii] The BE was performed in an undivided three-port cell with 8 mA current for 3 h (4 Farads or 4 equivalents of electrons per equivalent of complex **2**). Consistent with our hypothesis, the acetoxylated product **3** was formed in 30% yield (as determined by ^1H NMR spectroscopic analysis of the crude reaction mixture with trimethoxybenzene (TMB) as the internal standard). It was noted that **3** was not fully soluble in the MeCN/TMAOAc solution, and thus 20% v/v of AcOH was added. Under these conditions, an increase in yield of **3** to 52% was observed. These results clearly demonstrate the feasibility of the electrochemical oxidative functionalization of this catalytic intermediate.

(ii) The bulk study was conducted in collaboration with Dr. Anna L. Dunn.

Scheme 2.2. Bulk electrolysis of palladacycle **2** in an undivided cell with and without added AcOH

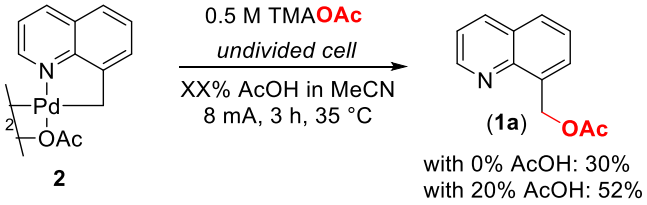

Yields were determined by ^{1}H NMR spectroscopic analysis of crude reaction mixture using trimethoxybenzene as an internal standard.

2.2.2. Translation to Catalytic Transformation

Next, translation of these stoichiometric results to a Pd-catalyzed electrochemical C(sp^3)–H acetoxylation of 8-methylquinoline was pursued. Notably, in the catalytic transformation, the C–H activation step to form **2** must occur prior to oxidation. As such, it was critical to optimize the reaction conditions to promote this step (which is often rate-determining)[42] while minimizing competing decomposition of the Pd catalyst. First, the experiment was performed under conditions analogous to the stoichiometric bulk electrolysis of **2**: in an undivided cell with 10 mol % of the $Pd(OAc)_2$ catalyst. However, under these conditions no product was formed, and the precipitation of Pd-black was observed (Table 2.1, entry 1), which is an indication of catalyst deactivation.

It was reasoned that the Pd catalyst was undergoing competitive reduction at the cathode, which would lead to the catalyst deactivation. Hence, a divided H-cell with a physical barrier (a fine frit) between the anodic (A) and cathodic (C) electrodes was next employed. This resulted in the formation of **1a** in 54% yield (Table 2.1, entry 2). However, a Pd-black precipitate was still observed on the working anode side at the completion of this reaction, indicating that some catalyst deactivation was still occurring under these conditions. This result was unexpected, as the working side of this cell should always be under oxidizing conditions, and thus no reduction should be occuring.

Table 2.1. Optimization of catalytic electrochemical C–H acetoxylation of **1**

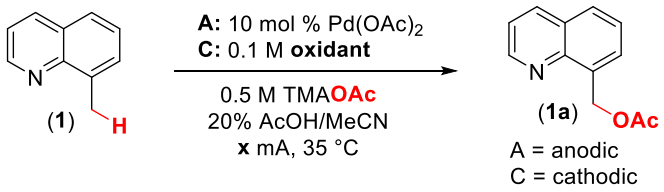

entry	mA or V	time/h	oxidant	1a (%)
1[b]	8 mA	6	-	0
2[c]	8 mA	6	-	54
3[c,d]	8 mA	6	BQ	70
4[c,e]	8 mA	6	BQ	73
5[c,e]	6 mA	8	BQ	71
6[c,e]	12 mA	4	BQ	58
7[c,e]	1.2 V	12	BQ	30 ± 16

[a] Reaction conditions: 0.4 mmol of **1**, 10 mol % of $Pd(OAc)_2$, 0.5 M TMAOAc, 20% AcOH in MeCN. Yield determined by ^1H NMR spectroscopic analysis of crude reaction mixture. [b]Conducted in an undivided cell. [c]Conducted in a divided H-cell. [d] 0.5 M (5 equiv) of benzoquinone (BQ) used as oxidant at counter electrode. [e] 0.1 M (1 equiv) of benzoquinone (BQ) used as oxidant at counter electrode.

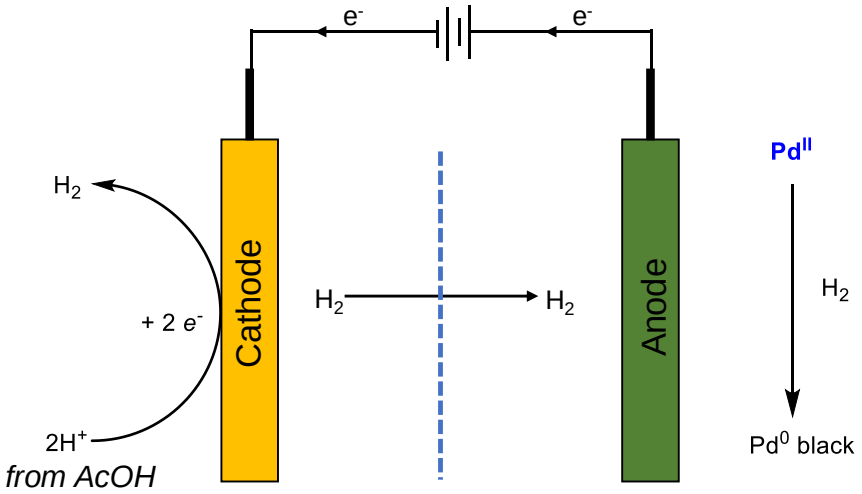

Figure 2.3. Schematic representation of production of hydrogen gas on cathode through proton reduction and hydrogen gas mediated catalyst deactivation

It was hypothesized that the Pd was being reduced chemically by products generated on the cathode side of the cell. Under these conditions, the electrochemical

reaction was balanced by proton reduction to form H_2 at the cathode. This H_2 gas could then diffuse to the anode chamber, leading to the chemical reduction of Pd^{II} to Pd^0 (Figure 2.3). To address this issue, benzoquinone (BQ) was selected as an alternative mild chemical oxidant on the cathodic chamber of the cell. Control studies show that BQ is incapable of oxidizing **2** by itself,[iii] and could also be recycled through an electrochemical oxidation of hydroquinone. Consistent with the hypothesis, the use of BQ resulted in a significant increase in yield to 70%; furthermore, no palladium black was observed under these conditions (Table 2.1, entry 3).[iv]

Several other parameters were optimized in this system, including solvent, cell configuration, electrode material, identity of the sacrificial oxidant at the counter electrode, and electrochemical settings (i.e., constant current versus constant potential). Selected details are discussed below, and more complete information is provided in the experimental details section, Table 2.3. We hypothesized that, in order to achieve productive oxidation, the rate of current discharged into the reaction would need to be slower than that of C–H activation. Consistent with this proposal, increasing the rate of current discharged into the reaction resulted in a decrease in yield, while decreasing the rate led to a similar yield over 8 h (Table 2.1, entries 6 and 5, respectively). Conducting this reaction using a controlled potential of 1.2 V rather than a controlled current led to lower yields and poor reproducibility (Table 2.1, entry 7). Ultimately, the optimal conditions for the C(sp^3)–H acetoxylation of 8-methylquinoline were identified as follows: 0.5 M TMAOAc, 20% AcOH v/v in MeCN, 0.4 mmol of benzoquinone on the counter side as a sacrificial oxidant, and 8 mA current passed over 6 h.

(iii) A control chemical reaction was run under identical conditions using benzoquinone (1.1 equiv) as an oxidant instead of electric current. No reaction was observed and starting material was recovered at the end of the reaction.

(iv) Upon closer evaluation of the working-side and counter-side potentials during the reaction, we observed that the potential on the counter side was significantly lower (by almost 1 V) with the addition of BQ (see experimental details below). The working side potential was also slightly reduced. We believe that both this reduction of overpotential on the working side as well as the prevention of H_2 formation benefit the overall yield of the reaction. In addition, a control chemical reaction with BQ as an oxidant did not yield any acetoxylated product. This result substantiates the fact that BQ alone cannot affect the oxidation of Pd (II) to Pd (IV).

Table 2.2. Substrate scope for the palladium C–H functionalization via electrochemical oxidation

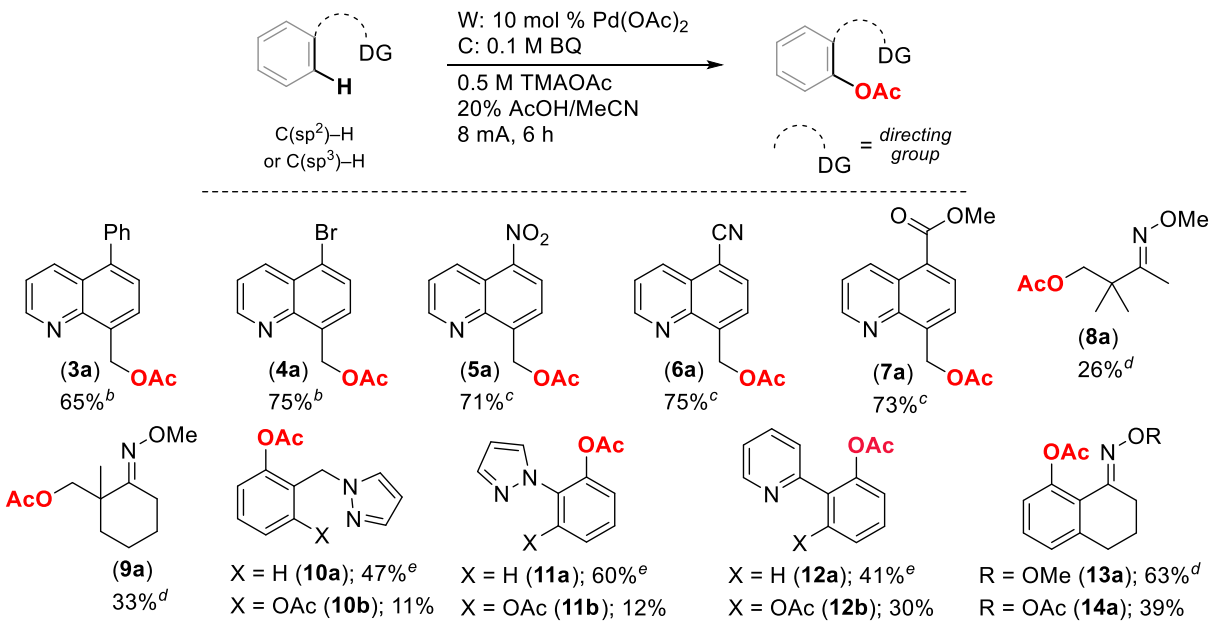

[a] Reaction conditions: 0.4 mmol substrate, 10 mol % of $Pd(OAc)_2$, 0.5 M TMAOAc, 20% AcOH v/v in MeCN. [b] 65 ºC. [c] 75 ºC. [d] Reaction conditions: 0.4 mmol substrate, 10 mol % of $Pd(OAc)_2$, 0.5 M TMAOAc, 20% AcOH, 10% Ac_2O in MeCN at 100 ºC. [e] 100 ºC.

The scope of this electrochemical C–H oxidation reaction was examined next with a variety of other substrates.[v] As mentioned above, previously reported electrochemical Pd-catalyzed C–H oxidation reactions were limited to phenylpyridine and phenylpyrazole substrates. In contrast, the current transformation is much more general. A series of different 8-methylquinoline derivatives with different functional groups at the 5-position underwent $C(sp^3)$–H acetoxylation in moderate to good yields (to form products **3a-14a** in Table 2). A variety of different directing groups were compatible with these reaction conditions, including pyridines, pyrazoles, oxime ethers, and *O*-acetyl oximes. Furthermore, both 5- and 6-membered palladacyclic intermediates underwent electrochemical C–H acetoxylation in moderate to high yields (for example, compare **10a/b** and **11a/b**). Finally, both $C(sp^3)$–H and $C(sp^2)$–H bonds can be functionalized without any modification of the reaction conditions. While the yields for oxygenation of

(v) The substrate scope was obtained in collaboration with Dr. Melissa Lee.

unactivated C(sp^3)–H bonds (for example to form **8a** and **9a**) are relatively modest under these conditions, we note that Mei has recently reported a related method that is specifically optimized for this class of substrates.[41]

2.2.3. Complementary Reactivities

Some interesting complementarities between electrochemical and chemical oxidation reactions were noted in this work. For example, as shown in Scheme 2.3, the acetanilide substrate **15** afforded none of the targeted C(sp^2)–H acetoxylation product **15a**[43] when subjected to the optimized Pd-catalyzed electrochemical oxidation conditions.[vi] Instead, N–N coupling occurred to afford **16** in 52% yield. This type of reactivity has been reported in the literature in the absence of a Pd catalyst.[44,45] Indeed, conducting the electrochemical reaction without Pd under otherwise identical conditions afforded **16** in 57% yield. We also explored the chemical oxidation of **15** using $PhI(OAc)_2$. Use of the electrochemical conditions (20% AcOH/MeCN, 0.5 M TMAOAc, 100 ºC, 6 h), but with 1 equivalent of $PhI(OAc)_2$ in place of electrical current, resulted in no detectable formation of either **15a** or **16** in the presence or absence of $Pd(OAc)_2$.[vii] In contrast, conducting the Pd-catalyzed oxidation with $PhI(OAc)_2$ under more standard chemical oxidation conditions (in $AcOH/Ac_2O$ at 100 ºC for 6 h) afforded 30% yield of **15a**. Only starting material was recovered under these conditions in the absence of Pd. Overall, these results demonstrate that there can be key differences in the relative rates of competing oxidation reactions under chemical versus electrochemical oxidation conditions, resulting in the formation of complementary products. Furthermore, the changes required to achieve an electrochemical reaction (often using different solvents as well as significant quantities of supporting electrolyte) can lead to fundamental changes in catalyst performance/reaction outcomes. Both of these points will be critical to consider for the future development and applications of electrochemistry in organic synthesis.

(vi) These studies were conducted in collaboration with Dr. Melissa Lee.

(vii) In general, the presence of MeCN and TMAOAc seems to have deteriorating effect on the overall C–H oxidation reaction. The reason behind this is not entirely clear, however, we hypothesize that the speciation of the palladium complex changes depending on the solvent and pH of the solution.

Scheme 2.3. Complementary electrochemical versus chemical oxidation of **15**

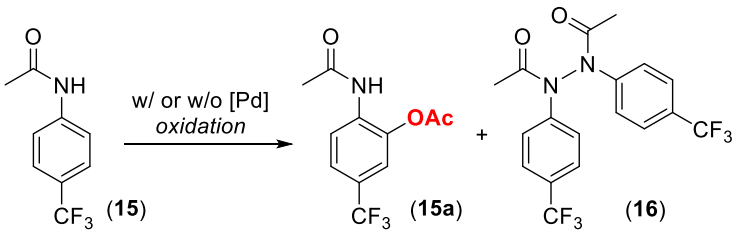

Conditions:

W: $Pd(OAc)_2$ or no Pd C: BQ (0.1 M) 20% AcOH/MeCN TMAOAc (0.5 M) **8 mA**, 6 h, 100 ºC	w/$Pd(OAc)_2$: <1% **15a**; 52% **16** w/o $Pd(OAc)_2$: <1% **15a**; 57% **16**
$Pd(OAc)_2$ or no Pd 2 equiv $PhI(OAc)_2$ 20% AcOH/MeCN TMAOAc (0.5 M) 48 h, 100 ºC	w/$Pd(OAc)_2$: <1% **15a**; <1% **16** w/o $Pd(OAc)_2$: <1% **15a**; <1% **16**
$Pd(OAc)_2$ or no Pd **2 equiv $PhI(OAc)_2$** 10% Ac_2O/AcOH 48 h, 100 ºC	w/$Pd(OAc)_2$: 30% **15a**; <1% **16** w/o $Pd(OAc)_2$: <1% **15a**; <5% **16**

2.3. Conclusion and Outlook

In conclusion, this work describes an electrochemical, Pd-catalyzed oxygenation of C(sp^2)–H and C(sp^3)–H bonds. By decoupling the C–H activation and oxidation steps, the oxidation of the palladacycle of 8-methylquinoline was studied. These studies ultimately led to the development and optimization of parameters for a catalytic system. We have shown that the addition of a mild oxidant to the cathode half-cell improves the overall reaction yield. Furthermore, we have shown that the choice of oxidant (chemical versus electrochemical) as well as the reaction medium (solvent and electrolyte) can lead to different reaction outcomes.

Since our report in 2018, this field of transition metal-catalyzed electrochemical C–H bond functionalization has received an upsurge in attention.[21,22] In addition to palladium, several methodologies utilizing other transition metals such as rhodium,[46–48] ruthenium[49–51] and cobalt[52,53] have been developed and have been shown to be effective for weakly coordinating directing groups such as amides and acids. Several new methods

to achieve functionalizations including halogenation,[36,54–56] alkylation,[57] alkenylation,[47,48] alkoxylation,[58] and amination[59–61] have been developed. The Ackermann group among others also pioneered synthesis of several heterocycles such as indoles,[62] isoquinolines,[51] and isocoumarins[50] via directed C–H activation.

The field of transition metal-catalyzed electrochemical C–H functionalization is still relatively nascent. Despite the advances already achieved, for a widespread utilization of these methodology, especially in industrial settings, several challenges need to be addressed. Establishing ways to recycle or designing reusable supporting electrolytes, (needed to maintain conductivity of the solution) is crucial for application in large scale reactions.[22] Additionally, diversification of transformations that can be mediated as well as the transitional metal catalysts that can participate in electrochemical oxidation would funnel in more interest in the field, especially from the synthetic community.

2.4. Experimental Details

2.4.1. Instrumental Information

NMR spectra were recorded on a Varian vnmrs 700 (700 MHz for ^{1}H; 176 MHz for ^{13}C) or a Varian vnmrs 500 (500 MHz for ^{1}H; 126 MHz for ^{13}C) spectrometer with the residual solvent peak ($CDCl_3$; ^{1}H: δ = 7.26 ppm, ^{13}C: δ = 77.16 ppm; CD_3CN; ^{1}H: δ = 1.94 ppm, 13C: δ = 1.32 ppm) as the internal reference unless otherwise noted. Chemical shifts are reported in parts per million (ppm, δ) relative to tetramethylsilane. Multiplicities are reported as follows: s (singlet), d (doublet), t (triplet), q (quartet), and m (multiplet). Coupling constants (*J*) are reported in Hz. High-resolution mass spectra were recorded on a Micromass AutoSpec Ultima Magnetic Sector mass spectrometer. A multi-channel potentiostat from Bio-Logic Instruments (model VSP-CHAS) was used for all the electrochemical studies.

2.4.2. Materials and Methods

All commercial reagents and solvents were used as received unless otherwise indicated. Tetramethylammonium acetate (TMAOAc) and 8-methylquinoline were purchased from TCI America and used without further purification. Benzoquinone,

purchased from Sigma Aldrich, was purified by sublimation before use. Anhydrous acetonitrile and acetic acid were purchased from Sigma Aldrich. Other chemicals were purchased from commercial sources (Alfa Aeser, Sigma Aldrich, TCI, Acros, Astatech, and Ark Pharm) and used without further purification. Thin layer chromatography (TLC) was performed on Macherey-Nagel SIL G-25 TLC plates pre-coated with silica gel UV254. Biotage® SNAP Ultra column cartridges were used for flash column chromatography. $CDCl_3$ and CD_3CN were purchased from Cambridge Isotope Laboratories, Inc. All reagents were weighed out under ambient conditions.

Bulk electrolysis experiments were performed in an H-cell with two compartments divided by an ultra-fine glass frit (10 mM P5 frit from Adams and Chittenden Scientific Glass). Each reaction utilized three electrodes: anode (working), cathode (counter), and reference. The two compartments in the H-cell were equipped with a graphite rod (anode and cathode), and a stir bar. The reference electrode on the working side of the cell consisted of a Ag wire in a fritted chamber containing a solution of $AgBF_4$ (0.01 M) and NBu_4PF_6 (0.1 M) in acetonitrile.

The substrates 8-methyl-5-nitroquinoline,[63] 5-bromo-8-methylquinoline,[63] 5-methoxy-8-methylquinoline,[63] 8-methylquinoline-5-carbonitrile,[64] methyl 8-methylquinoline-5-carboxylate[64] and 8-methyl-5-phenylquinoline[65] were prepared according to literature procedures.

2.4.3. Experimental Procedure for Cyclic Voltammetry

Cyclic voltammetry was performed in a three-electrode cell with a 3 mM glassy carbon disc as the working electrode, a Pt wire counter electrode, and a reference electrode consisting of a Ag wire in a fritted chamber containing a solution of $AgBF_4$ (0.01 M) and NBu_4PF_6 (0.1 M) in acetonitrile. A solution of the palladacycle **2** (0.02 M) and supporting electrolyte TMAOAc or tetramethylammonium hexafluorophosphate ($TMAPF_6$) (0.1 M) in a mixture of acetic acid and acetonitrile was added to the cell. The potential was swept from 0 to 1.5 V at a 100 mV/s scan rate.

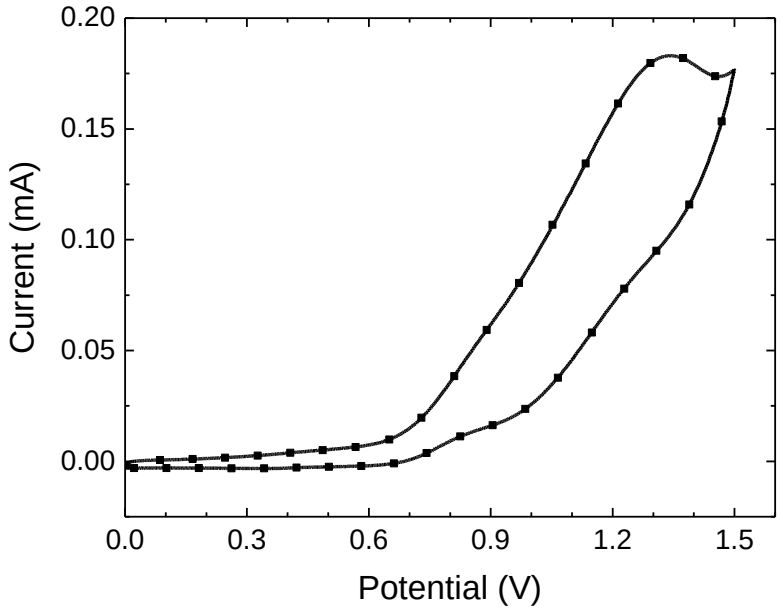

Figure 2.4. Cyclic Voltammogram of palladacycle **2** in 20% AcOH/MeCN and TMAOAc

A CV of the preformed palladium complex **2** in the reaction mixture is shown above. Compared to the CV of the same complex in absence of AcOH, a significant shift to higher potential was observed. The reason for this is still unclear.

2.4.4. Experimental Procedure for Stoichiometric Bulk Electrolysis

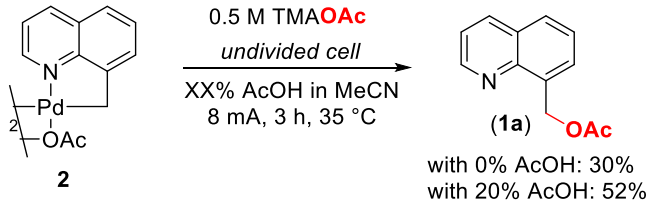

The electrochemical oxidation was conducted in an undivided three port cell. The cell was equipped with a stir bar, two graphite rod electrodes, and a Ag/Ag^+ reference electrode. A stock solution of TMAOAc (0.5 M) in either MeCN or in 20% acetic acid in MeCN was prepared (0.33 g of TMAOAc in 5 mL of solution). The palladacycle **2** (0.2 mmol,123 mg) was dissolved in the electrolyte solution (4 mL). This mixture was added to the three port cell and bulk electrolysis was conducted at 35 ºC under constant current settings with 8 mA passed through the solution over 6 h. The yield was determined by ^1H NMR spectroscopic analysis using trimethoxybenzene (0.2 mmol, 33.6 mg) as a standard. In MeCN, **1a** was formed in 23% yield (with 0.4 mmol of **1a** representing 100%

yield based on the dimeric nature of **2**). In 20% AcOH in MeCN, **1a** was formed in 52% yield.

2.4.5. General Procedure for the Catalytic Bulk Electrolysis

2.3.5.1. General Procedure for Optimization Reaction with 8-Methylquinoline

A stock solution of TMAOAc (0.5 M, 0.67 g) in acetic acid (2 mL) and acetonitrile (8 mL) was prepared.

When an undivided, three port cell was used: 8-Methylquinoline (0.4 mmol, 54 µL) and $Pd(OAc)_2$ (0.04 mmol, 8.9 mg) were dissolved in electrolyte solution (4 mL). This mixture was transferred to the cell and subjected to electrolysis at 35 ºC under constant current settings with 8 mA passed through the solution over 6 h.

When a divided H-cell was used: 8-Methylquinoline (0.4 mmol, 54 µL) and $Pd(OAc)_2$ (0.04 mmol, 8.9 mg) were dissolved in electrolyte solution (4 mL). This mixture was transferred to the anodic chamber of the H-cell. The cathodic chamber was loaded with either electrolyte solution or quinone dissolved in electrolyte, as appropriate. The bulk electrolysis was conducted at 35 ºC.

To quantify the yield of the reaction: The yield was determined by ^{1}H NMR spectroscopic analysis, using trimethoxybenzene (0.2 mmol, 33.6 mg) as a standard. The standard was added to the working (anodic) chamber after electrolysis was complete.

Table 2.3. Optimization of the Reaction the Reaction Conditions

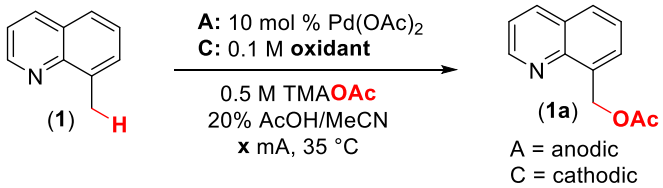

Entry	mA or V	Time/h	1a (%)	Modifications
1	8 mA	6	<1%	Undivided cell
2	8 mA	6	54	Divided cell, no oxidant
3	8 mA	6	32	Pt electrode on the counter side
4	8 mA	6	70	5 equiv. BQ on the counter side
5	8 mA	6	73	1 equiv. BQ on the counter side
6	8 mA	6	70	2,6-dichloro-1,4-benzoquinone on the counter side
7	8 mA	6	68	2,6-diphenyl-1,4-benzoquinone on the counter side

8	8 mA	6	70	2-methyl-1,4-benzoquinone on the counter side
9	8 mA	6	66	7% AcOH
10	8 mA	6	23	100% AcOH
11	4 mA	12	57	
12	6 mA	6	51	
13	6 mA	8	71	
14	12 mA	4	58	
15	1.2 V	12	30 ± 16	
16	1.2 V	12	17	RVC electrodes appended to Cu wire[a]
17	1.2 V	3.18	34 (35 SM)	Same mmol of e^- as 8 mA/6h

[a]AcOH dissolved Cu and the reaction got contaminated with Cu.

2.3.5.2. General Procedure for Obtaining Isolated Yields

The electrochemical oxidation was conducted in an H-cell divided by an ultra-fine glass frit. Both chambers of this cell were equipped with a stir bar and graphite rod electrodes. A stock solution was prepared of TMAOAc (0.5 M) in 20% acetic acid in acetonitrile. Substrate (0.4 mmol) and $Pd(OAc)_2$ (0.04 mmol, 8.9 mg) were dissolved in electrolyte solution (4 mL) and transferred to the anodic chamber of the H-cell. The cathodic chamber was loaded with benzoquinone (0.4 mmol, 43 mg) dissolved in electrolyte. A Ag/Ag^+ reference electrode was attached to the anodic chamber. The bulk electrolysis was conducted at 35-100 ºC under constant current settings with 8 mA being passed through the solution over 6 h. The solution was removed from the working (anodic) side of the cell, and this solution was passed through a silica plug and washed with acetonitrile (3 x 10 mL). The resulting solution and washings were combined and concentrated under vacuum, and the organic products were purified by column chromatography.

2.3.5.3. General Procedure for Isolations of Oximes and Oxime Ethers

Optimization studies showed that these reactions afforded higher yields using a slightly different solvent system (a 2 : 1 : 7 mixture of acetic anhydride (Ac_2O), acetic acid, and acetonitrile). After the bulk electrolysis, the reaction was concentrated, re-dissolved in DCM, and washed with $NaHCO_3$. The product was extracted into dichloromethane

(DCM) (3 X 5 mL), dried with Na_2SO_4, filtered, concentrated, and purified by column chromatography.

2.4.6. Synthesis and Isolation of Products from C–H Functionalization

Quinolin-8-ylmethyl acetate (1a)

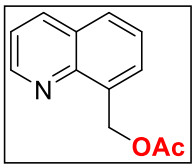

The product was formed from bulk electrolysis of 8-methylquinoline following general procedure B at 35 ºC. The product was isolated as a white powder in 73% yield (58.8 mg) via flash chromatography (gradient of 0-30% EtOAc in hexanes). The ^{1}H and ^{13}C NMR spectra of the product matched reported values.[12]

HRMS: ESI^+ (m/z): $[M+H^+]$ calcd for $C_{12}H_{11}NO_2$: 202.0863; found: 202.0860.

Scale-up:

8-Methylquinoline (1 mmol, 136 µL) and $Pd(OAc)_2$ (0.1 mmol, 22.4 mg) were dissolved in electrolyte solution (10 mL) and transferred to the anodic chamber of the H-cell. The cathodic chamber was loaded with benzoquinone (1 mmol, 108 mg) dissolved in electrolyte. A Ag/Ag^+ reference electrode was attached to the anodic chamber. The bulk electrolysis was conducted at 35 ºC under constant current settings with 8 mA being passed through the solution over 18 h. The solution was removed from the working (anodic) side of the cell, was passed through a silica plug and washed with acetonitrile (3 x 10 mL). The resulting solution and washings were combined and concentrated under vacuum, and the organic products were purified by column chromatography to yield product as a white powder in 66% yield (133 mg).

(5-phenylquinolin-8-yl)-methyl acetate (3a)

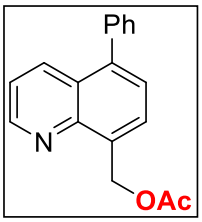

The product was formed from bulk electrolysis of 5-phenyl-8-methylquinoline following general procedure B at 65 ºC. The product was isolated as a white solid in 65% yield (72.1 mg) via flash chromatography (gradient of 0-45% EtOAc in hexanes).

HRMS: ESI$^+$ (m/z): [M+H$^+$] calcd for $C_{18}H_{15}NO_2$: 278.1176; found: 278.1180.

^{1}H NMR ($CDCl_3$, 700 MHz): δ 8.97 (dd, *J* = 4.2, 1.7 Hz, 1H), 8.25 (dd, *J* = 8.5, 1.7 Hz, 1H), 7.81 (d, *J* = 7.2 Hz, 1H), 7.51 (t, *J* = 7.3 Hz, 3H), 7.48-7.43 (multiple peaks, 3H), 7.39 (dd, *J* = 8.5, 4.1 Hz, 1H), 5.90 (s, 2H), 2.18 (s, 3H).

^{13}C NMR ($CDCl_3$, 126 MHz): δ 171.09, 149.66, 146.26, 140.79, 139.18, 134.62, 133.43, 129.99, 128.49, 128.28, 127.74, 126.79, 126.62, 121.20, 62.96, 21.21.

IR (cm^{-1}): 1725, 1446, 1241, 1047, 843.

mp: 58-59 ºC

(5-bromoquinolin-8-yl)methyl acetate (4a)

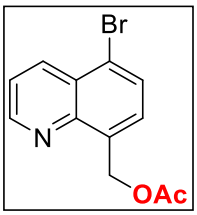

The product was formed from bulk electrolysis of 5-bromo-8-methylquinoline following general procedure B at 65 ºC. The product was isolated as a white solid in 75% yield (84.1 mg) via flash chromatography (gradient of 0-45% EtOAc in hexanes). The ^{1}H and ^{13}C NMR spectra of the product matched reported values.[66]

HRMS: ESI$^+$ (m/z): [M+H$^+$] calcd for $C_{12}H_{10}BrNO_2$: 279.9968; found: 279.9970.

(5-nitroquinolin-8-yl)methyl acetate (5a)

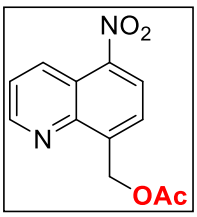

The product was formed from bulk electrolysis of 5-nitro-8-methylquinoline following general procedure B at 75 ºC. The product was isolated as a pale yellow solid

in 71% yield (69.9 mg) via a flash chromatography (gradient of 0-45% EtOAc in hexanes). The ^{1}H and ^{13}C NMR spectra of the product matched reported values.[66]

HRMS: ESI^{+} (m/z): [M+H^{+}] calcd for $C_{12}H_{10}N_2O_4$: 247.0713; found: 247.0718.

5-cyanoquinolin-8-yl)methyl acetate (6a)

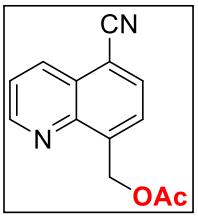

The product was formed from bulk electrolysis of 5-cyano-8-methylquinoline following general procedure B at 75 ºC. The product was isolated as a white solid in 75% yield (67.9 mg) via flash chromatography (gradient of 0-45% EtOAc in hexanes).

HRMS: ESI^{+} (m/z): [M+H^{+}] calcd for $C_{13}H_{10}N_2O_2$: 227.0815; found: 227.0818.

^{1}H NMR ($CDCl_3$, 700 MHz): δ 9.05 (d, *J* = 3.2 Hz, 1H), 8.56 (d, *J* = 8.4 Hz, 1H), 7.98 (d, *J* = 7.4 Hz, 1H), 7.81 (d, *J* = 7.4 Hz, 1H), 7.66 (dd, *J* = 8.5, 3.9 Hz, 1H), 5.90 (s, 2H), 2.21 (s, 3H).

^{13}C NMR ($CDCl_3$, 126 MHz): δ 170.65, 151.21, 145.07, 140.87, 133.55, 132.72, 127.59, 126.49, 123.41, 116.63, 109.96, 62.31, 21.01.

IR (cm^{-1}): 3029, 2218, 1744, 1732, 1230, 1054, 826.

mp: 109-111 ºC

Methyl 8-(acetoxymethyl)quinoline-5-carboxylate (7a)

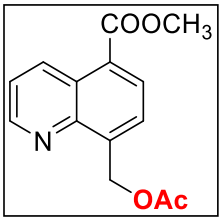

The product was formed from bulk electrolysis of methyl 8-methylquinoline-5-carboxylate following general procedure B at 75 ºC. The product was isolated as a white solid in 73% yield (75.7 mg) via flash chromatography (gradient of 0-45% EtOAc in hexanes).

HRMS: ESI$^+$ (m/z): [M+H$^+$] calcd for $C_{13}H_{14}NO_4$: 260.0917; found: 260.0925.

^{1}H NMR ($CDCl_3$, 700 MHz): δ 9.39 (d, *J* = 8.7 Hz, 1H), 8.98 (d, *J* = 3.8 Hz, 1H), 8.29 (d, *J* = 7.5 Hz, 1H), 7.78 (d, *J* = 7.6 Hz, 1H), 7.57 (dd, *J* = 8.8, 4.1 Hz, 1H), 5.91 (s, 2H), 4.01 (s, 3H), 2.20 (s, 3H).

^{13}C NMR ($CDCl_3$, 126 MHz): δ 170.79, 166.76, 149.66, 139.79, 134.88, 130.51, 126.85, 126.47, 126.29, 122.60, 62.83, 52.36, 21.08.

IR (cm^{-1}): 1742, 1706, 1247, 1218, 1055, 767.

mp: 81-82 ºC

(E)-3-(methoxyimino)-2,2-dimethylbutyl acetate (8a)

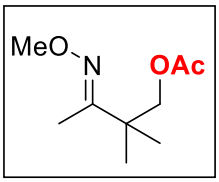

The product was formed from bulk electrolysis of (*E*)-3,3-dimethylbutan-2-one O-methyl oxime following general procedure C at 100 ºC. The product was isolated via flash chromatography (gradient of 0-10% EtOAc in hexanes) in 26% yield (19.7 mg) as a colorless oil. The ^{1}H and ^{13}C NMR spectra of the product matched reported values.[11]

HRMS: ESI$^+$ (m/z): [M+H$^+$] calcd for $C_9H_{18}NO_3$: 188.1281; found: 188.1280.

(E)-(2-(methoxyimino)-1-methylcyclohexyl)methyl acetate (9a)

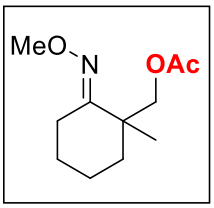

The product was formed from bulk electrolysis of (*E*)-2,2-dimethylcyclohexan-1-one O-methyl oxime following general procedure C at 100 ºC. The product was isolated via flash chromatography (gradient of 0-10% EtOAc in hexanes) in 33% yield (28.0 mg) as a colorless oil.

HRMS: ESI$^+$ (m/z): [M+H$^+$] calcd for $C_{11}H_{20}NO_3$: 214.1438; found: 214.1442.

^{1}H NMR ($CDCl_3$, 700 MHz): δ 4.29 (d, *J* = 10.5 Hz, 1H), 4.10 (d, *J* = 10.5 Hz, 1H), 3.79 (s, 3H), 2.61 (m, 1H), 2.34 (m, 1H), 2.05 (s, 3H), 1.55 (multiple peaks, 6H), 1.49 (s, 3H).

^{13}C NMR ($CDCl_3$, 176 MHz): δ 171.28, 161.23, 69.87, 61.37, 40.61, 36.13, 25.71, 22.10, 21.42, 21.29, 21.09.

IR (cm^{-1}): 2935, 1740, 1228,1046, 888.

2-((1H-pyrazol-1-yl)methyl)phenyl acetate (10a)

2-((1H-pyrazol-1-yl)methyl)-1,3-phenylene diacetate (10b)

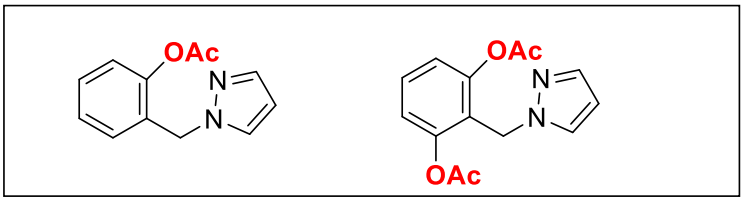

The products were formed from bulk electrolysis of 1-benzyl-1H-pyrazole following general procedure B at 100 ºC. The products were isolated via flash chromatography (gradient of 0-100% EtOAc in hexanes) in 47% yield (40.5 mg) of 10a as a colorless oil and 11% yield (12.3 mg) of 10b as a light yellow solid.

^{1}H NMR 10a ($CDCl_3$, 700 MHz): δ 7.53 (apparent s, 1H), 7.34 (t, *J* = 7.7 Hz, 1H), 7.32 (d, *J* = 2.1 Hz, 1H), 7.21 (t, *J* = 7.7 Hz, 1H), 7.12 (d, *J* = 7.7 Hz, 1H), 7.11 (d, *J* = 7.7 Hz, 1H), 6.26 (t, *J* = 2.1 Hz, 1H), 5.28 (s, 2H), 2.28 (s, 3H).

^{13}C NMR 10a ($CDCl_3$, 176 MHz): δ 169.15, 148.68, 139.49, 129.75, 129.52, 129.37, 128.71, 126.57, 122.84, 106.21, 51.15, 20.96.

IR 10a (cm^{-1}): 1762, 1368, 1200, 1086, 745.

HRMS 10a: ESI^+ (m/z): [M+H$^+$] calcd for $C_{12}H_{13}N_2O_2$: 217.0972; found: 217.0973.

^{1}H NMR 10b ($CDCl_3$, 700 MHz): δ 7.45 (apparent s, 1H), 7.40 (t, *J* = 8.4 Hz, 1H), 7.22 (d, *J* = 2.1 Hz, 1H), 7.05 (d, *J* = 8.4 Hz, 2H), 6.20 (t, *J* = 2.1 Hz, 1H), 5.25 (s, 2H), 2.27 (s, 6H).

^{13}C NMR 10b ($CDCl_3$, 176 MHz): δ 169.02, 150.39, 138.91, 129.85, 128.78, 121.24, 120.88, 106.37, 45.48, 20.96.

IR 10b (cm^{-1}): 1751, 1464, 1366, 1168, 1033, 760.

mp 10b: 62-64 ºC

HRMS 10b: ESI$^+$ (m/z): [M+H$^+$] calcd for $C_{14}H_{15}N_2O_4$: 275.1026; found: 275.1026.

2-(1H-pyrazol-1-yl)phenyl acetate (11a)

2-(1H-pyrazol-1-yl)-1,3-phenylene diacetate (11b)

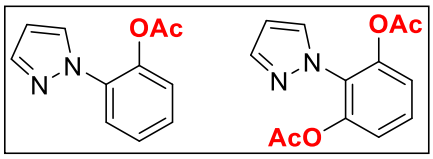

The products were formed from bulk electrolysis of 1-phenylpyrazole following general procedure B at 100 ºC. The products were isolated via flash chromatography (gradient of 0-70% EtOAc in hexanes) in 60% yield (48.5 mg) of 11a as a yellow oil and 12% yield (12.5 mg) of 11b as a yellow oil. The ^{1}H and ^{13}C NMR spectra of the products matched reported values.**Error! Bookmark not defined.**

HRMS of 11a: ESI$^+$ (m/z): [M+H$^+$] calcd for $C_{13}H_{11}NO_2$: 203.0815; found: 203.0812.

HRMS of 11b: ESI$^+$ (m/z): [M+H$^+$] calcd for $C_{15}H_{13}NO_4$: 261.0870; found: 261.0870.

2-(pyridin-2-yl)phenyl acetate (12a)

2-(pyridin-2-yl)-1,3-phenylene diacetate (12b)

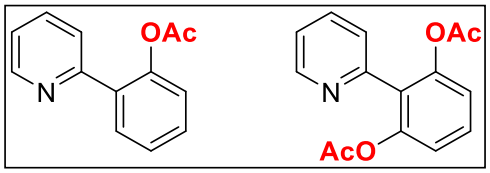

The products were formed from bulk electrolysis of 2-phenylpyridine following general procedure B at 100 ºC. The products were isolated via a flash chromatography (gradient of 0-70% EtOAc in hexanes) in 41% yield (35.0 mg) of 12a as a yellow oil and 30% yield (32.6 mg) of 12b as a yellow oil. The ^{1}H and ^{13}C NMR spectra of the products matched reported values.**Error! Bookmark not defined.**

HRMS of 12a: ESI$^+$ (m/z): [M+H$^+$] calcd for $C_{13}H_{11}NO_2$: 214.0863; found: 214.0860.

HRMS of 12b: ESI$^+$ (m/z): [M+H$^+$] calcd for $C_{15}H_{13}NO_4$: 272.0917; found: 272.0917.

(*E*)-8-(methoxyimino)-5,6,7,8-tetrahydronaphthalen-1-yl acetate (13a)

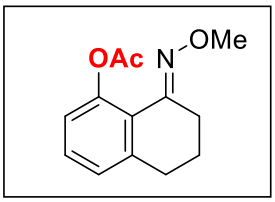

The product was formed from bulk electrolysis of (*E*)-3,4-dihydronaphthalen-1(2H)-one O-methyl oxime following general procedure C at 100 ºC. The product was isolated via flash chromatography (gradient of 0-70% EtOAc in hexanes) in 39% yield (40.3 mg) as a pink oil. The ^{1}H and ^{13}C NMR spectra of the product matched reported values.[67]

HRMS: ESI^{+} (m/z): [M+H^{+}] calcd for $C_{13}H_{16}NO_3$: 234.1125; found: 234.1129.

(*E*)-8-(acetoxyimino)-5,6,7,8-tetrahydronaphthalen-1-yl acetate (14a)

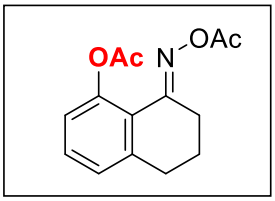

The product was formed from bulk electrolysis of (*E*)-3,4-dihydronaphthalen-1(2H)-one O-methyl oxime following general procedure C at 100 ºC. The product was isolated via flash chromatography (gradient of 0-100% EtOAc in hexanes) in 63% yield (58.6 mg) as an off-white solid. The ^{1}H and ^{13}C NMR spectra of the product matched reported values.[68]

HRMS: ESI^{+} (m/z): [M+H^{+}] calcd for $C_{14}H_{16}NO_4$: 262.1074; found: 262.1075.

2-acetamido-5-(trifluoromethyl)phenyl acetate (15a)

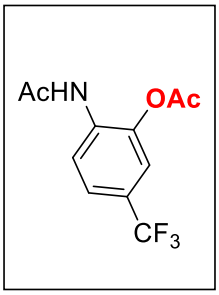

The product was isolated from a chemical oxidation with $PhI(OAc)_2$. A 4 mL vial was charged with a stir bar, N-(4-(trifluoromethyl)phenyl)acetamide (0.20 mmol, 40.6 mg), $Pd(OAc)_2$ (0.02 mmol, 4.5 mg), and $PhI(OAc)_2$ (0.40 mmol, 128.8 mg). A mixture of 9:1 AcOH:Ac_2O (2.0 mL) was added and the resulting solution was stirred at 100 ºC for 48 h. The reaction was diluted with dichloromethane, the organic layer was washed with aqueous Na_2CO_3, and the organic layer was separated and dried over sodium sulfate. The organic extracts were concentrated and the product was isolated via a flash chromatography (gradient of 0-100% EtOAc in hexanes) as a light pink solid in 30% yield (15.8 mg).

^{1}H NMR ($CDCl_3$, 700 MHz): δ 8.42 (d, *J* = 8.4 Hz, 1H), 7.48 (d, *J* = 8.4, 1H), 7.43 (s, 1H), 7.34 (br s, 1H), 2.43 (s, 3H), 2.26 (s, 3H).

^{13}C NMR ($CDCl_3$, 176 MHz): δ 168.19, 168.04, 139.27, 132.86, 126.12 (q, J_{C-F} = 32.7 Hz), 123.44 (q, J_{C-F} = 272.1 Hz), 123.54 (q, J_{C-F} = 14.7 Hz), 121.92, 119.45, 24.82, 21.05.

^{19}F NMR ($CDCl_3$, 376 MHz): –62.2.

IR (cm^{-1}): 1762, 1690, 1326, 1200, 1166, 1107.

mp: 104-106 ºC

HRMS: ESI^+ (m/z): [M+H^+] calcd for $C_{11}H_{10}F_3NO_3$: 262.0686; found: 262.0688.

N'-acetyl-N,N'-bis(4-(trifluoromethyl)phenyl)acetohydrazide (16)

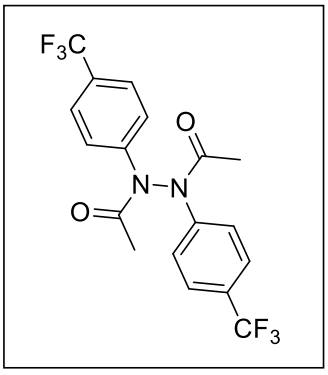

The product was formed from bulk electrolysis of N-(4-(trifluoromethyl)phenyl)acetamide following general procedure B at 100 ºC. The product was isolated via a flash chromatography (gradient of 0-100% EtOAc in hexanes) as a light yellow oil in 52% yield (41.9 mg).

^{1}H NMR (d_6-DMSO, 700 MHz, 100 ºC): δ 7.74 (d, *J* = 8.4 Hz, 4H), 7.63 (d, *J* = 8.4 Hz, 4H), 2.20 (s, 6H).

^{13}C NMR (d_6-DMSO, 176 MHz, 100 ºC): δ 169.23, 142.90, 127.18 (q, $J_{C\text{-}F}$ = 31.7 Hz), 125.84, 124.50, 123.34 (q, $J_{C\text{-}F}$ = 272.8 Hz), 21.47.

^{19}F NMR (d_6-DMSO, 376 MHz, 100 ºC): 61.21.

IR (cm^{-1}): 1704, 1613, 1319, 1165, 1116, 1066.

HRMS: ESI^+ (m/z): [M+H^+] calcd for $C_{18}H_{15}F_6N_2O_2$: 405.1032; found: 405.1030.

2.4.7. The Four Electrode Experiment

This electrochemical experiment was conducted to understand the impact of benzoquinone (the sacrificial oxidant added on the counter-side) on the overall reaction. The potentials at both the working (anodic) and the counter (cathodic) electrode were monitored during the reaction as detailed below. This allowed the potential to be directly compared in presence and absence of benzoquinone without being impacted by the resistance of the frit.

The electrochemical oxidation was conducted in an H-cell divided by ultra-fine glass frit. Both chambers of this cell were equipped with a stir bar and graphite rod electrodes. An electrolyte stock solution was prepared, consisting of TMAOAc (0.5 M) dissolved in 20% acetic acid in acetonitrile. 8-Methylquinoline (0.4 mmol, 57 mg) and 10 mol% $Pd(OAc)_2$ were dissolved in electrolyte solution (4 mL) and transferred into the working chamber of the H-cell. Separately, benzoquinone (0.4 mmol, 43 mg) was dissolved in electrolyte solution (4 mL)and transferred to the counter chamber of the H-cell. A Ag/Ag^+ reference electrode was attached to both working and counter chambers. Two channels from the potentiostat were utilized, with the first channel passing a current of 8 mA between the anode and cathode. The second channel recorded the open circuit potential of the cathode. In line with our hypothesis, the cathodic potential in presence of benzoquinone was lower compared to the cathodic potential in the absence of sacrificial oxidant. The observed cathodic potentials are consistent with the relative potentials for reduction of BQ versus protons. A slight increase in the anodic potential was observed, potentially indicating overpotential in the reaction.

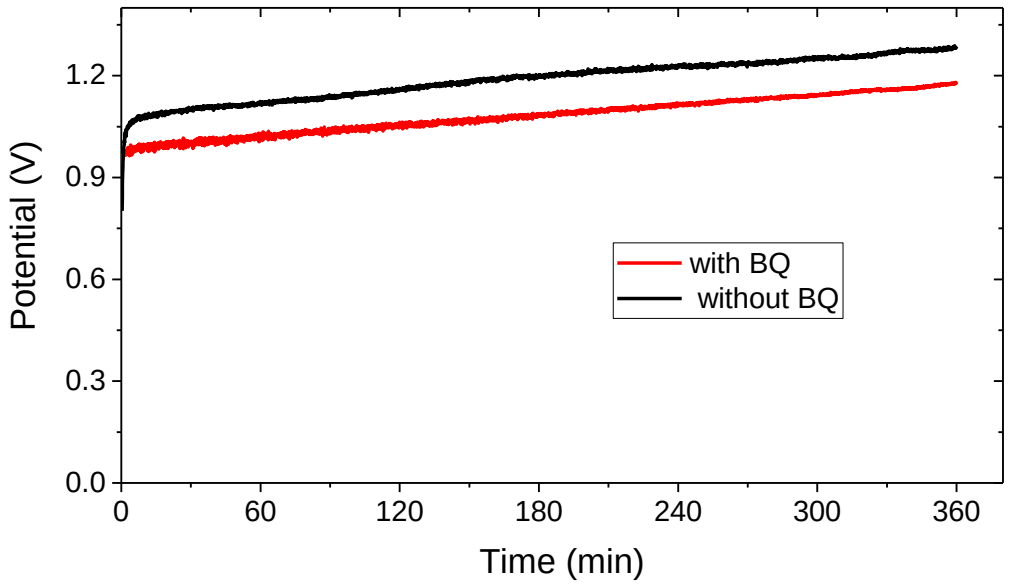

Figure 2.5. Profile of redox potential over time of the working side through the C–H functionalization reaction of 8-methylquinoline in presence and absence of benzoquinone on the counter side

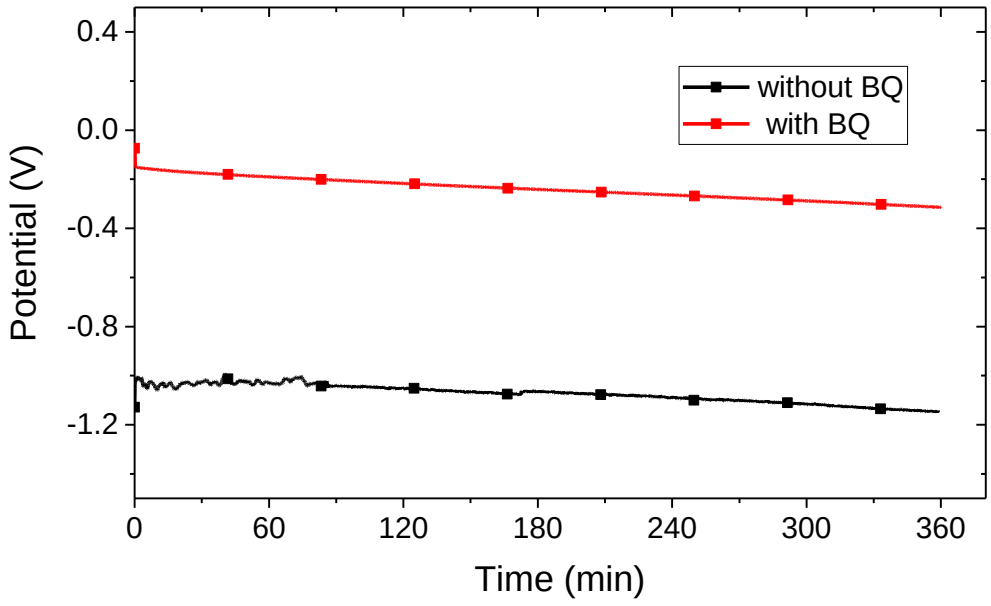

Figure 2.6. Profile of redox potential over time of the working side through the C–H functionalization reaction of 8-methylquinoline in presence and absence of benzoquinone on the counter side

2.5. References

(1) Daugulis, O.; Do, H.-Q.; Shabashov, D. Palladium- and Copper-Catalyzed Arylation of Carbon−Hydrogen Bonds. *Acc. Chem. Res.* **2009**, *42* (8), 1074–1086. https://doi.org/10.1021/ar9000058.

(2) Lyons, T. W.; Sanford, M. S. Palladium-Catalyzed Ligand-Directed C−H Functionalization Reactions. *Chem. Rev.* **2010**, *110* (2), 1147–1169. https://doi.org/10.1021/cr900184e.

(3) He, J.; Wasa, M.; Chan, K. S. L.; Shao, Q.; Yu, J.-Q. Palladium-Catalyzed Transformations of Alkyl C–H Bonds. *Chem. Rev.* **2017**, *117* (13), 8754–8786. https://doi.org/10.1021/acs.chemrev.6b00622.

(4) Powers, D. C.; Lee, E.; Ariafard, A.; Sanford, M. S.; Yates, B. F.; Canty, A. J.; Ritter, T. Connecting Binuclear Pd(III) and Mononuclear Pd(IV) Chemistry by Pd–Pd Bond Cleavage. *J. Am. Chem. Soc.* **2012**, *134* (29), 12002–12009. https://doi.org/10.1021/ja304401u.

(5) Deprez, N. R.; Sanford, M. S. Synthetic and Mechanistic Studies of Pd-Catalyzed C−H Arylation with Diaryliodonium Salts: Evidence for a Bimetallic High Oxidation State Pd Intermediate. *J. Am. Chem. Soc.* **2009**, *131* (31), 11234–11241. https://doi.org/10.1021/ja904116k.

(6) Powers, D. C.; Ritter, T. Bimetallic Redox Synergy in Oxidative Palladium Catalysis. *Acc. Chem. Res.* **2012**, *45* (6), 840–850. https://doi.org/10.1021/ar2001974.

(7) Hickman, A. J.; Sanford, M. S. High-Valent Organometallic Copper and Palladium in Catalysis. *Nature* **2012**, *484* (7393), 177–185. https://doi.org/10.1038/nature11008.

(8) Choy, P. Y.; Kwong, F. Y. Palladium-Catalyzed Ortho-CH-Bond Oxygenation of Aromatic Ketones. *Org. Lett.* **2013**, *15* (2), 270–273. https://doi.org/10.1021/ol303088z.

(9) Kalyani, D.; Dick, A. R.; Anani, W. Q.; Sanford, M. S. A Simple Catalytic Method for the Regioselective Halogenation of Arenes. *Org. Lett.* **2006**, *8* (12), 2523–2526. https://doi.org/10.1021/ol060747f.

(10) Hull, K. L.; Anani, W. Q.; Sanford, M. S. Palladium-Catalyzed Fluorination of Carbon−Hydrogen Bonds. *J. Am. Chem. Soc.* **2006**, *128* (22), 7134–7135. https://doi.org/10.1021/ja061943k.

(11) Desai, L. V.; Hull, K. L.; Sanford, M. S. Palladium-Catalyzed Oxygenation of Unactivated Sp3 C−H Bonds. *J. Am. Chem. Soc.* **2004**, *126* (31), 9542–9543. https://doi.org/10.1021/ja046831c.

(12) Dick, A. R.; Hull, K. L.; Sanford, M. S. A Highly Selective Catalytic Method for the Oxidative Functionalization of C−H Bonds. *J. Am. Chem. Soc.* **2004**, *126* (8), 2300–2301. https://doi.org/10.1021/ja031543m.

(13) Kalyani, D.; Deprez, N. R.; Desai, L. V.; Sanford, M. S. Oxidative C−H Activation/C−C Bond Forming Reactions: Synthetic Scope and Mechanistic Insights. *J. Am. Chem. Soc.* **2005**, *127* (20), 7330–7331. https://doi.org/10.1021/ja051402f.

(14) Deprez, N. R.; Kalyani, D.; Krause, A.; Sanford, M. S. Room Temperature Palladium-Catalyzed 2-Arylation of Indoles. *J. Am. Chem. Soc.* **2006**, *128* (15), 4972–4973. https://doi.org/10.1021/ja060809x.

(15) Dick, A. R.; Remy, M. S.; Kampf, J. W.; Sanford, M. S. Carbon−Nitrogen Bond-Forming Reactions of Palladacycles with Hypervalent Iodine Reagents. *Organometallics* **2007**, *26* (6), 1365–1370. https://doi.org/10.1021/om061052l.

(16) Canty, A. J.; Ariafard, A.; Sanford, M. S.; Yates, B. F. Mechanism of Pd-Catalyzed Ar–Ar Bond Formation Involving Ligand-Directed C–H Arylation and Diaryliodonium Oxidants: Computational Studies of Orthopalladation at Binuclear Pd(II) Centers, Oxidation To Form Binuclear Palladium(III) Species, and Ar···Ar Reductive Coupling. *Organometallics* **2013**, *32* (2), 544–555. https://doi.org/10.1021/om301013w.

(17) Brady, P. B.; Bhat, V. Recent Applications of Rh- and Pd-Catalyzed C(Sp3)–H Functionalization in Natural Product Total Synthesis. *Eur. J. Org. Chem.* **2017**, *2017* (35), 5179–5190. https://doi.org/10.1002/ejoc.201700641.

(18) Baudoin, O. Ring Construction by Palladium(0)-Catalyzed C(Sp3)–H Activation. *Acc. Chem. Res.* **2017**, *50* (4), 1114–1123. https://doi.org/10.1021/acs.accounts.7b00099.

(19) Ding, C.; Li, J.; Jiao, M.; Zhang, A. Catalyst-Free Sp3 C–H Acyloxylation: Regioselective Synthesis of 1-Acyloxy Derivatives of the Natural Product Tanshinone IIA. *J. Nat. Prod.* **2016**, *79* (10), 2514–2520. https://doi.org/10.1021/acs.jnatprod.6b00370.

(20) Sharpe, R. J.; Johnson, J. S. A Global and Local Desymmetrization Approach to the Synthesis of Steroidal Alkaloids: Stereocontrolled Total Synthesis of Paspaline. *J. Am. Chem. Soc.* **2015**, *137* (15), 4968–4971. https://doi.org/10.1021/jacs.5b02631.

(21) Sauermann, N.; Meyer, T. H.; Qiu, Y.; Ackermann, L. Electrocatalytic C–H Activation. *ACS Catal.* **2018**, *8* (8), 7086–7103. https://doi.org/10.1021/acscatal.8b01682.

(22) Ma, C.; Fang, P.; Mei, T.-S. Recent Advances in C–H Functionalization Using Electrochemical Transition Metal Catalysis. *ACS Catal.* **2018**, *8* (8), 7179–7189. https://doi.org/10.1021/acscatal.8b01697.

(23) Moeller, K. D. Synthetic Applications of Anodic Electrochemistry. *Tetrahedron* **2000**, *56* (49), 9527–9554. https://doi.org/10.1016/S0040-4020(00)00840-1.

(24) Jiao, K.-J.; Zhao, C.-Q.; Fang, P.; Mei, T.-S. Palladium Catalyzed CH Functionalization with Electrochemical Oxidation. *Tetrahedron Lett.* **2017**, *58* (9), 797–802. https://doi.org/10.1016/j.tetlet.2016.12.065.

(25) Dudkina, Yu. B.; Gryaznova, T. V.; Sinyashin, O. G.; Budnikova, Yu. H. Ligand-Directed Electrochemical Functionalization of C(Sp2)—H Bonds in the Presence of the Palladium and Nickel Compounds. *Russ. Chem. Bull.* **2015**, *64* (8), 1713–1725. https://doi.org/10.1007/s11172-015-1067-3.

(26) Horn, E. J.; Rosen, B. R.; Baran, P. S. Synthetic Organic Electrochemistry: An Enabling and Innately Sustainable Method. *ACS Cent. Sci.* **2016**, *2* (5), 302–308. https://doi.org/10.1021/acscentsci.6b00091.

(27) Yoshida, J.; Kataoka, K.; Horcajada, R.; Nagaki, A. Modern Strategies in Electroorganic Synthesis. *Chem. Rev.* **2008**, *108* (7), 2265–2299. https://doi.org/10.1021/cr0680843.

(28) Sperry, J. B.; Wright, D. L. The Application of Cathodic Reductions and Anodic Oxidations in the Synthesis of Complex Molecules. *Chem. Soc. Rev.* **2006**, *35* (7), 605–621. https://doi.org/10.1039/B512308A.

(29) Lund, H. A Century of Organic Electrochemistry. *J. Electrochem. Soc.* **2002**, *149* (4), S21. https://doi.org/10.1149/1.1462037.

(30) Badalyan, A.; Stahl, S. S. Cooperative Electrocatalytic Alcohol Oxidation with Electron-Proton-Transfer Mediators. *Nature* **2016**, *535* (7612), 406–410. https://doi.org/10.1038/nature18008.

(31) Kawamata, Y.; Yan, M.; Liu, Z.; Bao, D.-H.; Chen, J.; Starr, J. T.; Baran, P. S. Scalable, Electrochemical Oxidation of Unactivated C–H Bonds. *J. Am. Chem. Soc.* **2017**, *139* (22), 7448–7451. https://doi.org/10.1021/jacs.7b03539.

(32) Horn, E. J.; Rosen, B. R.; Chen, Y.; Tang, J.; Chen, K.; Eastgate, M. D.; Baran, P. S. Scalable and Sustainable Electrochemical Allylic C-H Oxidation. *Nature* **2016**, *533* (7601), 77–81. https://doi.org/10.1038/nature17431.

(33) Redden, A.; Perkins, R. J.; Moeller, K. D. Oxidative Cyclization Reactions: Controlling the Course of a Radical Cation-Derived Reaction with the Use of a Second Nucleophile. *Angew. Chem. Int. Ed Engl.* **2013**, *52* (49), 12865–12868. https://doi.org/10.1002/anie.201308739.

(34) Lips, S.; Wiebe, A.; Elsler, B.; Schollmeyer, D.; Dyballa, K. M.; Franke, R.; Waldvogel, S. R. Synthesis of Meta-Terphenyl-2,2''-Diols by Anodic C-C Cross-Coupling Reactions. *Angew. Chem. Int. Ed Engl.* **2016**, *55* (36), 10872–10876. https://doi.org/10.1002/anie.201605865.

(35) Wiebe, A.; Schollmeyer, D.; Dyballa, K. M.; Franke, R.; Waldvogel, S. R. Cover Picture: Selective Synthesis of Partially Protected Nonsymmetric Biphenols by Reagent- and Metal-Free Anodic Cross-Coupling Reaction (Angew. Chem. Int. Ed. 39/2016). *Angew. Chem. Int. Ed.* **2016**, *55* (39), 11689–11689. https://doi.org/10.1002/anie.201606627.

(36) Kakiuchi, F.; Kochi, T.; Mutsutani, H.; Kobayashi, N.; Urano, S.; Sato, M.; Nishiyama, S.; Tanabe, T. Palladium-Catalyzed Aromatic C−H Halogenation with Hydrogen Halides by Means of Electrochemical Oxidation. *J. Am. Chem. Soc.* **2009**, *131* (32), 11310–11311. https://doi.org/10.1021/ja9049228.

(37) Dudkina, Y. B.; Mikhaylov, D. Y.; Gryaznova, T. V.; Sinyashin, O. G.; Vicic, D. A.; Budnikova, Y. H. MII/MIII-Catalyzed Ortho-Fluoroalkylation of 2-Phenylpyridine. *Eur. J. Org. Chem.* **2012**, *2012* (11), 2114–2117. https://doi.org/10.1002/ejoc.201200050.

(38) Grayaznova, T. V.; Dudkina, Yu. B.; Islamov, D. R.; Kataeva, O. N.; Sinyashin, O. G.; Vicic, D. A.; Budnikova, Yu. H. Pyridine-Directed Palladium-Catalyzed Electrochemical Phosphonation of C(Sp2)–H Bond. *J. Organomet. Chem.* **2015**, *785*, 68–71. https://doi.org/10.1016/j.jorganchem.2015.03.001.

(39) Dudkina, Y. B.; Mikhaylov, D. Y.; Gryaznova, T. V.; Tufatullin, A. I.; Kataeva, O. N.; Vicic, D. A.; Budnikova, Y. H. Electrochemical Ortho Functionalization of 2-Phenylpyridine with Perfluorocarboxylic Acids Catalyzed by Palladium in Higher Oxidation States. *Organometallics* **2013**, *32* (17), 4785–4792. https://doi.org/10.1021/om400492g.

(40) Li, Y.-Q.; Yang, Q.-L.; Fang, P.; Mei, T.-S.; Zhang, D. Palladium-Catalyzed C(Sp2)–H Acetoxylation via Electrochemical Oxidation. *Org. Lett.* **2017**, *19* (11), 2905–2908. https://doi.org/10.1021/acs.orglett.7b01138.

(41) Yang, Q.-L.; Li, Y.-Q.; Ma, C.; Fang, P.; Zhang, X.-J.; Mei, T.-S. Palladium-Catalyzed C(Sp3)—H Oxygenation via Electrochemical Oxidation. *J. Am. Chem. Soc.* **2017**, *139* (8), 3293–3298. https://doi.org/10.1021/jacs.7b01232.

(42) Powers, D. C.; Geibel, M. A. L.; Klein, J. E. M. N.; Ritter, T. Bimetallic Palladium Catalysis: Direct Observation of Pd(III)−Pd(III) Intermediates. *J. Am. Chem. Soc.* **2009**, *131* (47), 17050–17051. https://doi.org/10.1021/ja906935c.

(43) Wang, G.-W.; Yuan, T.-T.; Wu, X.-L. Direct Ortho-Acetoxylation of Anilides via Palladium-Catalyzed Sp2 C−H Bond Oxidative Activation. *J. Org. Chem.* **2008**, *73* (12), 4717–4720. https://doi.org/10.1021/jo8003088.

(44) Gieshoff, T.; Schollmeyer, D.; Waldvogel, S. R. Access to Pyrazolidin-3,5-Diones through Anodic N-N Bond Formation. *Angew. Chem. Int. Ed Engl.* **2016**, *55* (32), 9437–9440. https://doi.org/10.1002/anie.201603899.

(45) Rosen, B. R.; Werner, E. W.; O'Brien, A. G.; Baran, P. S. Total Synthesis of Dixiamycin B by Electrochemical Oxidation. *J. Am. Chem. Soc.* **2014**, *136* (15), 5571–5574. https://doi.org/10.1021/ja5013323.

(46) Kong, W.-J.; Finger, L. H.; Oliveira, J. C. A.; Ackermann, L. Rhodaelectrocatalysis for Annulative C−H Activation: Polycyclic Aromatic Hydrocarbons through Versatile Double Electrocatalysis. *Angew. Chem. Int. Ed.* **2019**, *58* (19), 6342–6346. https://doi.org/10.1002/anie.201901565.

(47) Qiu, Y.; Kong, W.-J.; Struwe, J.; Sauermann, N.; Rogge, T.; Scheremetjew, A.; Ackermann, L. Electrooxidative Rhodium-Catalyzed C−H/C−H Activation: Electricity as Oxidant for Cross-Dehydrogenative Alkenylation. *Angew. Chem. Int. Ed.* **2018**, *57* (20), 5828–5832. https://doi.org/10.1002/anie.201803342.

(48) Qiu, Y.; Scheremetjew, A.; Ackermann, L. Electro-Oxidative C–C Alkenylation by Rhodium(III) Catalysis. *J. Am. Chem. Soc.* **2019**, *141* (6), 2731–2738. https://doi.org/10.1021/jacs.8b13692.

(49) Mei, R.; Koeller, J.; Ackermann, L. Electrochemical Ruthenium-Catalyzed Alkyne Annulations by C–H/Het–H Activation of Aryl Carbamates or Phenols in Protic Media. *Chem. Commun.* **2018**, *54* (91), 12879–12882. https://doi.org/10.1039/C8CC07732K.

(50) Qiu, Y.; Tian, C.; Massignan, L.; Rogge, T.; Ackermann, L. Electrooxidative Ruthenium-Catalyzed C−H/O−H Annulation by Weak O-Coordination. *Angew. Chem. Int. Ed.* **2018**, *57* (20), 5818–5822. https://doi.org/10.1002/anie.201802748.

(51) Xu, F.; Li, Y.-J.; Huang, C.; Xu, H.-C. Ruthenium-Catalyzed Electrochemical Dehydrogenative Alkyne Annulation. *ACS Catal.* **2018**, *8* (5), 3820–3824. https://doi.org/10.1021/acscatal.8b00373.

(52) Sauermann, N.; Meyer, T. H.; Ackermann, L. Electrochemical Cobalt-Catalyzed C−H Activation. *Chem. – Eur. J.* **2018**, *24* (61), 16209–16217. https://doi.org/10.1002/chem.201802706.

(53) Zeng, L.; Li, H.; Tang, S.; Gao, X.; Deng, Y.; Zhang, G.; Pao, C.-W.; Chen, J.-L.; Lee, J.-F.; Lei, A. Cobalt-Catalyzed Electrochemical Oxidative C–H/N–H Carbonylation with Hydrogen Evolution. *ACS Catal.* **2018**, *8* (6), 5448–5453. https://doi.org/10.1021/acscatal.8b00683.

(54) Kakiuchi, F.; Kochi, T.; Mutsutani, H.; Kobayashi, N.; Urano, S.; Sato, M.; Nishiyama, S.; Tanabe, T. Palladium-Catalyzed Aromatic C−H Halogenation with Hydrogen Halides by Means of Electrochemical Oxidation. *J. Am. Chem. Soc.* **2009**, *131* (32), 11310–11311. https://doi.org/10.1021/ja9049228.

(55) Aiso, H.; Kochi, T.; Mutsutani, H.; Tanabe, T.; Nishiyama, S.; Kakiuchi, F. Catalytic Electrochemical C–H Iodination and One-Pot Arylation by ON/OFF Switching of Electric Current. *J. Org. Chem.* **2012**, *77* (17), 7718–7724. https://doi.org/10.1021/jo3012286.

(56) Konishi, M.; Tsuchida, K.; Sano, K.; Kochi, T.; Kakiuchi, F. Palladium-Catalyzed Ortho-Selective C–H Chlorination of Benzamide Derivatives under Anodic Oxidation Conditions. *J. Org. Chem.* **2017**, *82* (16), 8716–8724. https://doi.org/10.1021/acs.joc.7b01137.

(57) Ma, C.; Zhao, C.-Q.; Li, Y.-Q.; Zhang, L.-P.; Xu, X.-T.; Zhang, K.; Mei, T.-S. Palladium-Catalyzed C–H Activation/C–C Cross-Coupling Reactions via Electrochemistry. *Chem. Commun.* **2017**, *53* (90), 12189–12192. https://doi.org/10.1039/C7CC07429H.

(58) Sauermann, N.; Meyer, T. H.; Tian, C.; Ackermann, L. Electrochemical Cobalt-Catalyzed C–H Oxygenation at Room Temperature. *J. Am. Chem. Soc.* **2017**, *139* (51), 18452–18455. https://doi.org/10.1021/jacs.7b11025.

(59) Yang, Q.-L.; Wang, X.-Y.; Lu, J.-Y.; Zhang, L.-P.; Fang, P.; Mei, T.-S. Copper-Catalyzed Electrochemical C–H Amination of Arenes with Secondary Amines. *J. Am. Chem. Soc.* **2018**, *140* (36), 11487–11494. https://doi.org/10.1021/jacs.8b07380.

(60) Sauermann, N.; Mei, R.; Ackermann, L. Electrochemical C-H Amination by Cobalt Catalysis in a Renewable Solvent. *Angew. Chem. Int. Ed Engl.* **2018**, *57* (18), 5090–5094. https://doi.org/10.1002/anie.201802206.

(61) Gao, X.; Wang, P.; Zeng, L.; Tang, S.; Lei, A. Cobalt(II)-Catalyzed Electrooxidative C-H Amination of Arenes with Alkylamines. *J. Am. Chem. Soc.* **2018**, *140* (12), 4195–4199. https://doi.org/10.1021/jacs.7b13049.

(62) Ackermann, L.; Lygin, A. V. Cationic Ruthenium(II) Catalysts for Oxidative C–H/N–H Bond Functionalizations of Anilines with Removable Directing Group: Synthesis of Indoles in Water. *Org. Lett.* **2012**, *14* (3), 764–767. https://doi.org/10.1021/ol203309y.

(63) Evans, P.; Hogg, P.; Grigg, R.; Nurnabi, M.; Hinsley, J.; Sridharan, V.; Suganthan, S.; Korn, S.; Collard, S.; Muir, J. E. 8-Methylquinoline Palladacycles: Stable and Efficient Catalysts for Carbon–

Carbon Bond Formation. *Tetrahedron* **2005**, *61* (41), 9696–9704. https://doi.org/10.1016/j.tet.2005.06.118.

(64) Tochilkin, A. I.; Gracheva, I. N.; Kovel'man, I. R.; Prokof'ev, E. P. Aromatic Chlorination and Iodination of 8-Methylquinoline. Benzyl Bromination of 5-Halo-8-Methylquinolines. *Chem. Heterocycl. Compd.* **1983**, *19* (10), 1093–1096. https://doi.org/10.1007/BF00505763.

(65) McMurtrey, K. B.; Racowski, J. M.; Sanford, M. S. Pd-Catalyzed C–H Fluorination with Nucleophilic Fluoride. *Org. Lett.* **2012**, *14* (16), 4094–4097. https://doi.org/10.1021/ol301739f.

(66) Zhang, J.; Khaskin, E.; Anderson, N. P.; Zavalij, P. Y.; Vedernikov, A. N. Catalytic Aerobic Oxidation of Substituted 8-Methylquinolines in PdII-2,6-Pyridinedicarboxylic Acid Systems. *Chem. Commun.* **2008**, No. 31, 3625–3627. https://doi.org/10.1039/B803156H.

(67) Pan, L.; Wang, L.; Chen, Q.; He, M. Palladium-Catalyzed Oxime Ether Directed Regioselective C-H Alkoxylation of Arenes. *Synth. Commun.* **2016**, *46* (24), 1981–1988. https://doi.org/10.1080/00397911.2016.1242749.

(68) Neufeldt, S. R.; Sanford, M. S. O-Acetyl Oximes as Transformable Directing Groups for Pd-Catalyzed C−H Bond Functionalization. *Org. Lett.* **2010**, *12* (3), 532–535. https://doi.org/10.1021/ol902720d.

Chapter 3

Realization of an Asymmetric Non-Aqueous Redox Flow Battery Through Molecular Design to Minimize Active Species Crossover and Decomposition

(A part of this work has been published in Shrestha, A.; Hendriks, K. H.; Sigman, M. S.; Minteer, S. D.; Sanford, M. S. “Realization of an Asymmetric Non-Aqueous Redox Flow Battery Through Molecular Design to Minimize Active Species Crossover and Decomposition” *Chemistry – A European Journal* **2020**¸ ASAP)

3.1. Introduction

The widespread adoption of renewable energy sources remains limited by a dearth of cost-effective and scalable methods for electrical energy storage (EES).[1,2] Several technologies have been explored for energy storage including pumped hydropower, compressed air energy storage and a variety of electrochemical energy storage technologies. Common energy storage technologies include lithium ion battery or lead-acid battery, but these technologies suffer from scalability and long-term stability. Redox flow batteries (RFBs) represent an attractive alternative to address limitations of these electrochemical EES.[3–8] In RFBs, energy is stored in solutions of redox active electrolytes (termed catholytes and anolytes) that in external reservoirs. To convert electrical energy into chemical energy, these redox active species are charged to their higher energy state. This energy conversion process occurs in the electrochemical chamber, that is equipped with inert electrodes (Figure 3.1a). A reverse process (discharge) to bring these redox active species to their lower energy state can release the stored energy. This configuration facilitates scaling of these systems, since power and storage capacity are dictated by independent factors (the area/number of electrodes and the volume of the

solutions, respectively). In addition to scalability, RFBs are also highly modular, as the system can be adopted for use with a wide variety of different anolyte/catholytes pairs.[9–14] Some of the favorable properties of a good electrolyte candidate include: (a) high oxidation potential for catholyte and low reduction potential for anolyte; (b) good solubility in the solvent of choice; (c) reversible electron transfer behavior; (d) solution stability in all charge states; and (e) stable cycling (charge/discharge) over a minimum of several hundreds of cycles. The scalability of RFBs and the tunability of the electrolytes in these systems has led to a recent rise in interest in the field of RFBs, with groups of diverse backgrounds tackling a multitude of challenges in this nascent field.

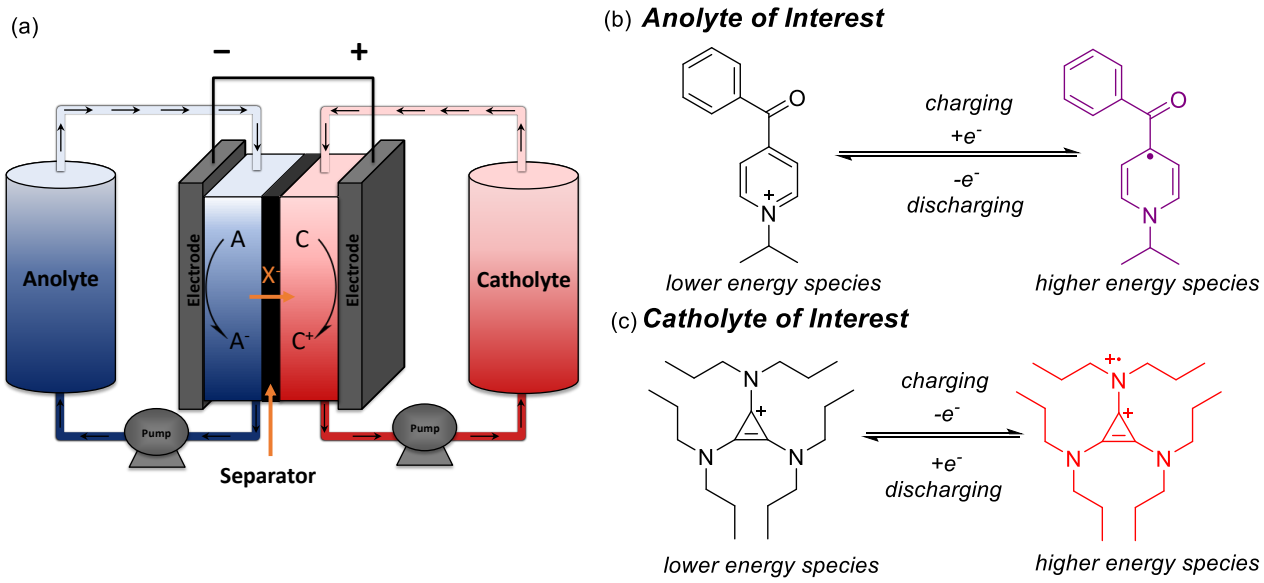

Figure 3.1. (a) A schematic representation of a redox flow battery during charge; (b) Pyridinium salts as anolyte of interest in this work; (c) Cyclopropenium salts as catholyte of interest in this work.

Although metal complexes and aqueous systems have been more commonly studied in the field, RFBs that consist of organic electrolytes in non-aqueous media have emerged over the last decade as particularly attractive targets. Non-aqueous solvents allow for operation under a wider potential window (~5 V vs 1.23 V for aqueous systems) as well as the ability to tailor the structures/properties of the organic active species.[15–21] To that end, recent work has uncovered a variety of different organic anolyte and catholyte candidates with promising individual properties (e.g., redox potentials, cycling stabilities, solubilities).[22–26] Nonetheless, the integration of organic anolyte/catholyte pairs into fully

operating non-aqueous flow batteries remained a significant challenge. This is because RFBs containing two different active materials often suffer from chemical/electrochemical compatibility issues, resulting in parasitic decay of the electrolytes.[27–32] While numerous examples of electrolyte incompatibility have been reported, to date, few strategies have been developed to fully characterize and mitigate these processes.[22–26]

Pyridinium salt (**Py1**[23]) and cyclopropenium salt (**CP**[22,24]) had been well studied in our group as a anolyte and catholyte candidates, respectively (Figure 3.1b). These electrolytes meet the preliminary requirements of having desirable redox properties, high solubility, and high stability in electrochemical half-cell cycling tests. However, all of these experiments were conducted for the individual molecules, independent of one another. This chapter describes a detailed investigation to study this anolyte/catholyte pair in a prototype flow cell. Electrochemical and chemical compatibility of this pair of electrolytes is tested. As described below, initial studies employing these electrolytes in a flow cell showed extensive parasitic decomposition. To address this issue, a systematic study was conducted to understand the mechanism of this decomposition and explore avenues to mitigate it. A detailed analysis of the decay pathways is presented, and these insights are used to design new electrolytes that mitigate this process. Ultimately, next-generation electrolytes are demonstrated that exhibit an order-of-magnitude enhancement in capacity retention during flow cell cycling.

3.2. Results and Discussion

3.2.1. Symmetric Redox Flow Battery

Py1 and **CP** each underwent stable individual cycling in half-cell experiments with MeCN as solvent and KPF_6 as the supporting electrolyte (>200 charge-discharge cycles over 36-48 h).[22–26] As such, the logical next step was to pair these materials in a flow cell. The standard configuration for a non-aqueous flow battery involves an equimolar mixture of anolyte/catholyte on both sides of the cell in conjunction with a microporous separator (Figure 3.2, symmetric).[33–36] This symmetric configuration requires compatibility between the anolyte/catholyte pair, which can be preliminarily assessed via cyclic voltammetry (CV).[33–36] The CV of a 1:1 mixture of **Py1** and **CP** (5 mM in MeCN/KPF_6) showed no difference in the peak position, shape and/or reversibility of electron transfer from the

individual CVs of each of the molecules (Figure 3.3). Furthermore, minimal change was observed after conducting the experiment for 10 CV cycles. This indicated that the two electrolytes of interest are compatible on the CV timescale.

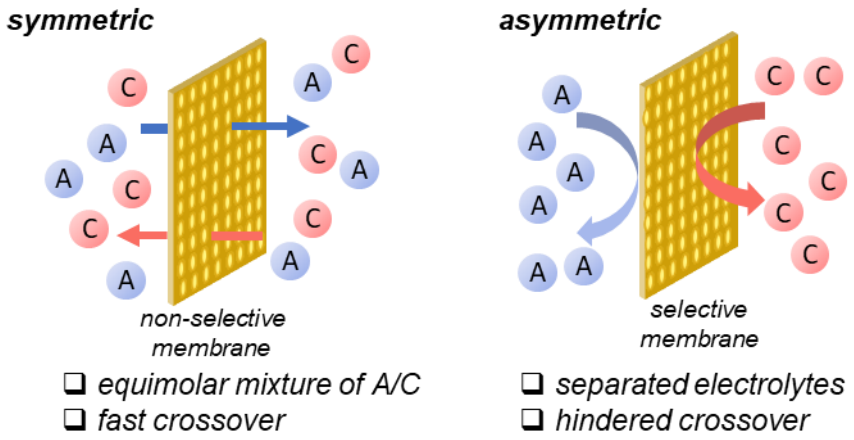

Figure 3.2. Symmetric and asymmetric configuration for a redox flow battery operation (A = anolyte and C = catholyte).

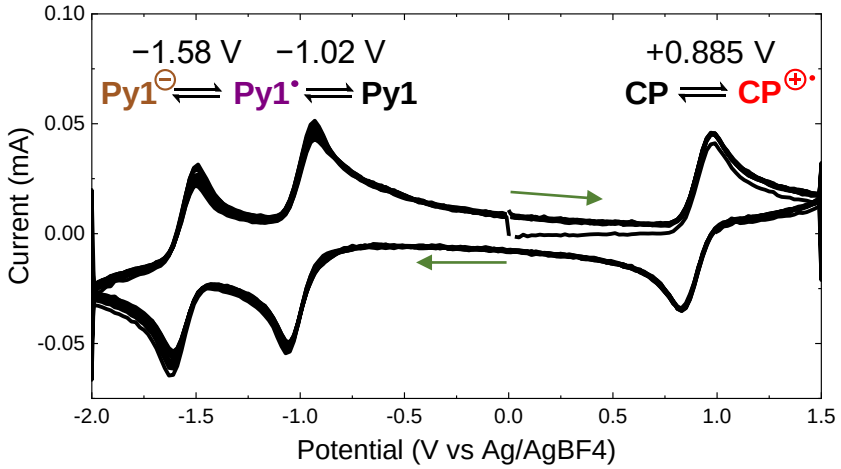

Figure 3.3. Cyclic Voltammogram of Py1 and CP for 10 continuous cycles. The cyclic voltammogram was conducted using glassy carbon as working electron, platinum wire as counter electrode and $Ag/AgBF_4$ as reference electrode in a solution of KPF_6 as supporting electrolyte and MeCN as solvent.

With the promising result from the CV experiment in hand, a flow cell with a 1:1 mixture of **Py1** and **CP** was constructed.[i] This flow cell[37,38] consisted of graphite charge collecting plates with an interdigitated flow field, in combination with 400 µm thick carbon felt electrodes and a microporous Celgard 2500 separator. The electrolyte solutions were flowed from the reservoir at the rate of 10 mL/min to the electrochemical chamber, where it was subjected to galvanostatic cycling at 10 mA/cm^2 over one redox couple of **Py1** (at -1.02 V vs Ag/Ag$^+$). This results in a cell potential of 1.90 V. As shown in Figure 3.4, despite the promising CV data, this system showed modest cycling performance. It initially charged to just 62% of the theoretical capacity and then faded by 62% over 55 h of cycling (Figure 3.4a). CV analysis of the spent solutions showed that the observed fade was likely due to decomposition of the anolyte (Figure 3.4b). In the CVs obtained after the experiment, the peak corresponding to cyclopropenium salt remained intact and reversible, while the peak corresponding to the pyridinium salt had greatly diminished in magnitude and exhibited an irreversible electron transfer event. Additionally, a new peak appeared at a potential lower than that of the pyridinium **Py1** (Figure 3.4b).

(i) The set-up was designed and parts constructed by Dr. Koen H. Hendriks.

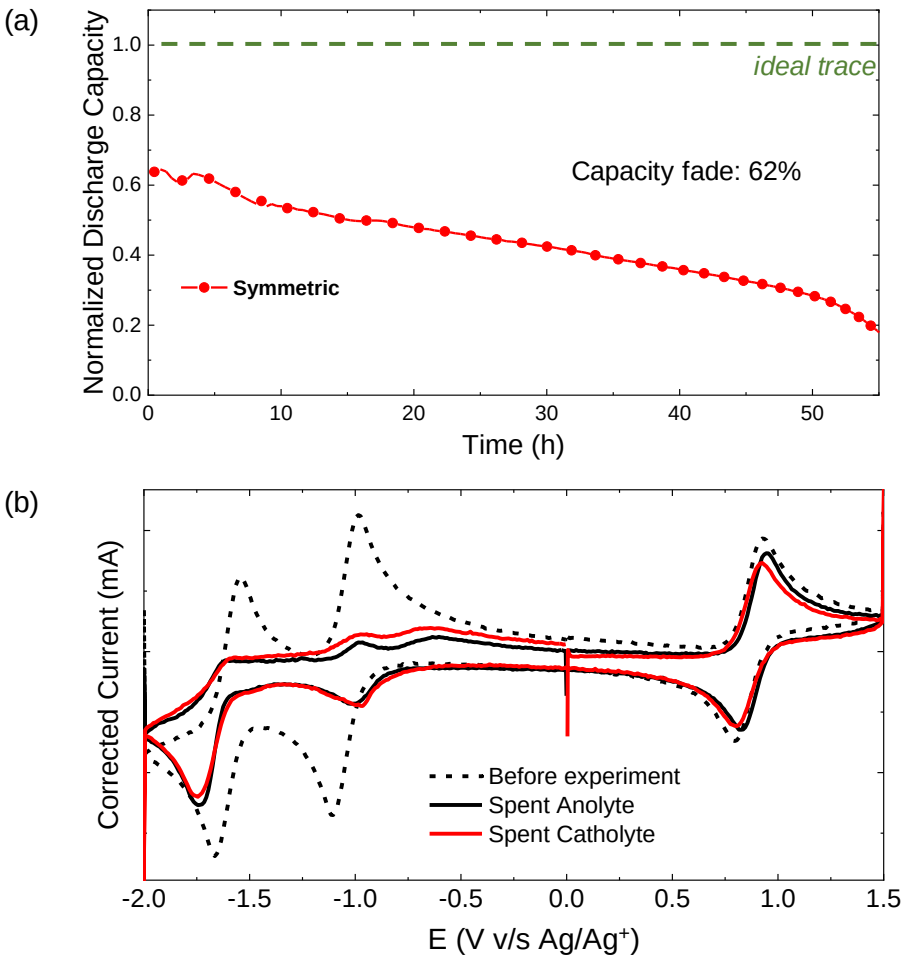

Figure 3.4. (a) Symmetrical electrochemical cycling of **Py1/CP** in a prototype RFB. Experiment conducted with each reservoir containing 6 mL of a 50 mM solution of both of the redox active species in 0.5 M KPF_6 in acetonitrile. The solutions were flowed at 10 mL/min, and the battery was charged/discharged with a current density of 10 mA/cm^2. Normalized discharge capacity (normalized against maximum theoretical capacity) is plotted against time; (b) Cyclic voltammetry of the solution before the symmetrical cycling experiment (dotted black line), of solution in anolyte (solid black line) and catholyte (solid red line) chamber after the cycling experiment.

Initial efforts thus focused on characterization of the anolyte decomposition pathway(s). In order to pinpoint the pathways through which the pyridinium salt was decomposing in solution, it was critical to identify the products of decomposition. For this, tools such as one- and two-dimensional NMR spectroscopic analysis of the spent

electrolyte solutions was useful. The ^{1}H NMR spectrum of the spent solution showed loss of 74% of the starting anolyte **Py1**. Based on the ^{1}H NMR spectrum, **Py1** had transformed into a mixture of two species with a ratio of 3 : 1 (Figure 3.4a). Upon further evaluation and independent synthesis of the compounds, the two species in solution were identified as: **Py1-OH** as the major species (57% in the spent solution) and **Py1-H$_2$** as the minor species (18% in the spent solution) as depicted in Figure 3.4.[ii,iii] It was hypothesized that **Py1-OH** derived from a two proton/two electron reduction of **Py-1**, while **Py1-H$_2$** derived from a subsequent two proton/two electron reduction of **Py1-OH** followed by loss of water (Figure 3.4b).[iv,39–41] Similar protonative decomposition of electrolytes containing carbonyl functional groups had been previously invoked in the literature, but no chemical solution to this problem had been developed.

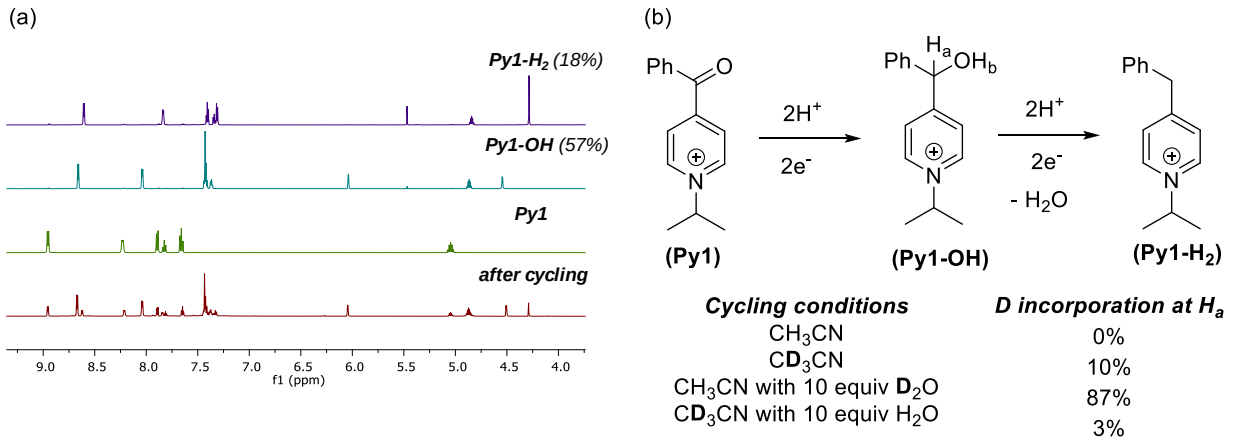

Figure 3.5. (a) Identification of anolyte decomposition through ^{1}H NMR spectra analysis of the spent solution (after cycling) and comparative analysis of the spent solution with the independently synthesized **Py1-OH** and **Py1-H$_2$**. (b) Pathway for anolyte decomposition during the electrochemical cycling and deuterium labeling experiments to

(ii) Both the decomposed compounds are reoxidized to ketone in presence of air.

(iii) Control experiments revealed that neither **A-1** nor **A-1**$^{\bullet}$ decomposes to **A-1 OH** or **A-1 H$_2$** when stored for 96 h in 0.5 M KPF_6 in MeCN. Furthermore, no decomposition is observed over this timescale during half-cell electrochemical cycling of **A-1**. Leventis et al. have reported on similar decomposition products for pyridinium salts in the presence of proton donors. Bulk electrolysis in the presence of superstoichiometric amounts of strong acids (5 equiv), such as acetic acid, led to quantitative conversion to the alcohol.

(iv) Protonation has frequently been invoked as a parasitic reaction leading to decomposition of ROMs, particularly those containing a carbonyl moiety. See ref. 39–41.

identify the source of anolyte decomposition. Deuterium labeling experiments were performed in a symmetric system with **CP** as catholyte. **Py1-H_2** was not detected under these conditions.

Deuterium labeling studies were conducted to determine the origin of the protons in this system (Figure 3.5b). When CD_3CN was used as the solvent for cycling, 10% deuteration was detected at H_a of **Py1-OH**. In contrast, in CH_3CN with 10 equivalents of added D_2O under otherwise analogous conditions, 87% deuteration was observed. These results suggest that the protons predominantly derive from adventitious water, which we were unable to completely remove even upon rigorous drying of the electrolyte solutions. Importantly, the decomposition of **Py-1** to **Py1-OH** and **Py1-H_2** is greatly accelerated by the presence of oxidized **CP**. When **Py1** is subjected to flow cell cycling in CH_3CN under analogous conditions *but in the absence of **CP***, only traces of **Py1-OH** or **Py1-H_2** were detected.

3.2.2. Asymmetric Redox Flow Battery

The results above, showing that the decomposition of anolyte is accelerated in presence of catholyte, suggested that such decomposition could be attenuated by minimizing contact between anolyte and catholyte. This could be achieved through the implementation of an asymmetric cell (Figure 3.2), in which **Py1** and **CP** are physically separated during the electrochemical cycling. This asymmetric configuration required a membrane that could impede the crossover of redox active species across to the other half of the cell, while maintaining fast equilibration of charge-balancing ions. Since both the electrolytes of interest are cationic in nature, it was reasoned that they could be effectively separated using an organic-compatible anion exchange membrane (AEM)[42,v] such as Fumasep FAPQ-375-PP.[43,44] As such, an asymmetric flow battery was assembled with 50 mM solutions of **Py1** and **CP** separated by Fumasep FAPQ-375-PP.[vi] Encouragingly, this system showed improved cycling performance relative to the original symmetric cell (compare black trace to red trace in Figure 3.6a). It initially charged to

(v) The idea of using an anion-exchange membrane was conceived during the discussions with Prof. Matthew S. Sigman, Prof. Shelley D. Minteer, Dr. Christo Sevov and Dr. Koen H. Hendriks.

(vi)This experiment was done in collaboration with Dr. Koen H. Hendriks.

>80% of the theoretical capacity and then faded by 50% over 96 h of cycling. ^{1}H NMR spectroscopic analysis of the spent electrolyte solutions revealed a significant enhancement in anolyte stability in this asymmetric system. Only 26% decomposition of **Py1** was observed over the 96 h of cycling, which compares favorably to 74% decomposition over just 55 h of cycling in the symmetric RFB. Instead, the major cause of capacity loss is crossover of the active species through the AEM. CV analysis of the spent solutions shows 30% crossover of **CP** and 26% crossover of **Py1** over 96 h of cycling (Figure 3.6b).

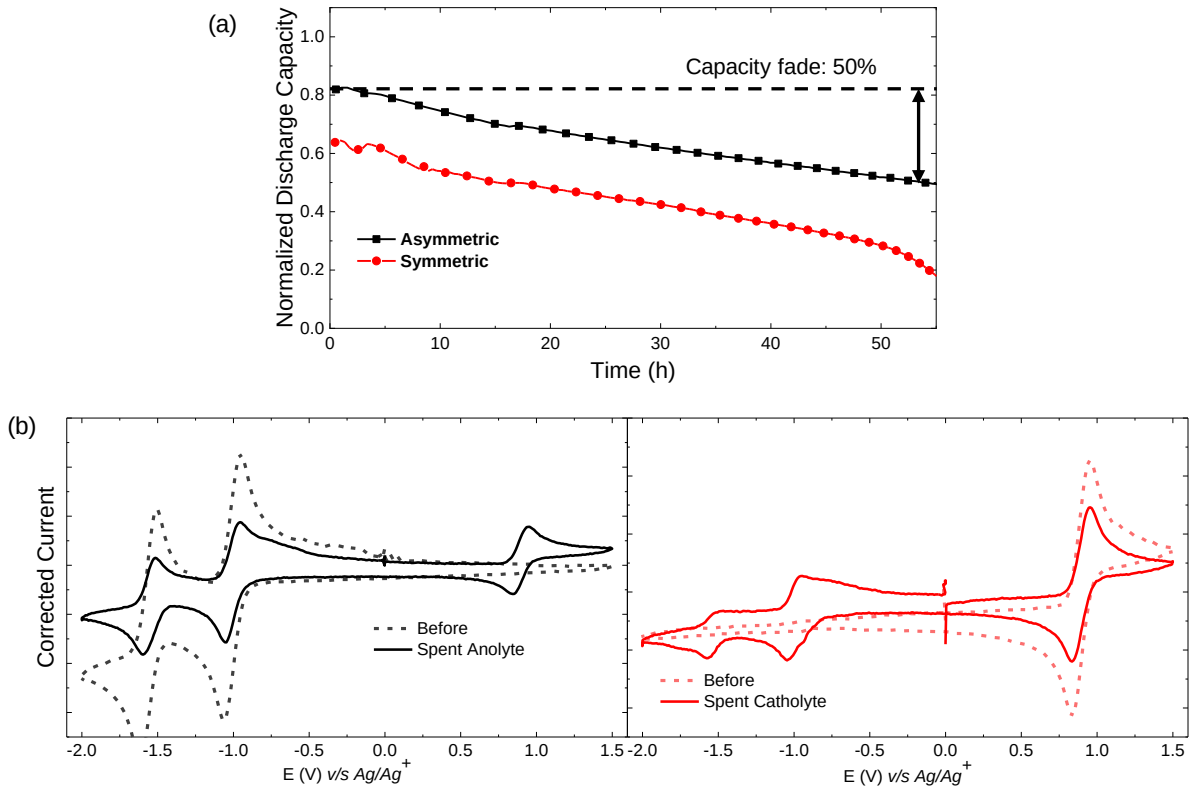

Figure 3.6. (a) Comparison of asymmetric electrochemical cycling of **Py1**/**CP** in a prototype RFB (black trace) to the symmetric cycling (red trace). Experiment conducted with each reservoir containing 6 mL of a 50 mM solution of each of the redox active species in their respective chambers with 0.5 M KPF_6 in acetonitrile. The solutions were flowed at 10 mL/min, and the battery was charged/discharged with a current density of 10 mA/cm^2. Normalized discharge capacity (normalized against maximum theoretical capacity) is plotted against time; (b) Comparison of cyclic voltammogram of the solution before the cycling experiment (dotted lines) to the solution obtained after the experiment

(solid lines) for both anolyte (black) and catholyte (red) solutions. These CVs are a clear indication of crossover of electrolytes during the cycling experiment.

Scheme 3.1. Molecular design to identify a new generation of (a) catholyte (**CP**) to trimer (**CP-tri**) and (b) anolyte (**Py1**) to dimer (**Py1-di**) to prevent crossover.

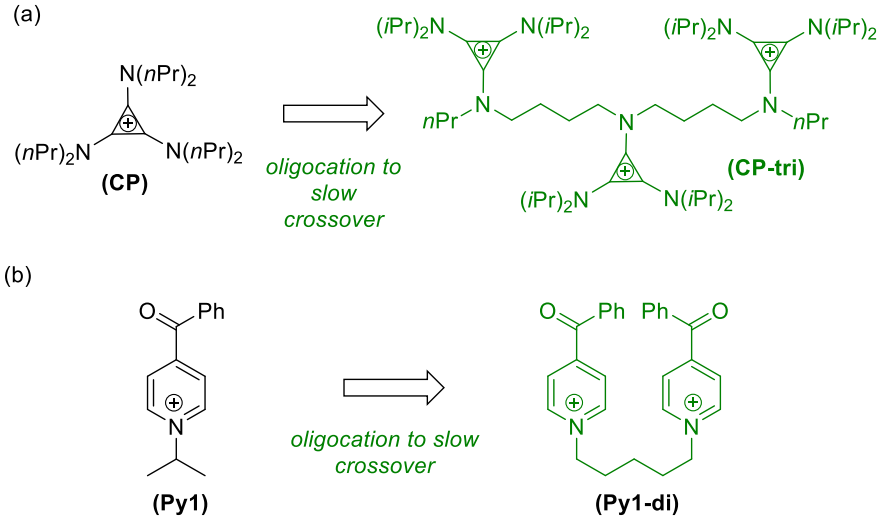

It was hypothesized that the crossover could be impeded by moving from the monocationic monomeric electrolytes to polycationic oligomers, which should exhibit enhanced electrostatic repulsions with the AEM. Recent literature has shown that oligomeric cyclopropenium derivatives containing C_4-hydrocarbon linkers (e.g., such as **CP-tri** in Scheme 3.1) maintain comparable electrochemical and solubility properties to their monomeric congeners.[24,45,46] Thus, we targeted **CP-tri**[vii] in conjunction with the similarly designed pyridinium dimer **Py1-di** as second generation electrolytes for this system (Scheme 3.1).[1] Asymmetric cycling of **Py1-di**/**CP-tri** in a Fumasep FAPQ-375-PP-separated flow cell (Figure 3.7a, green data) yielded a RFB with an open circuit potential of 1.95 V. As anticipated, electrolyte crossover was significantly reduced in this system (Figure 3.7b). CV analysis of the spent solutions showed <3% crossover of **CP-tri** and approximately 10% crossover of **Py1-di** over the 96 h cycling experiment. Decomposition of the anolyte was also attenuated relative to the monomeric system (17%

(vii) **CP-tri** was synthesized in collaboration with Dr. Koen H. Hendriks.

versus 26%, respectively), but this decay was the leading cause of capacity fade in this second-generation asymmetric system.

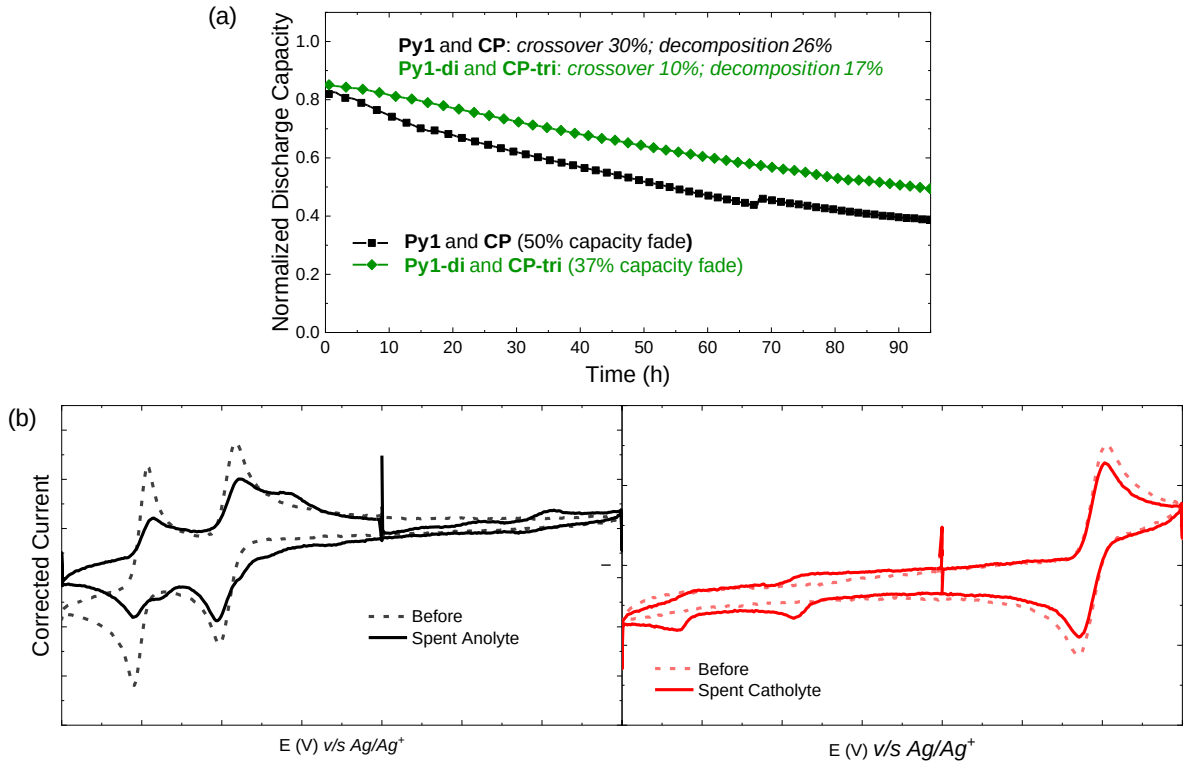

Figure 3.7. (a) Comparison of asymmetric electrochemical cycling of **Py1**/**CP** (black trace) and **Py1-di**/**CP-tri** (green trace) in a prototype RFB. Experiment conducted with each reservoir containing 6 mL of a 50 mM solution of the respective redox active species in 0.5 M KPF_6 in acetonitrile. The solution was flowed at 10 mL/min, and the battery was charged/discharged with a current density of 10 mA/cm^2. Normalized discharge capacity (normalized against maximum theoretical capacity) is plotted against time; (b) Comparison of cyclic voltammogram of the solution before the cycling experiment (dotted lines) to the solution obtained after the experiment (solid lines) for both anolyte (black) and catholyte (red) solutions.

A third-generation anolyte was then designed in order to limit decomposition of pyridinium during cycling. As discussed above, the conversion of **Py1** to **Py1-OH** involved a net two proton, two electron reduction, with the basic carbonyl moiety likely serving as the initial proton acceptor.[47] Thus, it was hypothesized that this undesired pathway could be attenuated by replacing the reactive carbonyl site with less basic malononitrile group

$(C(CN)_2)$.[48–53] Notably, malononitrile is pseudo-oxocarbon functionality.[48–53] The malononitrile-analog of **Py1-di** (**Py2-di**) was synthesized from **Py1-di** via a TiO_2-mediated

Scheme 3.2. Molecular design to identify a new generation of protected anolyte (**Py2-di**) to prevent anolyte decomposition.

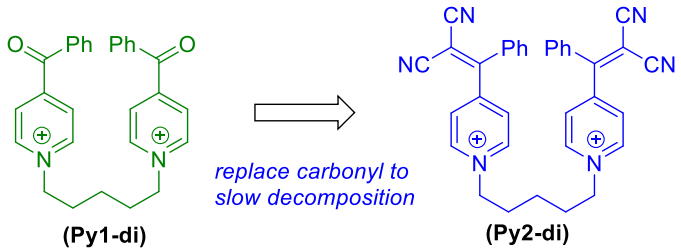

condensation reaction.[54] The cyclic voltammogram of **Py2-di** showed one electron redox couples at −0.626 V and −0.976 V vs Ag/Ag^+ (see Figure 3.9c). This represents a 0.4 V increase in the redox potential compared to the ketone analogue **Py1-di** (−1.01 V and −1.55 V vs Ag/Ag^+). However, as discussed below, this is accompanied by a large enhancement in cycling stability. Data for the asymmetric cycling of **Py2-di**/**CP-tri** in a Fumasep FAPQ-375-PP-separated flow cell is shown in Figure 3.8. This system yields an RFB with an open circuit voltage of 1.57 V. As a result of these modifications, <5% fade of capacity was detected over 96 h of cyclic (~200 charge-discharge cycles). This was largely due to the enhanced stability of **Py2-di** during cycling, as ^1H NMR spectroscopic analysis of the spent anolyte solution showed only traces (~3%) of products analogous to **Py1-OH**. Minimal crossover of the polycations **CP-tri** (<1%) or **Py2-di** (<3%) was detected during cycling.

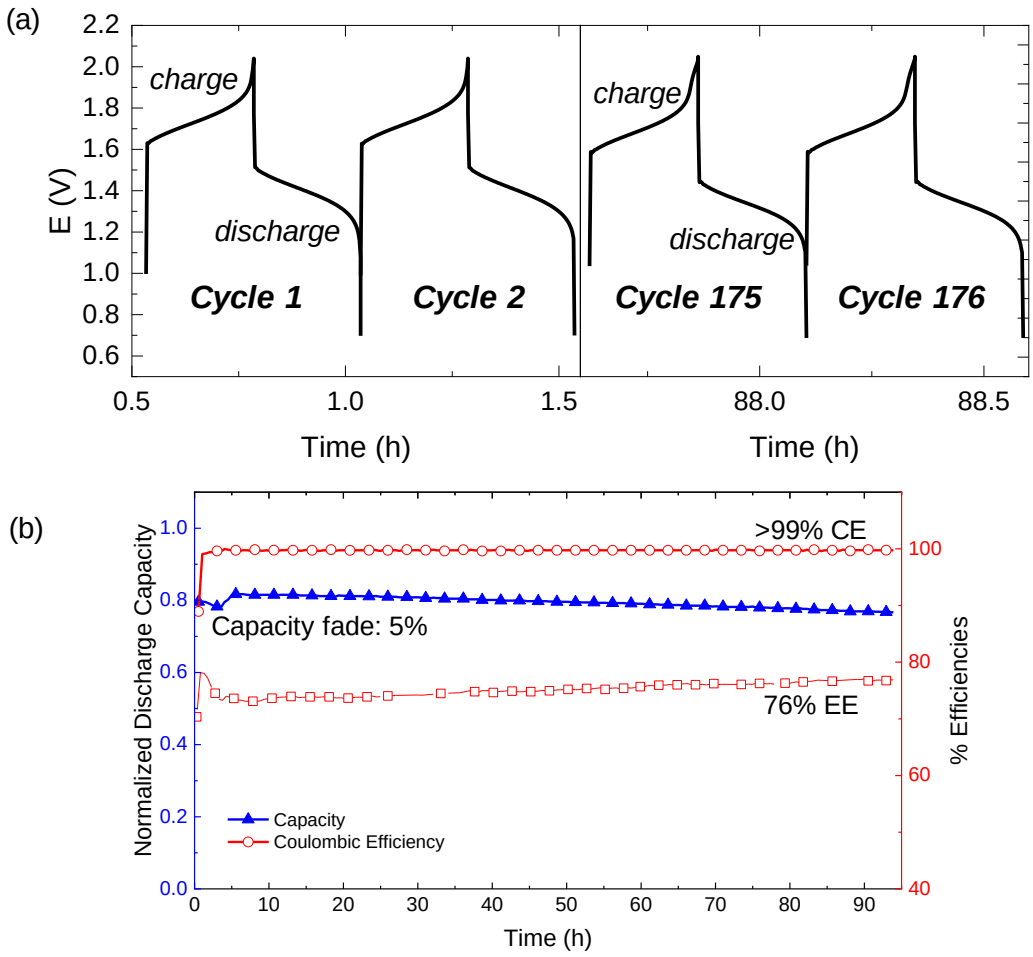

Figure 3.8. (a) Comparison of charge/discharge curves of early cycles (1-2) to later cycles (175-176) of the electrochemical cycling with **Py2-di**/**CP-tri**; (b) Electrochemical performance of **Py2-di**/**CP-tri** in asymmetric battery (blue trace). Experiment conducted with each reservoir containing 6 mL of a 50 mM solution of the respective redox active species in 0.5 M KPF_6 in acetonitrile. The solution was flowed at 10 mL/min, and the battery was charged/discharged with a current density of 10 mA/cm^2. Normalized discharge capacity (normalized against maximum theoretical capacity) is plotted against time. Coulombic efficiency (red circles) and energy efficiency (red squares) are also plotted against time.

3.3. Conclusion and Outlook

Overall, this chapter presents a mechanism-based approach to the molecular design of electrolytes for implementation in an asymmetric non-aqueous redox flow battery. Decomposition of the anolyte during battery cycling was demonstrated as a major

factor contributing to capacity fade in both symmetric and asymmetric systems. The asymmetric configuration helped to mitigate this decomposition but introduced crossover as another key factor that contributed to capacity fade. Two key modifications were required to achieve stable cycling of an asymmetric RFB in this system. First, oligomerization of the electrolytes generated oligocations that resisted crossover due to electrostatic repulsions with the anion exchange membrane. Second, proton-coupled anolyte decomposition was mitigated by the replacement of a basic carbonyl group in the anolyte scaffold. Overall, these studies demonstrated that detailed chemical analyses of RFB systems coupled with iterative design and synthesis of next generation electrolytes is an effective strategy for advancing electrolyte candidates for this application.

3.4. Experimental Details

3.4.1. Synthesis

3.4.1.1. ***Instrumental Information***

NMR spectra were recorded on a Varian vnmrs 700 (700 MHz for ^{1}H; 176 MHz for ^{13}C) or a Varian vnmrs 500 (500 MHz for ^{1}H; 126 MHz for ^{13}C) spectrometer with the residual solvent peak ($CDCl_3$; ^{1}H: δ = 7.26 ppm, ^{13}C: δ = 77.16 ppm; CD_3CN; ^{1}H: δ = 1.94 ppm, 13C: δ = 1.32 ppm) as the internal reference unless otherwise noted. Chemical shifts are reported in parts per million (ppm, δ) relative to tetramethylsilane. Multiplicities are reported as follows: s (singlet), d (doublet), t (triplet), q (quartet), and m (multiplet). Coupling constants (*J*) are reported in Hz. High-resolution mass spectra were recorded on a Micromass AutoSpec Ultima Magnetic Sector mass spectrometer. A multi-channel potentiostat from Bio-Logic Instruments (model VSP-CHAS) was used for all the electrochemical studies.

3.4.1.2. ***Materials and Methods***

All commercial reagents and solvents were used as received, unless otherwise noted. Anhydrous CH_2Cl_2 was obtained from an SDS solvent system. All reactions were performed under nitrogen atmosphere unless otherwise noted. Thin layer chromatography (TLC) was performed on Macherey-Nagel SIL G-25 TLC plates pre-coated with silica gel UV254. Biotage® SNAP Ultra column cartridges were used for flash

column chromatography. **Py1**,[23] **CP**,[22] and **CP-trimer**[24] were synthesized using previously reported procedures.

3.4.1.3. ***Synthesis of Py1-di***

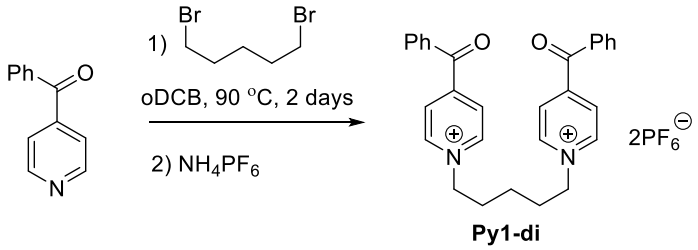

4-Benzoyl pyridine (2.20 g, 12.4 mmol, 4.0 equiv) was dissolved in *o*-dichlorobenzene (3 mL) in a 20 mL vial. 1,5-Dibromopentane (0.420 mL, 3.10 mmol, 1.0 equiv) was added. The vial was sealed with a Teflon-lined cap, and the reaction was stirred at 90 ºC for 2 d, during which time a pale-yellow precipitate formed. The precipitate was dissolved in CH_3CN (10 mL), and then CH_2Cl_2 (~60 mL) was added until a solid formed. The solid was collected and then taken up in an aqueous solution of NH_4PF_6 (2.53 g, 15.5 mmol, 5.0 equiv in 75 mL of water). This solution was extracted with 10% CH_3CN in CH_2Cl_2 (4 x 100 mL). The organic extracts were dried over $MgSO_4$ and concentrated under vacuum. The product was purified via three recrystallizations from boiling CH_3OH to yield **Py1-di** as a white crystalline solid (788 mg, 35% yield).

^{1}H NMR (500 MHz, CD_3CN) δ 8.87 (d, *J* = 6.3 Hz, 4H), 8.25 (d, *J* = 6.1 Hz, 4H), 7.91-7.86 (m, 4H), 7.83 (t, *J* = 7.5 Hz, 2H), 7.66 (t, *J* = 7.7 Hz, 4H), 4.63 (t, *J* = 7.6 Hz, 4H), 2.11 (dd, *J* = 9.0, 6.7 Hz, 4H), 1.52 (p, *J* = 8.2 Hz, 2H).

^{13}C NMR (176 MHz, CD_3CN) δ 191.76, 152.59, 145.44, 135.01, 134.31, 130.29, 129.16, 127.62, 61.63, 30.11, 22.13.

HRMS: $[M\text{-}PF_6]^+$ Calc. 581.1787, Measured: 581.1792

IR: 3131.89, 2954.84, 1664.16, 937.97 cm^{-1}

$E_{1/2}$: -1.01 V and -1.56 V vs Ag/Ag^+

3.4.1.4. ***Synthesis of Py2-di***

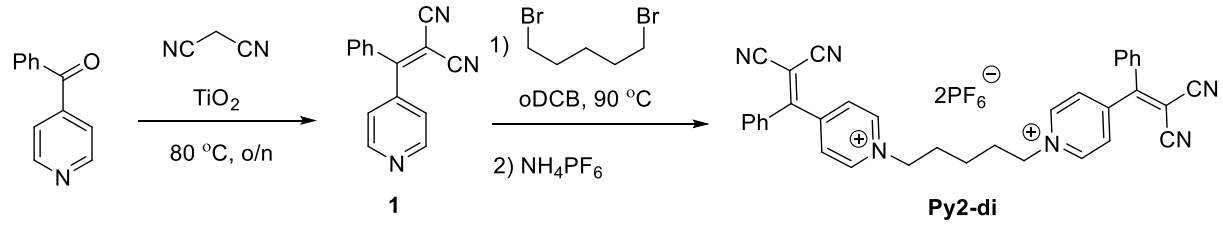

4-Benzoyl pyridine (4.00 g, 21.8 mmol, 1.0 equiv), malononitrile (1.44 g, 21.8 mmol, 1.0 equiv), and titanium dioxide (1.74 g, 21.8 mmol, 1.0 equiv) were combined in a vial. The vial was sealed with a Teflon-lined cap, and the neat reaction mixture was heated to 80 °C overnight. The resulting gray paste was cooled, the organics were dissolved in ethyl acetate, and the TiO_2 was removed by filtration. The filtrate was concentrated under vacuum, and the resulting solids were purified via flash chromatography on silica gel, eluting with a gradient of 0-20% ethyl acetate in CH_2Cl_2. The fractions containing the product were collected and concentrated under vacuum. The product was further purified via recrystallization from CH_3OH to afford **S1** as a white powder (3.33 g, 66% yield).

^{1}H NMR (700 MHz, CD_3CN) δ 8.82-8.78 (m, 2H), 7.84 (dd, *J* = 8.3, 1.4 Hz, 2H), 7.75-7.69 (m, 1H), 7.61-7.58 (m, 2H), 7.58-7.56 (m, 2H).

^{13}C NMR (176 MHz, CD_3CN) δ 171.85, 150.51, 143.73, 135.02, 132.95, 130.04, 129.02, 123.31, 113.45, 113.23, 84.97.

HRMS: Calc. 232.0869, Measured: 232.0870

IR: 3063.85, 2225.7, 1669.56, 820.74 cm^{-1}

Compound **S1** (800 mg, 3.46 mmol, 2.2 equiv) and dibromopentane (2.1 mL, 1.57 mmol, 1.0 equiv) were dissolved in *o*-dichlorobenzene (2 mL), and the reaction was heated at 90 °C for 3 d, during which time a pale yellow precipitate formed. The precipitate was dissolved in CH_3CN (10 mL), and then diethyl ether (150 mL) was added, resulting in the formation of a cream-colored precipitate. This precipitate was collected and then dissolved in an aqueous solution of NH_4PF_6 (1.28 g, 7.87 mmol, 5.0 equiv in 30 mL of water). The aqueous solution was extracted with 10% CH_3CN in CH_2Cl_2 (4 x 40 mL). The organic extracts were collected, dried over $MgSO_4$, and concentrated under vacuum. The

product was purified via five recrystallizations from CH_3CN/diethyl ether to afford **Py2-di** as a white solid (258 mg, 20% yield).

^{1}H NMR (700 MHz, CD_3CN) δ 8.82 (d, *J* = 6.6 Hz, 4H), 8.10 (d, *J* = 6.4 Hz, 4H), 7.77-7.72 (m, 2H), 7.63 (dd, *J* = 8.7, 7.2 Hz, 4H), 7.57-7.53 (m, 4H), 4.58 (t, *J* = 7.7 Hz, 4H), 2.10-2.08 (m, 4H), 1.52 (p, *J* = 7.8 Hz, 2H).

^{13}C NMR (176 MHz, CD_3CN) δ 166.96, 152.05, 145.54, 133.79, 133.49, 130.19, 129.41, 128.84, 112.63, 112.26, 87.93, 61.75, 29.95, 22.24.

HRMS: $[M\text{-}PF_6]^+$ Calc.: 677.2012, Measured: 677.2013

IR: 3071.52, 2234.32, 1641.44, 1557.29, 828.55 cm^{-1}

$E_{1/2}$: -0.626 V and -0.976 V vs Ag/Ag^+

3.4.1.5. ***Synthesis of Py1-OH***

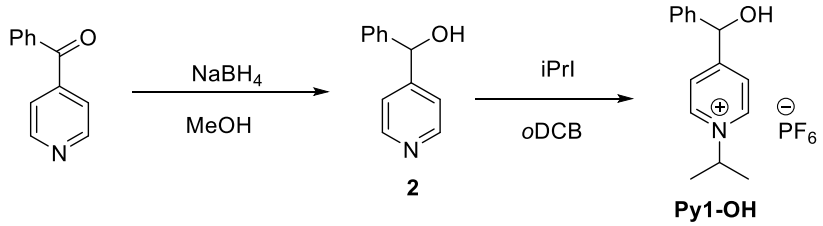

4-Benzoyl pyridine (200 mg, 1.09 mmol, 1.0 equiv) was dissolved in CH_3OH (3 mL). The solution was cooled to 0 °C, and $NaBH_4$ (53.7 mg, 1.41 mmol, 1.3 equiv) was added. The reaction was allowed to warm to room temperature and stirred under nitrogen for 3 h. The reaction was quenched by the addition of water (2 mL), and the resulting mixture was extracted with ethyl acetate (3 x 20 mL). The organic extracts were collected, dried over $MgSO_4$, and concentrated under vacuum. The product was further purified by tituration with hexanes (2 x 15 mL) to afford **S2** as a white solid (190 mg, 95% yield).

^{1}H NMR (700 MHz, CD_3CN) δ 8.52-8.49 (m, 2H), 7.40 (d, *J* = 6.9 Hz, 2H), 7.38-7.34 (multiple peaks, 4H), 7.31-7.27 (m, 1H), 5.79 (d, *J* = 3.8 Hz, 1H), 4.04-4.02 (m, 1H).

^{13}C NMR (176 MHz, CD_3CN) δ 153.53, 149.69, 143.88, 128.52, 127.63, 126.53, 121.04, 73.91.

HRMS: Calc. 186.0913, Measured: 186.0916

IR: 3133.56, 2825.64, 2723.77, 1597.69, 1063.47 cm^{-1}

Compound **S2** (189 mg, 1.02 mmol, 1.0 equiv) was dissolved in *o*-dichlorobenzene (0.22 mL). *iso*-Propyl iodide (0.74 mL, 7.43 mmol, 7.3 equiv) was added, and the mixture was heated at 50 °C overnight. The reaction was cooled to room temperature, the resulting paste was transferred to an Erlenmeyer flask using CH_3CN (5 mL), and diethyl ether (50 mL) was added, resulting in the formation of a precipitate. The precipitate was collected via filtration and dissolved in CH_2Cl_2 to afford a bright red solution. The organic layer was washed with a solution of NH_4PF_6 (499 mg, 3.06 mmol, 3.0 equiv) in 1 : 1 H_2O : brine (3 x 50 mL) after which the organic layer turned light yellow. The organic extracts were collected, dried over $MgSO_4$, and concentrated under vacuum. The product was purified via flash chromatography (0-15% CH_3OH in CH_2Cl_2) followed by recrystallization from boiling CH_3OH (x 2). **Py1-OH** was obtained as a white solid (258 mg, 68% yield).

^{1}H NMR (700 MHz, CD_3CN) δ 8.65-8.62 (m, 2H), 8.02 (d, *J* = 6.2 Hz, 2H), 7.43-7.38 (multiple peaks, 4H), 7.35 (ddt, *J* = 9.7, 5.7, 1.8 Hz, 1H), 6.02 (d, *J* = 3.3 Hz, 1H), 4.85 (hept, *J* = 6.8 Hz, 1H), 4.52 (d, *J* = 3.8 Hz, 1H), 1.60 (dd, *J* = 6.6, 2.3 Hz, 6H).

^{13}C NMR (176 MHz, CD_3CN) δ 165.25, 143.35, 142.62, 130.00, 129.63, 128.04, 126.20, 74.31, 65.58, 22.99.

HRMS: Calc. 228.1383, Measured: 228.1384

IR: 3134.73, 1635.87, 878.06 cm^{-1}

3.4.1.6. ***Synthesis of Py1-H_2***

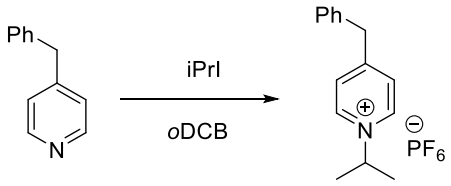

Py1-H_2

4-Benzyl pyridine (1.18 mmol, 200 mg, 1.0 equiv) was dissolved in *o*-dichlorobenzene (0.25 mL). *iso*-Propyl iodide (0.86 mL, 8.6 mmol, 7.3 equiv) was added, and the mixture was heated at 50 °C overnight. The reaction was cooled to room temperature, the creamy paste was transferred to an Erlenmeyer flask using CH_3CN, and diethyl ether (50 mL) was added leading to the formation of a precipitate. The precipitate was collected via filtration and then dissolved in CH_2Cl_2, affording a bright red solution. The organic layer was washed with NH_4PF_6 (32.4 mmol, 3 equiv) in 1 : 1 H_2O : brine (50

mL x 3) after which the solution turned light yellow. The organic extracts were collected, dried over $MgSO_4$, and concentrated under vacuum. The product was purified via flash chromatography (0-15% CH_3OH in CH_2Cl_2) followed by recrystallization from boiling ethyl acetate. The product, **Py1-H_2**, was obtained as white solid (307 mg, 73% yield).

^{1}H NMR (700 MHz, CD_3CN) δ 8.60 (d, *J* = 6.5 Hz, 2H), 7.84 (d, *J* = 6.2 Hz, 2H), 7.41 (t, *J* = 7.6 Hz, 2H), 7.34 (t, *J* = 7.4 Hz, 1H), 7.31 (d, *J* = 7.6 Hz, 2H), 4.84 (hept, *J* = 6.7 Hz, 1H), 4.28 (s, 2H), 1.61 (d, *J* = 6.7 Hz, 6H).

^{13}C NMR (176 MHz, CD_3CN) δ 163.12, 143.09, 138.09, 130.30, 130.14, 129.20, 128.41, 65.41, 41.66, 22.98.

HRMS: Calc. 212.1434, Measured: 212.1437

IR: 3570.84, 3071.27, 1672.30, 772.77 cm^{-1}

3.4.2. Electrochemistry and Cycling Studies

3.4.2.1. Materials and Methods

Acetonitrile (99.8% anhydrous) was obtained from Sigma Aldrich and used as received. Potassium hexafluorophosphate (≥99%) was obtained from Sigma Aldrich and dried under high vacuum at 100 °C for 48 h before use. 0.5 M stock solutions of KPF_6 in MeCN were prepared in a nitrogen-filled glovebox and dried over activated 3Å molecular sieves for at least two days prior to use. The molecular sieves were activated by heating at 200 °C under vacuum. All organic electrolytes were dried at 80 °C under high vacuum for 19 h before use and were then stored in an inert-atmosphere drybox.

For the laboratory-scale flow battery, a peristaltic pump (Cole-Parmer) was used in combination with Solveflex and PFA tubing. The cycling was performed with a zero-gap flow cell comprised of graphite charge-collecting plates containing an interdigitated flow field. Two layers of non-woven carbon felt electrodes, Sicracet 29AA, were used in each half-cell. ePTFE gaskets were used to achieve ~20% compression of the carbon felt. The exposed area of the membrane in the gasket window was used as the active area (2.55 cm^2). Fumasep FAPQ-375PP was purchased from FuMa-Tech and was ion exchanged prior to use by soaking pre-cut membranes in a saturated aqueous solution of KPF_6 (3 x 8-16 h). After each soak, the membrane was rinsed with deionized water. The membrane was stored outside the box, under ambient atmosphere. Prior to use, it

was dried *in vacuo*, at 50 °C, along with the rest of the glassware for battery cycling. A sample of Celgard 2500 was generously provided by Celgard LLC, and used without any further treatment.

3.4.2.2. ***General Procedure for Cyclic Voltammetry***

Cyclic voltammetry was performed in a nitrogen-filled drybox with a Biologic VSP multichannel potentiostat/galvanostat using a three-electrode setup. A glassy carbon electrode (0.07 cm^2, BASi) was used as the working electrode and a platinum wire was used as the counter electrode. An Ag/Ag^+ quasi-reference electrode (BASi) containing 0.01 M $AgBF_4$ (Sigma Aldrich) in 0.5 M KPF_6/MeCN was used. All potentials are referenced to Ag/Ag^+. The CVs were performed with a solution of 5 mM concentration of active species, a scan rate of 100 mV s^{-1}, using 0.5 M KPF_6 as supporting electrolyte in MeCN.

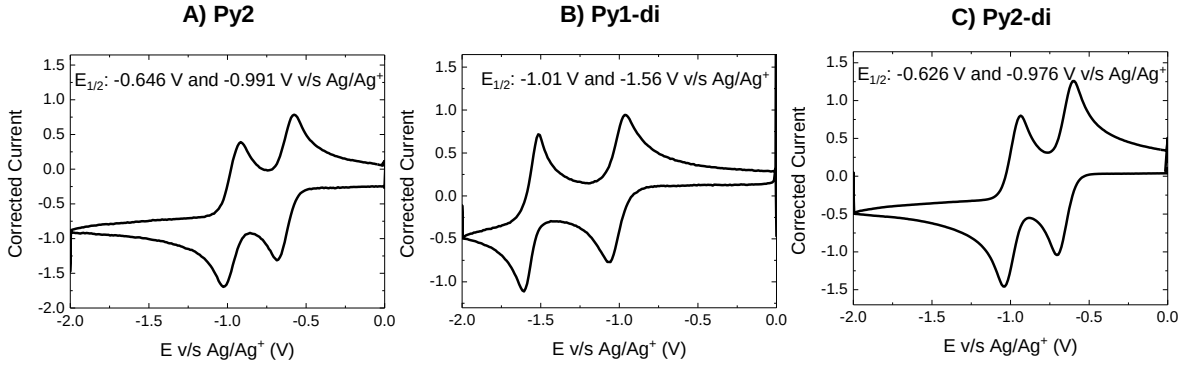

Figure 3.9. Representative cyclic voltammograms of **Py2**, **Py1-di** and **Py2-di** in MeCN with KPF_6 as a supporting electrolyte at 100 mVs^{-1}

3.4.2.3. ***General Procedure for Flow Cell Cycling***

All parts of the cell (including membrane, carbon felt electrodes, tubing) were dried in a vacuum oven at 50 °C overnight. The cell was assembled under ambient conditions and then brought into the glovebox. A 50 mM solution (per redox active unit) of the electrolyte was prepared in the glovebox using 0.5 M KPF_6 as the supporting electrolyte in MeCN (6 mL). To wet the membrane, the cell was pretreated by continuous flow of the electrolyte solution through the cell at 10 mL/min for 2 h. Electrochemical cycling was then performed under galvanostatic conditions using a BioLogic VSP galvanostat employing a charge/discharge current of 10 mA cm^{-2} (~4 C) using potential cutoffs of 1.7-

2.2 V during charge and 1.0-0.5 V during discharge. Under these conditions, the battery typically reached ~80% state of charge. EIS was performed from 500 kHz to 1 Hz at OCV using a 10 mV sine perturbation. Aliquots of the solution were taken before and after the experiments to determine crossover (by CV) and decomposition (by ^{1}H NMR). Fade of capacity was calculated by subtracting the measured charge capacity at the end of cycling from the measured charge capacity at cycle 0 and dividing that by the theoretical capacity (8 mAh).

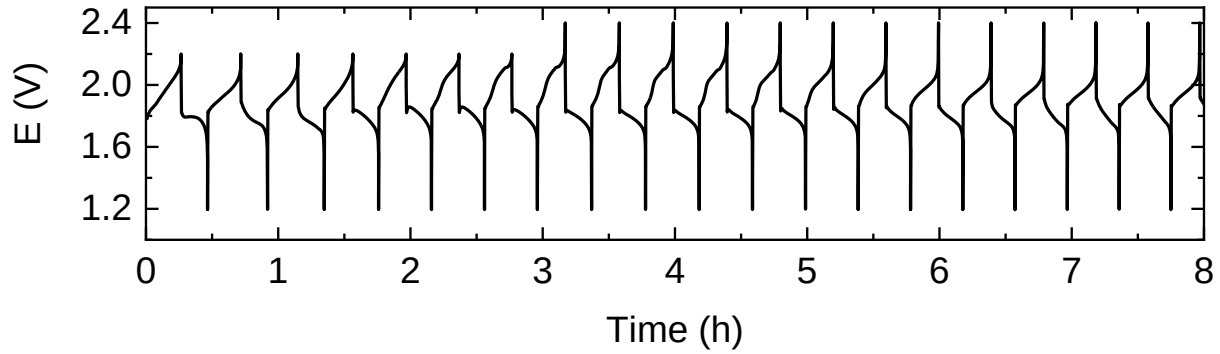

Figure 3.10. Flow cell cycling data showing the first few charge/discharge cycles of **Py1**/**CP** in a symmetric system

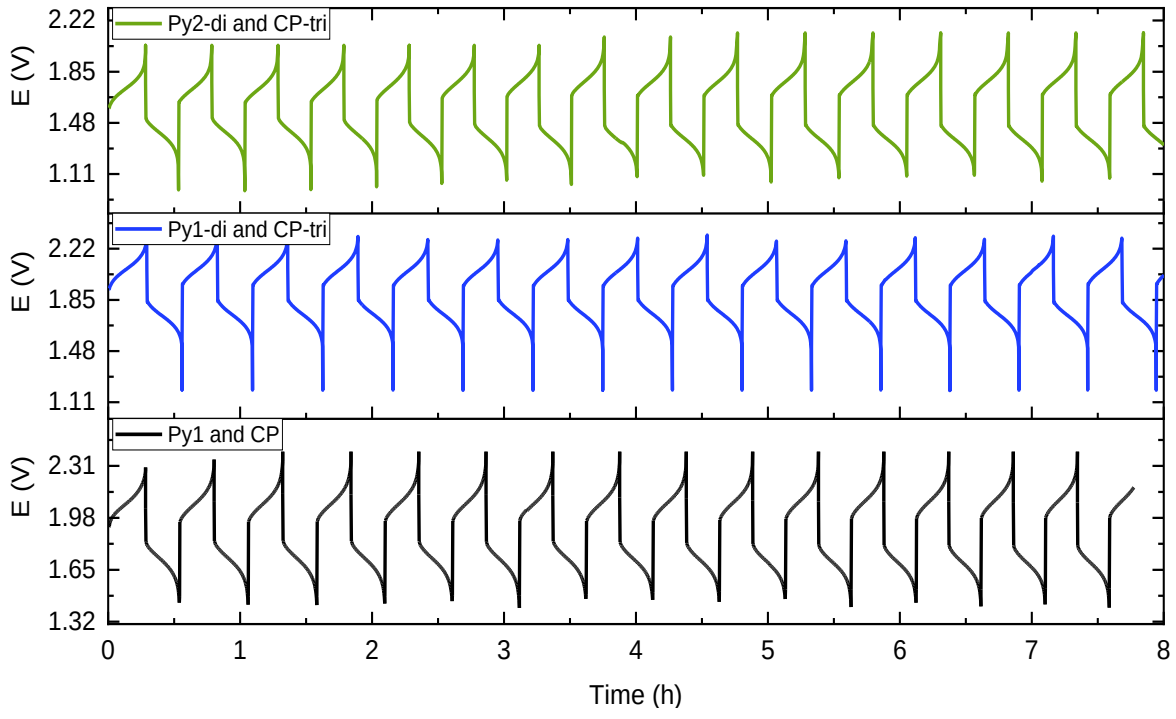

Figure 3.11. Flow cell cycling data showing the first few charge/discharge cycles for the asymmetric systems

3.4.2.4. ***Deuterium Labeling Experiments***

The deuterium labeling experiments conducted in custom glass H-cells equipped with stir bars and reticulated vitreous carbon (RVC) electrodes (100 ppi, ~70 cm^2 surface area, Duocell) in a nitrogen-filled glovebox with a BioLogic VSP galvanostat. A porous glass frit (P5, Adams and Chittenden) was used as a separator. H-cells, stir bars, and electrodes were dried in an oven at 150 °C for 30 min prior to use. A symmetrical configuration with 25 mM of each active species (5 mL in each chamber) was subjected on both halves of the cell. 0.5 M KPF_6 was used as a supporting electrolyte in CH_3CN or CD_3CN as solvent. Both chambers of the H-cell were stirred continously during the experiment. Electrochemical cycling was then performed under galvanostatic conditions employing a charge/discharge current of 1.2 mA cm^{-2} using potential cutoffs of 3.0 V during charge and 0.0 V during discharge.Three sets of experiments were run:

1. Using CD_3CN as a solvent and no added D_2O or H_2O
2. Using CH_3CN as the solvent and 10 equiv of D_2O added
3. Using CD_3CN as a solvent and 10 equiv of H_2O added

Integration of protons alpha to nitrogen was compared to that of H_a to track the amount of deuteration in the decomposition product.

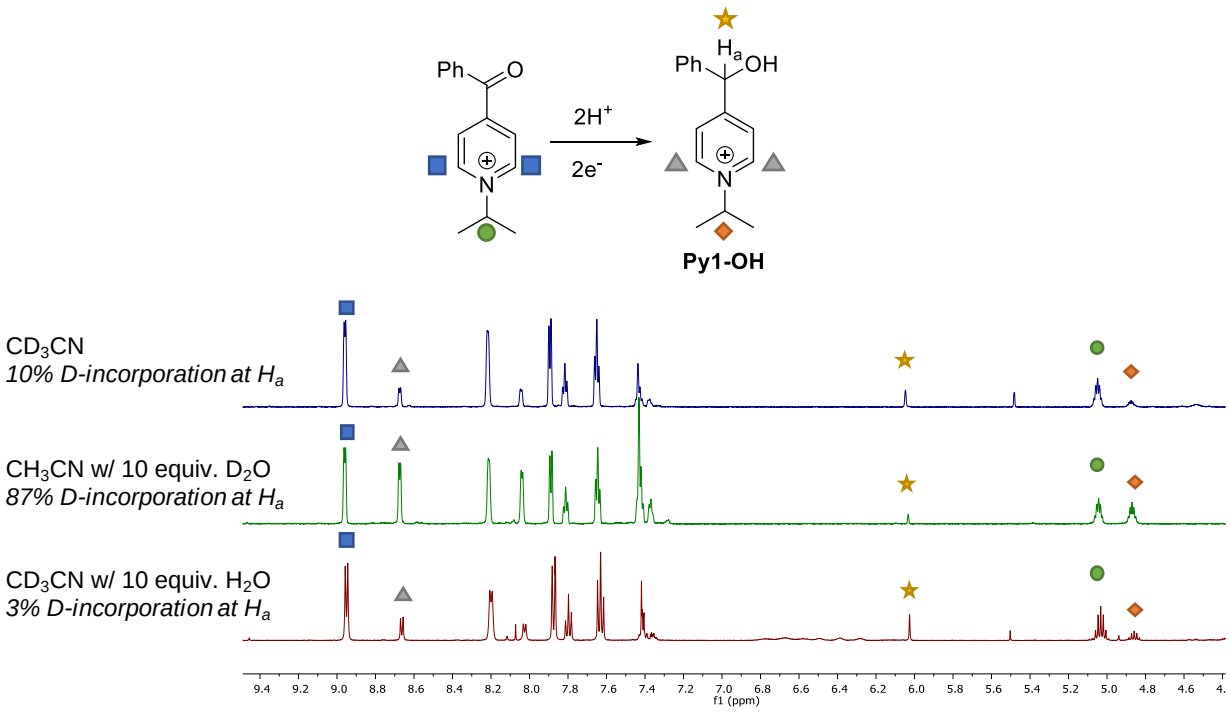

Figure 3.12. ^{1}H NMR of the deuterium labeling experiments

3.4.2.5. ***General Procedure for Determining Crossover***

An aliquot of known amount was taken out for analysis before the start of the cycling experiment and at the end of the experiment. These aliquots were analyzed by cyclic voltammetry to determine % crossover. Volumes of solutions on both sides of the cell were measured (to account for any solvent lost to evaporation or transfer between half-cells).

Quantification of Crossover:

ANOLYTE:

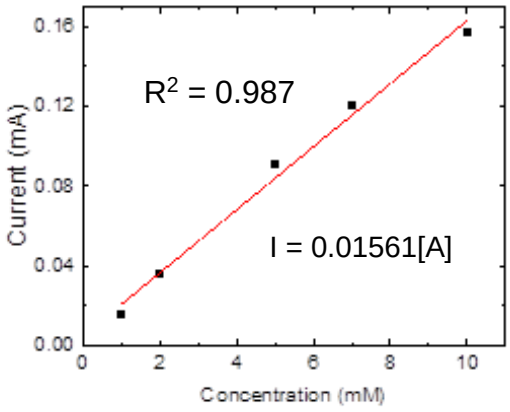

CATHOLYTE

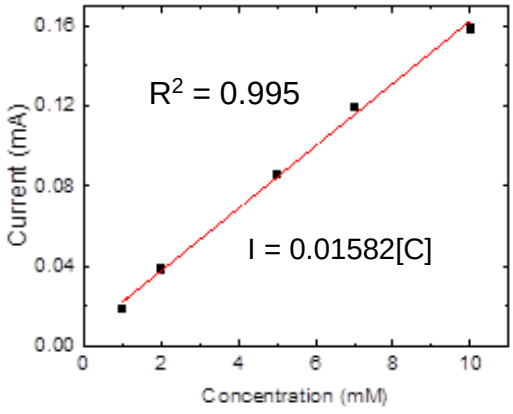

The aliquots collected at the beginning and end of the experiment were diluted with 0.5 M KPF_6 in MeCN solution (0.9 mL) and the cyclic voltammograms for each sample were measured. Calibration curves were used to calculate the concentration of this CV sample. This concentration was then normalized for the amount of aliquot taken out (by mass) and corrected for any volumetric change that occurred during the experiment (see calculation example below). Percent crossover was then calculated by dividing the concentration calculated for the blank side by the concentration of solution before the experiment.

To calculate crossover of CP monomer after 1 day of circulation:

-Mass of aliquot before experiment = 60 mg

-Mass of aliquot from crossover side after experiment = 61 mg

-Total volume of crossover side after the experiment = 5.67 mL

-Volumetric change = 5.67/6.0 = 0.945

*6.0 mL was the original volume of the solution

-CV peak height of sample before the experiment = 0.06659 mA. Concentration = 4.21 mM (by plugging peak height into the equation above)

-CV peak height of CV from the counter side sample after the experiment = 0.0175 mA. Concentration = 1.11 mM

-The peak heights were then normalized to their respective aliquot masses and the crossover calculated using the formula below.

$$\%crossover = \left(\frac{concentration(counter) * Volumetric\ change}{mass\ aliquot\ (counter)}\right) / \left(\frac{concentration(before)}{mass\ aliquote\ (before)}\right) * 100$$

For this example: Crossover = $\left(\frac{1.11*0.945}{61}\right) / \left(\frac{4.21}{60}\right) * 100$ = **24%**

When plotting the CVs, *corrected/normalized current* was plotted. Current was normalized by dividing the voltammogram by the mass of the aliquot and multiplying for volumetric change.

3.5 Spectroscopic Data

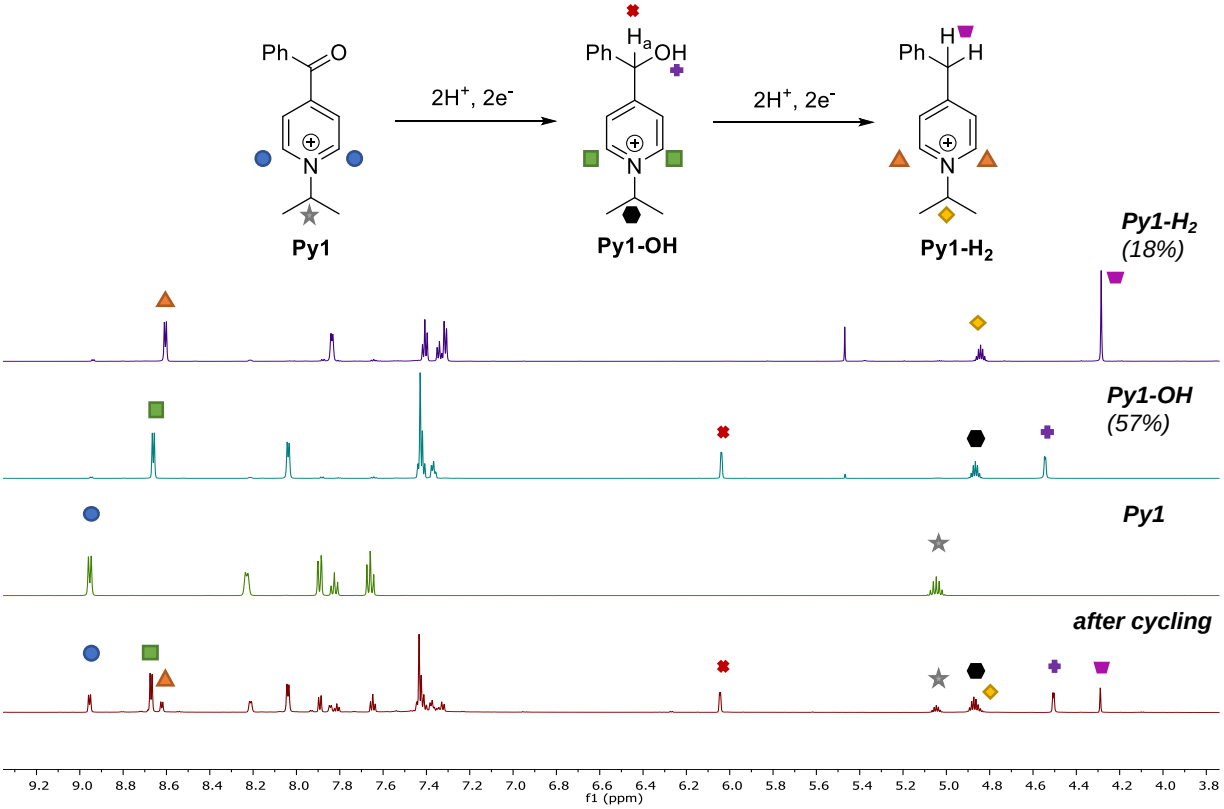

Figure 3.13. ^{1}H NMR spectra obtained after the symmetrical cycling experiment in Figure 1b along with independent spectra of **Py1**, **Py1-OH** and **Py1-H$_2$**.

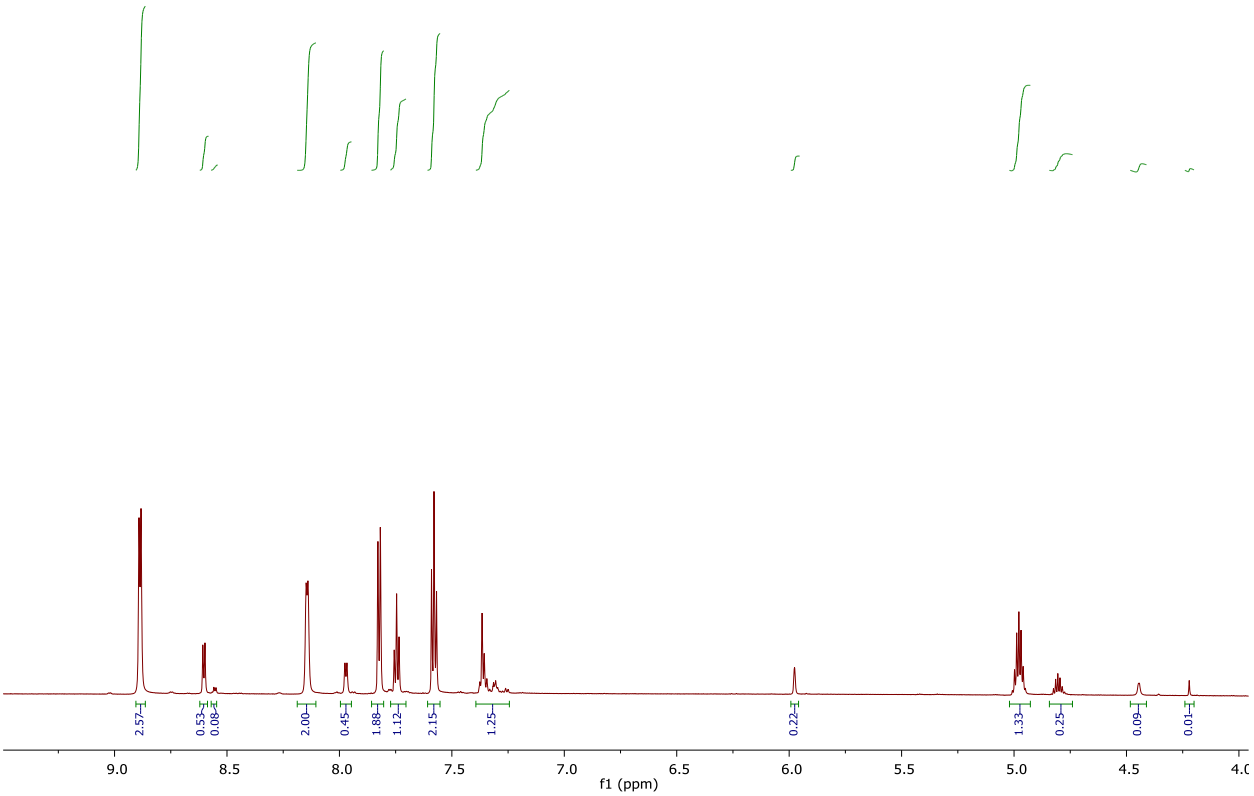

Figure 3.14. ^{1}H NMR spectrum of the anolyte solution after the electrochemical cycling of **Py1**/**CP** in asymmetric system (Figure 3.6, black)

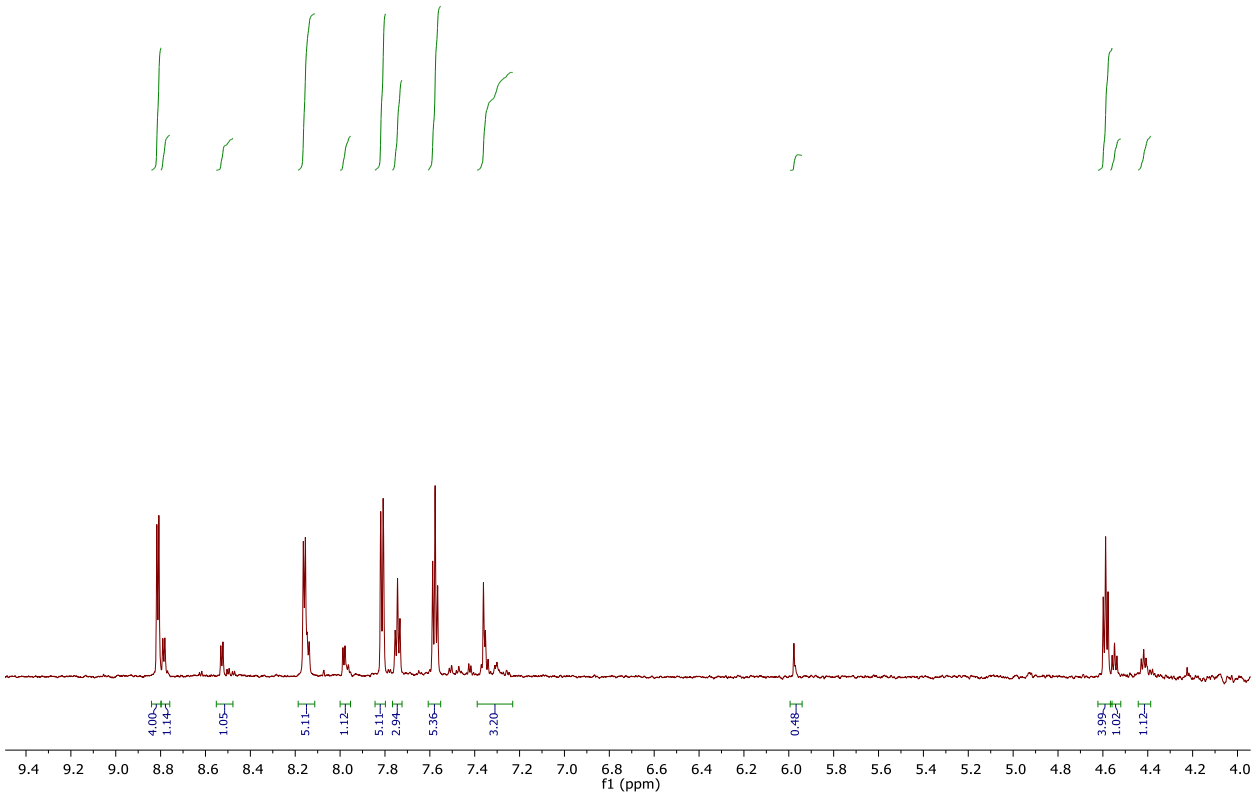

Figure 3.15. ^{1}H NMR spectrum of the anolyte solution after the electrochemical cycling of **Py1-di/CP-tri** in asymmetric system (Figure 3.7, green)

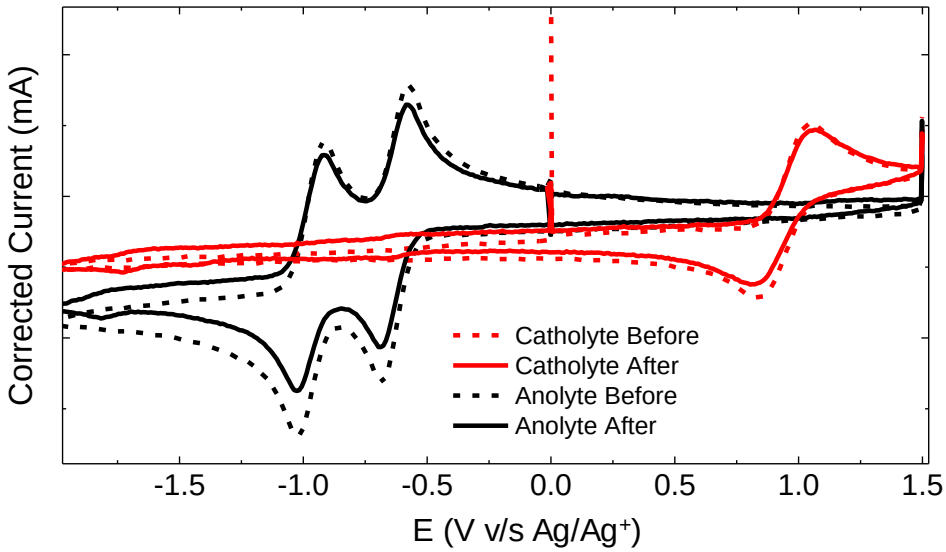

Figure 3.16. CVs after the cycling experiment with **Py2-di/CP-tri** (Figure 3.8)

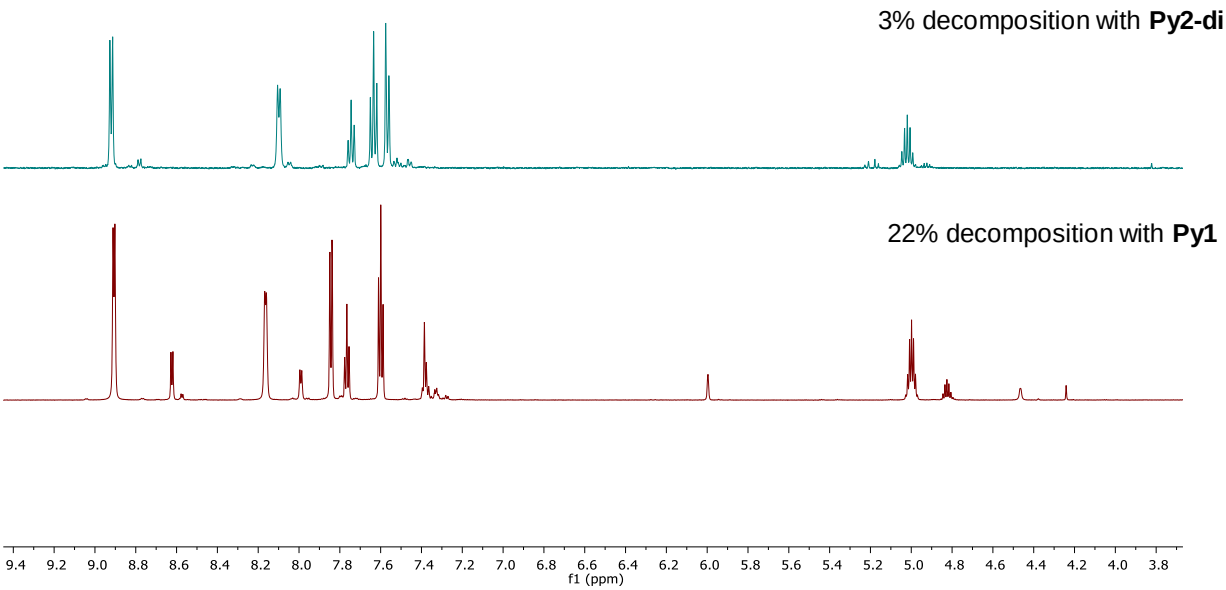

Figure 3.17. ^{1}H NMR spectra after the cycling experiments comparing **Py1/CP** to **Py2-di/CP-tri**

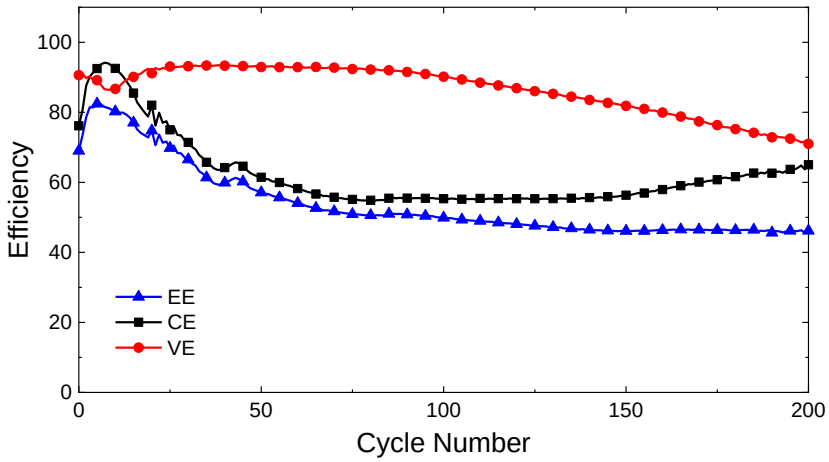

Figure 3.18. Coulombic (black), voltaic (red) and energy (blue) efficiencies of battery with **Py1/CP** in symmetric configuration

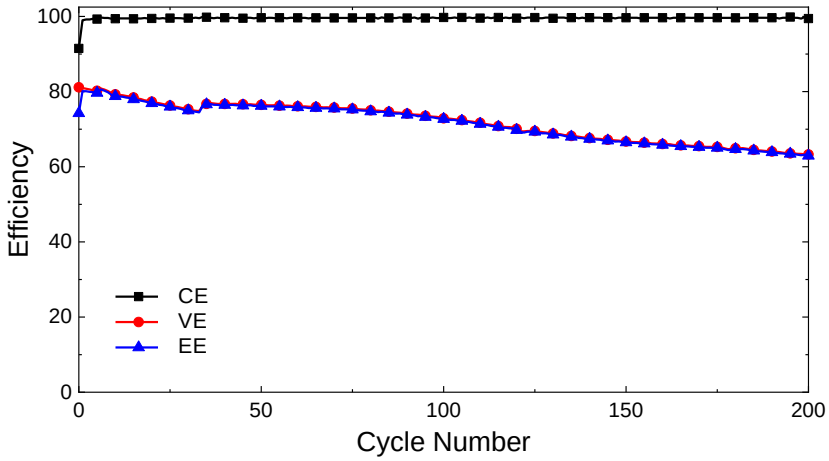

Figure 3.19. Coulombic (black), voltaic (red) and energy (blue) efficiencies of battery with **Py1/CP** in asymmetric configuration

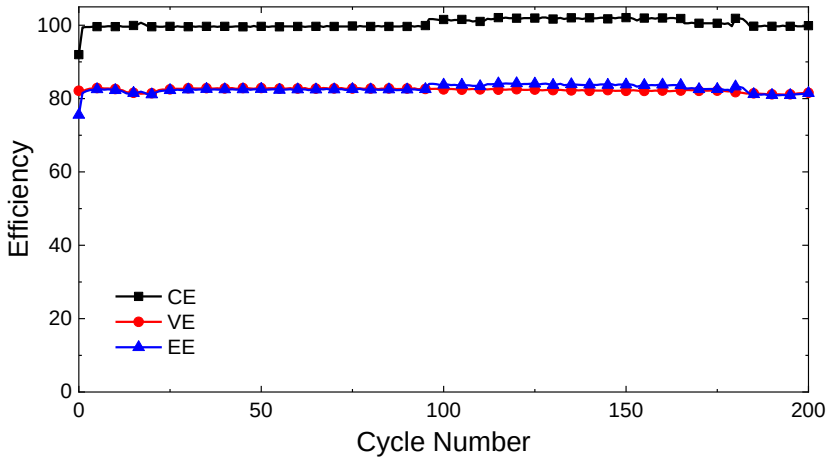

Figure 3.20. Coulombic (black), voltaic (red) and energy (blue) efficiencies of battery with **Py1-di/CP-tri** in asymmetric configuration

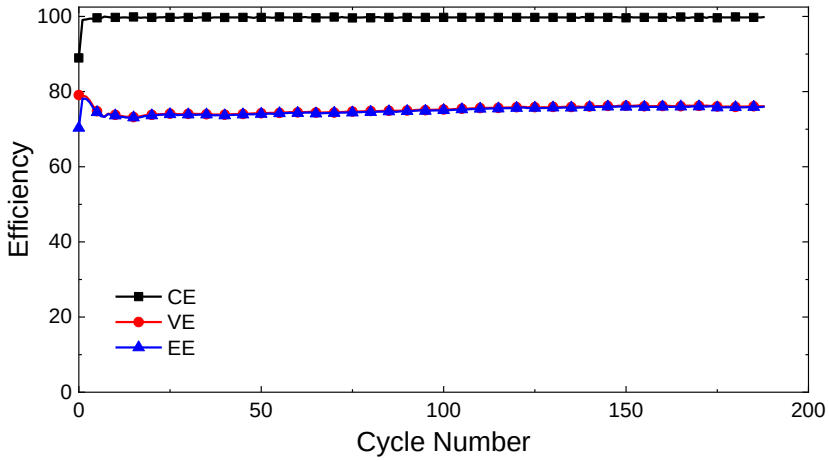

Figure 3.21. Coulombic (black), voltaic (red) and energy (blue) efficiencies of battery with **Py2-di/CP-tri** in asymmetric configuration

3.6 References

(1) Larcher, D.; Tarascon, J.-M. Towards Greener and More Sustainable Batteries for Electrical Energy Storage. *Nat. Chem.* **2015**, *7* (1), 19–29. https://doi.org/10.1038/nchem.2085.

(2) M. Gür, T. Review of Electrical Energy Storage Technologies, Materials and Systems: Challenges and Prospects for Large-Scale Grid Storage. *Energy Environ. Sci.* **2018**, *11* (10), 2696–2767. https://doi.org/10.1039/C8EE01419A.

(3) Soloveichik, G. L. Flow Batteries: Current Status and Trends. *Chem. Rev.* **2015**, *115* (20), 11533–11558. https://doi.org/10.1021/cr500720t.

(4) Wei, X.; Pan, W.; Duan, W.; Hollas, A.; Yang, Z.; Li, B.; Nie, Z.; Liu, J.; Reed, D.; Wang, W.; Sprenkle, V. Materials and Systems for Organic Redox Flow Batteries: Status and Challenges. *ACS Energy Lett.* **2017**, *2* (9), 2187–2204. https://doi.org/10.1021/acsenergylett.7b00650.

(5) Noack, J.; Roznyatovskaya, N.; Herr, T.; Fischer, P. The Chemistry of Redox-Flow Batteries. *Angew. Chem. Int. Ed.* **2015**, *54* (34), 9776–9809. https://doi.org/10.1002/anie.201410823.

(6) Rugolo, J.; Aziz, M. J. Electricity Storage for Intermittent Renewable Sources. *Energy Environ. Sci.* **2012**, *5* (5), 7151–7160. https://doi.org/10.1039/C2EE02542F.

(7) Winsberg, J.; Hagemann, T.; Janoschka, T.; Hager, M. D.; Schubert, U. S. Redox-Flow Batteries: From Metals to Organic Redox-Active Materials. *Angew. Chem. Int. Ed Engl.* **2017**, *56* (3), 686–711. https://doi.org/10.1002/anie.201604925.

(8) Kamat, P. V.; Schanze, K. S.; Buriak, J. M. Redox Flow Batteries. *ACS Energy Lett.* **2017**, *2* (6), 1368–1369. https://doi.org/10.1021/acsenergylett.7b00361.

(9) Ding, Y.; Zhao, Y.; Li, Y.; Goodenough, J. B.; Yu, G. A High-Performance All-Metallocene-Based, Non-Aqueous Redox Flow Battery. *Energy Environ. Sci.* **2017**, *10* (2), 491–497. https://doi.org/10.1039/C6EE02057G.

(10) Huskinson, B.; Marshak, M. P.; Suh, C.; Er, S.; Gerhardt, M. R.; Galvin, C. J.; Chen, X.; Aspuru-Guzik, A.; Gordon, R. G.; Aziz, M. J. A Metal-Free Organic–Inorganic Aqueous Flow Battery. *Nature* **2014**, *505* (7482), 195–198. https://doi.org/10.1038/nature12909.

(11) Lin, K.; Gómez-Bombarelli, R.; Beh, E. S.; Tong, L.; Chen, Q.; Valle, A.; Aspuru-Guzik, A.; Aziz, M. J.; Gordon, R. G. A Redox-Flow Battery with an Alloxazine-Based Organic Electrolyte. *Nat. Energy* **2016**, *1* (9), 1–8. https://doi.org/10.1038/nenergy.2016.102.

(12) Janoschka, T.; Martin, N.; Hager, M. D.; Schubert, U. S. An Aqueous Redox-Flow Battery with High Capacity and Power: The TEMPTMA/MV System. *Angew. Chem. Int. Ed Engl.* **2016**, *55* (46), 14427–14430. https://doi.org/10.1002/anie.201606472.

(13) Hu, B.; DeBruler, C.; Rhodes, Z.; Liu, T. L. Long-Cycling Aqueous Organic Redox Flow Battery (AORFB) toward Sustainable and Safe Energy Storage. *J. Am. Chem. Soc.* **2017**, *139* (3), 1207–1214. https://doi.org/10.1021/jacs.6b10984.

(14) Schon, T. B.; McAllister, B. T.; Li, P.-F.; Seferos, D. S. The Rise of Organic Electrode Materials for Energy Storage. *Chem. Soc. Rev.* **2016**, *45* (22), 6345–6404. https://doi.org/10.1039/C6CS00173D.

(15) Zhang, J.; Yang, Z.; Shkrob, I. A.; Assary, R. S.; Tung, S. on; Silcox, B.; Duan, W.; Zhang, J.; Su, C. C.; Hu, B.; Pan, B.; Liao, C.; Zhang, Z.; Wang, W.; Curtiss, L. A.; Thompson, L. T.; Wei, X.; Zhang, L. Annulated Dialkoxybenzenes as Catholyte Materials for Non-Aqueous Redox Flow Batteries: Achieving High Chemical Stability through Bicyclic Substitution. *Adv. Energy Mater.* **2017**, *7* (21), 1701272. https://doi.org/10.1002/aenm.201701272.

(16) Su, L.; Ferrandon, M.; Kowalski, J. A.; Vaughey, J. T.; Brushett, F. R. Electrolyte Development for Non-Aqueous Redox Flow Batteries Using a High-Throughput Screening Platform. *J. Electrochem. Soc.* **2014**, *161* (12), A1905. https://doi.org/10.1149/2.0811412jes.

(17) Wang, W.; Sprenkle, V. Redox Flow Batteries Go Organic. *Nat. Chem.* **2016**, *8* (3), 204–206. https://doi.org/10.1038/nchem.2466.

(18) Wang, W.; Luo, Q.; Li, B.; Wei, X.; Li, L.; Yang, Z. Recent Progress in Redox Flow Battery Research and Development. *Adv. Funct. Mater.* **2013**, *23* (8), 970–986. https://doi.org/10.1002/adfm.201200694.

(19) Winsberg, J.; Hagemann, T.; Muench, S.; Friebe, C.; Häupler, B.; Janoschka, T.; Morgenstern, S.; Hager, M. D.; Schubert, U. S. Poly(Boron-Dipyrromethene)—A Redox-Active Polymer Class for Polymer Redox-Flow Batteries. *Chem. Mater.* **2016**, *28* (10), 3401–3405. https://doi.org/10.1021/acs.chemmater.6b00640.

(20) Montoto, E. C.; Nagarjuna, G.; Moore, J. S.; Rodríguez-López, J. Redox Active Polymers for Non-Aqueous Redox Flow Batteries: Validation of the Size-Exclusion Approach. *J. Electrochem. Soc.* **2017**, *164* (7), A1688. https://doi.org/10.1149/2.1511707jes.

(21) Burgess, M.; Moore, J. S.; Rodríguez-López, J. Redox Active Polymers as Soluble Nanomaterials for Energy Storage. *Acc. Chem. Res.* **2016**, *49* (11), 2649–2657. https://doi.org/10.1021/acs.accounts.6b00341.

(22) Sevov, C. S.; Samaroo, S. K.; Sanford, M. S. Cyclopropenium Salts as Cyclable, High-Potential Catholytes in Nonaqueous Media. *Adv. Energy Mater.* **2017**, *7* (5), 1602027. https://doi.org/10.1002/aenm.201602027.

(23) Sevov, C. S.; Hickey, D. P.; Cook, M. E.; Robinson, S. G.; Barnett, S.; Minteer, S. D.; Sigman, M. S.; Sanford, M. S. Physical Organic Approach to Persistent, Cyclable, Low-Potential Electrolytes for Flow Battery Applications. *J. Am. Chem. Soc.* **2017**, *139* (8), 2924–2927. https://doi.org/10.1021/jacs.7b00147.

(24) Hendriks, K. H.; Robinson, S. G.; Braten, M. N.; Sevov, C. S.; Helms, B. A.; Sigman, M. S.; Minteer, S. D.; Sanford, M. S. High-Performance Oligomeric Catholytes for Effective Macromolecular Separation in Nonaqueous Redox Flow Batteries. *ACS Cent. Sci.* **2018**, *4* (2), 189–196. https://doi.org/10.1021/acscentsci.7b00544.

(25) Wei, X.; Xu, W.; Vijayakumar, M.; Cosimbescu, L.; Liu, T.; Sprenkle, V.; Wang, W. TEMPO-Based Catholyte for High-Energy Density Nonaqueous Redox Flow Batteries. *Adv. Mater.* **2014**, *26* (45), 7649–7653. https://doi.org/10.1002/adma.201403746.

(26) Hu, B.; Liu, T. L. Two Electron Utilization of Methyl Viologen Anolyte in Nonaqueous Organic Redox Flow Battery. *J. Energy Chem.* **2018**, *27* (5), 1326–1332. https://doi.org/10.1016/j.jechem.2018.02.014.

(27) Chen, Q.; Eisenach, L.; Aziz, M. J. Cycling Analysis of a Quinone-Bromide Redox Flow Battery. *J. Electrochem. Soc.* **2015**, *163* (1), A5057. https://doi.org/10.1149/2.0081601jes.

(28) Gerhardt, M. R.; Beh, E. S.; Tong, L.; Gordon, R. G.; Aziz, M. J. Comparison of Capacity Retention Rates During Cycling of Quinone-Bromide Flow Batteries. *MRS Adv.* **2017**, *2* (8), 431–438. https://doi.org/10.1557/adv.2016.667.

(29) Goulet, M.-A.; Tong, L.; Pollack, D. A.; Tabor, D. P.; Odom, S. A.; Aspuru-Guzik, A.; Kwan, E. E.; Gordon, R. G.; Aziz, M. J. Extending the Lifetime of Organic Flow Batteries via Redox State Management. *J. Am. Chem. Soc.* **2019**, *141* (20), 8014–8019. https://doi.org/10.1021/jacs.8b13295.

(30) Tong, L.; Jing, Y.; Gordon, R. G.; Aziz, M. J. Symmetric All-Quinone Aqueous Battery. *ACS Appl. Energy Mater.* **2019**, *2* (6), 4016–4021. https://doi.org/10.1021/acsaem.9b00691.

(31) Tong, L.; Goulet, M.-A.; Tabor, D. P.; Kerr, E. F.; De Porcellinis, D.; Fell, E. M.; Aspuru-Guzik, A.; Gordon, R. G.; Aziz, M. J. Molecular Engineering of an Alkaline Naphthoquinone Flow Battery. *ACS Energy Lett.* **2019**, *4* (8), 1880–1887. https://doi.org/10.1021/acsenergylett.9b01321.

(32) Zhang, J.; Shkrob, I. A.; Assary, R. S.; Tung, S. on; Silcox, B.; Curtiss, L. A.; Thompson, L.; Zhang, L. Toward Improved Catholyte Materials for Redox Flow Batteries: What Controls Chemical Stability of Persistent Radical Cations? *J. Phys. Chem. C* **2017**, *121* (42), 23347–23358. https://doi.org/10.1021/acs.jpcc.7b08281.

(33) Duan, W.; Huang, J.; Kowalski, J. A.; Shkrob, I. A.; Vijayakumar, M.; Walter, E.; Pan, B.; Yang, Z.; Milshtein, J. D.; Li, B.; Liao, C.; Zhang, Z.; Wang, W.; Liu, J.; Moore, J. S.; Brushett, F. R.; Zhang, L.; Wei, X. “Wine-Dark Sea” in an Organic Flow Battery: Storing Negative Charge in 2,1,3-Benzothiadiazole Radicals Leads to Improved Cyclability. *ACS Energy Lett.* **2017**, *2* (5), 1156–1161. https://doi.org/10.1021/acsenergylett.7b00261.

(34) Huang, J.; Duan, W.; Zhang, J.; Shkrob, I. A.; Assary, R. S.; Pan, B.; Liao, C.; Zhang, Z.; Wei, X.; Zhang, L. Substituted Thiadiazoles as Energy-Rich Anolytes for Nonaqueous Redox Flow Cells. *J. Mater. Chem. A* **2018**, *6* (15), 6251–6254. https://doi.org/10.1039/C8TA01059E.

(35) Huang, J.; Yang, Z.; Vijayakumar, M.; Duan, W.; Hollas, A.; Pan, B.; Wang, W.; Wei, X.; Zhang, L. A Two-Electron Storage Nonaqueous Organic Redox Flow Battery. *Adv. Sustain. Syst.* **2018**, *2* (3), 1700131. https://doi.org/10.1002/adsu.201700131.

(36) Wei, X.; Duan, W.; Huang, J.; Zhang, L.; Li, B.; Reed, D.; Xu, W.; Sprenkle, V.; Wang, W. A High-Current, Stable Nonaqueous Organic Redox Flow Battery. *ACS Energy Lett.* **2016**, *1* (4), 705–711. https://doi.org/10.1021/acsenergylett.6b00255.

(37) Milshtein, J. D.; Barton, J. L.; Darling, R. M.; Brushett, F. R. 4-Acetamido-2,2,6,6-Tetramethylpiperidine-1-Oxyl as a Model Organic Redox Active Compound for Nonaqueous Flow Batteries. *J. Power Sources* **2016**, *327*, 151–159. https://doi.org/10.1016/j.jpowsour.2016.06.125.

(38) Milshtein, J. D.; Kaur, A. P.; Casselman, M. D.; Kowalski, J. A.; Modekrutti, S.; Zhang, P. L.; Attanayake, N. H.; Elliott, C. F.; Parkin, S. R.; Risko, C.; Brushett, F. R.; Odom, S. A. High Current Density, Long Duration Cycling of Soluble Organic Active Species for Non-Aqueous Redox Flow Batteries. *Energy Environ. Sci.* **2016**, *9* (11), 3531–3543. https://doi.org/10.1039/C6EE02027E.

(39) Park, S.-K.; Shim, J.; Yang, J.; Shin, K.-H.; Jin, C.-S.; Lee, B. S.; Lee, Y.-S.; Jeon, J.-D. Electrochemical Properties of a Non-Aqueous Redox Battery with All-Organic Redox Couples. *Electrochem. Commun.* **2015**, *59*, 68–71. https://doi.org/10.1016/j.elecom.2015.07.013.

(40) Wei, X.; Xu, W.; Huang, J.; Zhang, L.; Walter, E.; Lawrence, C.; Vijayakumar, M.; Henderson, W. A.; Liu, T.; Cosimbescu, L.; Li, B.; Sprenkle, V.; Wang, W. Radical Compatibility with Nonaqueous Electrolytes and Its Impact on an All-Organic Redox Flow Battery. *Angew. Chem. Int. Ed.* **2015**, *54* (30), 8684–8687. https://doi.org/10.1002/anie.201501443.

(41) Naef, R. Polarographic Properties and Electrochemical Reduction of 1,2-Dimethyl-3-Indolyl Heteroaryl Ketones. *Helv. Chim. Acta* **1982**, *65* (6), 1734–1742. https://doi.org/10.1002/hlca.19820650608.

(42) Shin, S.-H.; Yun, S.-H.; Moon, S.-H. A Review of Current Developments in Non-Aqueous Redox Flow Batteries: Characterization of Their Membranes for Design Perspective. *RSC Adv.* **2013**, *3* (24), 9095–9116. https://doi.org/10.1039/C3RA00115F.

(43) Yan, Y.; Robinson, S. G.; Sigman, M. S.; Sanford, M. S. Mechanism-Based Design of a High-Potential Catholyte Enables a 3.2 V All-Organic Nonaqueous Redox Flow Battery. *J. Am. Chem. Soc.* **2019**, *141* (38), 15301–15306. https://doi.org/10.1021/jacs.9b07345.

(44) Robinson, S. G.; Yan, Y.; Hendriks, K. H.; Sanford, M. S.; Sigman, M. S. Developing a Predictive Solubility Model for Monomeric and Oligomeric Cyclopropenium-Based Flow Battery Catholytes. *J. Am. Chem. Soc.* **2019**, *141* (26), 10171–10176. https://doi.org/10.1021/jacs.9b04270.

(45) Baran, M. J.; Braten, M. N.; Montoto, E. C.; Gossage, Z. T.; Ma, L.; Chénard, E.; Moore, J. S.; Rodríguez-López, J.; Helms, B. A. Designing Redox-Active Oligomers for Crossover-Free, Nonaqueous Redox-Flow Batteries with High Volumetric Energy Density. *Chem. Mater.* **2018**, *30* (11), 3861–3866. https://doi.org/10.1021/acs.chemmater.8b01318.

(46) Doris, S. E.; Ward, A. L.; Baskin, A.; Frischmann, P. D.; Gavvalapalli, N.; Chénard, E.; Sevov, C. S.; Prendergast, D.; Moore, J. S.; Helms, B. A. Macromolecular Design Strategies for Preventing Active-Material Crossover in Non-Aqueous All-Organic Redox-Flow Batteries. *Angew. Chem. Int. Ed.* **2017**, *56* (6), 1595–1599. https://doi.org/10.1002/anie.201610582.

(47) Leventis, N.; Elder, I. A.; Gao, X.; Bohannan, E. W.; Sotiriou-Leventis, C.; Rawashdeh, A. M. M.; Overschmidt, T. J.; Gaston, K. R. The Redox Chemistry of 4-Benzoyl-N-Methylpyridinium Cations in Acetonitrile with and without Proton Donors: The Role of Hydrogen Bonding. *J. Phys. Chem. B* **2001**, *105* (17), 3663–3674. https://doi.org/10.1021/jp0107199.

(48) Thériault, K. D.; Radford, C.; Parvez, M.; Heyne, B.; Sutherland, T. C. Structure–Property Relationship of Donor–Acceptor Acridones – an Optical, Electrochemical and Computational Study. *Phys. Chem. Chem. Phys.* **2015**, *17* (32), 20903–20911. https://doi.org/10.1039/C5CP03222A.

(49) Rappoport, Z. Comparison of the Strengths of Dicyano-Methylene and Oxygen Acids. *Isr. J. Chem.* **1970**, *8* (4), 749–751. https://doi.org/10.1002/ijch.197000092.

(50) Wallenfels, K.; Friedrich, K.; Rieser, J.; Ertel, W.; Thieme, H. K. The Analogy between O and C(CN)2. *Angew. Chem. Int. Ed. Engl.* **1976**, *15* (5), 261–270. https://doi.org/10.1002/anie.197602611.

(51) Doane, L. M.; Fatiadi, A. J. Electrochemical Oxidation of Croconate Salts; Evidence of the Chemical Equivalence of the Carbonyl Oxygen Atom and the Dicyanomethylene Group. *Angew. Chem. Int. Ed. Engl.* **1982**, *21* (8), 635–636. https://doi.org/10.1002/anie.198206351.

(52) Xue, Z.-M.; Chen, C.-H. Theoretical Study of Electrical and Electrochemical Properties of Cyclopentanepentaone and Its Dicyanomethylene Derivatives. *Int. J. Quantum Chem.* **2007**, *107* (3), 637–646. https://doi.org/10.1002/qua.21170.

(53) Armstrong, C. G.; Hogue, R. W.; Toghill, K. E. Application of the Dianion Croconate Violet for Symmetric Organic Non-Aqueous Redox Flow Battery Electrolytes. *J. Power Sources* **2019**, *440*, 227037. https://doi.org/10.1016/j.jpowsour.2019.227037.

(54) Hosseini-Sarvari, M.; Sharghi, H.; Etemad, S. Solvent-Free Knoevenagel Condensations over TiO2. *Chin. J. Chem.* **2007**, *25* (10), 1563–1567. https://doi.org/10.1002/cjoc.200790288.

Chapter 4

Investigation of Molecular Structure on Crossover Through Anion Exchange Membrane in Non-Aqueous Redox Flow Batteries

(This chapter contains preliminary work that was conducted in collaboration with Brianna Jett and will be carried forward by her and Ryan Walser-Kuntz.)

4.1. Introduction

There is a growing interest in utilizing renewable sources of energy to meet global energy needs and tackle challenges such as carbon dioxide emissions, pollution, and climate change. A major limitation hindering the widespread adoption of renewable sources of energy is their inherent intermittency, which results in disparity between the times of availability of energy and the demand for that energy. This requires an intermediary energy storage technology that can store the energy on a grid scale. Redox flow batteries (RFBs) are one such example of an energy storage technology.[1–6] Their unique design allows for these systems to be scaled up to store energy at grid levels. Energy in RFBs is stored in solutions of redox active species (anolytes and catholytes), that are kept in external reservoirs and are flowed into an electrochemical cell which facilitates the energy conversion process. The electrochemical cell consists of two chambers, each equipped with inert electrodes. The two halves of the cell are separated by a partially permeable membrane.

The partially permeable membrane is a key component of an RFB.[7–9] The membrane must facilitate the transport of charge carrying-ions during the electrochemical cycling process to maintain electro-neutrality throughout the battery operation.[7–9] Contrastingly, in an asymmetric system, where the anolyte and catholyte solutions

contain distinct redox active species, the membrane needs to prevent crossover of these species to the other half of the cell. Crossover of the electrolytes can lead to irreversible loss of storage capacity while also lowering the overall coulombic efficiency of the system.

Crossover is a major challenge in the field of RFBs, particularly in non-aqueous systems. Many of the efforts to mitigate crossover have been focused on aqueous systems. Commercial membranes, such as Nafion (a cation exchange membrane), are widely utilized in aqueous RFBs.[10–13] Unfortunately, such membranes suffer from physical and mechanical failure when they come in contact with organic solvents such as acetonitrile.

Pioneers in the field of non-aqueous RFBs have circumvented some of the challenges presented by crossover by running the RFB experiment in a symmetric fashion (Figure 4.1a).[14,15,15–17] In this configuration, both halves of the cell are charged with an equimolar mixture of the anolyte and the catholyte. Although the molecules can crossover freely, there the concentration of redox active species does not change since the system is already at equilibrium. This configuration allows for investigation of redox active organic molecules (ROM) performance in a prototype flow battery, without crossover impacting the storage capacity. [14,15,15–17] A inexpensive polyolefin-based membrane, such as Celgard or Daramic, is typically used as a separator in these systems. However, half of the active species in solution do not take part in productive cycling and thus do not contribute to the capacity of the cell. While this is a good starting point to study behavior of ROMs in a prototype RFB system, ultimately, strategies to hinder crossover need to be devised for commercialization.

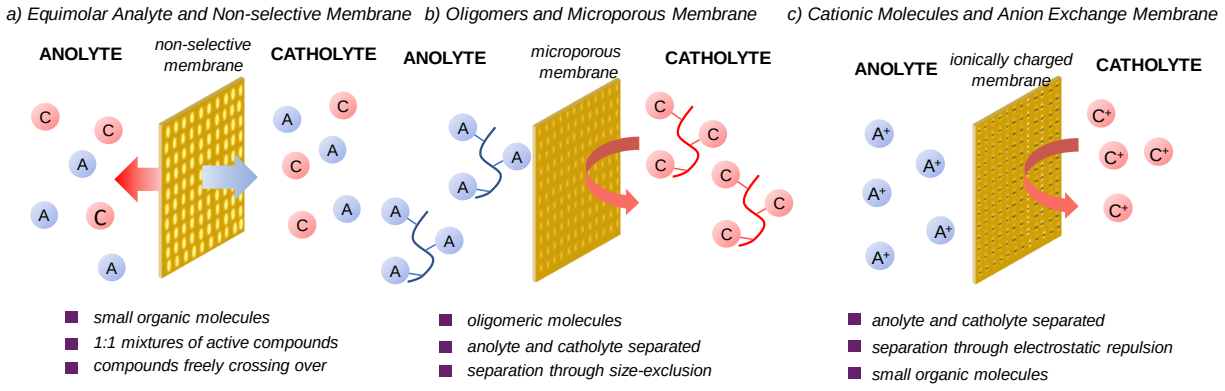

Figure 4.1. Strategies to circumvent and/or mitigate crossover in RFB systems

A tremendous amount of effort is currently underway to mitigating crossover in non-aqueous systems. A few examples have been reported with new designs of the membrane and/or electrolytes. In 2017, the Helms group reported the fabrication of a highly crosslinked polymeric membrane, known as Polymer of Intrinsic Microporosity (PIM-1).[18] This material is known to have pore sizes of approximately < 0.5 nm; furthermore, due to its high crosslinking, it does not swell significantly in organic media. By increasing the effective size of ROMs through oligomerization, crossover was reduced by several orders of magnitude via a size-sieving mechanism. Oligomers (dimers and trimers) of various redox active molecules were tested to demonstrate the generality of this approach.[18,19] They achieved a substantial selectivity through a combination strategy, where the pore size of the membrane was reduced via crosslinking and increase in effective size of the electrolyte through oligomerization.

A recent report from our group explored a complementary strategy where an electrostatic bias was placed on the system by employing an anion exchange membrane and cationic electrolytes.[20] Oligomerization of the electrolytes led to multi-cationic species, which exhibit enhanced interactions with the cationic membrane. With this strategy, crossover rates were slowed by approximately an order of magnitude.[20]

While these were considerable achievements, a deeper understanding of the various factors that impact crossover with a given membrane is still lacking. This is essential to guide the future design of systems with even lower rates of crossover. A fundamental understanding of how factors such as solvent, supporting electrolyte, as well as electrolyte charge, size, and functional groups affect crossover is necessary to outline better strategies to mitigate this process. Such systematic studies have not yet been conducted in this field. This chapter discusses some preliminary work and outline future directions toward this goal.

4.2. Results and Discussion

Electrochemical charge-discharge cycles are highly dynamic processes. The concentration of the parent molecules and their oxidized/reduced counterparts continually varies throughout the cycling experiment, changing the state of the charge of the molecule constantly. Additionally, as seen previously, electrolytes can undergo decomposition as a result of the electrochemical cycling. This dynamic behavior of electrolytes during the

electrochemical cycling process makes it difficult to gather unambiguous information on the crossover of a single species. Thus, in this work, crossover of the electrolytes across a given membrane was studied independent of electrochemical cycling. These experiments were conducted in a laboratory-scale flow cell containing a 50 mM solution of ROM in 0.5 M supporting electrolyte in acetonitrile (MeCN) on one side and a blank solution of 0.5 M supporting electrolyte on the other side. These two solutions were circulated through the electrochemical cell at a rate of 10 mL/min *without electrochemical charging/discharging*. Crossover of the ROM was measured by monitoring the blank side via cyclic voltammetry (CV).[i]

4.2.1. Preliminary Results

Initial efforts were directed toward investigating crossover of a series of electrolytes (pyridinium and cyclopropenium salts) that have been extensively studied in our lab. Previously studied commercial anion exchange membrane (AEM) Fumasep FAPQ-375-PP was selected as a separator for this study based on its known compatibility with organic solvents in the context of both methanol fuel cells and in RFBs.[21,22] Since AEMs contain a large density of cationic charges, this membrane should, theoretically, exclude molecules bearing an overall cationic charge based on electrostatic interactions. As an initial test of this approach, the crossover performance of Fumasep FAPQ-375-PP with monocationic electrolytes were benchmarked relative to that of Celgard, which is a size exclusion membrane that is commonly used in symmetrical RFBs. **Py1** and **CP** were chosen as electrolytes for this initial study. Upon only 4 h of circulation, the flow system with Celgard as a separator approached equilibrium, with 50% crossover observed for **CP** and 38% observed for **Py1** (Figure 4.2). This is consistent with literature results showing that Celgard is highly permeable to small organic molecules due to its large pore size (>20 nm).[14,15,15–17] In contrast, when the analogous experiment was conducted with Fumasep FAPQ-375-PP, <5% crossover of both **Py1** and **CP** was detected over the same period of 4 h. This demonstrated that the Fumasep membrane is effective at mitigating crossover of these cationic electrolytes, at least on a relatively short time scale. However,

(i) Note: The system equilibrates at 50% crossover, which is the maximum possible crossover.

a typical RFB experiment is conducted over several days. Thus, an analogous experiment was next carried out for 96 h, and over this extended period of time, both **Py1** and **CP** exhibited significantly higher crossover of ~38% (Figure 4.2).

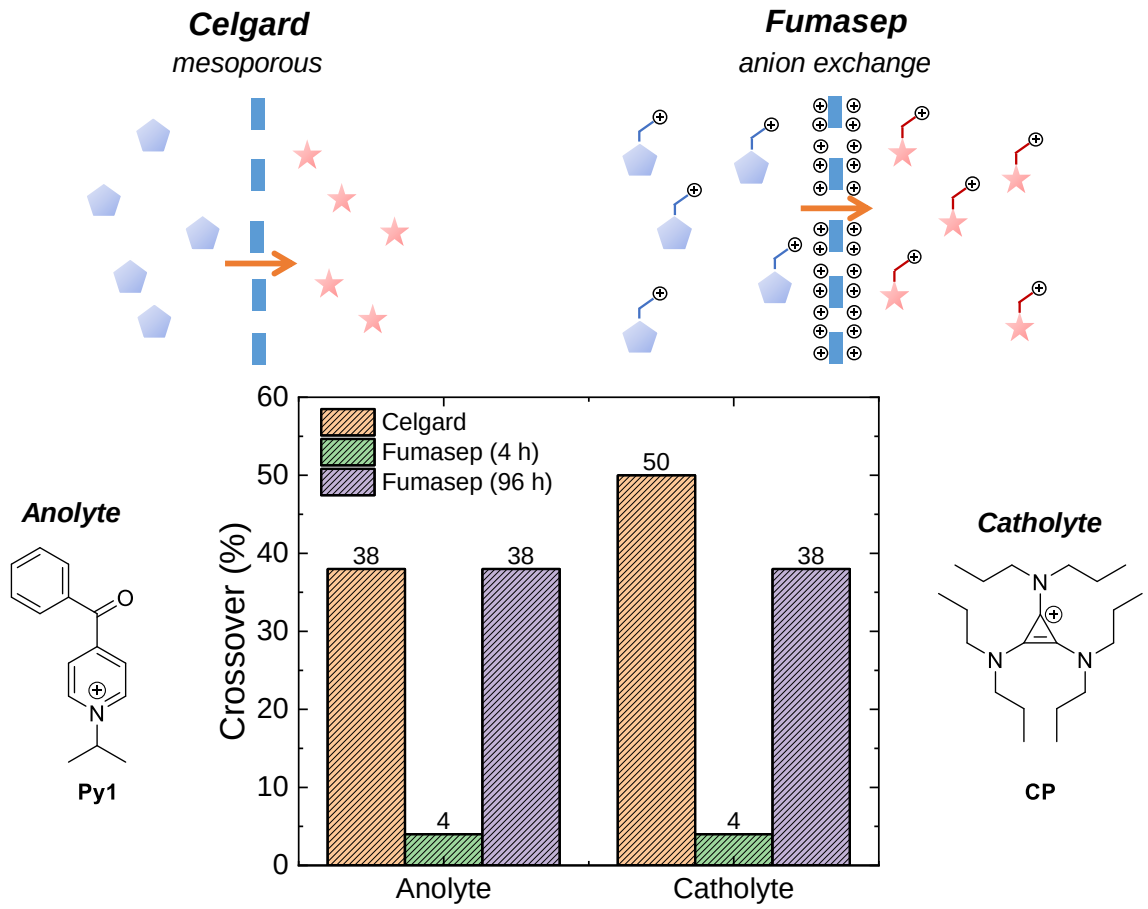

Figure 4.2. Examination of crossover of anolyte **Py1** and catholyte **CP** through size exclusion membrane, Celgard versus anion exchange membrane, Fumasep

Oligomerization of ROMs has been utilized as a strategy to mitigate crossover in several previous reports. Thus, for this work, we planned on synthesizing a series of oligomers and comparing their crossover across an anion exchange membrane.[ii] As such, crossover of a dimer and a trimer of **CP** (**CP-di** and **CP-tri**) and a dimer of **Py1** (**Py1-di**) was examined using the standard crossover assay. Synthesis of a trimer of **Py1** proved

(ii) We plan on repeating similar studies on specialized size exclusion membrane by collaborating with another group that specialize in fabrication of polymeric membrane materials.

challenging and is currently underway.[iii] Notably, in all three cases, the redox-active units are connected using at least a four-methylene tether, which minimizes electronic and/or electrostatic interactions between the redox-active moieties. The concentration during the crossover assay was adjusted to maintain an equivalent molarity of the pyridinium or cyclopropenium units (i.e., 50 mM for monomer, 25 mM for dimer, and 16.7 mM for trimer).[iv] The extent of crossover for each oligomer was assayed at 24 h and directly compared to that of the corresponding monomer (Figure 4.3). Consistent with our hypothesis and previous studies, oligomerization dramatically slowed crossover in all the cases, with **Py1-di** (<5%), **CP-di** (9%), and **CP-tri** (<5%) all showing <10% crossover after circulating the electrolyte solution for 24 h.[v]

(iii) The syntheses of a series of pyridinium trimers is currently being pursued by another graduate student, Ryan Walser-Kuntz.

(iv) Independent studies confirmed that concentration does not impact the rate of crossover for **CP** (see Experimental Details, Figure 4.X).

(v) A time study of the crossover was also conducted (up to 96 h), but no dramatic increase in crossover was observed after 24 h. Thus, most of the crossover experiments were conducted for 24 h.

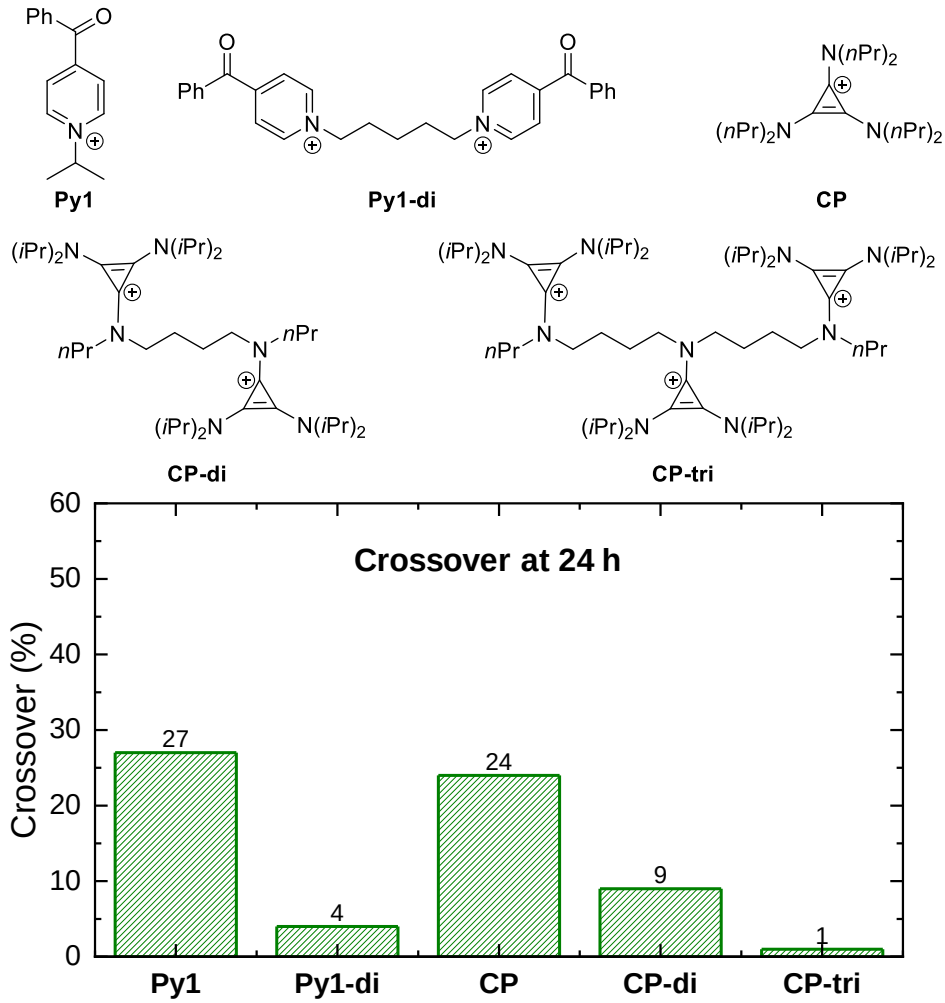

Figure 4.3. Comparison of crossover of oligomers (**Py1-di**, **CP-di** and **CP-tri**) to that of the monomers (**Py1** and **CP**) across AEM Fumasep

We noted that the oligomerization of an electrolyte increases both the charge of the molecule as well as its size. While the chemical structure of Fumasep FAPQ-375-PP is proprietary, AEMs typically contain a high density of positively charged functional groups appended to a polymer backbone. As such, we hypothesized that the overall charge of a ROM should have a large impact on crossover rates, with more positively charged molecules crossing over less through the AEM. In addition, the size of a molecule affects its diffusion coefficient, and hence is likely to have a large impact on the overall crossover rates. In order to dissect the impact of each of these variables, it was necessary to decouple charge from size of the molecule. The simplest way to modify the charge of **Py1** and **CP** while minimally altering their overall size and structure is to oxidize and/or

reduce these species. Reduction of monocationic **Py1** results in neutral **Py1•** whereas oxidation of **CP** results in dicationic **CP+•**. Again, a 24 h time point served as a useful comparison between the four species. After 24 h, both of the monocations, **Py1** and **CP**, display a comparable extent of crossover (27% and 24% respectively, Figure 4.4). In contrast, the neutral species **Py1•** shows a significantly more crossover (41%, Figure 4.4), while the dication **CP+•** shows significantly less (14%).[vi] As depicted in Table 4.1, these same trends hold at the longer time points as well. After circulating the electrolyte solution for 96 h, 45% crossover is observed for **Py1•**, 38% for **Py1** and **CP** and 20% for **CP+•**.

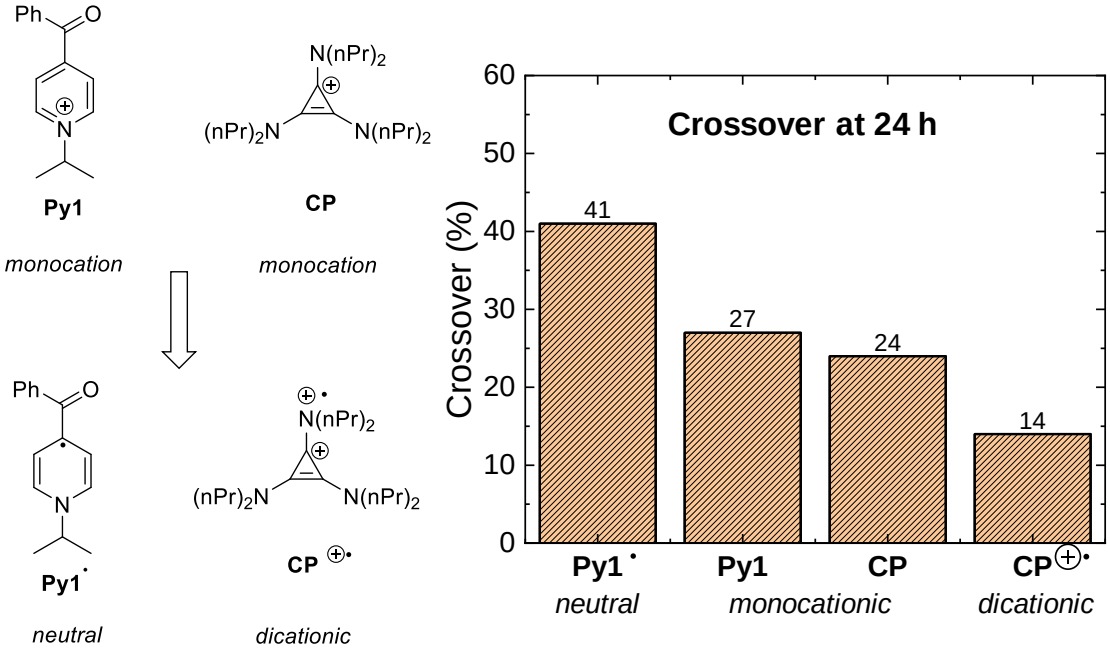

Figure 4.4. An analysis of effect of charge on crossover: Comparison of crossover of parent **Py1** and **CP** to their charged species **Py1•** and **CP+•**

To further interrogate the effect of charge and the size of the molecules on crossover, we next sought to decouple these factors by comparing the two monocations **Py1** and **Py2** to the dication **Py3** (Figure 4.5). Compounds **Py2** and **Py3** have a similar alkyl chain length/structure (and thus comparable size) but differ in terms of their overall charge (+1 versus +2). **Py1** has the same overall charge as **Py2** but a much more compact alkyl chain. After 24 h of circulation through a prototype flow battery, 27%, 17%

(vi) Notably, the crossover of oxidized **CP+•** stalls at ~20% rather than the 50% expected at equilibrium. We are still working to understand this unexpected behavior.

and 4% crossover were observed for **Py1**, **Py2**, and **Py3**, respectively. The progressively slower crossover in this series demonstrates a compounding effect of the charge and the size of the molecule on overall transport across the Fumasep FAPQ-375-PP membrane.

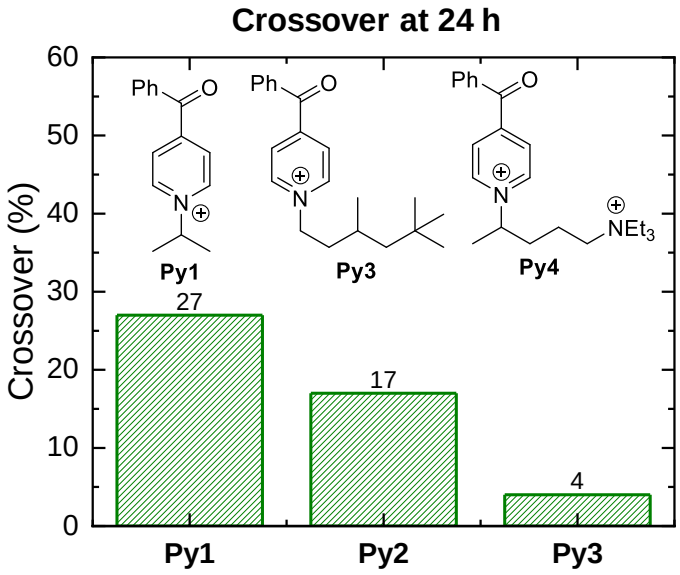

Figure 4.5. An analysis of effect of charge versus size on crossover of the electrolyte: Comparison of crossover of monocations **Py1** and **Py2** and dication **Py3**

4.3. Future Work

Preliminary efforts toward an systematic study of crossover and various factors that could affect crossover behavior of ROMs was conducted. This study uncovered valuable information on the effect of molecular charge on crossover through the AEM Fumasep FAPQ-375-PP. Oligomerization of cationic electrolytes lowered crossover via a compounding effect of an increase in charge as well as size of the molecule. However, a lot of work into the fundamental studies of crossover still remains unexplored. This section will outline a few directions to continue a more expansive investigation of this looming challenge in the field.

One such study that would coincide with recent efforts to explore the effect of solvent on performance and stability of ROMs, which has gained traction in recent time. For instance, studies in our group have recently illuminated that solvents such as DMF, which can form a tighter solvent shell around positively charged supporting electrolyte

salts (such as Li^+) as well as ROMs (such as pyridinium salts) and thereby affect their cycling behavior.[vii] Significant improvements in the stability of these electrolytes during cycling was observed by switching the solvent from MeCN to DMF. In particular, solvation of Li+ counterions by DMF suppressed decomposition pathways for the anionically charged anolyte. This drastic effect of solvent on the chemical behavior of electrolytes brought into question whether it could have any impact on crossover. Does the solvation shell, formed through non-covalent interactions between electrolyte and solvents, affect the crossover behavior of ROMs? Additionally, how do different solvents interact with the polymeric membrane? Polymers can swell when exposed to organic solvents, altering their ability to hinder crossover of ROMs.[23–25] To address these question, we envision an initial solvent screening study, where crossover of pyridinium and cyclopropenium salts will be tested with a variety of non-polar (DCM, toluene), polar aprotic (MeCN, DMF, DMA) and polar protic solvents (MeOH, H_2O).[viii] These solvents are expected to have different interactions with the cationic electrolytes that could alter the behavior of solvation shell. Indeed, a preliminary study with DMF showed a significant decrease in crossover of **Py1** and **CP** to ~10% (from >20% with MeCN).[ix] We hypothesize that this difference is due to the higher strength of solvation with DMF (as observed in the stability studies). In addition, it is possible the polymeric membrane swelled less in DMF than in MeCN. Experiments to quantify this by using microscopic analysis will be devised. This result points to potential impact that the strength of solvation can have on crossover. Studies with non-polar solvents (DCM, toluene), would be more telling of this behavior. Initial attempts to conduct these experiments suffered from physical incompatibility of various RFB components with these organic solvents.[x] The proposed solvent screen also suffered from lower solubility of **Py1** and **CP** in some of the solvents of interest (e.g. H_2O, toluene).

(vii) Manuscript with this work is currently in preparation by Ryan Walser-Kuntz.

(viii) The solvent screening study will be conducted outside the glovebox for ease of handling as well as wider variety of solvents.

(ix) This result was obtained by Brianna Jett.

(x) Different tubing materials that might have higher tolerance of organic solvents will be tested for experiment with these solvents.

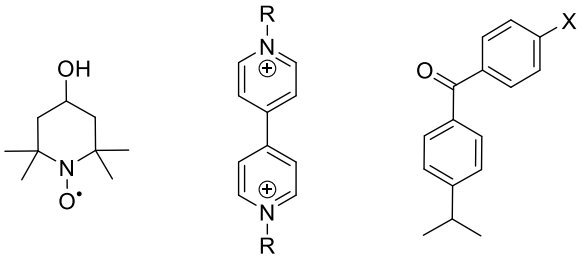

Figure 4.6. 4-OH TEMPO, viologen and a proposed molecule for crossover studies **A**

Solubility of molecules has hindered a comprehensive exploration of solvent effects. Therefore, an alternative strategy needs to be implemented, where the crossover of different molecules will be benchmarked to one solvent (i.e. MeCN). The library of electrolytes will be widened. Other electrolytes that have been employed in RFBs, such as 4-OH TEMPO and viologen (Figure 4.6), will be included. These electrolytes have better solubility in H_2O than **Py1** and **CP** and will allow better comparison of crossover as a function of solvent (MeCN/DMF vs H_2O). Molecules such as the amide **A** (Figure 4.6), which is structurally similar to **Py1** but is uncharged, will also be investigated. Solubility of **A** is anticipated to be better in non-polar solvents such as DCM and toluene, which will enable a better comparison for crossover with MeCN. In addition, derivatives of **A** containing different functional groups can be easily synthesized in a single coupling reaction. Polar functional groups (NH_2, OH, or other protected analogs) can be introduced to promote solubility in more polar solvents. Protonation of these functional groups can enhance the solubility in H_2O with little change in the molecular structure. Using this, any effect of different molecular conformations on crossover can be eliminated. Molecular dynamics simulation could impart valuable information on the solvation of these electrolytes and can be pursued in the future to understand the results better as well.

In addition to the solvent study, we have preliminary information on the crossover of some “hybrid” electrolytes, such as **B** (Figure 4.7).[xi] These hybrid electrolytes contain two cyclopropenium units tethered to a phenothiazine core. During RFB cycling

(xi) Synthesis, characterization and electrochemical evaluation of these hybrid molecules was conducted by Yichao Yan.

experiments, the “hybrid” electrolyte **B** exhibits no detectable crossover with Fumasep FAPQ-375-PP.[xi] This is in contrast to previously studied dimer of CP (**CP-di**) where ~9% crossover was detected under similar conditions. These data on crossover was obtained after ~4 days of cycling, at 10 mL/min at a concentration of 12.5 – 15 mM. Given these differences in crossover of electrolytes that are dimeric in the cyclopropenium unit, a way to quantify the kinetic molecular diameter of the molecules and understand the effect of conformational arrangement and flexibility is needed. A collaboration to compute these parameters could further enhance our understanding of crossover.

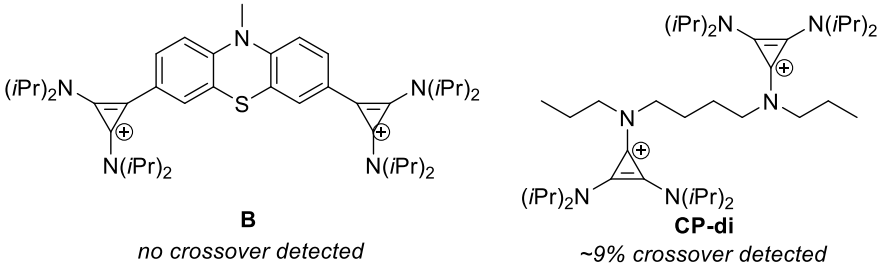

Figure 4.7. Electrolyte **B**, which is a hybrid of cyclopropenium and phenothiazine, and cyclopropenium dimer (**CP-di**)

Finally, until now, we have exclusively focused on a single anion exchange membrane: Fumasep FAPQ-375-PP. Since this is a commercial membrane, the chemical composition and structure of the membrane is proprietary. This prevents us from exploring effects of different interactions of electrolytes with the membrane. In the future, we plan on seeking a collaboration with polymer chemistry labs to obtain AEMs with known chemical composition. As one example, Geoff Coates’ group at Cornell is expert in synthesis and fabrication of AEMs for fuel cell purposes which could work well in RFBs as well.[26–28]

4.4. Conclusion

Crossover is one of the major challenges in the field of RFBs. While some efforts have been dedicated to mitigating crossover, systematic fundamental studies to understand how parameters such as solvent, molecular charge, molecular structure, and conformation, impact crossover have not been reported. This chapter outlines preliminary results obtained toward this goal. These results demonstrate a clear effect of charge on

crossover through an anion exchange membrane. A compounding effect of increasing charge as well as size of the electrolyte was observed upon oligomerization. While these were interesting results, a lot is yet to be done. For instance, a systematic study of solvent and solvation is proposed as a future direction for the overarching goal of studying crossover. Molecular dynamics simulations would be a valuable addition to our studies as well.

4.5. Experimental Details

4.5.1. Synthesis

4.5.1.1. Instrumental Information

NMR spectra were recorded on a Varian vnmrs 700 (700 MHz for ^{1}H; 176 MHz for ^{13}C) or a Varian vnmrs 500 (500 MHz for ^{1}H; 126 MHz for ^{13}C) spectrometer with the residual solvent peak ($CDCl_3$; ^{1}H: δ = 7.26 ppm, ^{13}C: δ = 77.16 ppm; CD_3CN; ^{1}H: δ = 1.94 ppm, 13C: δ = 1.32 ppm) as the internal reference unless otherwise noted. Chemical shifts are reported in parts per million (ppm, δ) relative to tetramethylsilane. Multiplicities are reported as follows: s (singlet), d (doublet), t (triplet), q (quartet), and m (multiplet). Coupling constants (*J*) are reported in Hz. High-resolution mass spectra were recorded on a Micromass AutoSpec Ultima Magnetic Sector mass spectrometer. A multi-channel potentiostat from Bio-Logic Instruments (model VSP-CHAS) was used for all the electrochemical studies.

4.5.1.2. Materials and Methods

All commercial reagents and solvents were used as received, unless otherwise noted. Anhydrous CH_2Cl_2 was obtained from an SDS solvent system. All reactions were performed under nitrogen atmosphere unless otherwise noted. Thin layer chromatography (TLC) was performed on Macherey-Nagel SIL G-25 TLC plates pre-coated with silica gel UV254. Biotage® SNAP Ultra column cartridges were used for flash column chromatography. **Py1**,[29] **Py1-di**,[20] **CP**,[30] **CP-di**[31] and **CP-tri**[31] were synthesized using previously reported procedures.

4.5.1.3. Synthesis of Py1-di

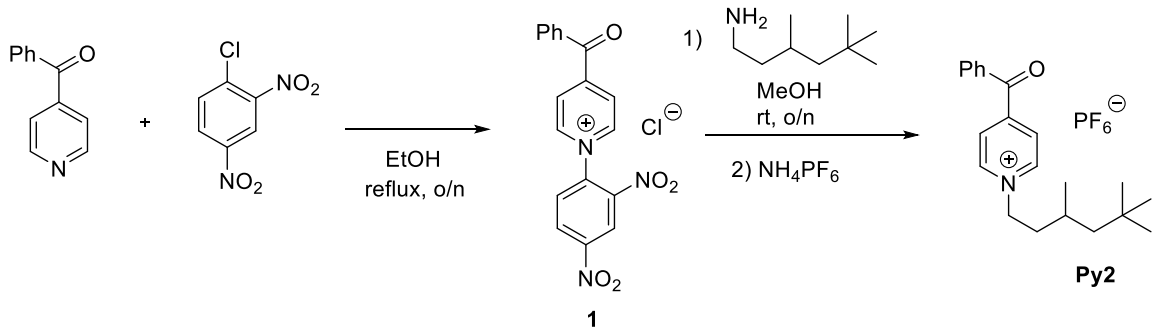

The Zincke reagent (**1**) was prepared according to the previously reported procedure.[29]

The Zincke reagent **1** (500 mg, 1.29 mmol, 1.0 equiv.) was dissolved in MeOH, and the amine (186 mg, 1.29 mmol, 1 equiv) was added dropwise. This mixture was stirred at room temperature overnight. The solvent was removed *in vacuo*, and the resulting residue was taken up in H_2O (15 mL) and washed with DCM (3 x 15 mL). The aqueous layer was collected, 1 M HCl (5 mL) was added, and the aqueous solution was concentrated under vacuum at elevated temperature (70 °C). This mixture was purified by flash chromatography on silica gel (0-15% MeOH:DCM). Fractions containing the product were collected and concentrated under vacuum. For further purification, the compound was dissolved in MeCN, and Et_2O was added until the solution turned cloudy. The product fuly precipitated from solution after standing overnight, and the precipitate was collected via filtration. To this solid was added a solution of NH_4PF_6 (424 mg, 2.59 mmol, 2 equiv) in water. The resulting solution was extracted with 10:1 DCM:MeCN (4 x 20 mL), and the organic extracts were dried over $MgSO_4$, and concentrated under vacuum. The resulting solid was purified by recrystallization from EtOAc to afford **Py2** as a white crystalline solid (325 mg, 55% yield).

^{1}H NMR (700 MHz, Acetonitrile-d_3) δ 8.86 (d, *J* = 6.7 Hz, 2H), 8.19 (d, *J* = 6.0 Hz, 2H), 7.84 (d, *J* = 7.0 Hz, 2H), 7.81-7.76 (m, 1H), 7.62 (dd, *J* = 8.3, 7.4 Hz, 2H), 4.65-4.56 (m, 2H), 2.04-1.98 (m, 1H), 1.89 (dddd, *J* = 13.2, 10.7, 7.6, 5.8 Hz, 1H), 1.71 (ddt, *J* = 13.3, 10.3, 6.4 Hz, 1H), 1.35 (dd, *J* = 14.1, 3.7 Hz, 1H), 1.20 (dd, *J* = 14.1, 6.3 Hz, 1H), 1.06 (d, *J* = 6.7 Hz, 3H), 0.93 (s, 9H).

^{13}C NMR (176 MHz, Acetonitrile-d_3) δ 194.49, 148.12, 137.64, 137.08, 134.75, 132.99, 131.84, 130.31, 63.41, 53.06, 43.12, 33.37, 31.83, 29.69, 24.29.

HRMS: Calc. 310.2165, Measured: 310.2169

IR: 3132.82, 2953.74, 2867.69, 1663.27, 1365.59 cm^{-1}

$E_{1/2}$: -0.996 V and -1.57 V v/s Ag/Ag^+

4.5.1.4. Synthesis of Py3

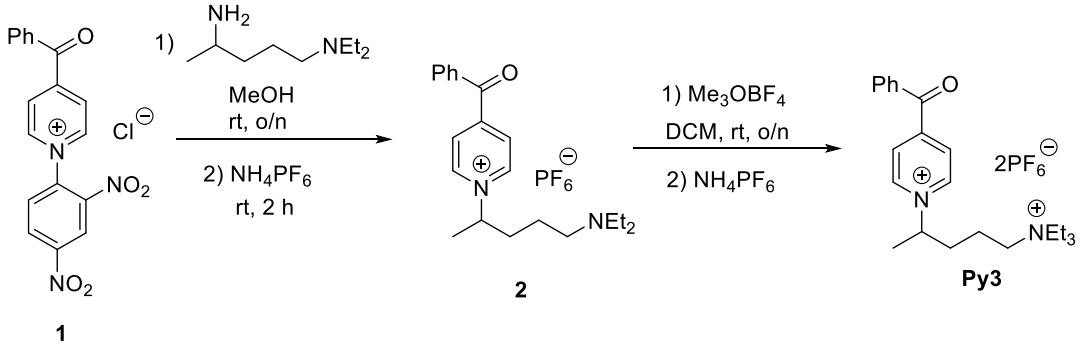

The Zincke reagent (**1**, 8.00 g, 20.7 mmol, 1.0 equiv.) was dissolved in MeOH (160 mL). The amine (12.0 mL, 62.2 mmol, 3 equiv.) was added dropwise to the reaction mixture, resulting in a color change from clear to dark red. The mixture was stirred overnight at room temperature. The solvent was removed *in vacuo*. The resulting residue was dissolved in H_2O (30 mL), and the aqueous layer was washed with DCM (3 x 30 mL). The aqueous layer was collected, 1 M HCl (24 mL) was added, and the aqueous solution was concentrated under vacuum at elevated temperature (~70 °C). This mixture was then purified by flash chromatography on silica gel, eluting with a gradient of 5-10% H_2O:MeCN. Fractions containing the product were collected and concentrated under vacuum. The product was taken up in a mixture of 1 M NaOH (40 mL) and brine (60 mL), and the resulting solution was stirred for 30 min. NH_4PF_6 (6.85 g, 41.4 mmol, 2 equiv.) was added, and the solution stirred for an additional 30 min. The resulting solution was extracted with 10:1 DCM:MeCN (4 x 100 mL), and the organic extracts were dried over $MgSO_4$ and concentrated under vacuum. Product **2** was obtained as a yellow oil (5.93 g, 61% yield).

^{1}H NMR (500 MHz, Acetonitrile-d_3) δ 8.93 (d, J = 6.8 Hz, 2H), 8.25 (d, J = 6.3 Hz, 2H), 7.94-7.87 (m, 2H), 7.86-7.80 (m, 1H), 7.66 (dd, J = 8.4, 7.4 Hz, 2H), 4.89 (h, J = 6.9 Hz,

1H), 2.78-2.58 (m, 6H), 2.07 (q, *J* = 7.7 Hz, 2H), 1.74 (d, *J* = 6.7 Hz, 3H), 1.60 (dp, *J* = 15.2, 7.5 Hz, 1H), 1.45-1.32 (m, 1H), 1.08 (t, *J* = 7.2 Hz, 6H).

^{13}C NMR (176 MHz, Acetonitrile-d_3) δ 192.78, 153.79, 144.92, 135.96, 135.36, 131.32, 130.14, 128.76, 70.99, 61.77, 52.59, 47.79, 45.88, 35.34, 21.43.

HRMS: Calc. 499.2307, Measured: 499.2310

IR: 2970.41, 1671.14, 1639.32, 1450.43 cm^{-1}

Compound **2** (6.00 g, 12.7 mmol, 1.0 equiv) was dissolved in dry DCM (65 mL), and Et_3OBF_4 (2.50 g, 16.6 mmol, 1.3 equiv) was added inside a glovebox. The reaction was stirred overnight at room temperature under an atmosphere of N_2. A solution of NH_4PF_6 (6.21 g, 38.1 mmol, 3.0 equiv) in H_2O (30 mL) was then added, and the resulting mixture was stirred vigorously for 10 min. MeCN (20 mL) was added, and the mixture was stirred for an additional 3 h. The produt was extracted into a 4:1 solution of DCM:MeCN (4 x 50 mL). The organic extracts were dried over $MgSO_4$ and then concentrated under vacuum. The product was purified via flash chromatography on silica gel, eluting with a gradient of 5-20% MeOH:DCM. The fractions containing the product were collected and concentrated. The product was further purified via two recrystallizations from MeOH to afford **Py3** as a white powder (3.35 g, 40% yield).

^{1}H NMR (500 MHz, Acetonitrile-d_3) δ 8.92 (d, *J* = 6.3 Hz, 2H), 8.28 (d, *J* = 6.1 Hz, 2H), 7.93-7.89 (m, 2H), 7.84 (t, *J* = 7.5 Hz, 1H), 7.67 (t, *J* = 7.7 Hz, 2H), 4.88 (app hex, *J* = 6.9 Hz, 1H), 3.20 (q, *J* = 7.2 Hz, 6H), 3.08 (pd, *J* = 13.9, 5.2 Hz, 2H), 2.04 (q, *J* = 7.8 Hz, 2H), 1.77 (d, *J* = 6.7 Hz, 3H), 1.74 – 1.68 (m, 1H), 1.47 (td, *J* = 11.9, 10.9, 5.2 Hz, 1H), 1.25 (t, *J* = 7.2 Hz, 9H).

^{13}C NMR (176 MHz, Acetonitrile-d_3) δ 191.78, 153.09, 143.96, 135.05, 134.32, 130.32, 129.17, 127.92, 69.46, 55.71, 52.82, 32.80, 20.14, 18.19, 6.75.

HRMS: Calc. 499.2307, Measured: 499.2310

IR: 2954.79, 1669.37, 1323.85, 950.90 cm^{-1}

$E_{1/2}$: -0.951 V and -1.52 V v/s Ag/Ag^+

4.5.1.5. Synthesis of Py1-surrogate

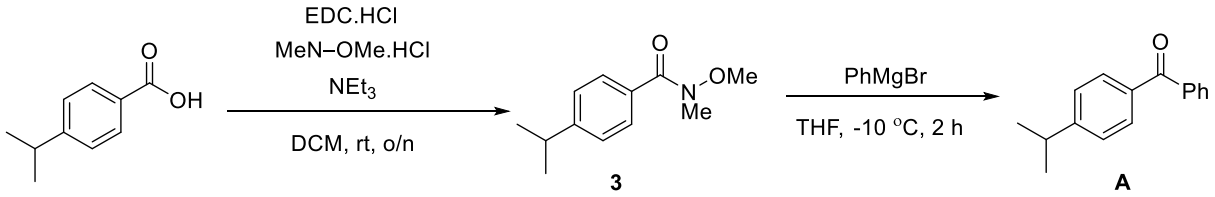

4-iso-Propylbenzoic acid (1.00 g, 6.09 mmol, 1.0 equiv) was dissolved in DCM (35 mL). Triethylamine (19.4 mmol, 2.6 mL, 3.2 equiv) was added, followed by *N*-(3-dimethylaminopropyl)-*N'*-ethylcarbodiimide hydrochloride (EDC•HCl) (1.87 g, 9.74 mmol, 1.6 equiv) and *N,O*-dimethylhydroxylamine hydrochloride (891 mg, 9.13 mmol, 1.5 equiv). The reaction was stirred overnight at room temperature. The resulting mixture was extracted with water (2 x 50 mL) and brine (1 x 30 mL), and the organic layer was dried over $MgSO_4$ and concentrated under vacuum. The compound was then passed through a plug of silica, which was washed with copious amount of EtOAc (to get rid of any remaining organic salts). Compound **3** was 85% pure (15% remaining starting material) and was used without further purification.

Amide **3** (600 mg, 2.89 mmol, 1.0 equiv) was dissolved in dry THF (6 mL). This solution was cooled to −10 °C, and freshly prepared phenyl magnesium bromide (7 mL of a 0.62 M solution in THF, 4.34 mmol, 1.5 equiv) was added dropwise. The reaction was stirred at −10 °C for 2 h and then quenched with a saturated aqueous solution of ammonium chloride (5 mL). DCM (20 mL) was added, and the organic layer was collected, dried over $MgSO_4$, and concentrated under vacuum. The product was purified via flash chromatography using a gradient of 10-50% EtOAc in hexanes. The fractions containing the product were collected and concentrated under vacuum to afford **A** as a clear oil (518 mg, 85% yield).

^{1}H NMR (700 MHz, Chloroform-*d*) δ 7.81-7.79 (m, 2H), 7.76 (d, *J* = 8.2 Hz, 2H), 7.58 (td, *J* = 7.4, 1.6 Hz, 1H), 7.48 (t, *J* = 7.7 Hz, 2H), 7.34 (d, *J* = 8.1 Hz, 2H), 3.00 (hept, *J* = 6.9 Hz, 1H), 1.30 (d, *J* = 6.9 Hz, 6H).

^{13}C NMR (176 MHz, Chloroform-*d*) δ 196.61, 154.10, 138.11, 135.39, 132.28, 130.57, 130.09, 128.34, 126.52, 34.42, 23.87.

HRMS: Calc. 225.1274, Measured: 225.1272

IR: 2960.30, 1655.10, 1605.18, 1446.06 cm^{-1}

4.5.2. Crossover Studies

4.5.2.1. Materials and Methods

Acetonitrile (99.8% anhydrous) was obtained from Sigma Aldrich and used as received. Potassium hexafluorophosphate (≥99%) was obtained from Sigma Aldrich and dried under high vacuum at 100 °C for 48 h before use. 0.5 M stock solutions of KPF_6 in MeCN were prepared in a nitrogen-filled glovebox and dried over activated 3Å molecular sieves for at least two days prior to use. The molecular sieves were activated by heating at 200 °C under vacuum. All organic electrolytes were dried at 80 °C under high vacuum for 19 h before use and were then stored in an inert atmosphere drybox.

For the laboratory-scale flow battery, a peristaltic pump (Cole-Parmer) was used in combination with Solveflex and PFA tubing. The cycling was performed with a zero-gap flow cell comprised of graphite charge-collecting plates containing an interdigitated flow field. Two layers of non-woven carbon felt electrodes, Sicracet 29AA, were used in each half-cell. ePTFE gaskets were used to achieve ~20% compression of the carbon felt. The exposed area of the membrane in the gasket window was used as the active area (2.55 cm^2). Fumasep FAPQ-375PP was purchased from FuMa-Tech and was ion exchanged prior to use by soaking pre-cut membranes in a saturated aqueous solution of KPF_6 (3 x 8-16 h). After each soak, the membrane was rinsed with deionized water. The membrane was stored outside the box, under ambient atmosphere. Prior to use, it was dried *in vacuo*, at 50 °C, along with the rest of the glassware for battery cycling. A sample of Celgard 2500 was generously provided by Celgard LLC, and used without any further treatment.

4.5.2.2. General Procedure for Cyclic Voltammetry

Cyclic voltammetry was performed in a nitrogen-filled drybox with a Biologic VSP multichannel potentiostat/galvanostat using a three-electrode setup. A glassy carbon electrode (0.07 cm^2, BASi) was used as the working electrode and a platinum wire was used as the counter electrode. An Ag/Ag^+ quasi-reference electrode (BASi) containing

0.01 M $AgBF_4$ (Sigma Aldrich) in 0.5 M KPF_6/MeCN was used. All potentials are referenced to Ag/Ag^+. The CVs were performed with a solution of 5 mM concentration of active species, a scan rate of 100 mV s^{-1}, using 0.5 M KPF_6 as supporting electrolyte in MeCN.

4.5.2.3. General Procedure for Determining Crossover

An aliquot of known amount was taken out for analysis before the start of the cycling experiment and at the end of the experiment. These aliquots were analyzed by cyclic voltammetry to determine % crossover. Volumes of solutions on both sides of the cell were measured (to account for any solvent lost to evaporation or transfer between half-cells).

Quantification of Crossover:

ANOLYTE:

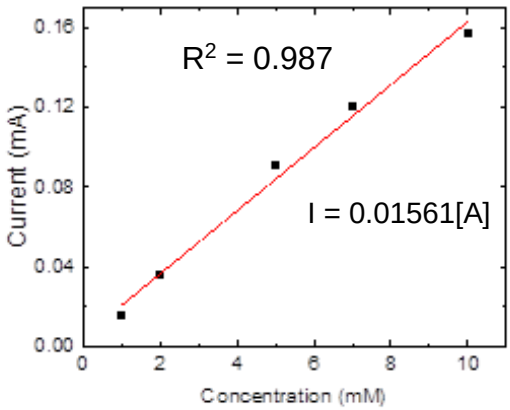

CATHOLYTE

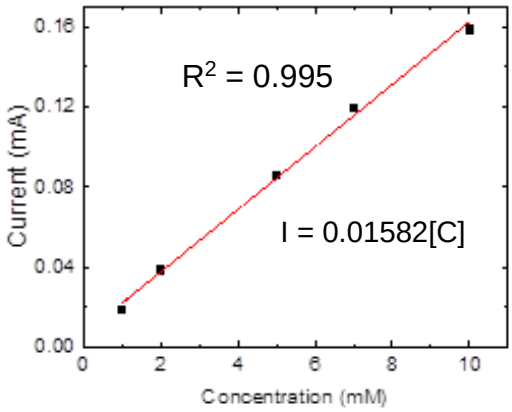

The aliquots collected at the beginning and end of the experiment were diluted with 0.5 M KPF_6 in MeCN solution (0.9 mL) and the cyclic voltammograms for each sample were measured. Calibration curves were used to calculate the concentration of this CV sample. This concentration was then normalized for the amount of aliquot taken out (by mass) and corrected for any volumetric change that occurred during the experiment (see calculation example below). Percent crossover was then calculated by dividing the concentration calculated for the blank side by the concentration of solution before the experiment.

To calculate crossover of CP monomer after 1 day of circulation:

-Mass of aliquot before experiment = 60 mg

-Mass of aliquot from crossover side after experiment = 61 mg

-Total volume of crossover side after the experiment = 5.67 mL

-Volumetric change = 5.67/6.0 = 0.945

*6.0 mL was the original volume of the solution

-CV peak height of sample before the experiment = 0.06659 mA. Concentration = 4.21 mM (by plugging peak height into the equation above)

-CV peak height of CV from the counter side sample after the experiment = 0.0175 mA. Concentration = 1.11 mM

-The peak heights were then normalized to their respective aliquot masses and the crossover calculated using the formula below.

$$\%crossover = \left(\frac{concentration(counter) * Volumetric\ change}{mass\ aliquot\ (counter)}\right) / \left(\frac{concentration(before)}{mass\ aliquote\ (before)}\right) * 100$$

For this example: Crossover = $\left(\frac{1.11*0.945}{61}\right) / \left(\frac{4.21}{60}\right) * 100$ = **24%**

When plotting the CVs, *corrected/normalized current* was plotted. Current was normalized by dividing the voltammogram by the mass of the aliquot and multiplying for volumetric change.

For crossover of **A**, 0.15 mmol trimethoxybenzene was added to the spent solution and a 1H NMR was taken. Using the internal standard, number of mmol of the **A** in the solution was calculated.

Tables with Crossover Data:

Table 4.1. Time-study of charged and uncharged **Py1** and **CP**

Time	$Py1^{\cdot}$	Py1	CP	$CP^{2+\cdot}$
4 h	14%	4%	4%	2%
24 h	41%	27%	24%	14%
48 h	46%	33%	32%	18%
96 h	45%	38%	38%	20%

Table 4.2. Crossover of various electrolytes at 24 h and 96 h

Compound	24 h	96 h
Py1	27	38
A	42%	52%
Py2	17%	33%
CP	24%	38%
Py3	4%	16%
Py1-dimer	4%	16%
CP-dimer	9%	20%
CP-trimer	<1%	4%

4.6. References

(1) Flow Batteries: Current Status and Trends | Chemical Reviews https://pubs.acs.org/doi/10.1021/cr500720t (accessed Mar 11, 2020).

(2) Wei, X.; Pan, W.; Duan, W.; Hollas, A.; Yang, Z.; Li, B.; Nie, Z.; Liu, J.; Reed, D.; Wang, W.; Sprenkle, V. Materials and Systems for Organic Redox Flow Batteries: Status and Challenges. *ACS Energy Lett.* **2017**, *2* (9), 2187–2204. https://doi.org/10.1021/acsenergylett.7b00650.

(3) Noack, J.; Roznyatovskaya, N.; Herr, T.; Fischer, P. The Chemistry of Redox-Flow Batteries. *Angew. Chem. Int. Ed.* **2015**, *54* (34), 9776–9809. https://doi.org/10.1002/anie.201410823.

(4) Kamat, P. V.; Schanze, K. S.; Buriak, J. M. Redox Flow Batteries. *ACS Energy Lett.* **2017**, *2* (6), 1368–1369. https://doi.org/10.1021/acsenergylett.7b00361.

(5) Winsberg, J.; Hagemann, T.; Janoschka, T.; Hager, M. D.; Schubert, U. S. Redox-Flow Batteries: From Metals to Organic Redox-Active Materials. *Angew. Chem. Int. Ed Engl.* **2017**, *56* (3), 686–711. https://doi.org/10.1002/anie.201604925.

(6) Rugolo, J.; Aziz, M. J. Electricity Storage for Intermittent Renewable Sources. *Energy Environ. Sci.* **2012**, *5* (5), 7151–7160. https://doi.org/10.1039/C2EE02542F.

(7) Gubler, L. Membranes and Separators for Redox Flow Batteries. *Curr. Opin. Electrochem.* **2019**, *18*, 31–36. https://doi.org/10.1016/j.coelec.2019.08.007.

(8) Shin, S.-H.; Yun, S.-H.; Moon, S.-H. A Review of Current Developments in Non-Aqueous Redox Flow Batteries: Characterization of Their Membranes for Design Perspective. *RSC Adv.* **2013**, *3* (24), 9095–9116. https://doi.org/10.1039/C3RA00115F.

(9) Wang, W.; Luo, Q.; Li, B.; Wei, X.; Li, L.; Yang, Z. Recent Progress in Redox Flow Battery Research and Development. *Adv. Funct. Mater.* **2013**, *23* (8), 970–986. https://doi.org/10.1002/adfm.201200694.

(10) Wei, X.; Li, B.; Wang, W. Porous Polymeric Composite Separators for Redox Flow Batteries. *Polym. Rev.* **2015**, *55* (2), 247–272. https://doi.org/10.1080/15583724.2015.1011276.

(11) Reed, D.; Thomsen, E.; Wang, W.; Nie, Z.; Li, B.; Wei, X.; Koeppel, B.; Sprenkle, V. Performance of Nafion® N115, Nafion® NR-212, and Nafion® NR-211 in a 1 KW Class All Vanadium Mixed Acid Redox Flow Battery. *J. Power Sources* **2015**, *285*, 425–430. https://doi.org/10.1016/j.jpowsour.2015.03.099.

(12) Noh, C.; Jung, M.; Henkensmeier, D.; Nam, S. W.; Kwon, Y. Vanadium Redox Flow Batteries Using Meta-Polybenzimidazole-Based Membranes of Different Thicknesses. *ACS Appl. Mater. Interfaces* **2017**, *9* (42), 36799–36809. https://doi.org/10.1021/acsami.7b10598.

(13) Porcellinis, D. D.; Mecheri, B.; D'Epifanio, A.; Licoccia, S.; Granados-Focil, S.; Aziz, M. J. Communication—Sulfonated Poly (Ether Ether Ketone) as Cation Exchange Membrane for Alkaline Redox Flow Batteries. *J. Electrochem. Soc.* **2018**, *165* (5), A1137. https://doi.org/10.1149/2.1291805jes.

(14) Duan, W.; Huang, J.; Kowalski, J. A.; Shkrob, I. A.; Vijayakumar, M.; Walter, E.; Pan, B.; Yang, Z.; Milshtein, J. D.; Li, B.; Liao, C.; Zhang, Z.; Wang, W.; Liu, J.; Moore, J. S.; Brushett, F. R.; Zhang, L.; Wei, X. "Wine-Dark Sea" in an Organic Flow Battery: Storing Negative Charge in 2,1,3-Benzothiadiazole Radicals Leads to Improved Cyclability. *ACS Energy Lett.* **2017**, *2* (5), 1156–1161. https://doi.org/10.1021/acsenergylett.7b00261.

(15) Hu, B.; Liu, T. L. Two Electron Utilization of Methyl Viologen Anolyte in Nonaqueous Organic Redox Flow Battery. *J. Energy Chem.* **2018**, *27* (5), 1326–1332. https://doi.org/10.1016/j.jechem.2018.02.014.

(16) Huang, J.; Duan, W.; Zhang, J.; Shkrob, I. A.; Assary, R. S.; Pan, B.; Liao, C.; Zhang, Z.; Wei, X.; Zhang, L. Substituted Thiadiazoles as Energy-Rich Anolytes for Nonaqueous Redox Flow Cells. *J. Mater. Chem. A* **2018**, *6* (15), 6251–6254. https://doi.org/10.1039/C8TA01059E.

(17) Wei, X.; Duan, W.; Huang, J.; Zhang, L.; Li, B.; Reed, D.; Xu, W.; Sprenkle, V.; Wang, W. A High-Current, Stable Nonaqueous Organic Redox Flow Battery. *ACS Energy Lett.* **2016**, *1* (4), 705–711. https://doi.org/10.1021/acsenergylett.6b00255.

(18) Doris, S. E.; Ward, A. L.; Baskin, A.; Frischmann, P. D.; Gavvalapalli, N.; Chénard, E.; Sevov, C. S.; Prendergast, D.; Moore, J. S.; Helms, B. A. Macromolecular Design Strategies for Preventing Active-Material Crossover in Non-Aqueous All-Organic Redox-Flow Batteries. *Angew. Chem. Int. Ed.* **2017**, *56* (6), 1595–1599. https://doi.org/10.1002/anie.201610582.

(19) Baran, M. J.; Braten, M. N.; Montoto, E. C.; Gossage, Z. T.; Ma, L.; Chénard, E.; Moore, J. S.; Rodríguez-López, J.; Helms, B. A. Designing Redox-Active Oligomers for Crossover-Free, Nonaqueous Redox-Flow Batteries with High Volumetric Energy Density. *Chem. Mater.* **2018**, *30* (11), 3861–3866. https://doi.org/10.1021/acs.chemmater.8b01318.

(20) Sanford, M.; Shrestha, A.; Hendriks, K.; Sigman, M.; Minteer, S. Realization of an Asymmetric Non-Aqueous Redox Flow Battery Through Molecular Design to Minimize Active Species Crossover and Decomposition. *Chem. – Eur. J.* **2020**, *n/a* (n/a). https://doi.org/10.1002/chem.202000749.

(21) Santasalo-Aarnio, A.; Peljo, P.; Aspberg, E.; Kontturi, K.; Kallio, T. Methanol, Ethanol and Iso-Propanol Performance in Alkaline Direct Alcohol Fuel Cell (ADAFC). *ECS Trans.* **2010**, *33* (1), 1701. https://doi.org/10.1149/1.3484660.

(22) Santasalo-Aarnio, A.; Hietala, S.; Rauhala, T.; Kallio, T. In and Ex Situ Characterization of an Anion-Exchange Membrane for Alkaline Direct Methanol Fuel Cell (ADMFC). *J. Power Sources* **2011**, *196* (15), 6153–6159. https://doi.org/10.1016/j.jpowsour.2011.03.028.

(23) Liu, J.; Xu, Q.; Jiang, J. A Molecular Simulation Protocol for Swelling and Organic Solvent Nanofiltration of Polymer Membranes. *J. Membr. Sci.* **2019**, *573*, 639–646. https://doi.org/10.1016/j.memsci.2018.12.035.

(24) Lee, J. N.; Park, C.; Whitesides, G. M. Solvent Compatibility of Poly(Dimethylsiloxane)-Based Microfluidic Devices. *Anal. Chem.* **2003**, *75* (23), 6544–6554. https://doi.org/10.1021/ac0346712.

(25) Vinothkumar, T. S.; Deivanayagam, K.; Ganesh, A.; Kumar, D. Influence of Different Organic Solvents on Degree of Swelling of Poly (Dimethyl Siloxane)-Based Sealer. *J. Conserv. Dent. JCD* **2011**, *14* (2), 156–159. https://doi.org/10.4103/0972-0707.82621.

(26) Noonan, K. J. T.; Hugar, K. M.; Kostalik, H. A.; Lobkovsky, E. B.; Abruña, H. D.; Coates, G. W. Phosphonium-Functionalized Polyethylene: A New Class of Base-Stable Alkaline Anion Exchange Membranes. *J. Am. Chem. Soc.* **2012**, *134* (44), 18161–18164. https://doi.org/10.1021/ja307466s.

(27) You, W.; Padgett, E.; MacMillan, S. N.; Muller, D. A.; Coates, G. W. Highly Conductive and Chemically Stable Alkaline Anion Exchange Membranes via ROMP of Trans-Cyclooctene Derivatives. *Proc. Natl. Acad. Sci.* **2019**, *116* (20), 9729–9734. https://doi.org/10.1073/pnas.1900988116.

(28) You, W.; Hugar, K. M.; Coates, G. W. Synthesis of Alkaline Anion Exchange Membranes with Chemically Stable Imidazolium Cations: Unexpected Cross-Linked Macrocycles from Ring-Fused ROMP Monomers. *Macromolecules* **2018**, *51* (8), 3212–3218. https://doi.org/10.1021/acs.macromol.8b00209.

(29) Sevov, C. S.; Hickey, D. P.; Cook, M. E.; Robinson, S. G.; Barnett, S.; Minteer, S. D.; Sigman, M. S.; Sanford, M. S. Physical Organic Approach to Persistent, Cyclable, Low-Potential Electrolytes for Flow Battery Applications. *J. Am. Chem. Soc.* **2017**, *139* (8), 2924–2927. https://doi.org/10.1021/jacs.7b00147.

(30) Sevov, C. S.; Samaroo, S. K.; Sanford, M. S. Cyclopropenium Salts as Cyclable, High-Potential Catholytes in Nonaqueous Media. *Adv. Energy Mater.* **2017**, *7* (5), 1602027. https://doi.org/10.1002/aenm.201602027.

(31) Hendriks, K. H.; Robinson, S. G.; Braten, M. N.; Sevov, C. S.; Helms, B. A.; Sigman, M. S.; Minteer, S. D.; Sanford, M. S. High-Performance Oligomeric Catholytes for Effective Macromolecular Separation in Nonaqueous Redox Flow Batteries. *ACS Cent. Sci.* **2018**, *4* (2), 189–196. https://doi.org/10.1021/acscentsci.7b00544.

Chapter 5

Synthesis and Investigation of Trimeric Cyclopropeniums on Physical and Electrochemical Properties

(This chapter contains work that is still unpublished. Future work for publication is being conducted in collaboration with Ryan Walser-Kuntz. Computational analysis is being conducted by Seyedeh (Nazanin) Maryamdokht Taimoory.)

5.1. Introduction

Redox flow batteries (RFBs) represent an emerging intermediary energy storage technology.[1–6] One of the most attractive features of RFBs are their scalability, which makes them a viable technology for large scale energy storage that can be used in conjunction with renewable sources of energy. This feature results from the use of soluble redox active species (anolytes and catholytes) to store energy that are housed in external reservoirs. The electrodes in an RFB merely facilitate the energy conversion process, and do not undergo any physical changes as a result.[7] This is in marked contrast with other electrochemical energy storage technologies, such as lithium ion batteries. Recent efforts in the field of RFB has been directed toward (1) the use of non-aqueous solvents, to widen the output voltage of the battery (~5 V window with acetonitrile), and (2) organic electrolytes, whose structures can be more readily tuned compared to metal-complexes.[1–6]

A key component of the redox flow battery setup is a partially permeable membrane that separates the two halves of the cell.[8] This membrane serves two crucial, and often contradicting, purposes. Firstly, the membrane must facilitate the transport of charge balancing ions during the charge-discharge cycling process. This maintains the electro-neutrality in the battery throughout its operation. Additionally, in a

asymmetric system, the membrane must prevent the diffusion of the redox active units to the other half of the cell. Such crossover of the electrolytes can directly lead to irreversible loss of storage capacity and can also result in lower overall coulombic efficiency. Crossover of redox active species can also induce parasitic reactions between the electrolytes of opposite polarity.

In fact, crossover of redox active species remains one of the largest current challenges in the field of RFBs. Several leading research groups have focused on developing strategies to overcome this challenge. One of such strategies involves utilization of redox active polymers (RAPs) as the electrolyte (Figure 5.1).[9] Due to the size of the polymers, crossover in these systems are significantly lower compared to systems that use small organic monomers as electrolytes. Additionally, specialized and expensive membranes are not required in these systems, which significantly reduces the cost of a flow battery.

An early example of the use of RAPs in RFBs was reported by the Schubert group, where they utilized water-soluble 2,2,6,6-tetramethylpiperidinyloxyl (TEMPO) and 4,4'-bipyridinium (viologen) with a widely available cellulose-based dialysis membrane in a RFB.[10,11] The authors were able to charge-discharge this polymer-based aqueous battery in a static cell for ~10,000 cycles. However, the authors reported limitations of the system arising from viscosity of the solution as a result of using polymers. More recently, the Rodriguez-Lopez and Moore groups have focused on design of RAPs for non-aqueous systems.[12–16] They have explored RAPs that include several redox active moieties, including viologen,[14,16] ferrocene,[15] nitrobenzene,[12] and cyclopropenium.[13] In their work,

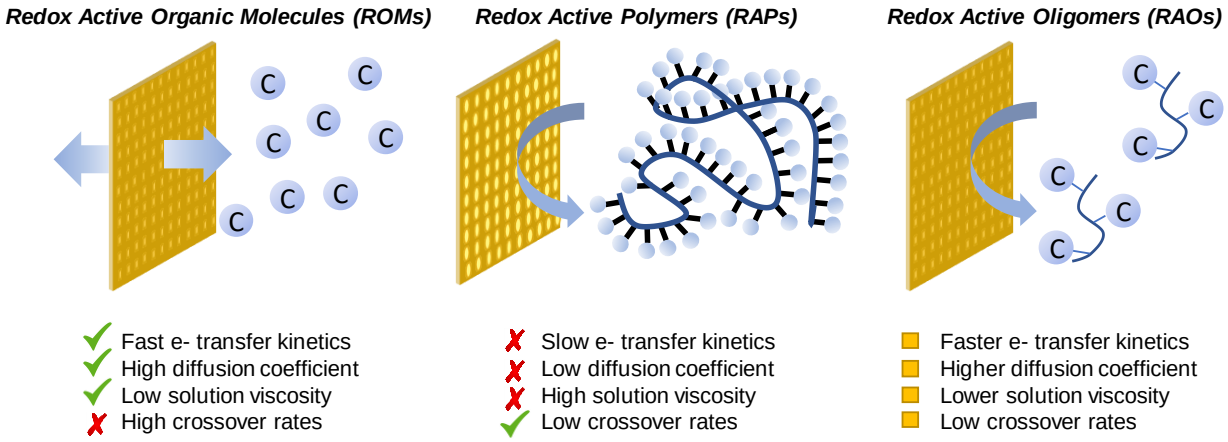

Figure 5.1. Comparison of various properties between redox active small organic molecules (ROMs), redox active polymers (RAPs) and redox active oligomers (RAOs). RAOs are the least studied class of electrolytes out of the three.

they have attempted to elucidate the impact of different features of polymer, such as polymer molecular weight or backbone tether on the electrochemical and physical properties of the RAPs.

While RAPs present an effective strategy to prevent crossover using simple and inexpensive membranes, they have several limitations that would prevent their use in a RFB (Figure 5.1). Solubility of these RAPs, especially in presence of supporting electrolyte salts, remains low (on the order of 1.2 Ah/L.[9] RAPs tend to salt out during the battery cycling processes. Concentrated solutions of RAPS also tend to be significantly more viscous and harder to pump through the cell than analogous solutions of monomeric electrolytes.[9,10,17] This can result poor mass transport as well as mechanical failures of the RFB parts. Additionally, their mass transport[14] and electron transfer kinetics suffer due to the size of the polymers.[18]

Redox-active oligomers (RAOs) overcome some of the presented limitations of RAPs (Figure 5.1). They possess desirable properties of both small organic molecules (rapid electron transfer kinetics, higher diffusion coefficients, lower viscosity, etc.) and redox active polymers (lower crossover).[18] In 2017, the Helms group first reported the suppression of crossover using a combination of a polymer of intrinsic microporosity (PIM) as the membrane and oligomers bearing tethered redox active moieties such as viologen, pyridinium, and dialkoxybenzene.[19] This report was followed by a systematic study of a series of linear cyclopropenium oligomers.[20] Dimers with different linker lengths were studied, and an interesting impact of the linker length on the overall electrochemical behavior of the oligomer was found. Inductive and stereoelectronic effects on the oxidation of the redox active cores were observed in the cyclic voltammograms. However, given sufficient spacers between the redox active units, the oligomers exhibit electrochemical behavior akin to an isolated monomeric cyclopropenium.[20]

RAOs present an exciting avenue for macromolecular design of redox-active species with promise for overcoming the limitations of small organic electrolytes as well

as redox active polymers. However, research in this field is still in its infancy. Fundamental studies on the impact of various structural morphologies of the oligomers on their electrochemical and physical properties as well as crossover behavior could prove invaluable. Changes in the oligomeric scaffold has already shown to have an influence on the RAO performance.[20] This Chapter focuses on systematically studying the impact of the three-dimensional morphology of RAOs on their redox potential, electron transfer kinetics, electrochemical stability, solubility, and crossover behavior. Cyclopropenium salt was chosen as the redox active core for this study due to the large amount of available data on this catholyte as well as the synthetic ease of appending it to various linkers. A small library of scaffolds that would provide different macromolecular arrangements were chosen. To append the cyclopropenium group on the oligomer, the corresponding oligoamines were first synthesized. Synthesis and purification of these oligoamines was the bottleneck of this process. Synthetic routes to cyclic trimers (**C2-C4**) were optimized, and the electrochemical behavior of these molecules was studied. Efforts to other oligoamines are still underway (*vide infra*).

5.2. Results and Discussion

5.2.1. Synthesis of the Cyclic Trimers

Previous work in the Sanford group focused on studying a series of linear oligomers.[20] In order to directly compare the effects of oligomer architecture on properties, our initial focus was directed toward an analogous series of cyclic trimers (Figure 5.2). Similar to the linear scaffold, these cyclic scaffolds of interest contain secondary amine functionalities in the backbone. This amine group can serve as an anchor for the attachment of redox-active bisaminocyclopropenium core. This symmetric series of RAOs consists of a 9-membered (**C2**), a 12-membered (**C3**), and a 15-membered (**C4**) ring with two, three, and four *carbon spacings* between the amine groups, respectively. We hypothesize that restricting the arrangement of the redox active cores in a ring in this fashion would: (a) alter the through-space interactions of the cationic redox-active molecules, which could affect the redox behavior of the oligomer; (b) potentially impact various physical properties such as solubility, rheology of the solution, and/or conductivity; and (c) change the kinetic diameter of the molecule, affecting the crossover behavior of

the oligomer. These are the parameters that will be studied as a result of changes in the three-dimensional morphology of these trimers.

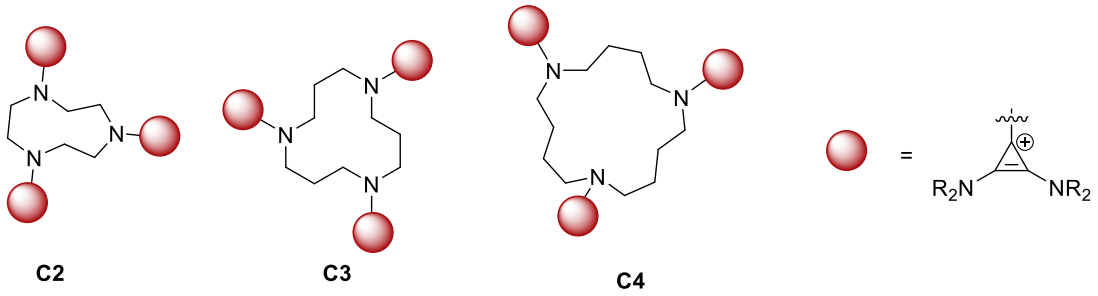

Figure 5.2. Series of cyclic trimers of interest for this study.

Most of these scaffolds are not commercially available; thus, they needed to be synthesized in order to conduct the fundamental studies. A general synthesis of the trimer from 1-chloro-2,3-bis(diisopropylamino)cyclopropenium chloride (**CP-Cl**) and the corresponding oligoamine has been previously reported (Scheme 5.1).[20] While the corresponding **C2-NH** oligoamine (triazonane) was commercially available, the **C3-NH** (triazacyclododecane) and the **C4-NH** (triazacyclopentadecane) oligoamines were either not commercially available or prohibitively expensive. Thus, synthetic routes to access **C3-NH** and **C4-NH** had to be mapped out. Importantly, the devised synthetic routes need to be readily scalable, since large quantities of the compound (>250 mg per experiment run at 25 mM concentration at 6 mL scale) is required to test the trimers in a RFB.

Scheme 5.1. Previous strategy to append cyclopropenium core to an oligoamine. Only the **C2** (triazonane) oligoamine is commercially available out of the three cyclic oligoamines.

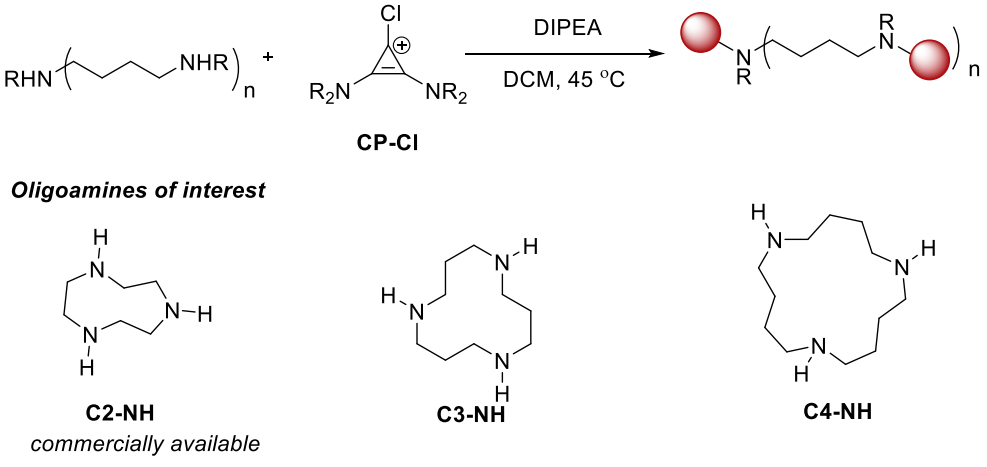

5.2.1.1. Synthetic Route to 1,5,9-Triazacyclododecane

The synthetic route to the macrocycle triazacyclododecane was inspired by the Atkins-Richman cyclization method for synthesis of polyazamacrocylic structures.[21,22] In the retrosynthetic analysis, the macrocyclic core was initially deconstructed into two simpler fragments (Scheme 5.2): a triamine (**I**) and a propyl fragment with two leaving groups on each of the terminal positions (**II**). Through a double substitution of the nucleophilic amine fragment (**I**) on the electrophilic propyl fragment (**II**), the desired ring could be constructed. The requisite starting materials, (3-aminopropyl)propanediamine (**I**) and 1,3 dibromopropane, are both commercially available, making this forward route a viable approach as shown in Scheme 5.3.

Scheme 5.2. Retrosynthetic bond disconnection to access triazacyclododecane.

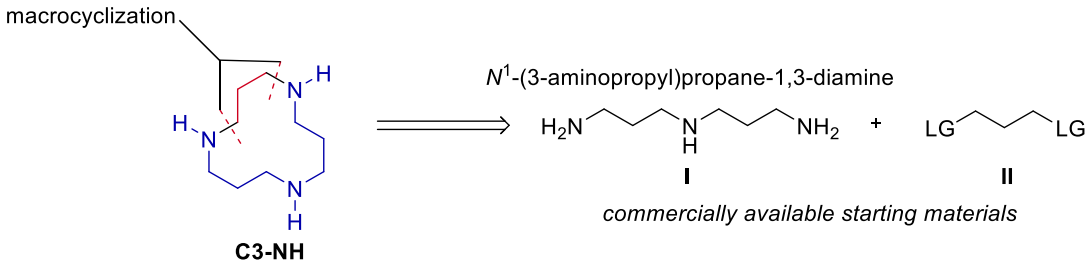

Protection of the starting triamine **I** is necessary to prevent overalkylation during the cyclization step. The Atkins-Richman cyclization employs a tosyl (Ts) protecting group on the amine fragment. The bulky sulfonamide group assists in the preorganization of the intermediates after the first substitution such that the transition state for the second substitution favors the intramolecular cyclization over intermolecular oligomerization.[23] For this reason, these reactions do not typically require high dilution of the starting materials. However, the tosyl protecting group requires harsh conditions to cleave. Thus, other protecting groups that are easier to deprotect, such as carboxybenzyl (Cbz) and nosyl (Ns), were also explored in this study. **I-Ts**, **I-Cbz** and **I-Ns** were prepared in high yields using well established base-assisted protection conditions.

Scheme 5.3. Proposed synthetic sequence to triazacyclododecane.

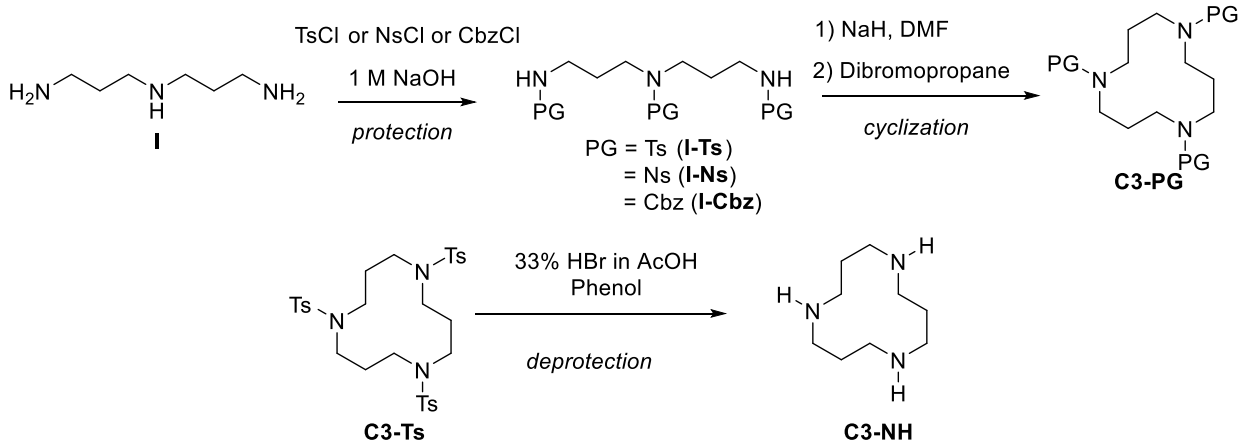

Following the protection of the triamine, the macrocyclization reaction was attempted under reported experimental conditions, using all three of the differently protected amines (**I-Ts**, **I-Cbz** and **I-Ns**) and 1,3-dibromopropane.[24] Sequential treatment of the amine with NaH in DMF (N–H deprotonation), followed by dropwise addition of a DMF solution of 1,3-dibromopropane resulted in different results with each protecting group. The desired product was only observed when using **I-Ts**. Based on ^{1}H NMR analysis, the starting material (**I-Cbz** and **I-Ns**) underwent complete decomposition during the reaction. It was believed that stirring **I-Cbz** or **I-Ns** with NaH caused deprotection of the Cbz or the Ns groups. Thus, milder reaction conditions using bases such as Cs_2CO_3, a non-nucleophilic base, that could potentially prevent such decomposition of **I-Cbz** or **I-Ns** and facilitate the macrocyclization could be examined in the future. However, in this study, we moved ahead with the tosyl protecting group rather than optimizing for a different protecting group. Detosylation was achieved by stirring **C3-Ts** in a mixture of 33% hydrobromic acid in acetic acid and phenol over 36 h.

Scheme 5.4. Addition of Boc-protecting group to purify the free-amine and deprotection to the free amine.

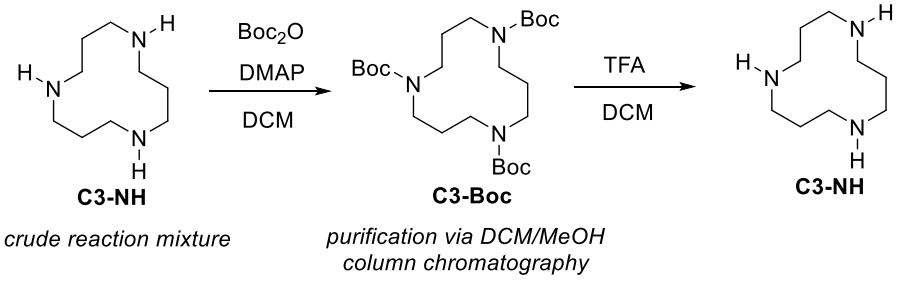

Purification of the free triamine **C3-NH** was challenging, requiring the use of a Boc protecting group and the formation of an intermediary **C3-Boc** species for isolation of the free **C3-NH**. The crude reaction mixture that was obtained after the detosylation reaction was directly subjected to Boc-protection conditions (Scheme 5.4). Addition of the Boc group allowed for facile purification via column chromatography using MeOH/DCM as eluents. The Boc protecting group was then cleaved under acidic conditions to obtain the pure, free amine **C3-NH** in quantitative yield.

5.2.1.2. Synthetic Route to 1,6,11-Triazacyclopentadecane

Given the success of the approach for **C3-NH**, our initial synthetic strategy for **C4-NH** was to construct the macrocycle from two similar fragments: a triamine and dibromobutane (Scheme 5.5). However, (4-aminobutyl)-butanediamine is not commercially available which necessitates a different approach.

Scheme 5.5. Initial disconnection strategy

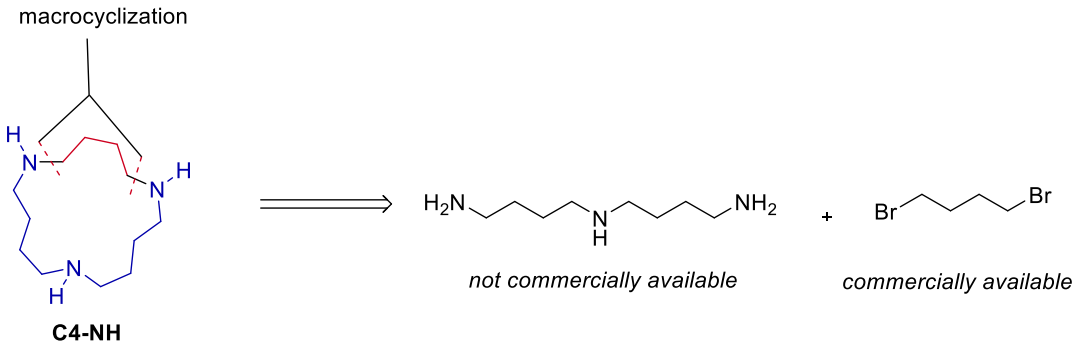

Another disconnection strategy to construct the triazacyclopentadecane ring is shown in Scheme 5.6. In this case, the macrocycle is disconnected to nucleophilic fragment diaminobutane (**IV**) and the corresponding electrophile **III**, with two terminal leaving groups on each end.[25] The macrocylization would then occur through two subsequent nucleophilic substitution reactions. The fragment **III** could be further deconstructed to an amine source and a butyl chain with two leaving groups on each end, such as 1,4-dibromobutane. Monosubstitution of the amine group in to two individual butyl fragments **V** would result in **III**. This strategy would have fewer overall linear synthetic steps compared to the initial strategy discussed above.

Scheme 5.6. Alternative disconnection strategy

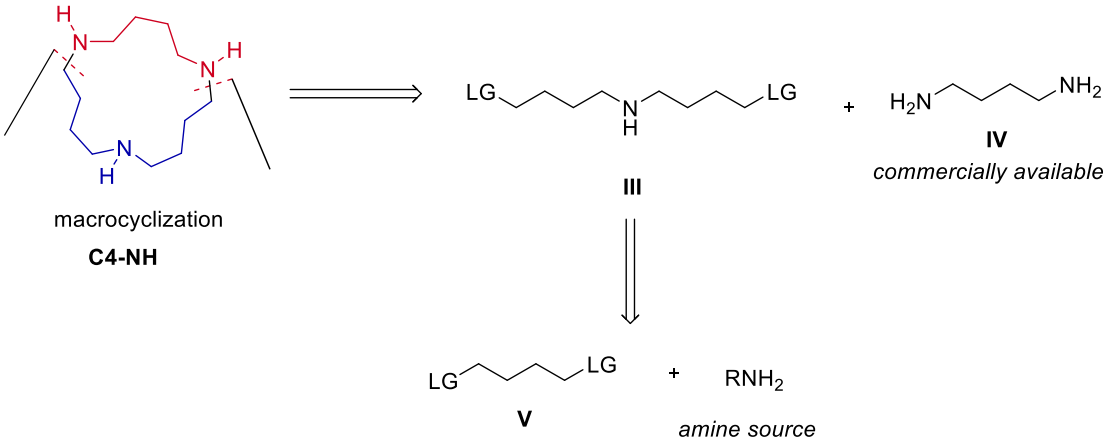

Since the tosyl protecting group worked well in synthesis of **C3-NH** and the conditions for detosylation were already optimized, *p*-toluenesulfonamide was chosen as the amine source. To facilitate monosubstitution of the sulfonamide with the alkyl halide, a solution of the sulfonamide was added dropwise to a solution containing 10 equivalents of alkyl halide. However, instead of the desired **III-Br**, double substitution into the alkylhalide occurred to yield a pyrrolidine ring (Scheme 5.7).

Scheme 5.7. Slow addition of *p*-toluenesulfonamide into dibromobutane

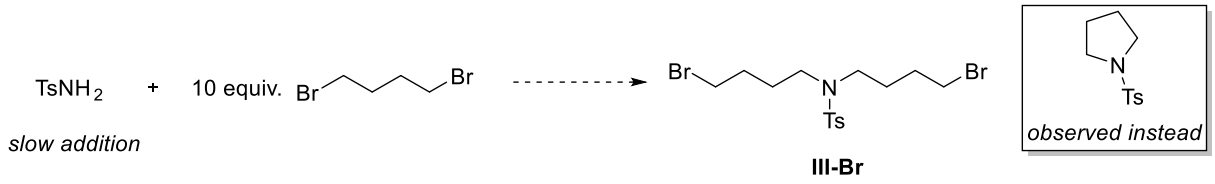

To overcome this challenge of intramolecular double alkylation of the sulfonamide, a different electrophilic partner was explored. 4-Chloro-1-tetrahydropyranylbutanol[26] was chosen as the electrophile, where the chloride would act as the leaving group while the tetrahydropyran (THP) protected alcohol would be unreactive to a subsequent nucleophilic attack. In the presence of NaH as the base, the nucleophilic substitution results in the desired **III-OTHP** in good yield (Scheme 5.8). Deprotection of the THP groups (using catalytic TsOH in methanol), followed by double mesylation afforded **III-OMs** in good yield (Scheme 5.8).

Scheme 5.8. Nucleophilic substitution of *p*-toluenesulfonamide into 4-chloro-1-tetrahydropyranylbutanol

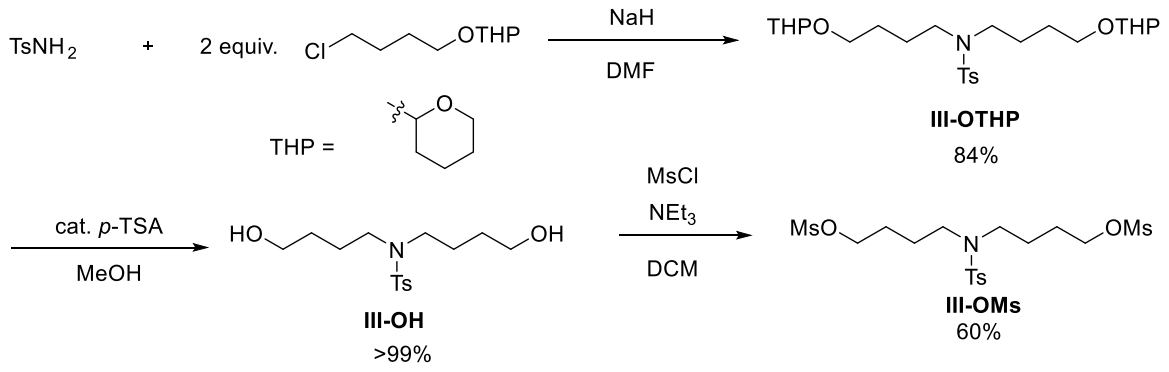

Ultimately, **III-OMs** was subjected to the macrocyclization reaction with the nucleophilic partner **IV-Ts**, that was synthesized via the previously established tosylation reaction (Scheme 5.9). An equimolar solution containing **III-OMs** and **IV-Ts** in DMF was added dropwise over 6 h to a suspension of base Cs_2CO_3 in DMF to yield **C4-Ts** in >90% yield. Again, high dilution was not necessary for this macrocyclization reaction because, upon first substitution, the sulfonamide protecting group leads to a transition state that favors intramolecular cyclization over intermolecular oligomerization. Detosylation was achieved under standard conditions (33% HBr in AcOH, PhOH) to generate the free amine **C4-NH**. **C4-NH** was purified using similar strategy as **C3-NH** via introduction of Boc-protecting group, column chromatography with MeOH/DCM, and then acid-catalyzed deprotection of Boc group.

Scheme 5.9. Synthesis of **C4-NH** from **III-OTHP** and **IV**

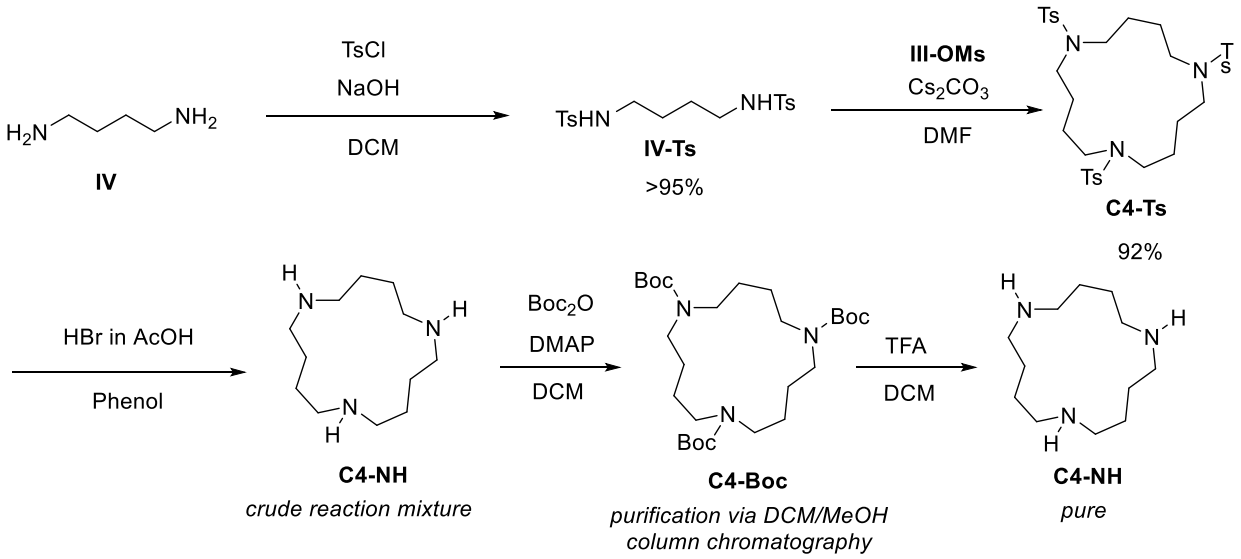

5.2.1.3. Synthesis and Electrochemical Analyses of the Cyclic Trimers

With all three free amines (**C2-NH**, **C3-NH**, **C4-NH**) in hand, the trimers were synthesized using previously reported conditions (Scheme 5.1).[20] In a solution containing the chloro-bispropylaminocyclopropenium salt, Hünig's base, and DCM, the amine solution in DCM was added at low temperatures. Each of the trimers was purified under different conditions. The **C2** trimer was purified via column chromatography using a MeOH/DCM eluent system, while pure **C3** trimer was obtained via recrystallization from hot MeOH. However, purification of the **C4** trimer was not as straightforward and required several iterations of oiling out the impurity with toluene followed by column chromatography with H_2O/MeCN to obtain pure **C4** trimer.

After the synthesis and purification of these trimers of interest, the electrochemical properties of these trimers were assessed. The cyclic voltammogram of trimer was collected (Figure 5.3) and compared to that of the previously studied linear dimers. The **C2** trimer underwent oxidation at +1.09 V vs Ag/Ag^+, the **C3** trimer underwent oxidation at +1.05 V vs Ag/Ag^+, and the **C4** timer underwent oxidation at +0.95 V vs Ag/Ag^+. These oxidation events were reversible in nature (see peak height ratios, Figure 5.3), and occurred at a potential that was higher than the oxidation of the monomeric tris(bisalkylamino)cyclopropenium salt itself (+0.88 V vs Ag/Ag^+). This indicates an inductive effect of the electron-withdrawing cyclopropenium groups on each other, thereby shifting the redox potential higher. Additionally, the peaks for **C2** and **C3** trimers are split while the peak for **C4** trimer is broadened. This splitting of the redox peaks indicates a stereoelectronic interaction of the redox-active cyclopropenium core due to the rigid structure of the macrocyclic scaffold.

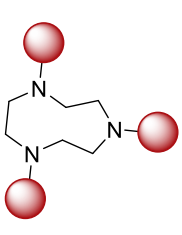

C2

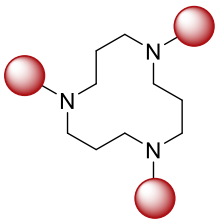

C3

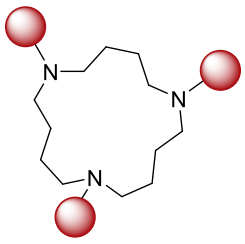

C4

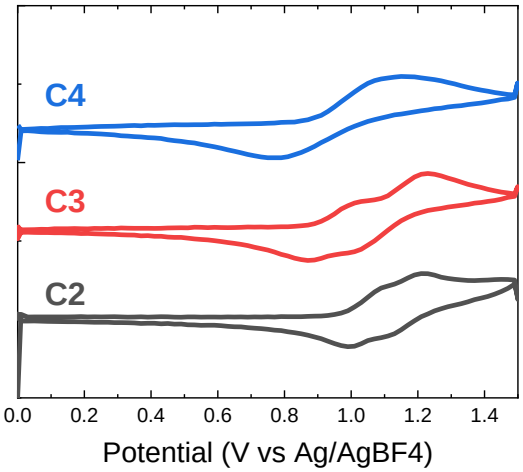

	$E_{1/2}$ vs $Ag/AgBF_4$	$\frac{i_{ox}}{i_{red}}$
Monomer	+0.88 V	
C4 trimer	+0.95 V	1.03
C3 trimer	+1.05 V	1.05
C2 trimer	+1.09 V	0.78

Figure 5.3. Cyclic Voltammogram of **C2**, **C3**, and **C4** trimers in KPF_6/MeCN solution at 100 mVs^{-1} scan rate. The CV was taken inside a nitrogen filled dry box, free from air and moisture. Glassy carbon was used as working electrode, platinum wire was used as counter electrode and $Ag/AgBF_4$ was used as reference.

Comparative analysis of the cyclic voltammogram of linear dimers (Figure 5.4) from the previous study[20] to those obtained for the cyclic trimers in this study was also conducted. Significant differences in the redox behavior of cyclic trimers and linear dimers were observed. For instance, **L2** exhibits an irreversible oxidative couple while the oxidation for **C2** was reversible by CV. Similarly, the CV for **L3** had a single peak, which indicates minimal stereoelectronic interaction in the linear dimer, whereas the **C3** trimer demonstrated drastic stereoelectronic interactions. These differences between the linear dimers and cyclic trimers indicates an effect of the three-dimensional structure on the redox behavior. More in-depth study is currently underway on the electrochemical stability of the cyclic trimers, any variations in physical properties, and their crossover across an anion-exchange membrane as well as a size-exclusion membrane. These studies require large quantities of the trimers, and the synthesis and purification of these trimers are a bottleneck of this process and are currently underway.

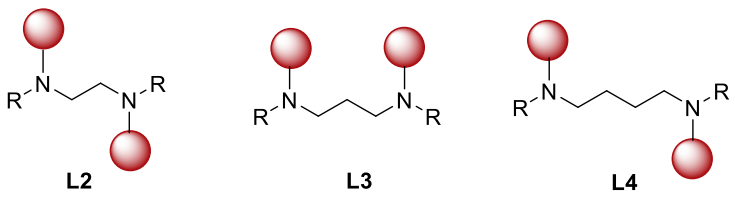

Figure 5.4. Linear dimers from the previous study

5.2.2. Attempted Synthesis of Different Triamine Scaffolds

The observed differences in the electrochemical behavior between the three-dimensional arrangements of the trimeric species prompted investigation into other scaffolds that would give the molecule different three-dimensional structure. To that end, a preliminary library of scaffolds was envisioned (Figure 5.5), including trimers with benzyl (**Bz**), cyclohexyl (**Cy**) and tripodal (**Tp**) scaffolds. Similar to the cyclic trimers, a synthetic route to access the corresponding triamines is required to synthesize these trimers.

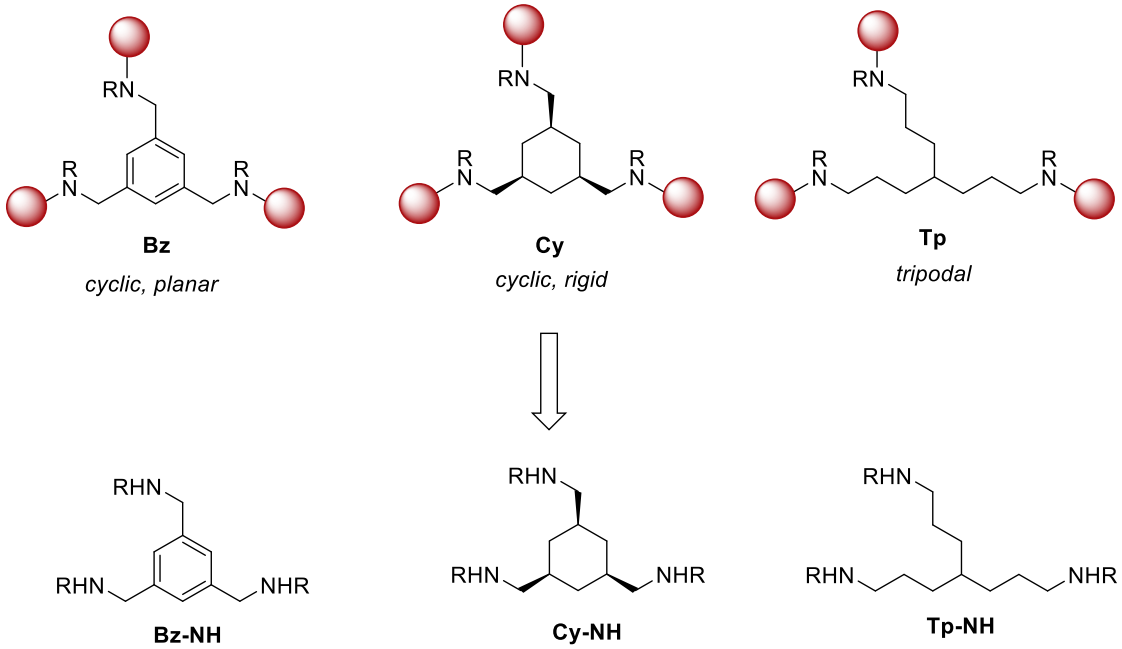

Figure 5.5. Preliminary scaffolds of interest and their corresponding oligoamines

5.2.2.1. Synthesis and Electrochemical Analysis of the Benzylic Trimer

The synthesis of **Bz-NH** was originally envisioned via a base-mediated three-fold nucleophilic substitution by alkylamine on tris(bromomethyl)benzene. However, despite several attempts to optimize the reaction by altering temperature, exploring additives that are known to facilitate such reactions (*e.g.,* AgOTf, NaI), and testing different solvents such (*e.g.,* acetone, THF, DMF) complete conversion to **Bz-NH** was never observed. Instead, the reactions afforded complex mixtures of mono-, di- and tri-substituted products, which proved to be difficult to separate. Instead, an alternative strategy was explored where the oligoamine **Bz-NH** was prepared via sequential reductive amination

reaction. Here, the benzyl-1,3,5-tricarbaldehyde was first stirred with propylamine in THF to afford a tris-imine intermediate. This tris-imine was then reduced to **Bz-NH** with $NaBH_4$. This sequence provided the desired product in excellent yield of 94%.

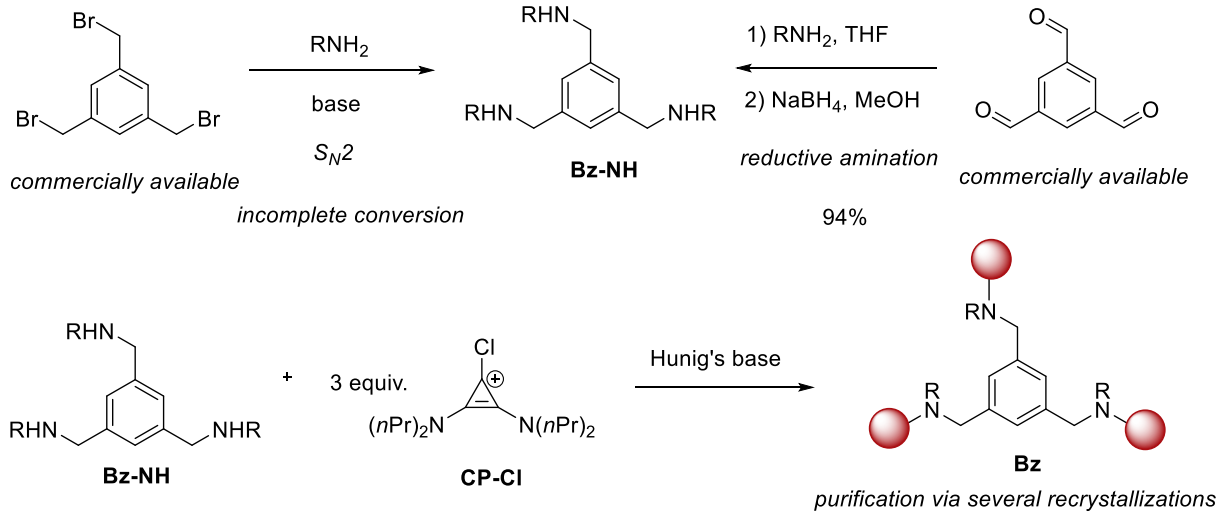

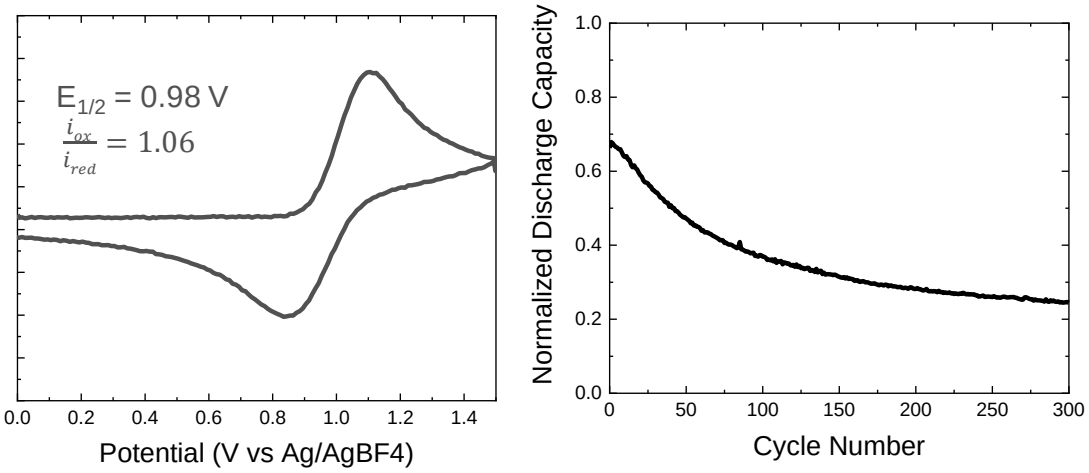

Figure 5.6. Synthetic route to benzylic trimer **Bz** and its electrochemical behavior. The CV was taken inside a nitrogen filled dry box, free from air and moisture in KPF_6/MeCN solution at 100 mVs^{-1} scan rate. Glassy carbon was used as working electrode, platinum wire was used as counter electrode and $Ag/AgBF_4$ was used as reference.

The trimer **Bz** was then synthesized from **Bz-NH** and the 1-chloro-2,3-bisaminocyclopropenium salt (**CP-Cl**) in the presence of Hünig's base. Pure samples of **Bz** were obtained after several rounds of recrystallization from MeOH. The electrochemical properties of **Bz** was then analyzed via CV, which showed a highly

reversible oxidative couple at +0.98 V vs Ag/$AgBF_4$ (Figure 5.6). This is higher than the parent trisaminocyclopropenium salt by 0.1 V (+0.88 V vs Ag/$AgBF_4$). The presence of electron withdrawing benzene ring close to the redox active cyclopropenium core is likely the reason for this shift in oxidation potential. Although **Bz** was stable on a cyclic voltammetry timescale, when the trimer was subjected to half-cell charge-discharge cycling, it lost 63% of its initial capacity over 300 cycles. ^{1}H NMR spectroscopic analysis showed complete decomposition of the starting trimer (**Bz**) and the concomitant formation of peaks that correspond to an aldehyde functional group. This implicates potential hydrolysis of the benzyl amine fragment and oxidation to an aldehyde. When the trimer is charged, the radical cation generated is highly acidic and electrophilic, making the scaffold susceptible to nucleophilic attack from any water molecules present in solution.

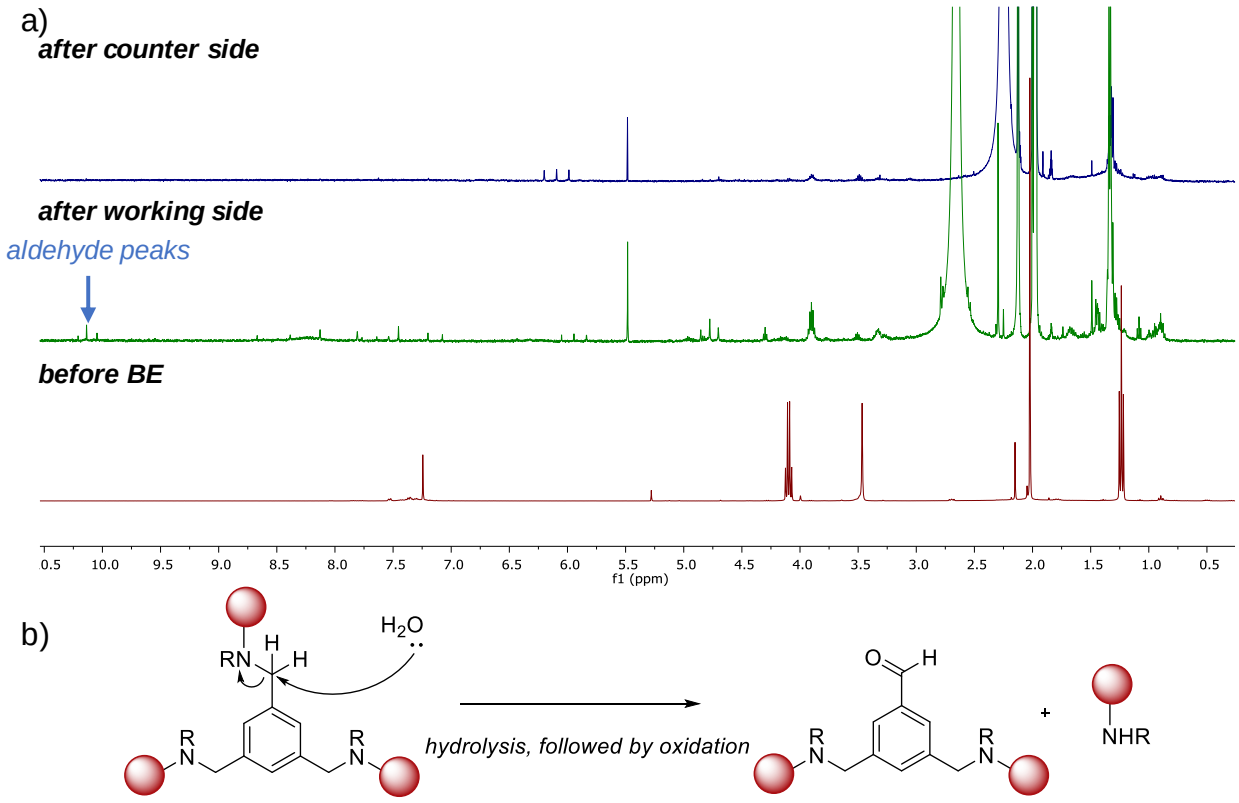

Figure 5.7. a) Postmortem ^{1}H analysis of the bulk electrolysis experiment with **Bz** that indicates complete consumption of starting material in both halves of the cell. b) A plausible mechanism of decomposition based on peaks observed in ^{1}H NMR.

5.2.2.2. Attempted Synthesis of Cy-NH and Tp-NH

The initial strategy to access **Cy-NH** led to an initial route via sequential amidation followed by exhaustive reduction of the corresponding amides (Scheme 5.10). This process uses a cheap and commercially available starting material: 1,3,5-cyclohexanetricarboxylic acid.[27,28]1-Ethyl-3-(3-dimethylaminopropyl)carbodiimide (EDC) coupling of the carboxylic acid and *n*-propyl amine was attempted under different temperatures, solvents, with added catalytic DMAP, and pre-stirring of the carboxylic acid and EDC with base before adding the amine nucleophile. However, the desired product was not observed. Instead, only adducts of the amine and EDC were observed (Scheme 5.10).

Scheme 5.10. Initial strategy to synthesize the oligoamine **Cy-NH** and attempts at amidation

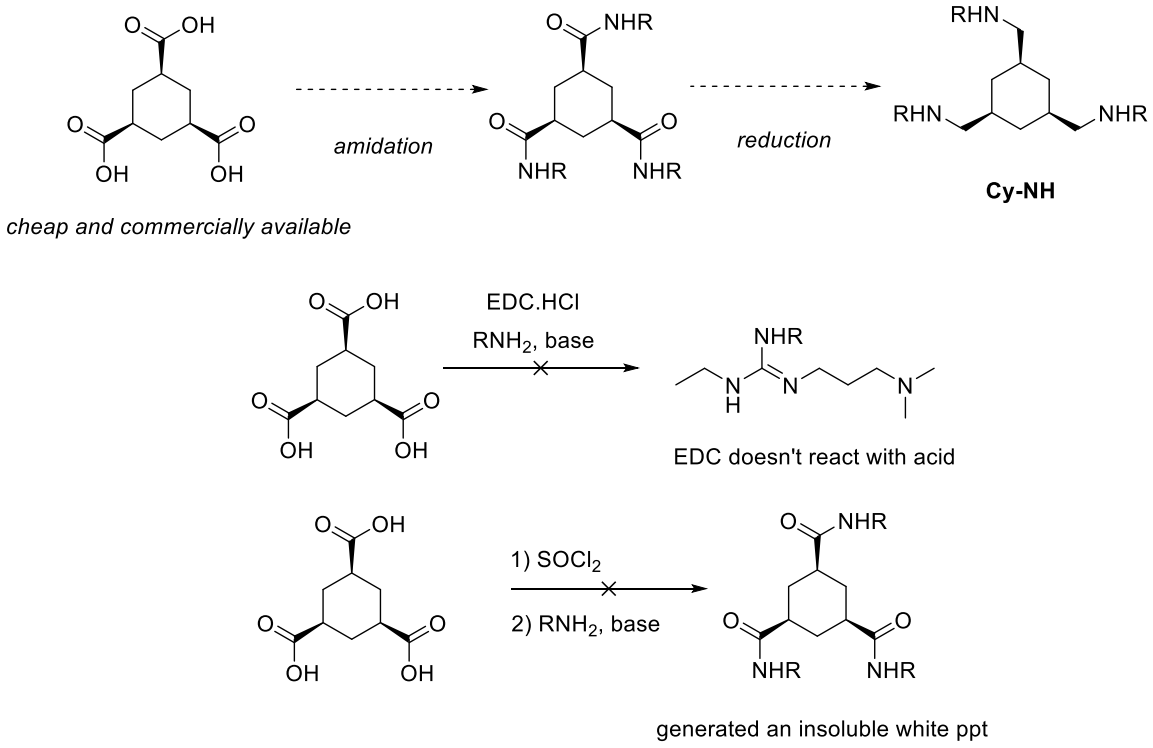

Amidation was also attempted through an acid chloride intermediate (Scheme 5.10). Stirring the tricarboxylic acid in thionyl chloride, with catalytic DMF yielded full conversion to the acyl chloride (based on ^{1}H NMR spectroscopic analysis). However, no amide product was detected upon addition of *n*-propylamine. Instead a white precipitate formed at the end of the reaction that was insoluble in a wide range of solvents (MeCN,

acetone, DCM, THF, water, DMSO, and 2 M HCl solution). The reaction was tested with a variety of solvents and bases at different temperatures to suppress the formation of the insoluble precipitate. Structures like 1,3,5-cyclohexylcarbamide are reported to self-assemble into macromolecular structures. Additives such as LiCl have been used to enhance solubility of the product but did not help to isolate the desired triamide.[27]

An alternative strategy to access **Cy-NH** was then proposed that would utilize a reductive amination reaction from an aldehyde and *n*-propylamine. This approach was successfully used to yield **Bz-NH** (Scheme 5.11). Since the cyclohexyltricarboxaldehyde (**Cy-CHO**) was not commercially available, we attempted the conversion of the tricarboxylic acid (**Cy-COOH**) to the desired trialdehyde. For this, the triacid (**Cy-COOH**) was completely converted to triol (**Cy-OH**) via an $LiAlH_4$ reduction at 60 °C. This reaction took ~7 days to completely consume the starting material, and the pure triol could be obtained in 50% yield after column chromatography. Subsequently, oxidation of the triol to aldehyde (**Cy-CHO**) was then attempted. Various oxidizing reagents were tested for this oxidation, including Bobbit's salt, Dess-Martin periodinane (DMP), and the Parikh-Doering reagent. The reaction mostly suffered from incomplete conversion to the trialdehyde (based on ^{1}H NMR and HRMS analyses). Furthermore, it was also noted that the trialdehyde (**Cy-CHO**) was highly unstable at room temperature and underwent decomposition in a matter of hours.

Scheme 5.11. Reductive amination route to synthesis of **Cy-NH**

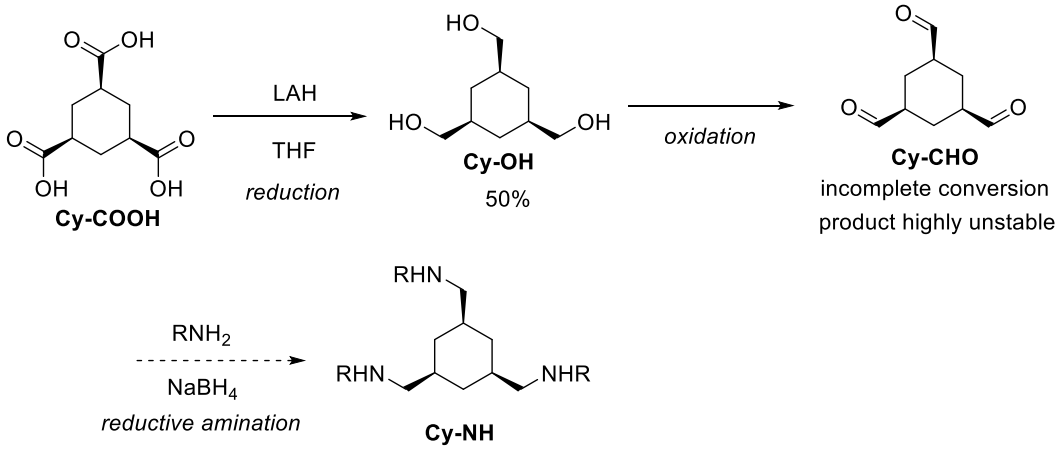

In the future, **Cy-NH** could be accessed through ring hydrogenation of **Bz-NH** (Scheme 5.12). Various heterogeneous catalysis systems are known for aromatic ring

hydrogenation that can tolerate the presence of the benzyl amine functional group. These include Ru/C in presence of $LiNO_3$,[29] titanium(III) oxo clusters,[30] and rhodium-platinum bimetallic nanoparticles,[31] among others.

Scheme 5.12. Future direction for synthesis of **Cy-NH**

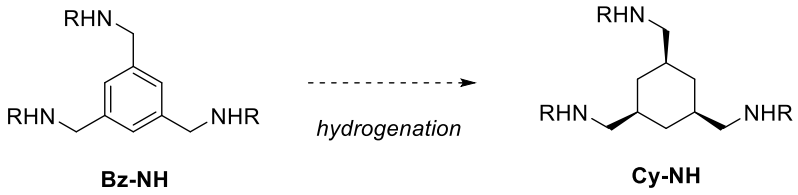

Bz-NH **Cy-NH**

Lastly**, Tp-NH** was proposed to be synthesized through reductive amination of the tripodal triamine (**Tp-NH_2**) and propionaldehye (Scheme 5.13). **Tp-NH_2** was prepared in 2 steps from the commercially available **Tp-NO_2** through a radical denitration reaction to form **Tp-CN**, followed by reduction of the nitrile groups with $LiAlH_4$ (Scheme 5.13). While **Tp-NH_2** could be synthesized through this route (as confirmed by ^{1}H NMR spectroscopic analysis), purification of this intermediate proved challenging. Protection of the free amine using a Boc-protecting group was attempted. Precipitation of the ammonium salt was also attempted. Additionally, reductive amination of the crude reaction mixture to directly access the imine was also evaluated. However, all these attempts led to decomposition of the free amine instead.

Scheme 5.13. Attempted synthesis of **Tp-NH**

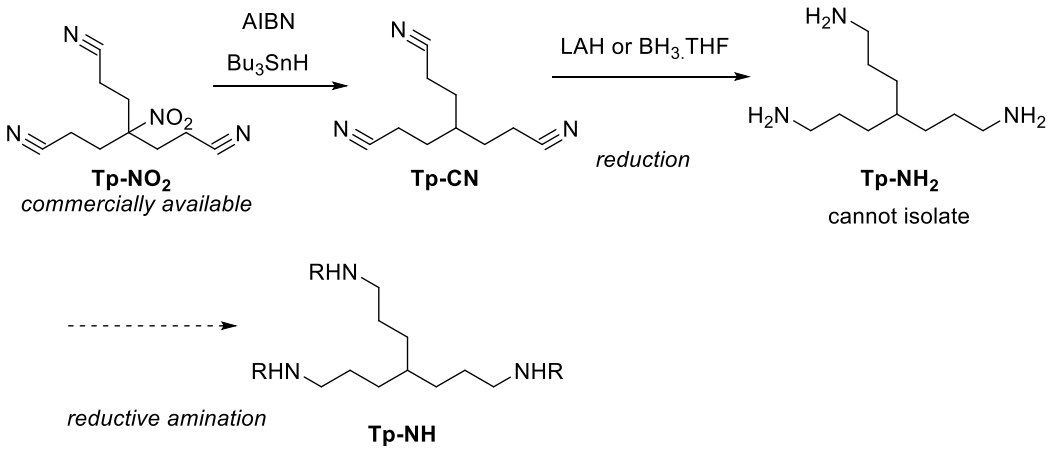

Future attempts at synthesis of a tripodal scaffold will focus on commercially available tetraamines such as **Tp2-N4** and **Tp3-N4** (Figure 5.7). First, the terminal amines would be alkylated, followed by addition of a protecting group (such as Boc or Cbz). This

would allow for quaternization of the central tertiary amine. In addition to preventing the oxidation of the tertiary amine in the scaffold, this quaternization would also enhance the solubility of the trimer. Appending ammonium groups to a redox active core has previously been studied as an effective strategy to promote solubility of electrolytes.[32–34]

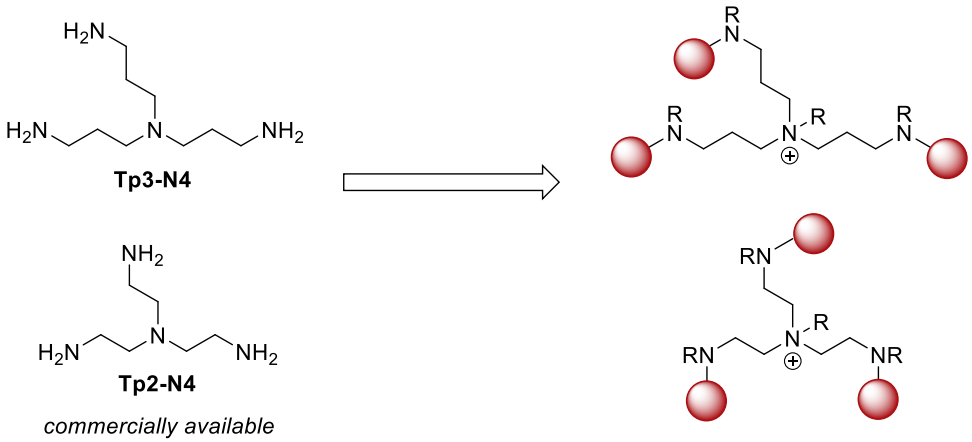

Figure 5.8. Future direction to access tripodal trimers

5.3. Conclusion and Outlook

This chapter summarizes efforts toward the synthesis of trimers with different three-dimensional arrangements as well as the preliminary investigation of the effects such variations have on the electrochemical behavior of these molecules. To that end, our initial focus was geared toward the synthesis of cyclic analogues of the linear oligomers. Linear oligomers of cyclopropenium salt were previously studied in our group. Tying the backbone chain into a cyclic configuration would give the trimer a different 3D structure, and the redox-active units within the trimer would interact with each other differently. This is evident in differences observed in cyclic voltammetry of these cyclic trimers. Any effects on other physical properties such as solubility, diffusion coefficient, or crossover will be a subject of future studies. In addition, synthesis of a small collection of scaffolds was also attempted and will be continued in future.

The differences in electrochemical behavior observed with the cyclic trimers warrants further investigation to study their origins. Current efforts are aimed at utilizing computational analyses as a tool for these investigations. The lowest energy conformer of the trimers can be identified to assess through space interactions of redox active units. Differences in thermodynamics for the sequential oxidation of each appended CP unit

along with any variation in HOMO or SOMO of the trimers will also be calculated. Using computational analyses to aid the experimental observations will provide critical information that will guide the design of future generations of RAOs.

5.4. Experimental Details

5.4.1. Synthesis

5.4.1.1 Instrumental Information

NMR spectra were recorded on a Varian vnmrs 700 (700 MHz for ^{1}H; 176 MHz for ^{13}C) or a Varian vnmrs 500 (500 MHz for ^{1}H; 126 MHz for ^{13}C) spectrometer with the residual solvent peak ($CDCl_3$; ^{1}H: δ = 7.26 ppm, ^{13}C: δ = 77.16 ppm; CD_3CN; ^{1}H: δ = 1.94 ppm, 13C: δ = 1.32 ppm) as the internal reference unless otherwise noted. Chemical shifts are reported in parts per million (ppm, δ) relative to tetramethylsilane. Multiplicities are reported as follows: s (singlet), d (doublet), t (triplet), q (quartet), and m (multiplet). Coupling constants (*J*) are reported in Hz. High-resolution mass spectra were recorded on a Micromass AutoSpec Ultima Magnetic Sector mass spectrometer. A multi-channel potentiostat from Bio-Logic Instruments (model VSP-CHAS) was used for all the electrochemical studies.

5.4.1.2 Materials and Methods

All commercial reagents and solvents were used as received, unless otherwise noted. Anhydrous CH_2Cl_2 was obtained from an SDS solvent system. All reactions were performed under nitrogen atmosphere unless otherwise noted. Thin layer chromatography (TLC) was performed on Macherey-Nagel SIL G-25 TLC plates pre-coated with silica gel UV254. Biotage® SNAP Ultra column cartridges were used for flash column chromatography.

5.4.1.3 General Procedure for Cyclopropenium Oligomers

A solution of 1-chloro-2,3-bis(diisopropylamino)cyclopropenium chloride (615 mg, 2.0 mmol) and Hünig's base (388 mg, 3.0 mmol) in DCM (10 mL) was cooled to 0 °C and one equivalent of the selected oligoamine was added dropwise. After stirring for 15 minutes, the solution was allowed to warm to room temperature and subsequently heated to 45 °C. After 16 hours, the solution was washed with a 1:1 brine and 2 M HCl solution

(20 mL). The aqueous layer was further extracted with DCM (2 × 30 mL) and the combined organic fractions were reduced *in vacuo*. The residue was dissolved in water (20 mL) and under vigorous stirring, a solution of ammonium hexafluorophosphate (652 mg, 4.0 mmol) in water (5 mL) was added. The resulting white precipitate was extracted with DCM (3 × 30 mL) and the combined organic fractions were dried with $MgSO_4$ and reduced. The oligomer was subsequently purified as described in the procedures below.

5.4.1.4 Synthesis of 1,5,9-Triazacyclododecane Scaffold

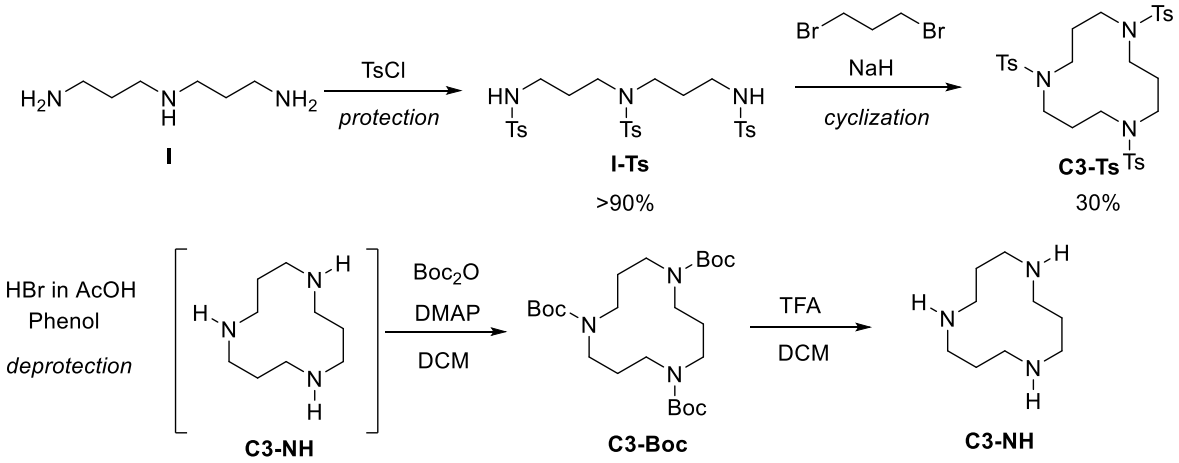

Tosylchloride (12.4 g, 65.3 mmol, 3.1 equiv.) was taken in dichloromethane (40 mL) in a 250 mL round-bottom flask equipped with a stir bar. The flask was cooled to 0 °C. To this flask, a solution of *N*-(3-aminopropyl)-propane-1,3-diamine (3.0 mL, 21.4 mmol, 1.0 equiv.) in 1 M NaOH (50 mL) was added dropwise with the use of an addition funnel. Upon completion of the addition, the reaction was allowed to warm up to room temperature and stir for 12 h. The organics were extracted into DCM, and the aqueous solution was washed with DCM (50 mL). The combined organics were dried over $MgSO_4$, filtered, and concentrated *in vacuo*. A silica plug was run to purify the desired compound. The plug was washed with DCM first until TLC was clear (to wash away the remaining tosylchloride in the reaction mixture). The solvent was then switched to EtOAc and the desired product **I-Ts** was collected in XX% yield (XX g).

^{1}H NMR (700 MHz, Chloroform-d) δ 7.72 (d, J = 8.3 Hz, 4H), 7.63 (d, J = 8.3 Hz, 2H), 7.30 (m, J = 8.7 Hz, 6H), 3.10 (t, J = 6.7 Hz, 4H), 2.96 (q, J = 6.4 Hz, 4H), 2.43 (s, 3H), 2.41 (s, 6H), 1.71 (p, J = 6.5 Hz, 4H).

^{13}C NMR (176 MHz, cdcl$_3$) δ 143.85, 143.42, 136.92, 135.33, 129.93, 129.75, 127.10, 127.00, 46.91, 39.97, 29.40, 21.52, 21.50.

HRMS: Calc. 593.1688, Measured: XX

For the macrocyclization, a dry 20 mL vial equipped with a stir bar was charged with the tosyl-protected triamine (**1**, 219 mg, 0.37 mmol, 1.0 equiv.) in DMF (2.75 mL). The solution was cooled to 0 °C, and NaH (33 mg, 0.83 mmol, 2.2 equiv.) was added to the solution. The mixture was stirred for 1 h at room temperature. Meanwhile, dibromopropane (38 µL, 0.37 mmol, 1.0 equiv.) was dissolved in 1.85 mL DMF and taken up in a syringe. The reaction vial was heated up to 100 °C and the solution of dibromopropane was added to the reaction flask dropwise over a period of 4 h. The reaction was stirred for 18 h. Upon completion, the reaction was cooled to 60 °C, and the DMF was distilled off the reaction flask. Once concentrated, the reaction was cooled to room temperature, 5 % LiCl solution (10 mL) was added to the reaction flask and the organic were extracted into DCM (10 mL X 3). The combined organics were dried over $MgSO_4$, filtered, and concentrated *in vacuo*. The macrocycle was purified via flash chromatography with a solvent gradient of 40% - 80% EtOAc/hexanes to yield 76.6 mg (32%) of **C3-Ts**.

^{1}H NMR (500 MHz, Chloroform-*d*) δ 7.65 (d, *J* = 8.2 Hz, 6H), 7.32 (d, *J* = 8.1 Hz, 6H), 3.22 (t, *J* = 6.7 Hz, 11H), 2.44 (s, 9H), 1.92 (t, *J* = 6.8 Hz, 4H).

^{13}C NMR (176 MHz, cdcl$_3$) δ 143.60, 135.07, 129.81, 127.27, 127.17, 45.45, 26.28, 21.50.

HRMS: Calc. [M + H$^+$] 634.2078, Measured: 634.2065

For deprotection of **C3-Ts**, the tosyl protected alkylamine (665 mg, 1.05 mmol, 1.0 eauiv.) taken in a vial equipped with a stir bar. To this, hydrobomic acid (24 mL, 33% in acetic acid) and phenol (2.4 g, 1 g/mL of acid) were added. The solution was gradually heated to 90 °C and stirred for 16 h while excess HBr gas was captured with a base trap. After cooling down the dark mixture, water (30 mL) was added and the solution was stirred for 15 minutes. The resulting mixture was washed with DCM (4 × 100 mL) after which it was basified to pH > 11 using a 10 M sodium hydroxide solution and extracted with ethyl

acetate (4 × 100 mL). The combined organic fractions were dried with $NaSO_4$ (not $MgSO_4$), filtered and concentrated *in vacuo*.

For purification, the triamine was protected with a Boc protecting group. The crude reaction was taken in a 20 mL vial equipped with a stir bar. To it, Boc_2O (1.5 g, 6.8 mmol, 6.6 equiv.), dimethylaminopyridine (DMAP, 50 mg, 0.41 mmol, 0.4 equiv.) and DCM (10.5 mL) were added. The reaction was stirred for 12 h at room temperature. The reaction was then washed with water (10 mL). The organic layer was dried over $MgSO_4$, filtered and concentrated. The compound was purified via flash chromatography using 0%-10% MeOH in DCM. $KMnO_4$ stain was used to locate the compound in TLC. The pure compound **C3-Boc** was obtained in 35% yield after purification (169 mg).

^{1}H NMR (700 MHz, Chloroform-*d*) δ 3.33 (t, *J* = 6.8 Hz, 12H), 1.88 (p, *J* = 6.8 Hz, 6H), 1.45 (s, 26H).

^{13}C NMR (176 MHz, cdcl$_3$) δ 156.12, 79.59, 45.60, 28.45.

HRMS: Calc. [M + H$^+$] 472.3387, Measured: XX

For Boc deprotection, **C3-Boc** was stirred in a solution with 0.4 mL TFA and 0.9 mL DCM at room temperature for 12 h. The reaction was concentrated, washed with 1 M NaOH (3 mL) and the desired product extracted into DCM (3 mL X 3). The combined organics were dried over $NaSO_4$, filtered and concentrated to yield 62 mg of the free amine **C3-NH**.

^{1}H NMR (401 MHz, Chloroform-*d*) δ 2.81 – 2.73 (m, 12H), 1.67 (p, *J* = 5.9, 5.4 Hz, 6H).

^{13}C NMR (176 MHz, cdcl$_3$) δ 48.80, 28.76.

HRMS: Calc. [M + H$^+$] 172.1814, Measured: XX

5.4.1.5 Synthesis of (tosylazanediyl)bis(butane-4,1-diyl) dimethanesulfonate (6)

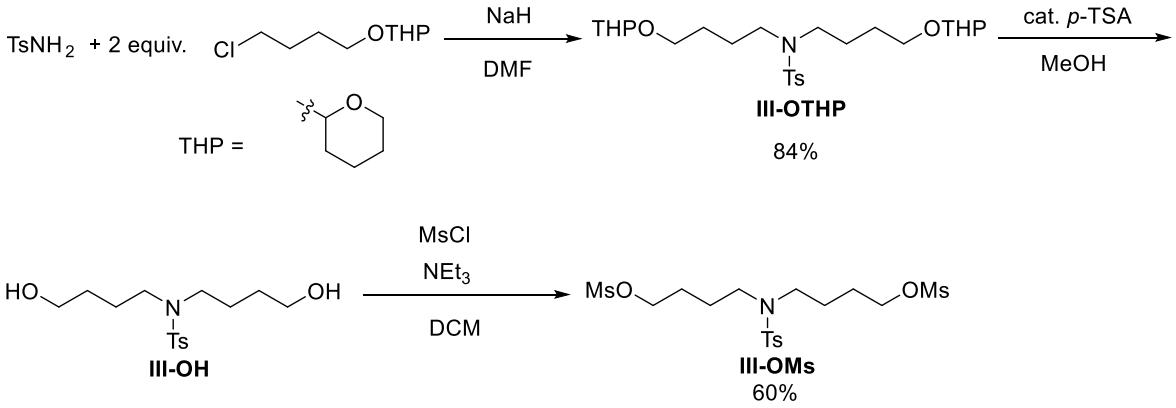

In a dry 250 mL round bottom flask equipped with a stir bar, tosylamide (4.44 g, 26 mmol, 1.0 equiv.) and DMF (116 mL) was taken. The flask was cooled to 0 °C and NaH (2.5 g, 62 mmol, 2.4 equiv.) was added to the reaction flask. The flask was slowly warmed up to 70 °C, and stirred at this temperature for 1.5 h. The reaction bubbled a lot upon heating. 2-(4-Chlorobutoxy)tetrahydro-2*H*-pyran (9.34 mL, 52 mmol, 2 equiv.) was added to the reaction mixture. The reaction was stirred for 18 h and monitored by TLC. In case of any remaining starting material or mono-substituted product, more alkylchloride was added to the reaction. This is critical, because separation of monosubstituted compound from disubstituted product is rather difficult. Upon completion, DMF was distilled from the reaction. 5% LiCl (100 mL) was added to the reaction flask, and the desired product extracted into DCM (100 mL X 3). The combined organics were dried over $MgSO_4$, filtered and concentrated. The product was purified via flash chromatography using 20% - 60% EtOAc/Hexanes to yield 10.6 g (85%) of **III-OTHP**.

^{1}H NMR (500 MHz, Chloroform-*d*) δ 7.69 (d, *J* = 8.3 Hz, 2H), 7.29 (d, *J* = 8.2 Hz, 2H), 3.85 (ddd, *J* = 11.1, 7.8, 3.1 Hz, 2H), 3.73 (dt, *J* = 9.7, 6.2 Hz, 2H), 3.54 – 3.47 (m, 2H), 3.38 (dt, *J* = 9.6, 6.0 Hz, 2H), 3.15 (t, *J* = 7.3 Hz, 4H), 2.42 (s, 3H), 1.81 (ddd, *J* = 14.7, 8.1, 4.6 Hz, 2H), 1.75 – 1.68 (m, 2H), 1.68 – 1.48 (m, 14H), 0.94 – 0.81 (m, 2H).

^{13}C NMR (176 MHz, $cdcl_3$) δ 142.91, 137.10, 129.56, 127.10, 98.86, 66.91, 62.35, 48.13, 30.72, 26.93, 25.64, 25.45, 21.46, 19.64.

HRMS: Calc. [M + H^+] 484.2733, Measured: XX

For THP deprotection, in a 250 mL round bottom flask equipped with a stir bar, **III-OTHP** (8 g, 16 mmol, 1.0 equiv.), catalytic amount of TsOH (57 mg, 2 mol%) and MeOH (160 mL) were taken. The mixture was stirred at room temperature for 16 h. The reaction mixture was concentrated, washed with $NaHCO_3$ (60 mL) and organic compound extracted into EtOAc (50 mL X 3). The combined organics were dried over $MgSO_4$, filtered and concentrated to yield a quantitative conversion to **III-OH** (5.0 g).

^{1}H NMR (500 MHz, Chloroform-*d*) δ 7.67 (d, *J* = 8.3 Hz, 2H), 7.29 (d, *J* = 8.0 Hz, 2H), 3.64 (t, *J* = 6.1 Hz, 4H), 3.12 (t, *J* = 7.3 Hz, 4H), 2.41 (s, 3H), 1.64 (tt, *J* = 7.4, 5.6 Hz, 4H), 1.60 – 1.53 (m, 4H).

^{13}C NMR (176 MHz, cdcl$_3$) δ 143.28, 136.80, 129.80, 127.26, 62.47, 48.50, 29.68, 25.44, 21.65.

HRMS: Calc. [M + H$^+$] 316.1583, Measured: XX

For mesyl protection, **III-OH** (4 g, 12.7 mmol, 1 equiv.) was taken in a 50 mL round bottom flask equipped with a stir bar. DCM (15 mL) was added and the flask was cooled to 0 °C. Triethylamine (4.06 mL, 29.2 mmol, 2.3 equiv.) was then added, followed by mesylchloride (2.06 mL, 26.6 mmol, 2.1 equiv.). The reaction was stirred at room temperature for 16 h. Then, the reaction was washed with water (10 mL X 2), followed by brine (10 mL). The organic layer was dried over $MgSO_4$, filtered and concentrated. The product was purified via flash chromatography with 40% - 80% EtOAc/hexanes to yield product **III-OMs** in 67% yield (4 g).

^{1}H NMR (700 MHz, Chloroform-*d*) δ 7.67 (d, *J* = 8.2 Hz, 2H), 7.32 (d, *J* = 8.0 Hz, 2H), 4.25 (t, *J* = 6.2 Hz, 4H), 3.13 (t, *J* = 7.3 Hz, 5H), 3.02 (s, 6H), 2.43 (s, 3H), 1.79 (dt, *J* = 8.1, 6.3 Hz, 5H), 1.69 (p, *J* = 7.3 Hz, 4H).

^{13}C NMR (176 MHz, cdcl$_3$) δ 143.65, 136.38, 129.97, 127.26, 69.51, 48.32, 37.52, 26.38, 25.15, 21.66.

HRMS: Calc. [M + H$^+$] 472.1134, Measured: XX

5.4.1.6 Synthesis of 1,6,11-triazacyclopentadecane

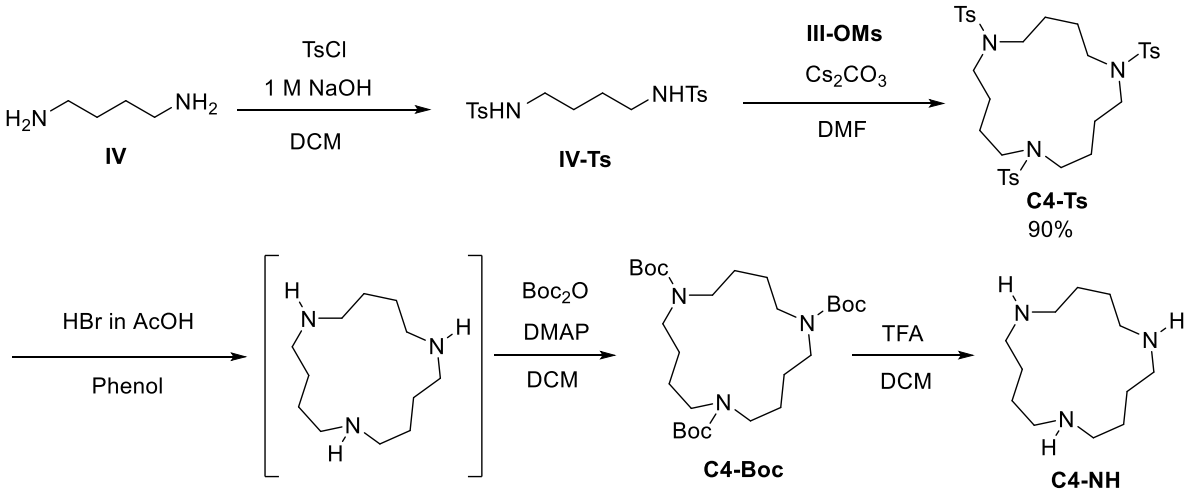

Tosylchloride (4.84 g, 25.4 mmol, 2.0 equiv.) was taken with dichloromethane (30 mL) in a 100 mL round-bottom flask equipped with a stir bar. The flask was cooled to 0 °C. To this flask, a solution of 1,4-diaminobutane (1.12 g, 12.7 mmol, 1.0 equiv.) in 1 M NaOH (28 mL) was added dropwise with the use of an addition funnel. Upon completion of the addition, the reaction was allowed to warm up to room temperature and stir for 12 h. The organics were extracted into DCM, and the aqueous solution was washed with DCM (50 mL). The combined organics were dried over $MgSO_4$, filtered, and concentrated *in vacuo*. A silica plug was run to purify the desired compound. The plug was washed with DCM first until TLC was clear (to wash away the remaining tosylchloride in the reaction mixture). The solvent was then switched to EtOAc and the desired product **IV-Ts** was collected in XX% yield (XX g).

^{1}H NMR (700 MHz, Chloroform-*d*) δ 7.72 (d, *J* = 8.3 Hz, 4H), 7.31 (d, *J* = 8.0 Hz, 4H), 2.95 – 2.89 (m, 4H), 2.43 (s, 6H), 1.53 – 1.47 (m, 4H).

^{13}C NMR (176 MHz, cdcl$_3$) δ 143.71, 136.94, 129.93, 127.22, 42.74, 26.69, 21.69.

HRMS: Calc. [M + H$^+$] 397.1256, Measured: XX

For macrocyclization, a solution of **III-OMs** (200 mg, 0.425 mmol, 1.0 equiv.) and **IV-Ts** (169 mg, 0.425 mmol, 1.0 equiv.) in DMF (2.25 mL) was prepared. In a 20 mL vial equipped with a stir bar, Cs_2CO_3 (692 mg, 2.13 mmol, 5.0 equiv.) was charged with DMF

(2 mL) and heated to 85 °C. The solution of **III-OMs** and **IV-Ts** were added to reaction flask dropwise over a period of 6 h. The reaction was stirred for 18 h. Then, DMF was removed via distilled. After cooling the reaction to room temperature, DCM (15 mL) was added to the flask, and the solution was filtered through a pad of Celite into a separatory funnel. The filtrate was then washed with 5% LiCl solution (15 mL). Organics were extracted into DCM. Combined organics were dried over $MgSO_4$, filtered and concentrated. The product was purified via flash chromatography with 40% - 80% EtOAc/hexanes to yield product **C4-Ts** in 92% yield (265 mg).

^{1}H NMR (700 MHz, Chloroform-*d*) δ 7.65 (d, *J* = 8.2 Hz, 6H), 7.31 (d, *J* = 8.0 Hz, 6H), 3.04 (d, *J* = 5.6 Hz, 12H), 2.43 (s, 9H), 1.70 (d, *J* = 4.4 Hz, 12H).

^{13}C NMR (176 MHz, $cdcl_3$) δ 143.48, 135.58, 129.85, 127.46, 50.20, 27.06, 21.65.

HRMS: Calc. [M + H^+] 676.2549, Measured: XX

For tosyl deprotection, the tosyl protected alkylamine **C4-Ts** (400 mg, 0.59 mmol, 1.0 eauiv.) taken in a vial equipped with a stir bar. To this, hydrobomic acid (7 mL, 33% in acetic acid) and phenol (0.7 g, 1 g/mL of acid) were added. The solution was gradually heated to 90 °C and stirred for 16 h while excess HBr gas was captured with a base trap. After cooling down the dark mixture, water (5 mL) was added and the solution was stirred for 15 minutes. The resulting mixture was washed with DCM (4 × 10 mL) after which it was basified to pH > 11 using a 10 M sodium hydroxide solution and extracted with DCM (4 × 10 mL). The combined organic fractions were dried with $NaSO_4$ (not $MgSO_4$), filtered and concentrated *in vacuo*.

For purification, the triamine was protected with a Boc protecting group. The crude reaction was taken in a 20 mL vial equipped with a stir bar. To it, Boc_2O (0.924 g, 4.24 mmol, 6.6 equiv.), dimethylaminopyridine (DMAP, 31 mg, 0.26 mmol, 0.4 equiv.) and DCM (6.5 mL) were added. The reaction was stirred for 12 h at room temperature. The reaction was then washed with water (10 mL). The organic layer was dried over $MgSO_4$, filtered and concentrated. The compound was purified via flash chromatography using 0%-10% MeOH in DCM. $KMnO_4$ stain was used to locate the compound in TLC. The pure compound **C4-Boc** was obtained in 87% yield after purification (266 mg).

^{1}H NMR (500 MHz, Chloroform-*d*) δ 3.21 (, 12H), 1.57 (s, 12H), 1.45 (s, *J* = 1.4 Hz, 27H).

^{13}C NMR (176 MHz, cdcl$_3$) δ.

HRMS: Calc. [M + Na$^+$] 536.3676, Measured: 536.3686.

For Boc deprotection, **C4-Boc** was stirred in a solution with 0.4 mL TFA and 0.9 mL DCM at room temperature for 12 h. The reaction was concentrated, washed with 1 M NaOH (3 mL) and the desired product extracted into DCM (3 mL X 3). The combined organics were dried over $NaSO_4$, filtered and concentrated to yield 62 mg of the free amine **C4-NH**.

^{1}H NMR (700 MHz, Chloroform-*d*) δ 2.69 – 2.65 (m, 12H), 1.57 (dq, *J* = 5.7, 3.0 Hz, 12H).

^{13}C NMR (176 MHz, cdcl$_3$) δ 48.48, 27.13.

HRMS: Calc. [M + H$^+$] 214.2283, Measured: XX

5.4.1.7 Synthesis of (benzene-1,3,5-triyltris(methylene))tris(propanamine)

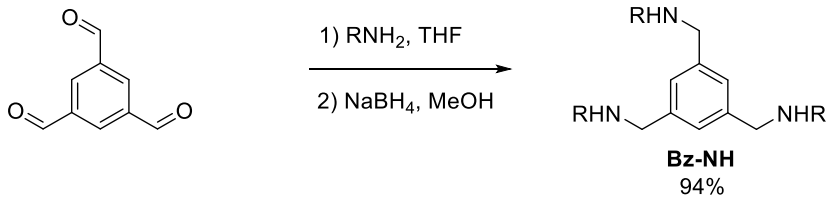

Bz-NH
94%

The oligoamine **Bz-NH** was synthesized via reductive amination.[16]

In a 50 mL round bottom flask equipped with a stir bar, tribenzaldehyde (1.0 g, 6.17 mmol, 1.0 equiv.), n-propylamine (3.0 mL, 37.0 mmol, 6.0 equiv.) and THF (12 mL) was added. A scoop of $MgSO_4$ was added to the flask and the reaction was stirred for 16 h at room temperature. The reaction was then filtered and concentrated *in vacuo*. This crude mixture was used in the reduction step without further purification.

In a 100 mL round bottom flask equipped with a stir bar, the crude tris-imine was taken up in MeOH (50 mL). This mixture is cooled to 0 °C and $NaBH_4$ (820 mg, 21.6 mmol, 3.5 equiv.) was added. The reaction was allowed to warm to room temperature and was stirred for 3 h. The solution is then filtered and concentrated *in vacuo* to give the pure oligoamine **Bz-NH** in 92 % yield (1.6 g).

^{1}H NMR (700 MHz, Chloroform-*d*) δ 7.16 (s, 3H), 3.77 (s, 6H), 2.60 (t, *J* = 7.2 Hz, 7H), 1.53 (h, *J* = 7.4 Hz, 6H), 0.92 (t, *J* = 7.4 Hz, 9H).

^{13}C NMR (176 MHz, cdcl$_3$) δ 140.98, 126.61, 54.16, 51.69, 23.34, 11.95.

HRMS: Calc. [M + H$^+$] 676.2549, Measured: XX

5.4.1.8 Synthesis of the Trimers

C2 trimer:

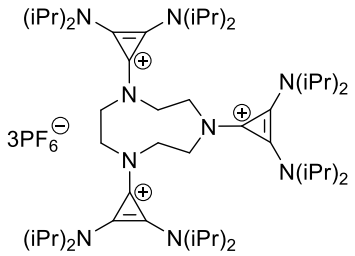

The trimer was synthesized according to the general procedure outlined above and purified via a column chromatography with eluent 10% MeOH/DCM followed by a recrystallization from EtOH.

^{1}H NMR (500 MHz, Acetonitrile-d_3) δ 3.89 (hept, *J* = 6.9 Hz, 12H), 3.77 (d, *J* = 2.5 Hz, 12H), 1.35 (d, *J* = 6.9 Hz, 70H).

^{13}C NMR (176 MHz, cdcl$_3$) δ 137.44, 126.78, 118.97, 117.23, 54.67, 52.50, 51.60, 21.88, 21.17, 10.50.

HRMS: Calc. [(M – 2PF$_6^-$)/2] 489.8710, Measured: [(M – 2PF$_6^-$)/2]: 489.8721

C3 trimer:

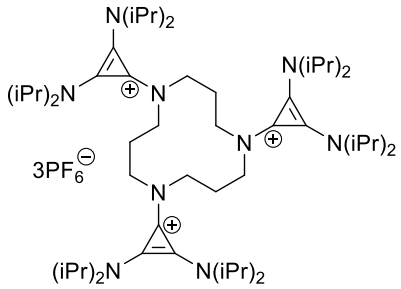

The trimer was synthesized according to the general procedure outlined above and was purified via recrystallization from MeOH.

^{1}H NMR

^{13}C NMR

HRMS: Calc. [M + H$^+$] 676.2549, Measured: XX

C4 trimer:

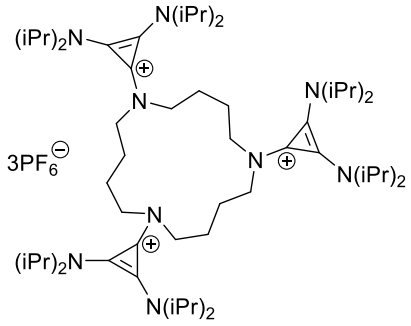

The trimer was synthesized according to the general procedure outlined above.

^{1}H NMR

^{13}C NMR

HRMS: Calc. [(M – 3PF_6^-)/3] 306.2904, [(M – 2PF_6^-)/2] 531.9180, [M – PF_6^-] 1208.8006, Measured: [(M – 3PF_6^-)/3] 306.2924, [(M – 2PF_6^-)/2] 531.9201, [M – PF_6^-] 1208.7977

Bz trimer:

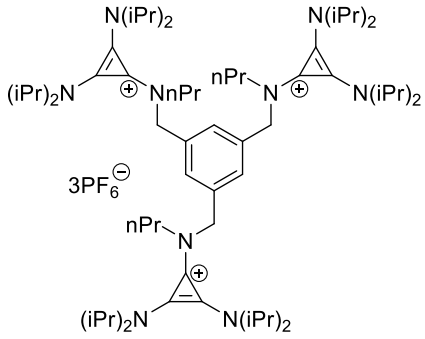

The trimer was synthesized according to the general procedure outlined above.

^{1}H NMR (500 MHz, Acetonitrile-d_3) δ 7.16 (s, 3H), 4.67 (s, 6H), 3.88 (hept, J = 6.9 Hz, 12H), 3.29 – 3.22 (m, 6H), 1.62 (h, J = 7.4 Hz, 6H), 1.32 (d, J = 6.9 Hz, 72H), 0.86 (t, J = 7.3 Hz, 8H).

^{13}C NMR (176 MHz, cdcl$_3$)

HRMS: Calc. [(M – 3PF_6^-)/3] 332.2060, [(M – 2PF_6^-)/2] 570.9414, Measured: [(M – 3PF_6^-)/3] 332.3082, [(M – 2PF_6^-)/2] 570.9435

5.4.2 Electrochemistry and Cycling Studies

5.4.2.1 Materials and Methods

Acetonitrile (99.8% anhydrous) was obtained from Sigma Aldrich and used as received. Potassium hexafluorophosphate (≥99%) was obtained from Sigma Aldrich and

dried under high vacuum at 100 °C for 48 h before use. 0.5 M stock solutions of KPF_6 in MeCN were prepared in a nitrogen-filled glovebox and dried over activated 3Å molecular sieves for at least two days prior to use. The molecular sieves were activated by heating at 200 °C under vacuum. All organic electrolytes were dried at 80 °C under high vacuum for 19 h before use and were then stored in an inert-atmosphere drybox.

5.4.1.1 General Procedure for Cyclic Voltammetry

Cyclic voltammetry was performed in a nitrogen-filled drybox with a Biologic VSP multichannel potentiostat/galvanostat using a three-electrode setup. A glassy carbon electrode (0.07 cm^2, BASi) was used as the working electrode and a platinum wire was used as the counter electrode. An Ag/Ag^+ quasi-reference electrode (BASi) containing 0.01 M $AgBF_4$ (Sigma Aldrich) in 0.5 M KPF_6/MeCN was used. All potentials are referenced to Ag/Ag^+. The CVs were performed with a solution of 5 mM concentration of active species, a scan rate of 100 mV s^{-1}, using 0.5 M KPF_6 as supporting electrolyte in MeCN.

5.5. References

(1) Flow Batteries: Current Status and Trends | Chemical Reviews https://pubs.acs.org/doi/10.1021/cr500720t (accessed Mar 11, 2020).

(2) Wei, X.; Pan, W.; Duan, W.; Hollas, A.; Yang, Z.; Li, B.; Nie, Z.; Liu, J.; Reed, D.; Wang, W.; Sprenkle, V. Materials and Systems for Organic Redox Flow Batteries: Status and Challenges. *ACS Energy Lett.* **2017**, *2* (9), 2187–2204. https://doi.org/10.1021/acsenergylett.7b00650.

(3) Noack, J.; Roznyatovskaya, N.; Herr, T.; Fischer, P. The Chemistry of Redox-Flow Batteries. *Angew. Chem. Int. Ed.* **2015**, *54* (34), 9776–9809. https://doi.org/10.1002/anie.201410823.

(4) Kamat, P. V.; Schanze, K. S.; Buriak, J. M. Redox Flow Batteries. *ACS Energy Lett.* **2017**, *2* (6), 1368–1369. https://doi.org/10.1021/acsenergylett.7b00361.

(5) Winsberg, J.; Hagemann, T.; Janoschka, T.; Hager, M. D.; Schubert, U. S. Redox-Flow Batteries: From Metals to Organic Redox-Active Materials. *Angew. Chem. Int. Ed Engl.* **2017**, *56* (3), 686–711. https://doi.org/10.1002/anie.201604925.

(6) Rugolo, J.; Aziz, M. J. Electricity Storage for Intermittent Renewable Sources. *Energy Environ. Sci.* **2012**, *5* (5), 7151–7160. https://doi.org/10.1039/C2EE02542F.

(7) Chalamala, B. R.; Soundappan, T.; Fisher, G. R.; Anstey, M. R.; Viswanathan, V. V.; Perry, M. L. Redox Flow Batteries: An Engineering Perspective. *Proc. IEEE* **2014**, *102* (6), 976–999. https://doi.org/10.1109/JPROC.2014.2320317.

(8) Gubler, L. Membranes and Separators for Redox Flow Batteries. *Curr. Opin. Electrochem.* **2019**, *18*, 31–36. https://doi.org/10.1016/j.coelec.2019.08.007.

(9) Lai, Y. Y.; Li, X.; Zhu, Y. Polymeric Active Materials for Redox Flow Battery Application. *ACS Appl. Polym. Mater.* **2020**, *2* (2), 113–128. https://doi.org/10.1021/acsapm.9b00864.

(10) Janoschka, T.; Martin, N.; Martin, U.; Friebe, C.; Morgenstern, S.; Hiller, H.; Hager, M. D.; Schubert, U. S. An Aqueous, Polymer-Based Redox-Flow Battery Using Non-Corrosive, Safe, and Low-Cost Materials. *Nature* **2016**, *534* (7607), S9–S10. https://doi.org/10.1038/nature18909.

(11) Janoschka, T.; Morgenstern, S.; Hiller, H.; Friebe, C.; Wolkersdörfer, K.; Häupler, B.; Hager, M. D.; Schubert, U. S. Synthesis and Characterization of TEMPO- and Viologen-Polymers for Water-Based Redox-Flow Batteries. *Polym. Chem.* **2015**, *6* (45), 7801–7811. https://doi.org/10.1039/C5PY01602A.

(12) Burgess, M.; Hernández-Burgos, K.; Cheng, K. J.; Moore, J. S.; Rodríguez-López, J. Impact of Electrolyte Composition on the Reactivity of a Redox Active Polymer Studied through Surface Interrogation and Ion-Sensitive Scanning Electrochemical Microscopy. *Analyst* **2016**, *141* (12), 3842–3850. https://doi.org/10.1039/C6AN00203J.

(13) Montoto, E. C.; Cao, Y.; Hernández-Burgos, K.; Sevov, C. S.; Braten, M. N.; Helms, B. A.; Moore, J. S.; Rodríguez-López, J. Effect of the Backbone Tether on the Electrochemical Properties of Soluble Cyclopropenium Redox-Active Polymers. *Macromolecules* **2018**, *51* (10), 3539–3546. https://doi.org/10.1021/acs.macromol.8b00574.

(14) Nagarjuna, G.; Hui, J.; Cheng, K. J.; Lichtenstein, T.; Shen, M.; Moore, J. S.; Rodríguez-López, J. Impact of Redox-Active Polymer Molecular Weight on the Electrochemical Properties and Transport Across Porous Separators in Nonaqueous Solvents. *J. Am. Chem. Soc.* **2014**, *136* (46), 16309–16316. https://doi.org/10.1021/ja508482e.

(15) Montoto, E. C.; Nagarjuna, G.; Moore, J. S.; Rodríguez-López, J. Redox Active Polymers for Non-Aqueous Redox Flow Batteries: Validation of the Size-Exclusion Approach. *J. Electrochem. Soc.* **2017**, *164* (7), A1688. https://doi.org/10.1149/2.1511707jes.

(16) Burgess, M.; Chénard, E.; Hernández-Burgos, K.; Nagarjuna, G.; Assary, R. S.; Hui, J.; Moore, J. S.; Rodríguez-López, J. Impact of Backbone Tether Length and Structure on the Electrochemical Performance of Viologen Redox Active Polymers. *Chem. Mater.* **2016**, *28* (20), 7362–7374. https://doi.org/10.1021/acs.chemmater.6b02825.

(17) Iyer, V. A.; Schuh, J. K.; Montoto, E. C.; Pavan Nemani, V.; Qian, S.; Nagarjuna, G.; Rodríguez-López, J.; Ewoldt, R. H.; Smith, K. C. Assessing the Impact of Electrolyte Conductivity and Viscosity on the Reactor Cost and Pressure Drop of Redox-Active Polymer Flow Batteries. *J. Power Sources* **2017**, *361*, 334–344. https://doi.org/10.1016/j.jpowsour.2017.06.052.

(18) Baran, M. J.; Braten, M. N.; Montoto, E. C.; Gossage, Z. T.; Ma, L.; Chénard, E.; Moore, J. S.; Rodríguez-López, J.; Helms, B. A. Designing Redox-Active Oligomers for Crossover-Free, Nonaqueous Redox-Flow Batteries with High Volumetric Energy Density. *Chem. Mater.* **2018**, *30* (11), 3861–3866. https://doi.org/10.1021/acs.chemmater.8b01318.

(19) Doris, S. E.; Ward, A. L.; Baskin, A.; Frischmann, P. D.; Gavvalapalli, N.; Chénard, E.; Sevov, C. S.; Prendergast, D.; Moore, J. S.; Helms, B. A. Macromolecular Design Strategies for Preventing Active-Material Crossover in Non-Aqueous All-Organic Redox-Flow Batteries. *Angew. Chem. Int. Ed.* **2017**, *56* (6), 1595–1599. https://doi.org/10.1002/anie.201610582.

(20) Hendriks, K. H.; Robinson, S. G.; Braten, M. N.; Sevov, C. S.; Helms, B. A.; Sigman, M. S.; Minteer, S. D.; Sanford, M. S. High-Performance Oligomeric Catholytes for Effective Macromolecular Separation in Nonaqueous Redox Flow Batteries. *ACS Cent. Sci.* **2018**, *4* (2), 189–196. https://doi.org/10.1021/acscentsci.7b00544.

(21) Richman, J. E.; Atkins, T. J. Nitrogen Analogs of Crown Ethers. *J. Am. Chem. Soc.* **1974**, *96* (7), 2268–2270. https://doi.org/10.1021/ja00814a056.

(22) MACROCYCLIC POLYAMINES: 1,4,7,10,13,16-HEXAÄZACYCLOÖCTADECANE. *Org. Synth.* **1978**, *58*, 86. https://doi.org/10.15227/orgsyn.058.0086.

(23) Hoye, R. C.; Richman, J. E.; Dantas, G. A.; Lightbourne, M. F.; Shinneman, L. S. Synthesis of Polyazamacrocyclic Compounds via Modified Richman−Atkins Cyclization of β-Trimethylsilylethanesulfonamides. *J. Org. Chem.* **2001**, *66* (8), 2722–2725. https://doi.org/10.1021/jo001639o.

(24) Bell, T. W.; Choi, H.-J.; Harte, W.; Drew, M. G. B. Syntheses, Conformations, and Basicities of Bicyclic Triamines. *J. Am. Chem. Soc.* **2003**, *125* (40), 12196–12210. https://doi.org/10.1021/ja030236d.

(25) Parker, L. L.; Gowans, N. D.; Jones, S. W.; Robins, D. J. A Practical Method for Building Linear and Cyclic Triamines from (2-Trimethylsilyl)Ethanesulfonamides (SES-Amides). *Tetrahedron* **2003**, *59* (51), 10165–10171. https://doi.org/10.1016/j.tet.2003.10.067.

(26) Marecek, J. F.; Fischer, P. A.; Burrows, C. J. Complexation of ATP to a Synthetic [15]-N3 Macrocyclic Polyammonium Receptor. *Tetrahedron Lett.* **1988**, *29* (48), 6231–6234. https://doi.org/10.1016/S0040-4039(00)82312-6.

(27) Timme, A.; Kress, R.; Albuquerque, R. Q.; Schmidt, H.-W. Phase Behavior and Mesophase Structures of 1,3,5-Benzene- and 1,3,5-Cyclohexanetricarboxamides: Towards an Understanding of the Losing Order at the Transition into the Isotropic Phase. *Chem. – Eur. J.* **2012**, *18* (27), 8329–8339. https://doi.org/10.1002/chem.201103216.

(28) Kersch, M.; Schmidt, H.-W.; Altstädt, V. Influence of Different Beta-Nucleating Agents on the Morphology of Isotactic Polypropylene and Their Toughening Effectiveness. *Polymer* **2016**, *98*, 320–326. https://doi.org/10.1016/j.polymer.2016.06.051.

(29) Kim, Y. J.; Lee, J. H.; Widyaya, V. T.; Kim, H. S.; Lee, H. Effect of Alkali Metal Nitrates on the Ru/C-Catalyzed Ring Hydrogenation of m-Xylylenediamine to 1,3-Cyclohexanebis(Methylamine). *Bull. Korean Chem. Soc.* **2014**, *35* (4), 1117–1120. https://doi.org/10.5012/bkcs.2014.35.4.1117.

(30) Ji, P.; Song, Y.; Drake, T.; Veroneau, S. S.; Lin, Z.; Pan, X.; Lin, W. Titanium(III)-Oxo Clusters in a Metal–Organic Framework Support Single-Site Co(II)-Hydride Catalysts for Arene Hydrogenation. *J. Am. Chem. Soc.* **2018**, *140* (1), 433–440. https://doi.org/10.1021/jacs.7b11241.

(31) Miyamura, H.; Suzuki, A.; Yasukawa, T.; Kobayashi, S. Polysilane-Immobilized Rh–Pt Bimetallic Nanoparticles as Powerful Arene Hydrogenation Catalysts: Synthesis, Reactions under Batch and Flow Conditions and Reaction Mechanism. *J. Am. Chem. Soc.* **2018**, *140* (36), 11325–11334. https://doi.org/10.1021/jacs.8b06015.

(32) Ding, Y.; Zhang, C.; Zhang, L.; Zhou, Y.; Yu, G. Molecular Engineering of Organic Electroactive Materials for Redox Flow Batteries. *Chem. Soc. Rev.* **2018**, *47* (1), 69–103. https://doi.org/10.1039/C7CS00569E.

(33) Ding, Y.; Yu, G. Molecular Engineering Enables Better Organic Flow Batteries. *Chem* **2017**, *3* (6), 917–919. https://doi.org/10.1016/j.chempr.2017.11.010.

(34) Beh, E. S.; De Porcellinis, D.; Gracia, R. L.; Xia, K. T.; Gordon, R. G.; Aziz, M. J. A Neutral PH Aqueous Organic–Organometallic Redox Flow Battery with Extremely High Capacity Retention. *ACS Energy Lett.* **2017**, *2* (3), 639–644. https://doi.org/10.1021/acsenergylett.7b00019.

(35) Leclaire, J.; Husson, G.; Devaux, N.; Delorme, V.; Charles, L.; Ziarelli, F.; Desbois, P.; Chaumonnot, A.; Jacquin, M.; Fotiadu, F.; Buono, G. CO2 Binding by Dynamic Combinatorial Chemistry: An Environmental Selection. *J. Am. Chem. Soc.* **2010**, *132* (10), 3582–3593. https://doi.org/10.1021/ja909975q.